AN ABSTRACT OF THE THESIS OF

JERRY EUGENE DONOVAN for the degree of Master of Science in Mechanical Engineering presented on June 6, 1979

Title: A STUDY OF FORCES ON SIMULATED HEAT EXCHANGE TUBES IMMERSED IN A COLD FLUIDIZED BED

Abstract approved: Redacted for Privacy

(Timothy C. Kennedy)

The object of this research project was to study how different parameters effect the magnitude and frequency composition of forces exerted on simulated heat exchange tubes immersed in a cold fluidized bed. Two arrays of tubes were assembled with the tubes mounted in an equilateral triangular pitch pattern. The center column of tubes in each array was instrumented with bi-directional strain gage load cells. The parameters varied and studied during this experimental research were the superficial air velocity, the spacing between centers of the tubes, the distance between the distributor plate and the bottom tube, and the mean particle diameter. A digital force-time series of the force exerted on each of the instrumented tubes was obtained in both the vertical and horizontal planes.

Results are given in the form of a plot of the force-time history and a statistical analysis for both the tube in the array experiencing the most severe loading

and the simultaneous sum of the loads experienced by all of the instrumented tubes. The statistical analysis includes the mean and variance of the digital force-time series and a plot of power spectral density verses frequency. Also shown are plots indicating how the statistical results vary with changes in superficial air velocity while holding all other parameters constant. The severity of loads on single tubes as well as the sum of the loads on all of the instrumented tubes varied with changes in the tube spacing, the height of the tubes above the distributor plate, and the air velocity. Peak vertical loads exceeded 140 lbs on individual tubes and 200 lbs on a complete column of instrumented tubes, while the horizontal loads were always less than half as severe as the vertical loads.

# A Study of Forces on Simulated Heat Exchange Tubes Immersed in a Cold Fluidized Bed

by

Jerry Eugene Donovan

A THESIS

submitted to

Oregon State University

in partial fulfillment of
the requirements for the
degree of

Master of Science

Completed June 6, 1979

Commencement June 1980

APPROVED:

Redacted for Privacy

Assistant Professor, School of Engineering in charge of major

Redacted for Privacy

Head of Department of Mechanical Engineering

Redacted for Privacy

Dean of Graduate School

Date thesis is presented JUNE 6, 1979

Typed by Miriam R. Donovan for Jerry Eugene Donovan

ACKNOWLEDGEMENT

First, I wish to express thanks to the Electric Power Research Institute for their support of the project through grant number RP-315-1, and to the following individuals, without whose assistance this would have been a much longer and more difficult project:

To Dr. Thomas Fitzgerald, who always had another good idea when I needed one.

To Mr. Steven Crane, who was a great assistance in the mechanics of the project.

To Mr. Rich Fobes, for the help in the use and programming of the Nova minicomputer, without which, it would have been impossible to collect over seven million points of data.

And finally to the person who was the most helpful and the one I could always get advice and support from, my major professor, Dr. Timothy C. Kennedy.

TABLE OF CONTENTS

LIST OF ILLUSTRATIONS

# A STUDY OF FORCES ON SIMULATED HEAT EXCHANGE TUBES IMMERSED IN A COLD FLUIDIZED BED

## I. INTRODUCTION

### Background

The United States is currently facing the problem of an increasing dependence on foreign oil resources. There are many different sources of energy which are possible solutions to this problem. Fossil fuels, and nuclear and hydroelectric power will continue to play a large part in supplying the energy that the United States will need in the future. Wind, solar, and geothermal sources will also be supplying some energy in the future. However, none of these sources of energy are without problems. [6]

Coal, which comprises eighty-five percent of the United States' fossil fuel resources, will continue to play a major role in supplying energy for a long time into the future, as it has in the past. However, it also has problems which currently make it less desirable than it could be. Even though it has a very large proven reserve, which is about two hundred times the current annual consumption rate, it is difficult to obtain. And after it is recovered from the ground, it has sulfur mixed in with it. This sulfur is released, along with oxides of nitrogen, when it is burned. These by-products

must be dealt with somehow in order for the coal to be burned in a way which is ecologically acceptable. One of the technologies used to combat this problem is the fluidized bed boiler, which will burn the coal more evenly, efficiently, and will absorb the unwanted emissions while burning the coal. [10

## History

In the late 1700's, it was recognized that if coal was finely divided, i.e., pulverized, it might be burned in a suspension similar to a gas. But suitable techniques for pulverizing were not available yet. Not until the 1890's did pulverizing methods appear in the cement industry, and in 1921, when Fritz Winkler patented his "Winkler Gas Generator", the first significant application of a pulverized coal firing boiler was made. His device gasified a bed of coal suspended by a gentle upward flow of air. His process used the technique of suspending the coal with air because of its natural mixing properties of the bed material and its even distribution of heat. Fluidized beds were also used in the 1940's by the petroleum industry in catalytic cracking processes.

Interest in using fluidized beds in boiler applications has been increasing significantly over the past decade. The feasibility of burning coal in a fluidized bed combustor has been shown in many studies. Proven

advantages of a fluidized bed boiler over a conventional boiler include compactness and economy in burning high sulfur coal in an environmentally acceptable manner. [10]

## Fluidized Bed Boilers

A fluidized bed consists simply of a container of small solid particles which are subjected to a uniform upward flow of a gas or liquid. When the bed is composed of limestone particles, and crushed coal is introduced and burned, the resulting combustion has a great number of attractions. The coal is burned evenly without "hot" or "cold" spots and at a much lower temperature than conventional boilers. Sulfur in the coal reacts with the limestone to form an ash instead of escaping as a gas into the atmosphere. The lower temperatures, 1500°F to 1600°F, rather than 2600°F plus for conventional boilers, produce less $NO_x$ and other undesirable gases. Also, because of temperatures below the melting point of the ashes, no slag is formed, thus allowing heat exchange tubes to be placed directly in the fluidized bed where the heat transfer coefficient is five times as great as the heat transfer for tubes above in the hot gases. Finally, the fluidized bed combustors can burn almost any grade of coal or oil. [4]

## The Problem

Many different types of studies have been made on various aspects of fluidized bed boilers, such as in the fields of

heat transfer from the bed to immersed heat exchange tubes and walls, movements of solids and gases within the bed, and elutriation of particles. Also of concern is the life expectancy of heat exchange tubes which are immersed in the hostile environment of a fluidized bed.

A number of factors combine to limit the lifetime of tubes in a fluidized bed boiler. Erosion of tube material itself may be augmented by chemical attack or corrosion caused by gas phase constituents found in a fluidized bed combustor. In order to study this effect it is necessary to conduct tests in which various tube materials under consideration are subjected to the actual environment of a fluidized bed combustor. Mechanical stresses on heat exchange tubes may also contribute to failures, not only of the tubes, but possibly also of the support system which holds the tubes in place. Unlike corrosion, the data on mechanical stresses on heat exchange tubes in a cold bed can be applied in the design of a hot bed.

Knowledge of the magnitude and frequency composition of applied forces is necessary in order to predict the fatigue life of a structure. The forces on an immersed heat exchange tube include the effect of buoyancy, because of the liquid-like behavior of the fluidized bed material, form drag related to the rate of change of momentum as the solids flow around the tube, and some viscous drag related to the velocity of particles passing the tube. [7, 8, 9]

This study deals with finding the magnitude and frequency composition of the applied forces on the immersed tubes in a cold fluidized bed. Tests were performed to measure forces on the tubes near the center of triangular pitched arrays. Results are given for both key individual tubes and the overall column of instrumented tubes under a wide range of operating conditions.

# II. EXPERIMENTAL RESEARCH

## Description of Equipment

### General Information

The fluidized bed facility is located in the main lab of the Chemical Engineering Building and extends from the basement to the roof. The experimental equipment can be thought of as two separate interlocking parts. One part is connected together by air ducts while the other is connected together by electrical wires. The first part consists of the fluidizing column and its associated apparatus needed to operate it, such as the engine and blower. The other part consists of the instrumented tube array bundle and its associated items, such as the electrical console and the computer which is used to collect the data.

### The Fluidized Bed

The fluidized bed, as shown in Figure 1, consists of a fluidizing column, an engine, a blower, a venturi meter, a water seal, and associated duct work. The fluidizing air is supplied by a Roots Positive Displacement Lobe Blower. The maximum output from the blower is 8000 cfm at 7.5 psi (3.78 $m^3/s$ at 51.7 kPa). The blower is powered by a 325 hp Caterpillar diesel engine. The engine and blower are installed in a specially constructed sound-suppression chamber. The air passes through a butterfly valve and

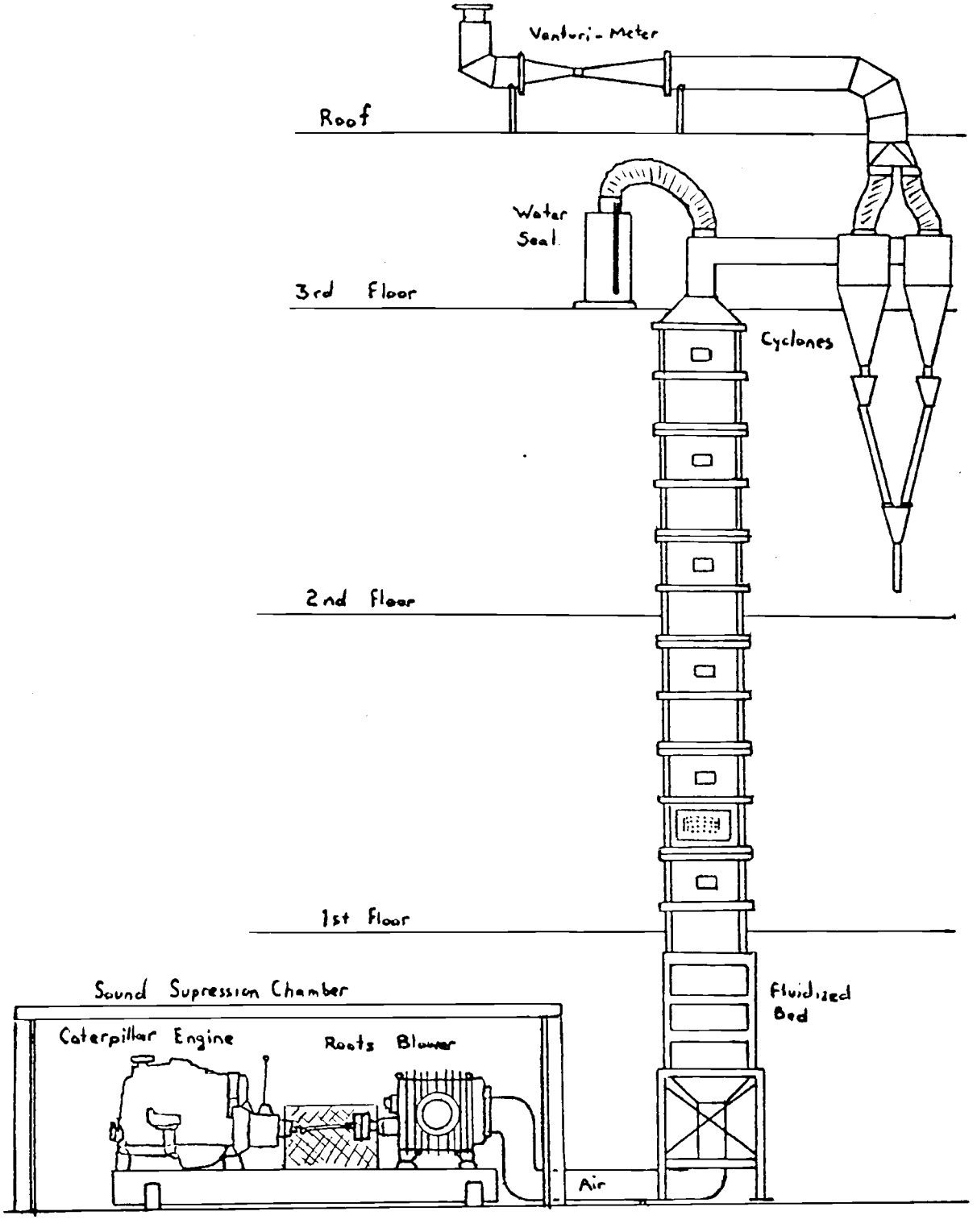


Figure 1. General layout of test facility.

enters the bed from an inverted pyramid shaped wind box, serving as a plenum chamber. Next, the air flows through a distributor plate and then into the fluidizing column. The distributor plate consists of two ten gauge mild steel plates with a wire screen mesh (No. 20 Tyler mesh) placed between the plates as shown in Figure 2. The plates are punched with 7/32" (0.556 cm) diameter holes placed on 3/4" (1.905 cm) centers in a square pitch pattern. The open area of the plate is 6.68% which allows velocities as high as 12.5 ft/sec (3.81 m/s). The pressure drop across the distributor plate is sufficiently high as to achieve equal flow through the openings. The ratio of $\Delta P_{distributor}/\Delta P_{bed}$ is in the vicinity of 40% and higher.

The test section of the bed is nine $ft^2$ (0.83 $m^2$) with the dimensions of three feet by three feet (0.914 m by 0.914 m). The transport disengaging height is 25 ft (7.5 m). At the top of the fluidizing column exists a water seal which would open whenever the system exceeded safety levels due to mal-operation. The air stream passes through four cyclone separators, operating in parallel, which remove the airborne particle which may not have dropped back into the bed before reaching the top. The particle-free air passes through a venturi and out into the atmosphere. A calibrated differential manometer is connected to the venturi and is located in the engine room. This allows the superficial air velocity to be adjusted by varying

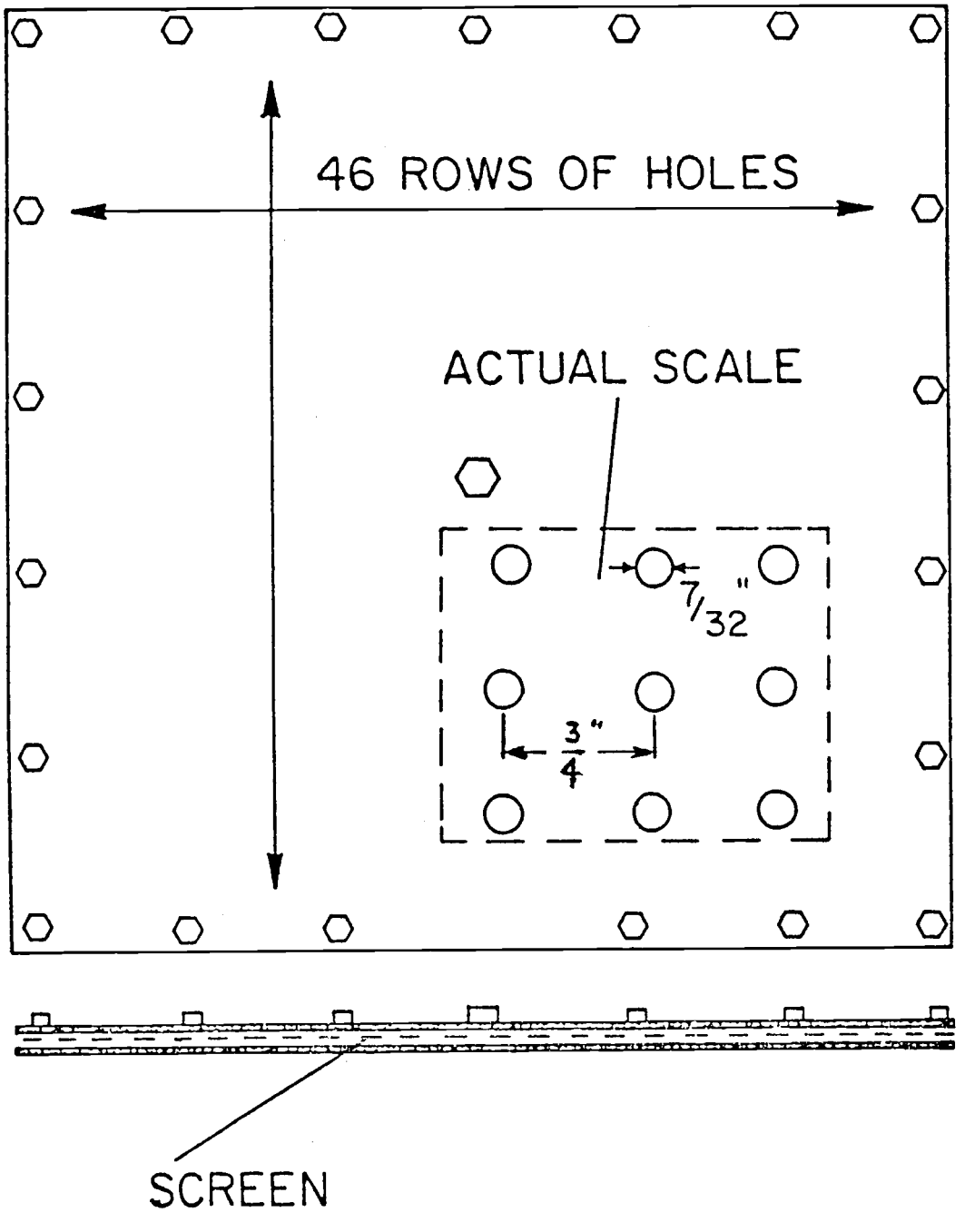


Figure 2. The distributor plate.

the engine speed.

Also, located parallel, and adjacent to the three foot by three foot bed, is a smaller one foot by one foot (0.3 m by 0.3 m) bed. The distributor plate in the smaller bed consists of two plates with 7/32" (0.556 cm) hole drilled on 1" (2.54 cm) centers in a square pitch pattern. These plates "sandwich" a No. 20 Tyler mesh wire screen. Ducting with butterfly valves allows air to flow from the same blower and out through the same cyclones as the larger bed.

Instrumentation of tubes.

Two similar immersed dummy heat exchange tube bundles were used, one for each spacing of tubes studied. Both bundles were held by a frame which could be bolted firmly into the fluidizing column. These frames could be supported at either the 10" (25 cm) or 20" (51 cm) distance from the distributor plate to the bottom tube. Each array used nearly equilateral triangular pitch. The array with center to center distances of 4" (10.1 cm) used 1.9" (4.8 cm) OD fiberglass tubes supported by rods with vertical spaces on each end. The array with center to center distances of 6" (15.2 cm) used 1.9" (4.8 cm) OD plastic pipe supported by plywood panels at each end. This can be seen in Figure 3. The instrumented column of tubes, shown in Figure 4, was made such that it could be assembled

Figure 3. Photograph of a tube array.

Figure 4. Photograph of an instrumented column of tubes.

outside the array and slipped into either array as one unit, occupying a zig-zag column of tubes in the center of the array.

The column of instrumented tubes consists of a series of aluminum tubes supported at each end by a load cell. These load cells are mounted on parallel plates with a triangular pitch matching the triangular pitch of the tubes in the array within which the column will be placed. The load cells, shown in Figures 5 and 6, consist of a thin-walled tube acting as a cantilever beam which supports the dummy heat exchange tubes. The load on the tube is determined by measuring the bending strains on the surface of the beam with strain gages. The beam itself is made of a thin-walled aluminum tube with circular disks at each end. One end of the tube is pressed into a 1/4" (6.3 mm) thick flat aluminum disk with a turned spherical radius of 7/8" (2.22 cm) at the outer edge. This disk fits inside the dummy heat exchange tube which is made from seamless, 1-1/2" Schedule 40, aluminum pipe. The inside of the pipe is bored to an ID of 1.751 inches (4.44 cm) for a distance of 2 inches (5 cm) along its axis to accept the disk. Friction between the tube and the aluminum disk is reduced by the use of silicon grease. A flexible molded butyl tube sleeve is placed over the end of the tube and extends over the strain gage support. These sleeves are held in place by hose clamps and can be

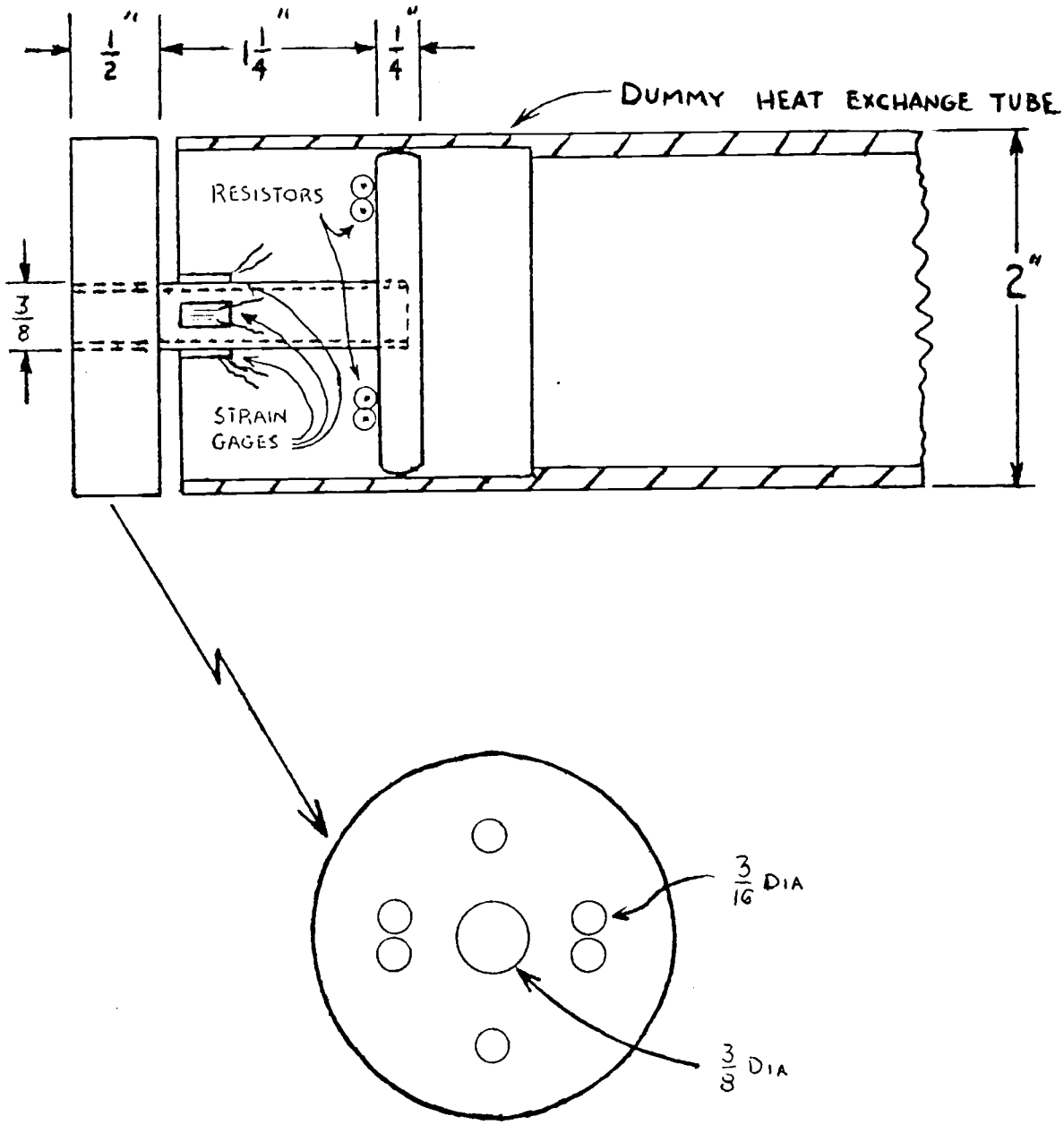


Figure 5. Drawing of a load cell.

Figure 6. Photograph of a load cell.

seen in Figure 4. The sleeves have no appreciable effect on the measured strain gage readings, but do prevent bed material from entering the annular region around the strain gages. The strain gage elements are bonded on opposite sides of the beam so that bending causes one to contract and the other to expand. When mounted in this fashion, bending strains add on output while temperature induced strains cancel on output. This is necessary because the fluidized bed heats up into the neighborhood of 140°F (60 c) when operating. Strains due to bending are measured in both vertical and horizontal planes on all load cells. Also included in the load cells are two pairs of resistors, one for each plane of measurement. These resistors are connected with the strain gages to form two complete but separate electrical bridges. Wires from each junction on the bridge pass out of the load cell through the back disk and connect up to the electrical console located outside of the fluidized bed.

Amplifier cards, like the one shown in Figure 7, supply a one-volt signal to the load cells and amplify the output from the load cells. A schematic drawing of an amplifier card is shown in Figure 8. The maximum gain on the amplifiers is 2000. The amplifier cards fit into slots located within the electrical console. These slots are wired to connectors on one of the faces of the console which can have wires from the load cells or from the computer

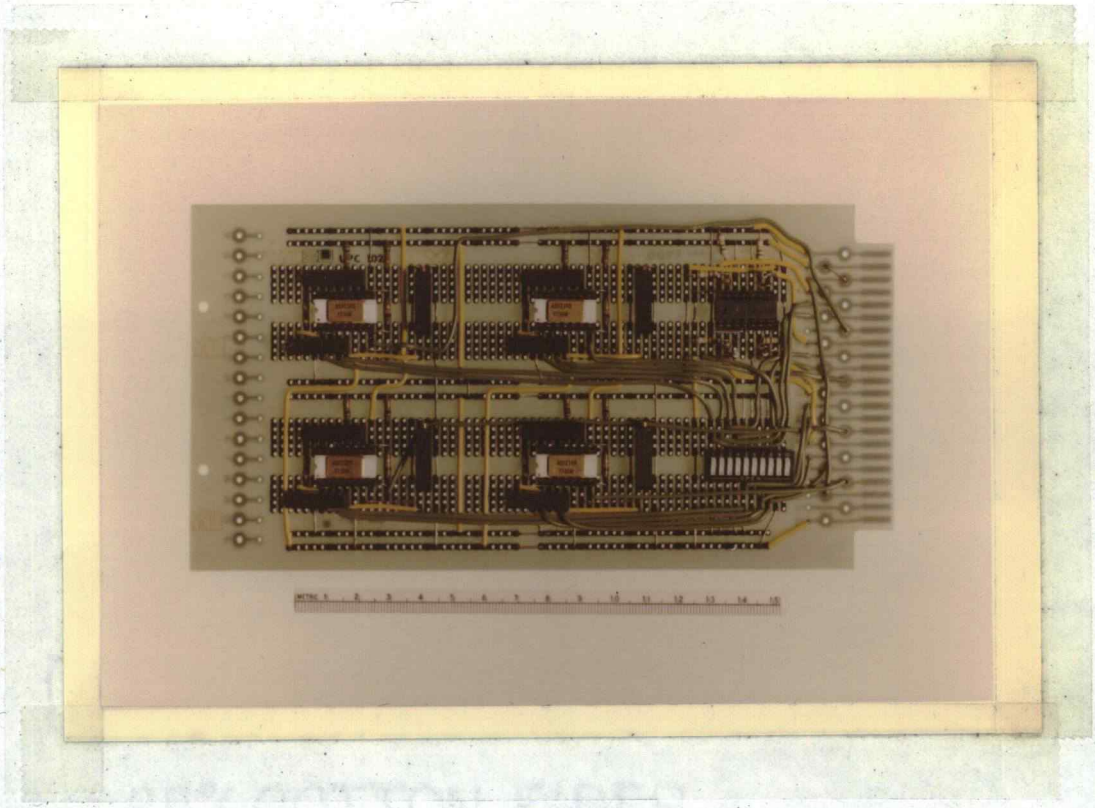

Figure 7. Photograph of an amplifier card.

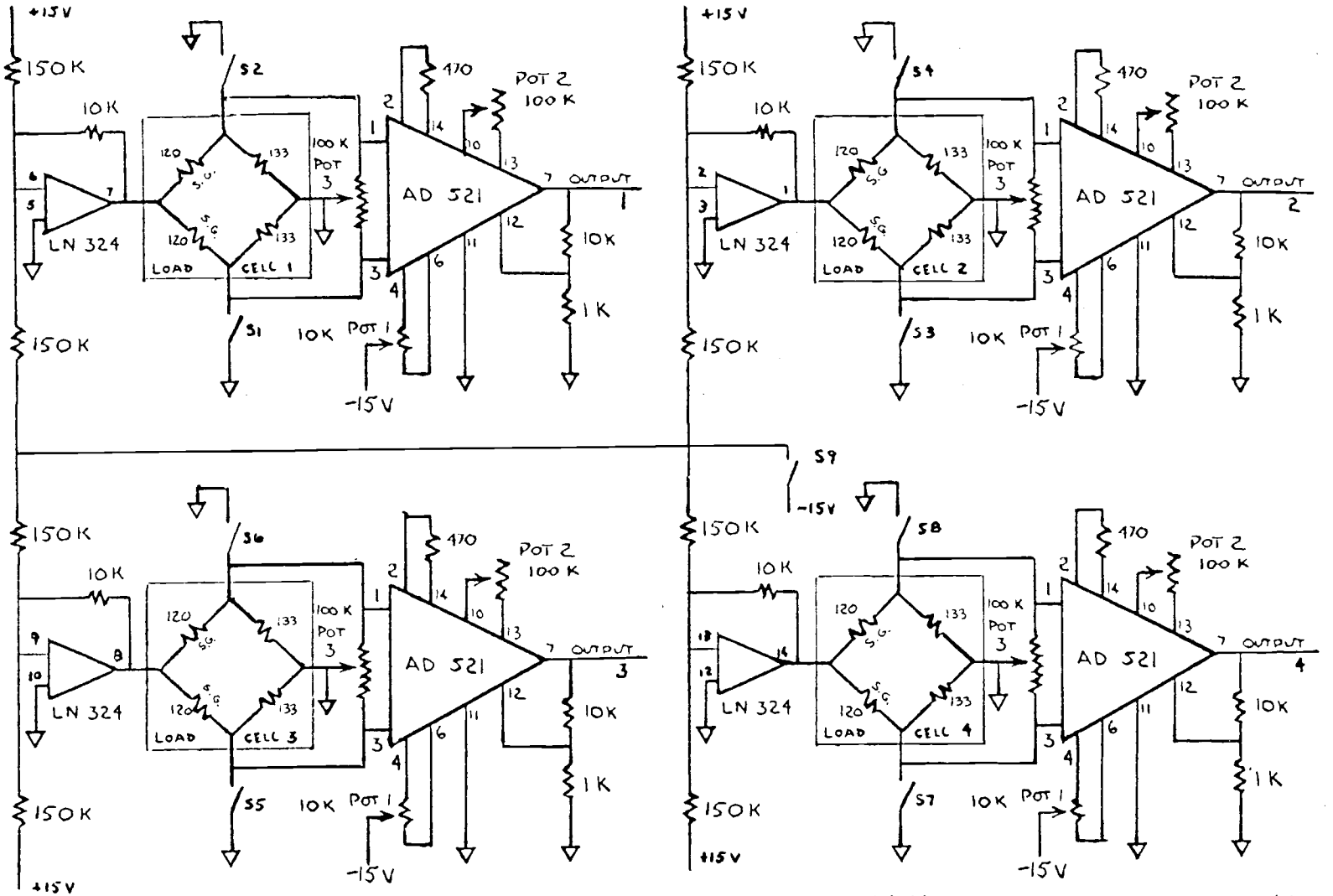


Figure 8. The schematic drawing of the amplifier card.

attached.

Data acquisition is accomplished by the use of a Data General Model 840 Nova minicomputer. It has 128 analog-to-digital input channels and can sample at rates up to over 10,000 samples per second. Programs have been written in machine language to collect data at pre-specified time intervals and store the digital data on files which can be stored on the interchangeable disks or magnetic tape. Preliminary plots are constructed on a plotter or a display screen with the help of another program located on the disks. The data files are then converted to a format which the Cyber computer, located in the Computer Center, can read. The power spectral density plots and short time series plots are created by programs located in the Cyber computer. These plots are drawn by the Gerber plotter, also located in the Computer Center.

Calibration of the load cells was done statically. This calibration is also valid for dynamic loading as long as the frequency components of the dynamic load are well below the natural frequency of resonance of the tubes. An amplication factor vs frequency of the dummy heat exchange tubes is found in Appendix A.

## Experimental Procedure

### Preliminary Tests

From reviewing literature on the subject of fluidized

beds, we were unable to estimate what magnitudes of forces would exist against the immersed tubes. Observing the fluidized bed in operation showed the bed materials bubbling violently, similar to a boiling liquid. Before instrumenting a full column of tubes in the large bed, we decided that a series of preliminary tests should be carried out and studied.

The first preliminary test was to determine the order of magnitude of loads experienced by individual tubes. This was done in the one foot square bed with a fiberglass tube. Mounted as shown in Figure 9, the tube was supported on one end by a Uni Measure/80 load cell and the other end by a single bolt through the wall of the bed. A short time history of the force on the one end of the tube with an air velocity of 12 ft/sec (3.7 m/s) is shown in Figure 10. The peak load was typically about 5 or 6 lb ($\sim$25N) in the upward direction with occasionally a spike up to 10 lbs ($\sim$45N) or more. The duration of each peak was about 0.1 sec and the time between peaks was about 0.3 sec. Downward forces were negligible compared to the upward forces. Unknown at this time was any indication of the magnitude of loading in the horizontal plane, because the commercial load cell, which was used, only measured loads in one direction. However, Donlevy [2] concluded that most of the flow is in the vertical direction in a fluidized bed.

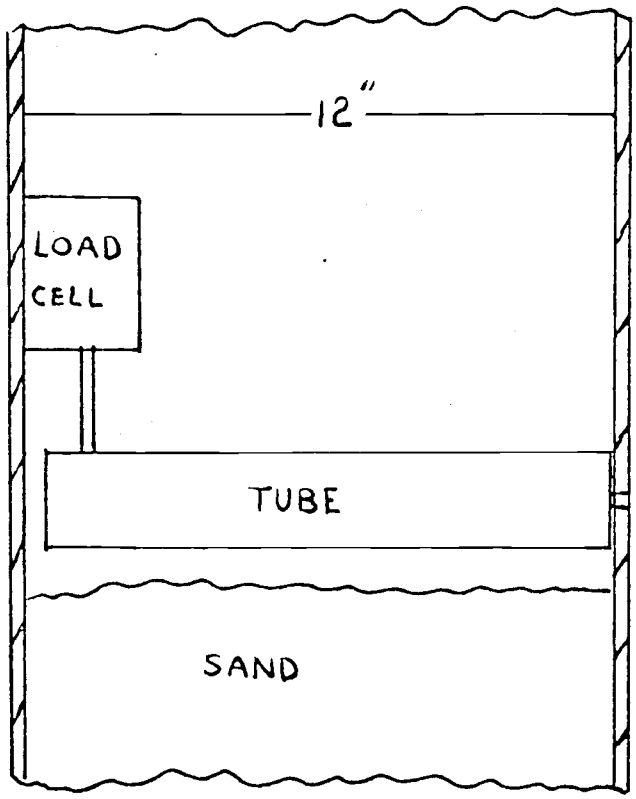


Figure 9. First preliminary test set-up.

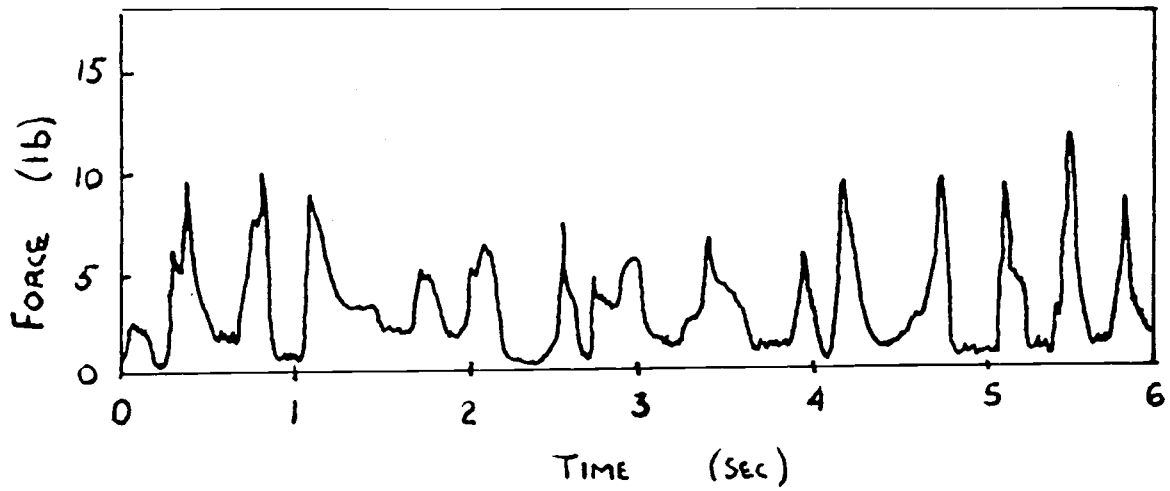


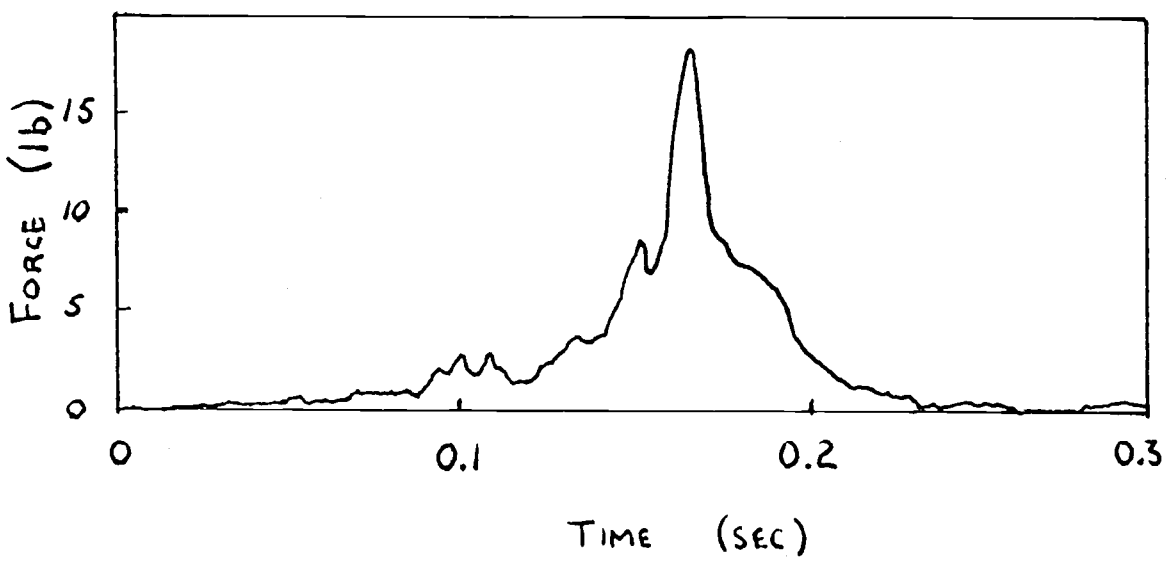


Figure 10. A short force-time history of the first test.

At this time it was realized that the use of commercial load cells in the larger tests would be prohibitive in cost. After considering many possibilities in the design of some specialized load cells, a pair of bidirectional load cells with the use of strain gages was manufactured. These load cells were similar to the final design with minor differences in the back plate and doorknob-like disk. The back plate was made larger so that it could be easily bolted to the walls of the smaller bed. The other disk was more rounded than the final design, and was machined to just fit inside the fiberglass tube. At the same time a bread-board design of the amplifiers was made. Tests were run in the one foot square bed with these load cells and amplifiers. Results of the tests compared well with the results from the Uni Measure/80 load cells. The tests also showed that the horizontal loads were similar to the vertical loads in shape, but with the magnitudes of peak loads in the horizontal plane of only about one-third of the magnitudes of peak loads in the vertical plane. Tests were also run with a small array of three tubes in a five-inch triangular pitch, shown in Figure 11, below the instrumented tube which indicated that the upper tube was protected somewhat by the surrounding tubes at the higher velocities.

The next step was to use the knowledge gained from these tests in the larger bed. The longer length of tubes in the larger bed brought concern of a natural frequency

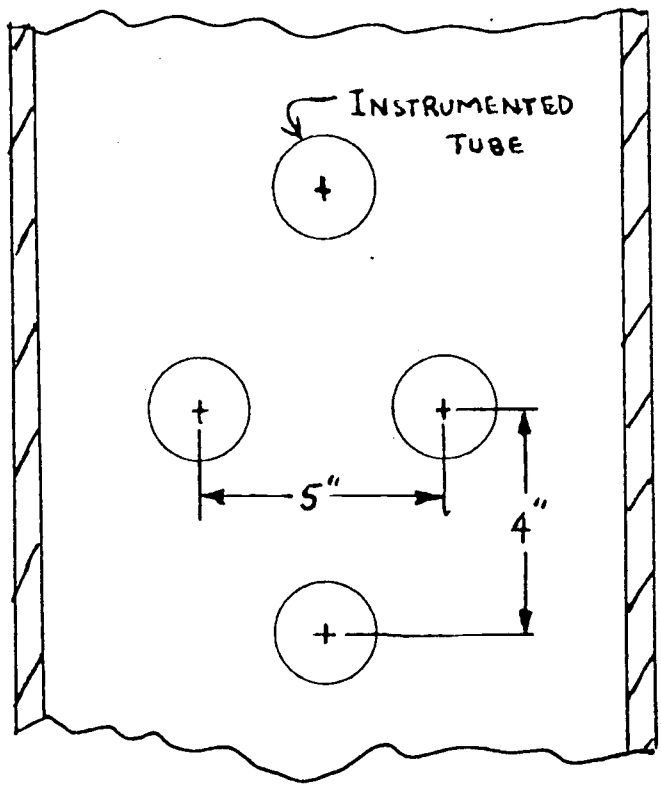


Figure 11. Four tube array test set-up.

of resonance of the tube being lowered to a point where the output signal would be distorted. Tests with the use of a shaker table showed that an aluminum tube would be better than a fiberglass tube. The tests brought about the final design of load cells and tubes, which was previously described. Shaker tests yielded the amplification factor vs. frequency curve, which is found in Appendix A. Another shaker test showed that when silicon grease was used to lubricate the place where the load cell touched the tube, the output best resembled the input signal. From this point on, all of the tests were performed with the aluminum tubes and load cells mounted on plates which fit into the simulated heat exchange tube arrays.

## Collection of Data

Collection of data consisted of calibration of the load cells, operation of the fluidized bed and operation of the Nova minicomputer. Calibration was done by placing a known weight on the tubes, one at a time, and adjusting the gain on the amplifier cards such that the Nova minicomputer yielded the desired change in output. This was done with the column of instrumented tubes standing outside of the rest of the array. Calibration of the tubes was done every time the array was removed from the fluidized bed facility. Next, the array was assembled and mounted in the empty bed. Before the sand was added to the bed,

the zero adjustment on the amplifier card was set. This was done always just before loading the bed to execute a set of runs. After filling the bed with the proper amount of sand, the "TAKEDATA" program, on the Nova minicomputer, which was used to collect data, was initialized. The data collection process started when the data start button, located for these tests, in the engine room, was activated. The engine speed was adjusted such that the manometer from the venturi showed the correct pressure differential for the superficial air velocity desired. Then the desired conditions of the test were achieved, the computer program was allowed to collect the data. Data collection proceeded for approximately thirty seconds after which the bed was defluidized until the next run was made so that the instrumented tubes would not receive any unnecessary wear. The data was then transferred to magnetic tapes for storage until further analysis was desired. The data collection process was continued by re-initializing the data collection program and changing whichever parameters needed to be changed, such as superficial air velocity.

Analysis of Data

Shortly after completing a set of runs, plots were made with the use of the Nova minicomputer. The plots showed magnitudes of peaks and valleys for each of the load cells, along with showing any problems that may have occurred during the data collection process. When it was determined

that the data collected was satisfactory, i.e., the load cells and amplifiers worked, it was transferred to the Cyber computer. On Cyber there exists a program in the IMSL library which does a fast fourier transorm of the data which yielded the power spectral density values. The parameters used in this program are listed in Appendix B. The values of the power spectral densities were plotted using the COMPLOT program, also in the Cyber library. Also plotted at the same time were the short force-time history plots.

Description of Parameters

Four parameters were varied through the course of the study. All combinations of the four parameters were tested, with one exception which was that only one bed media size (EI 16) was tested with the six-inch tube array spacing. The test parameters were:

1. Tube spacing - the two tube array spacings that were considered were four-inch and six-inch distances between centers on an approximately equilateral triangular pitch, as shown in Figures 12 and 13.
2. Bed media size - the two beds media were EI 8 sand with mean diameter of 0.04" (1.0 mm) and EI 16 sand with mean diameter of 0.03" (0.76 mm). Approximately 2000 lbs (900 kg) of sand was always used.

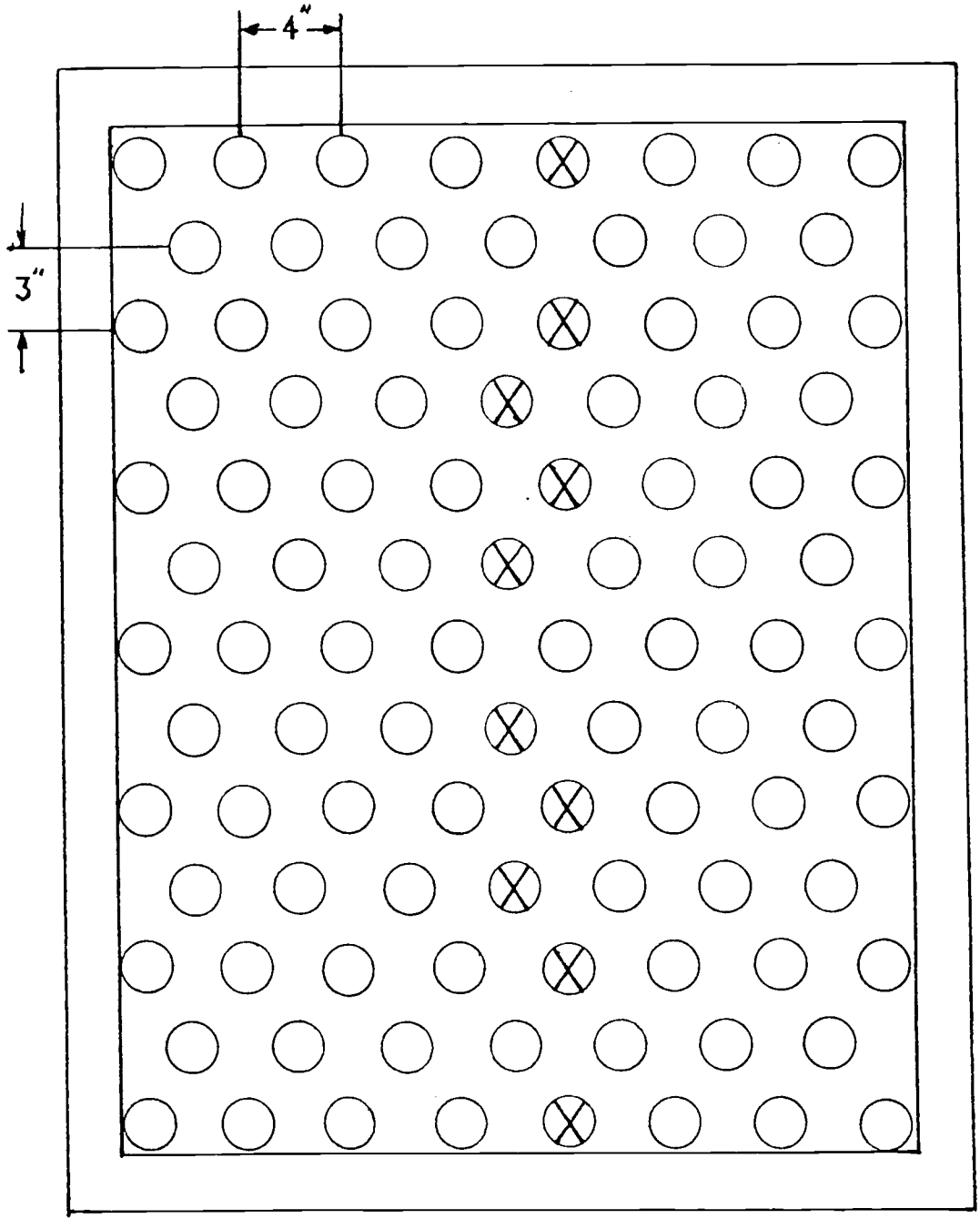


Figure 12. Array set-up with 4" tube spacing.

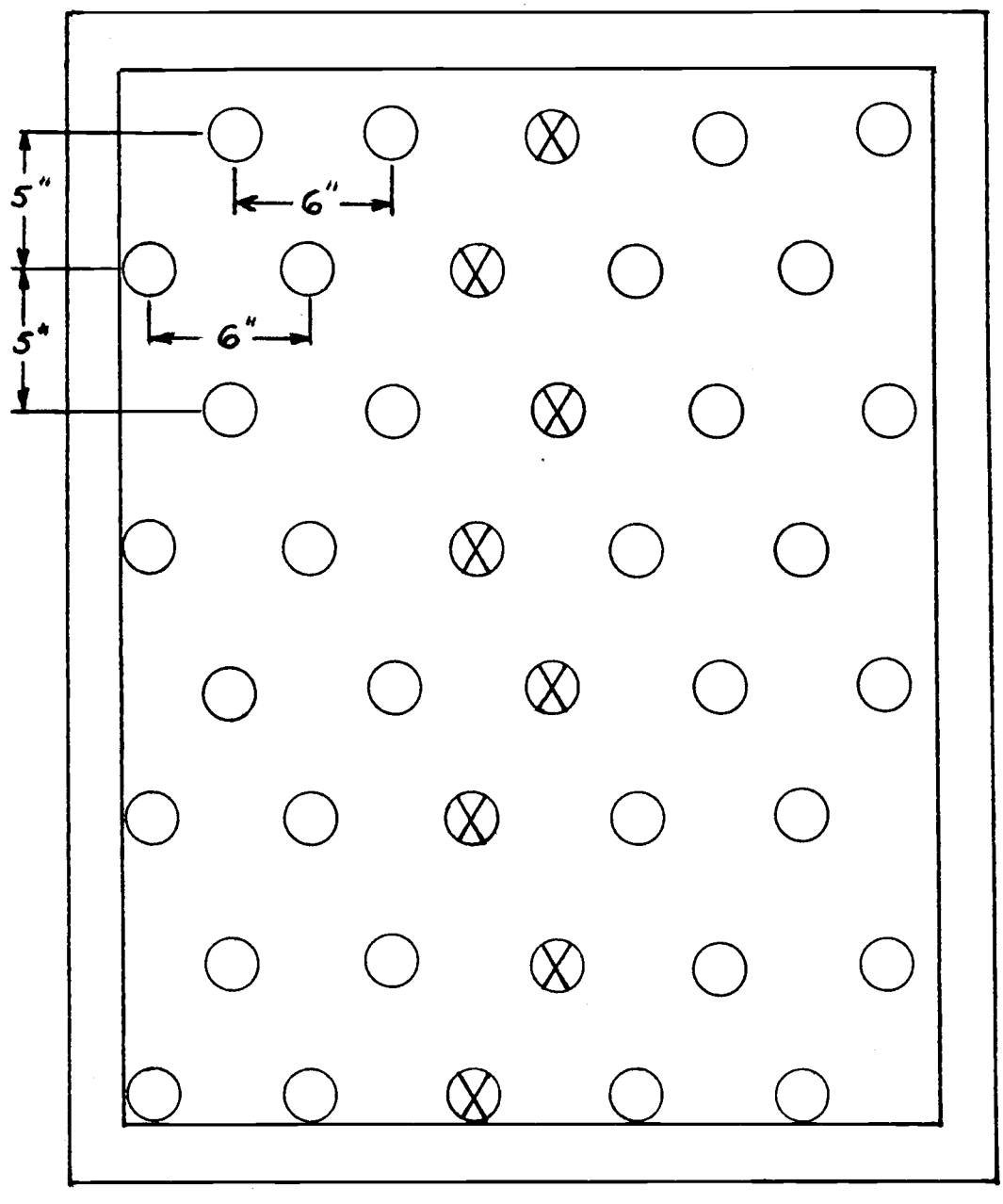


Figure 13. Array set-up with 6" tube spacing.

3. Tube array height - the two tube array heights were 10" (25 cm) and 20" (51 cm). This distance was measured from the top of the distributor plate to the bottom of the bottom row of tubes.
4. Superficial air velocity - the four superficial air velocities were 5, 7, 9 and 11 ft/sec. (1.5, 2.1, 2.7 and 3.4 m/s). Measurement of this parameter was with the differential manometer which was connected to the venturi flow meter.

Not varied in the tests were:

1. Size of tubes - all tubes were 2" (5 cm) in diameter and 28" (71 cm) in length.
2. Amount of bed material - all tests used 2000 lbs. (900 kg) of sand.

# III. RESULTS

## Description of Results

For each set of parameters, a series of four sets of results are given. Each set of results includes a short force-time history from the load cell output and a statistical analysis, which includes the mean, the variance, and a plot of power spectral density verses frequency. For each test run, the four sets of results consist of:

1. The vertical load on a single tube. The tube with the most severe loading was chosen. For most cases this was the bottom tube. However, when the six-inch spacing was mounted at the ten-inch array height, the middle tube had the most severe loads and it was chosen.
2. The horizontal load on a single tube. The same tube as for the vertical case was chosen.
3. The total vertical load on the entire instrumented array. The total vertical load was obtained by simultaneous superposition of the vertical loads on each of the individual instrumented tubes.
4. The total horizontal load on the entire instrumented array. The total horizontal load was obtained by simultaneous superposition of the horizontal loads on each of the individual instrumented tubes.

Also for each array spacing, plots are given showing how the statistical data varies with different superficial air velocities for the single tube and the sum of the instrumented tubes.

The results can be applied in the design of tubes and supports by various methods. Some of the methods are given by Crandall and Mark [1] or by Wirsching and others [8, 9, 10].

## The Array with Four-inch Tube Spacing

In all of the tests run with the four-inch tube spacing between centers, the bottom tube experienced the most severe loads. Most of the middle and lower tubes, except the bottom tube, showed nearly equal leads, but with a magnitude of less than three-quarters the magnitude of the forces on the bottom tube. The upper part of the array showed that the magnitude of the forces decreased with increasing height of the tubes. With the array at the 10" height, the forces were about three-quarters as severe on the middle tubes and half as severe on the top tubes when compared to the bottom tubes. When the array was placed at the 20" height, these figures dropped to half and nearly zero, respectively.

Typical peak loads in the vertical direction at the 10" array height were in the range of 20 to 30 lbs (90 to 130 N) for the bottom tube and 60 to 100 lbs (270 to 450 N)

for the 10-tube array. When the array was at the 20" height, peak vertical forces reached 50 to 80 lbs (220 to 360 N) for the bottom tube and 80 to 150 lbs (360 to 670 N) for the 10-tube array. In each case the horizontal forces were approximately one-third as severe as the corresponding vertical forces.

Figure 14 shows simultaneous loading of two tubes, the upper curve is the load on one of the middle tubes and the lower curve is the load on the next tube located diagonally upward in the instrumented array. Both the magnitude change and shift in time can be noticed as the load propagated up through the array. The rate of propagation of the load up through the array varied from 2 to 5 ft/sec.

Figures 15 - 18 show four sets of results for the combination parameters, which includes EI 16 sand, 20" array height and 4" tube spacing. The force-time history in Figure 15 indicates that the force in the vertical direction on a single tube is nearly zero about half of the time with upward pulses occurring approximately every half second. The major peak in the power spectral density plots in Figures 15 and 16 occurs at about 2 Hz, but the magnitude of the power spectral density is much lower for the entire curve in the horizontal case compared to the vertical case. The power spectral density curve for the horizontal direction also had a second peak around 70 Hz. This peak corresponds to the frequency of pulses created by the type of blower used. The location

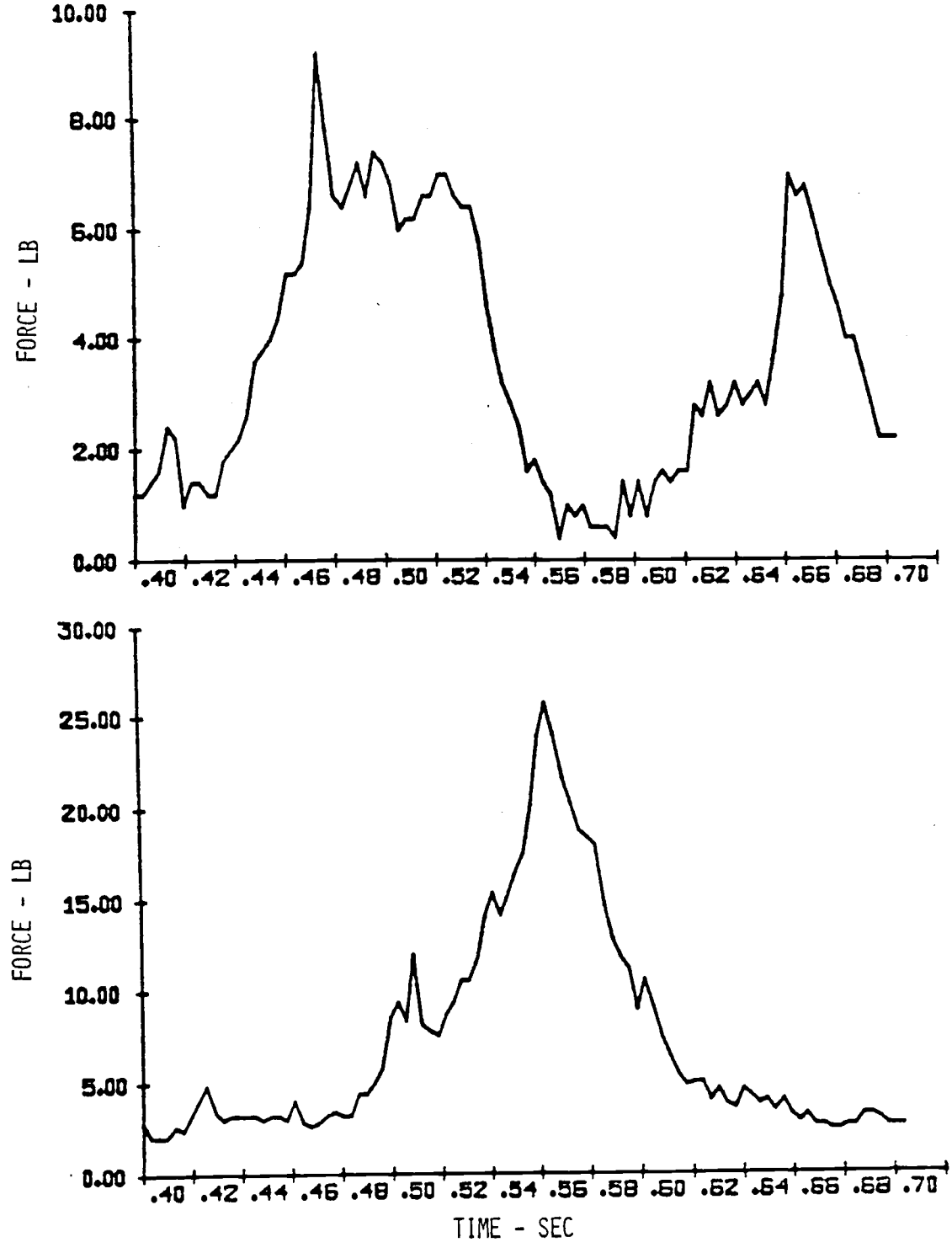


Figure 14. The vertical load on two consecutive tubes.

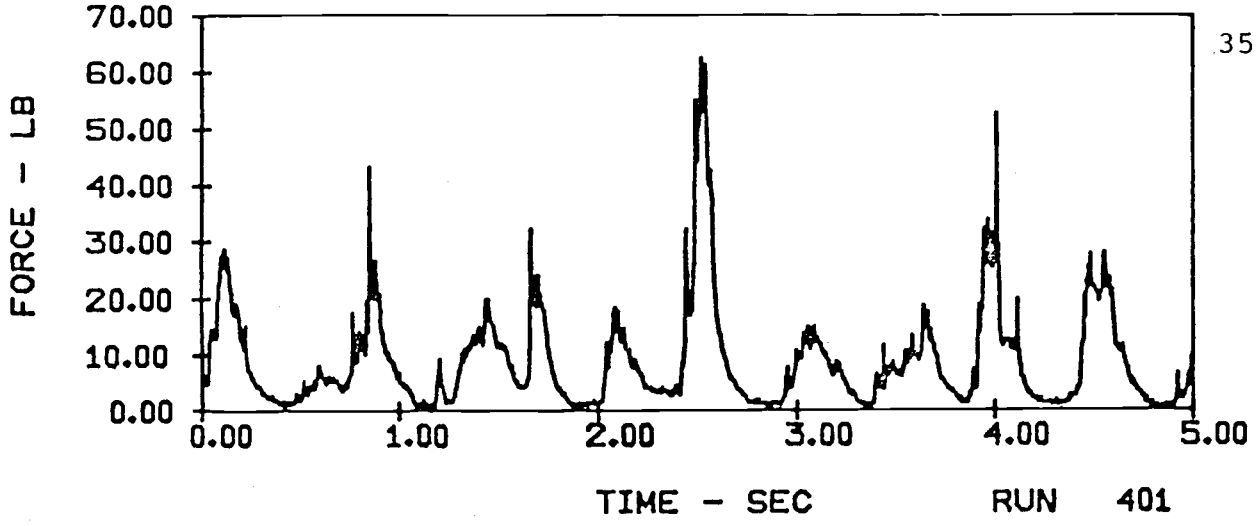


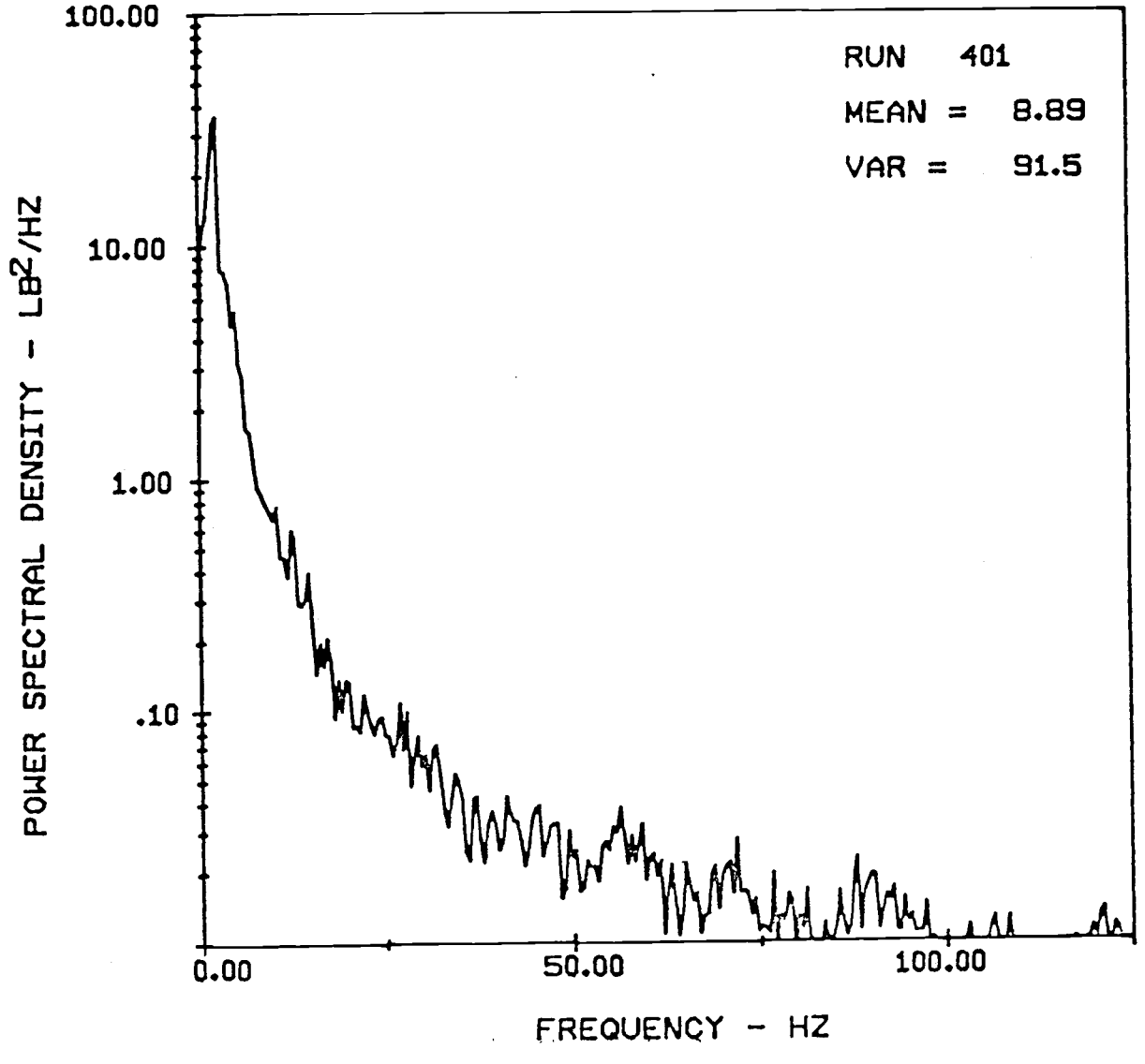


Figure 15. Vertical forces on a single tube (v = 9 ft/sec) in EI 16 sand with 20" array height and 4" tube spacing.

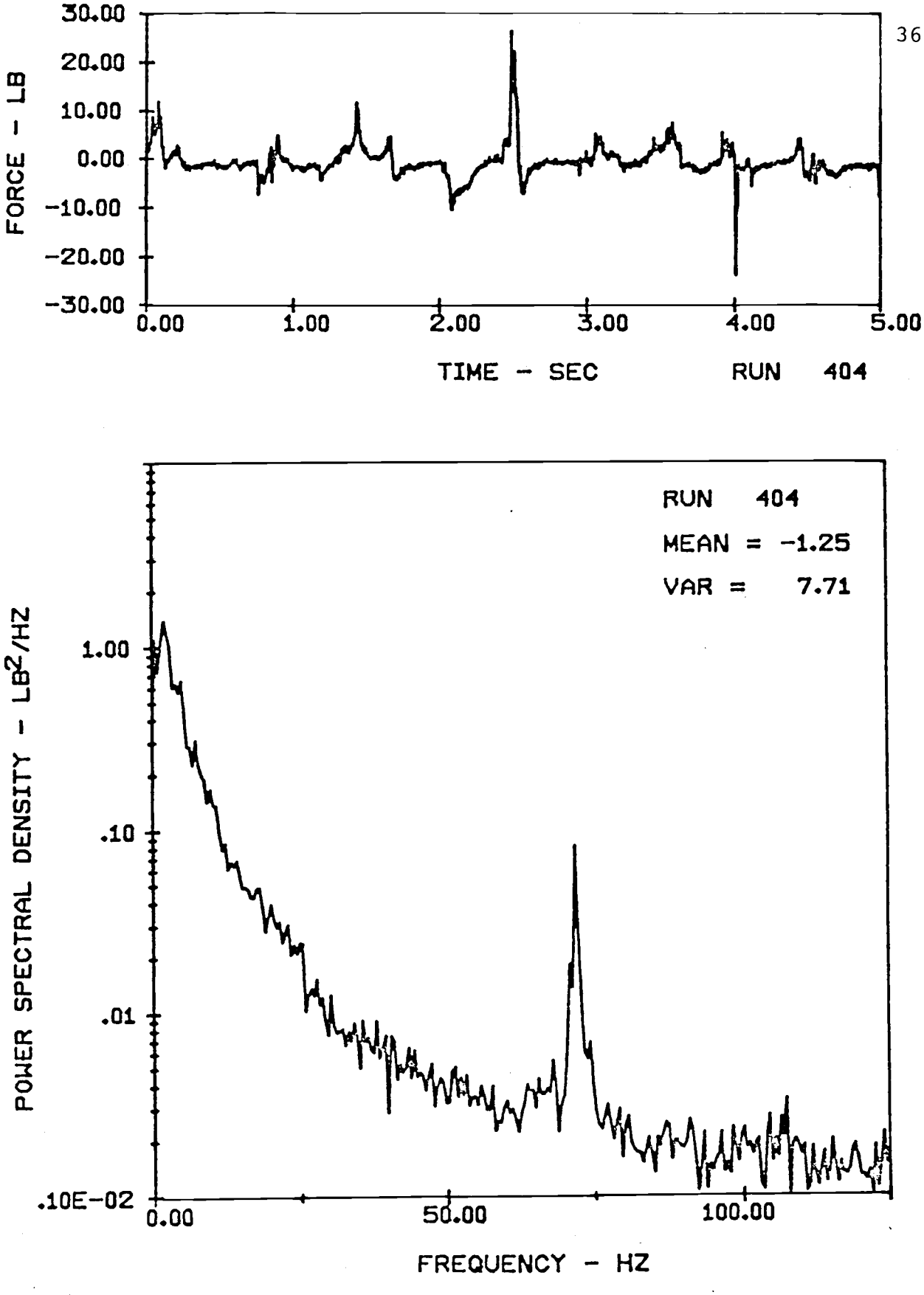


Figure 16. Horizontal forces on a single tube (v - 9 ft/sec) in EI 16 sand with 20" array height and 4" tube spacing

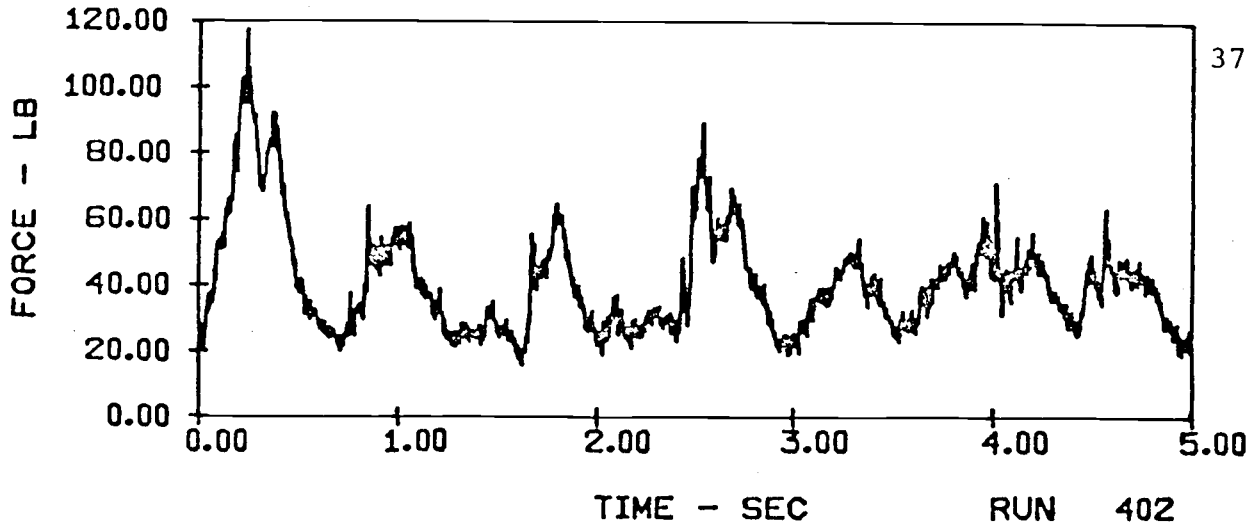


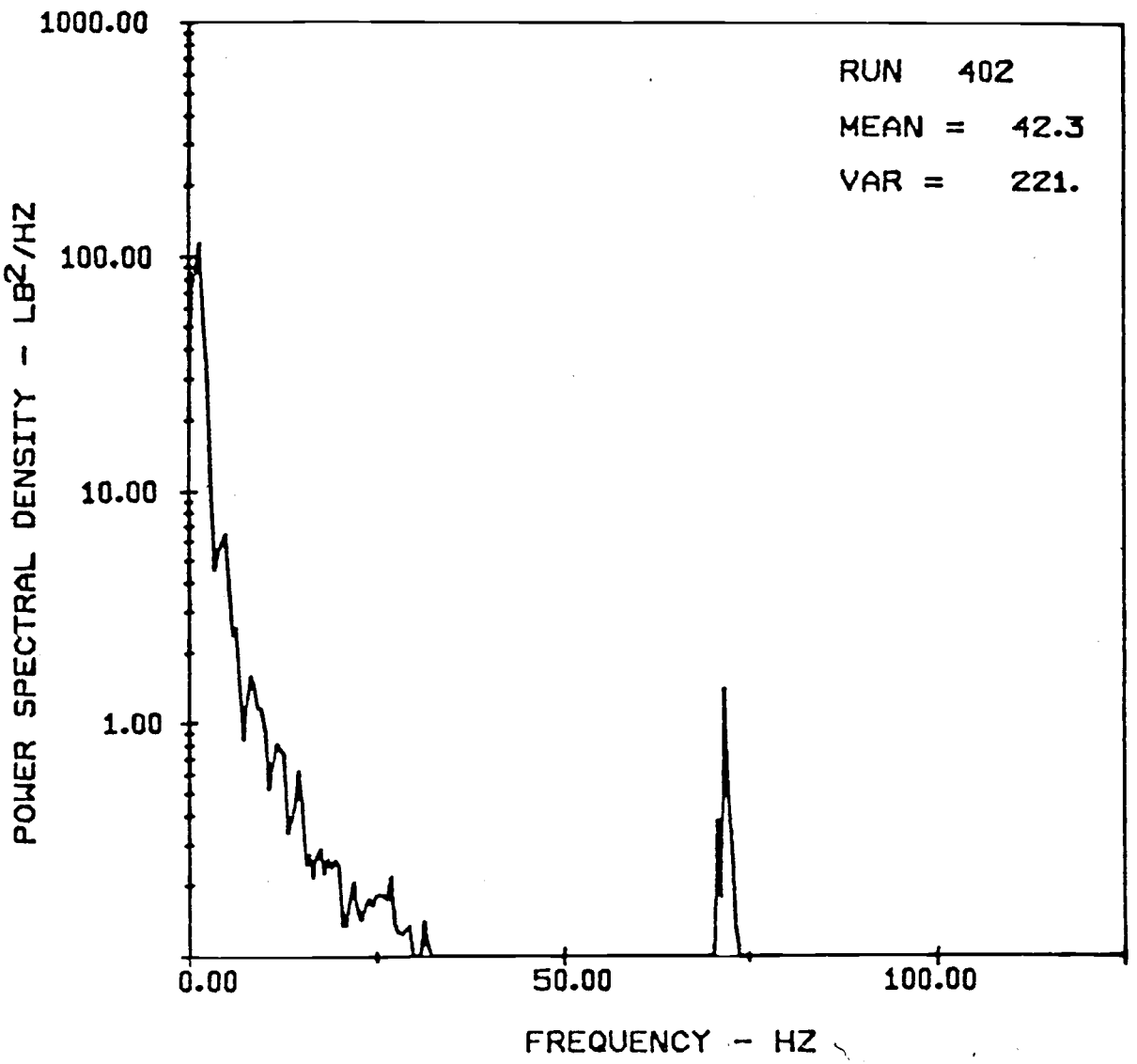


Figure 17. Vertical forces on a 10-tube array (v = 9 ft/sec) in EI 16 sand with 20" array height and 4" tube spacing.

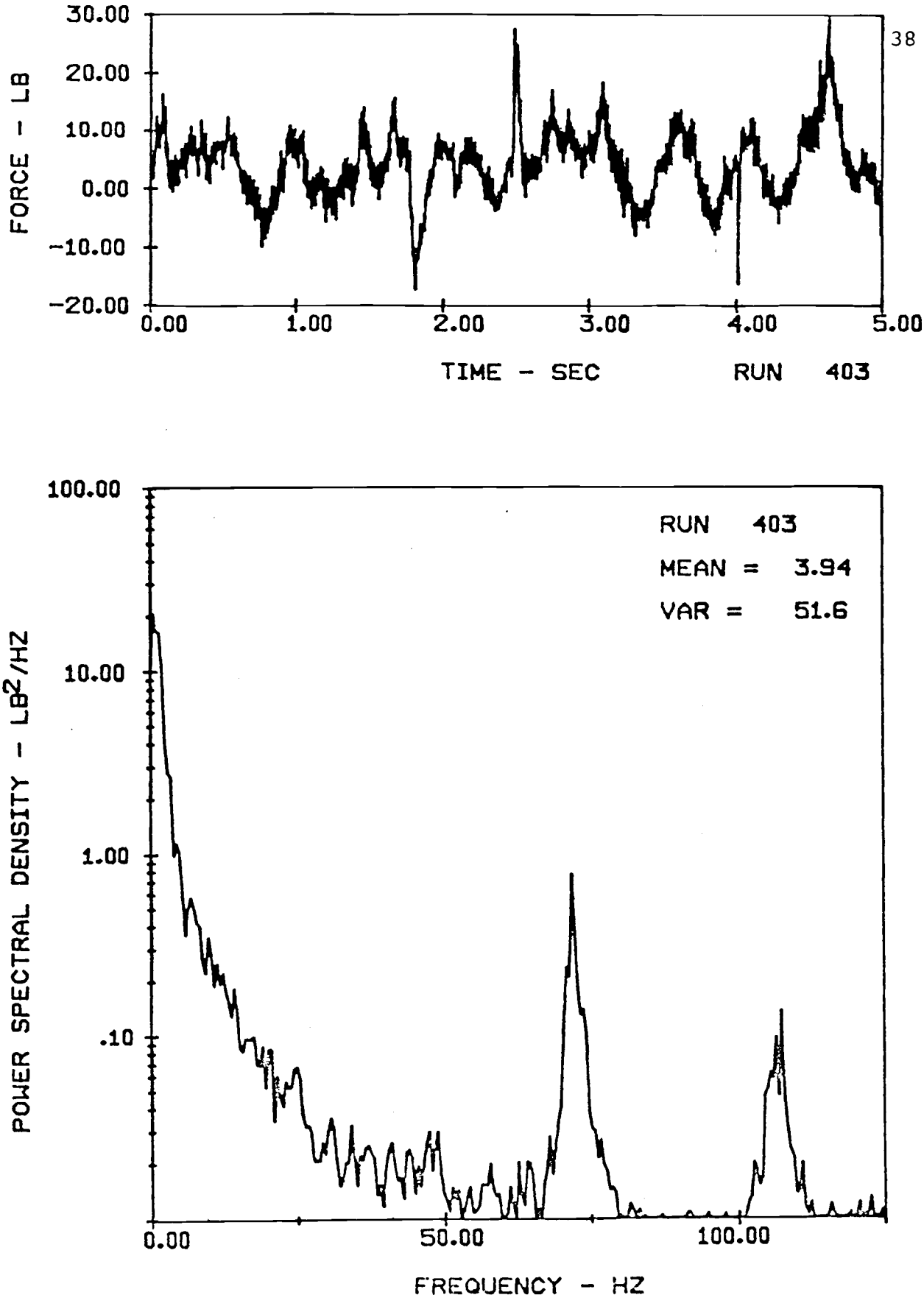


Figure 18. Horizontal forces on a 10-tube array (v = 9 ft/sec) in EI 16 sand with 20" array height and 4" tube spacing.

of this peak is a function of the number of lobes in the blower and the rotation rate the blower is driven at. The force-time history plot in Figure 16 indicates that the loading in the horizontal direction occurred in both directions and that the peak loads more or less alternated back and forth. The magnitude of these peak loads in the horizontal direction is noticeably smaller than the magnitude of the peak loads in the vertical direction.

In Figures 17 and 18 are the plots for the total load on the entire instrumented column for both vertical and horizontal directions. For this combination of parameters, the minimum total vertical load is always higher than 20 lbs (90 N) as seen in Figure 17. The peak total vertical loads occur at intervals of about three-quarters of a second and reached nearly 120 lbs (530 N) during the sampling period shown. The peak frequency in both the vertical and horizontal directions for the total load on the instrumented column was around 1 Hz. A second peak is noticed for both the total vertical load and the total horizontal load at around 70 Hz which is due to the frequency of pulses from the blower similar to the case of the horizontal load on a single tube. These peaks were typical for all of the cases where the total load was considered in either the vertical or horizontal direction. All four of the power spectral density plots in Figures 15 - 18 showed that the major frequency component of force occurs between 0 and 25 Hz with the power spectral

density at 25 Hz down by a factor of between 100 and 1000 from that of the peak power spectral density. Similar plots for different values of the parameters are given in Appendix C.

Figures 19 - 23 show how the statistical data varies with changes in the superficial air velocity. In all of the cases, both the mean and the standard deviation dropped off when the superficial air velocity was raised from 9 ft/sec to 11 ft/sec. Most of the plots indicate that the 20" array height was the most severe, both in terms of magnitude of mean force and standard deviation. However, when the total load in the vertical direction was considered, as in Figure 20, the mean total vertical load at the 20" array height was slightly lower than the mean total vertical load at the 10" array height. All five of these plots also show a tendency of the tests with EI 16 and EI 8 sands to be paired up. In most of the cases, the difference between the curves with EI 16 sand and EI 8 sand is negligible and the rest of the time the difference is still small when compared to the difference in loads at different array heights. The mean vertical force, Figures 19 and 20, generally increased slightly as the air velocity was increased, with the peak occurring at either 7 ft/sec or 9 ft/sec; then it dropped off sharply as the air velocity was raised to 11 ft/sec. The standard deviation of vertical force, Figures 21 and 22, showed much the same pattern as

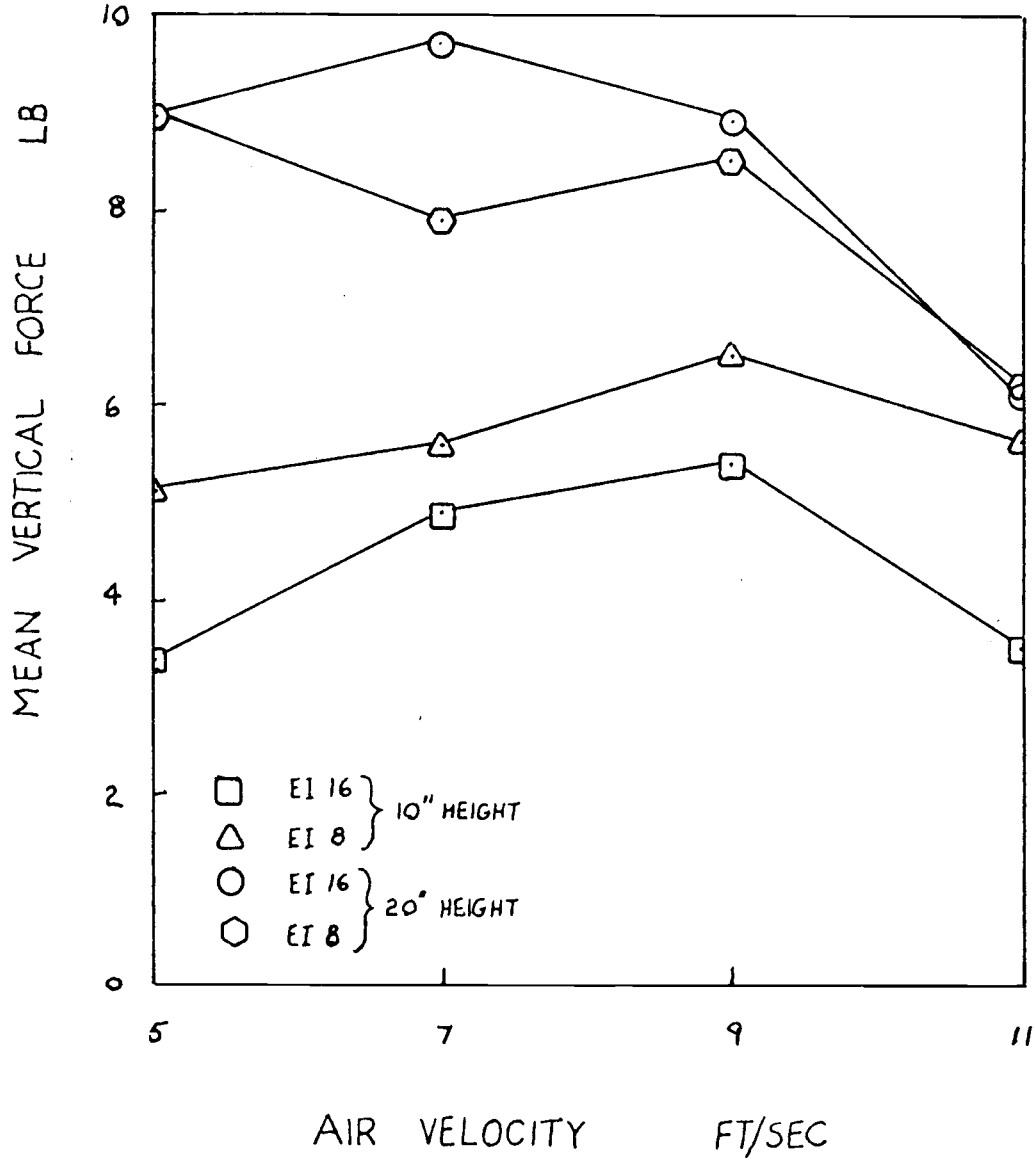


Figure 19. Mean vertical force vs air velocity on a single tube with 4" tube spacing.

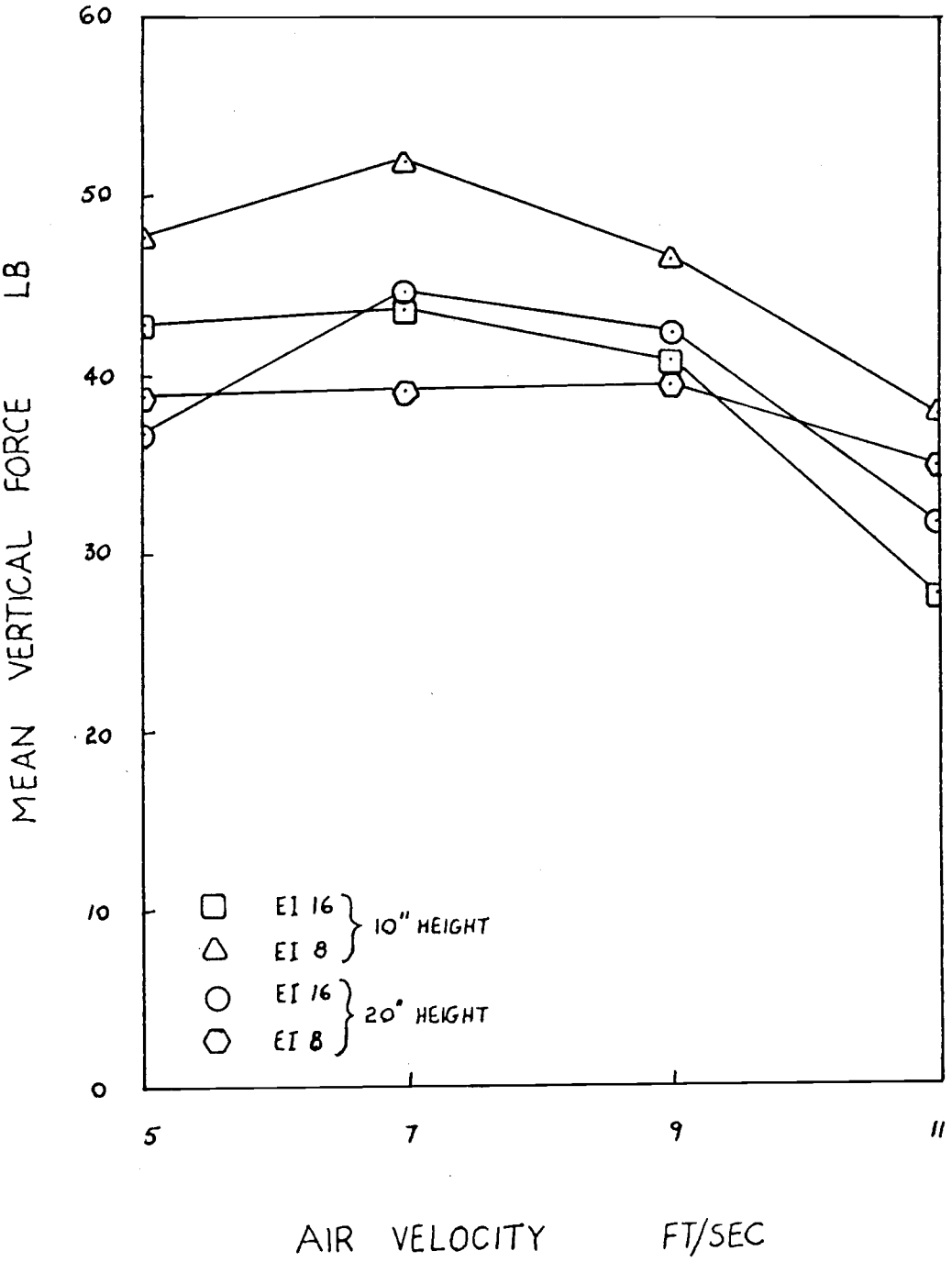


Figure 20. Mean vertical force vs velocity on a 10-tube array with 4" tube spacing.

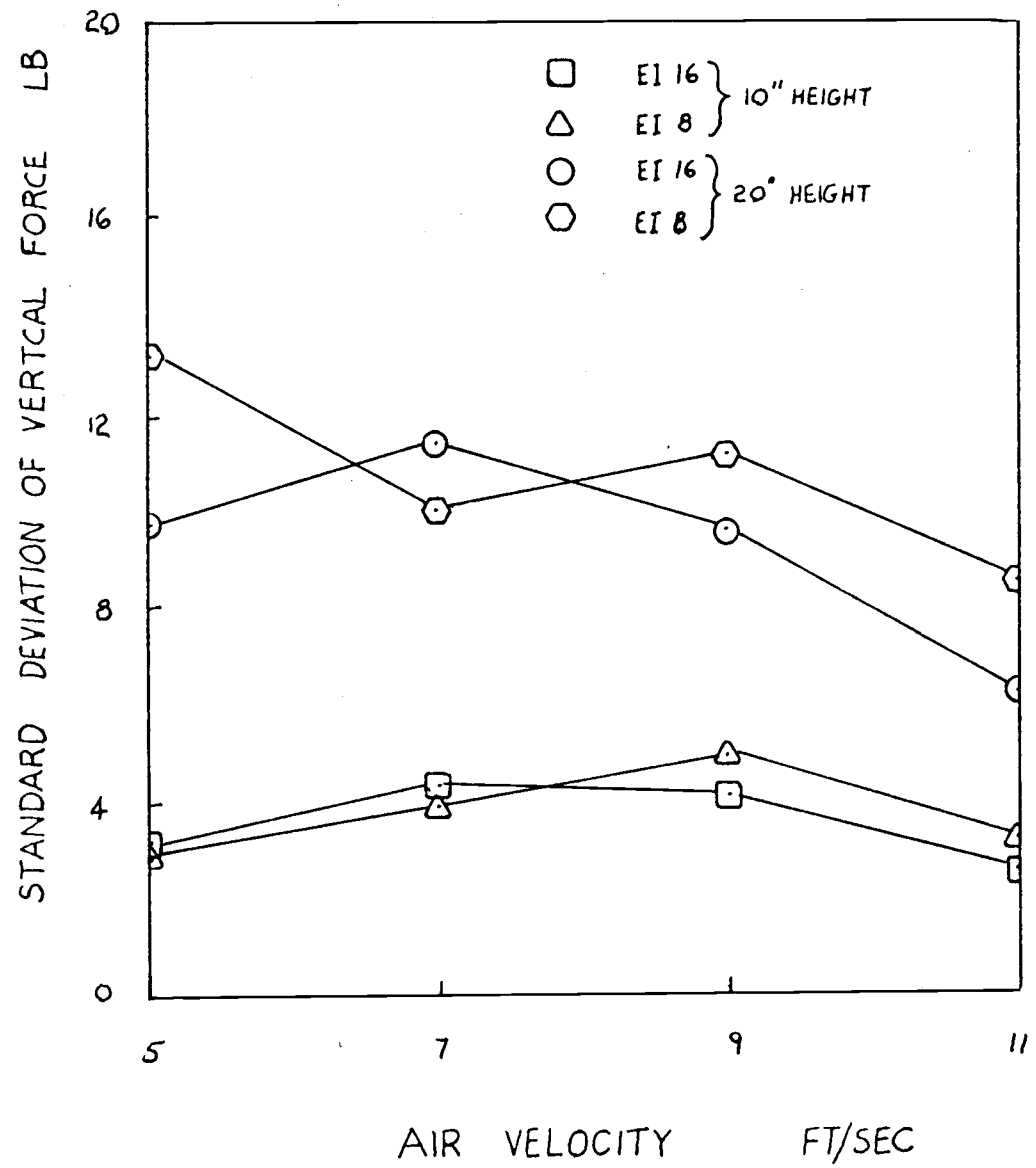


Figure 21. Standard deviation of vertical force vs air velocity on a single tube with 4" tube spacing.

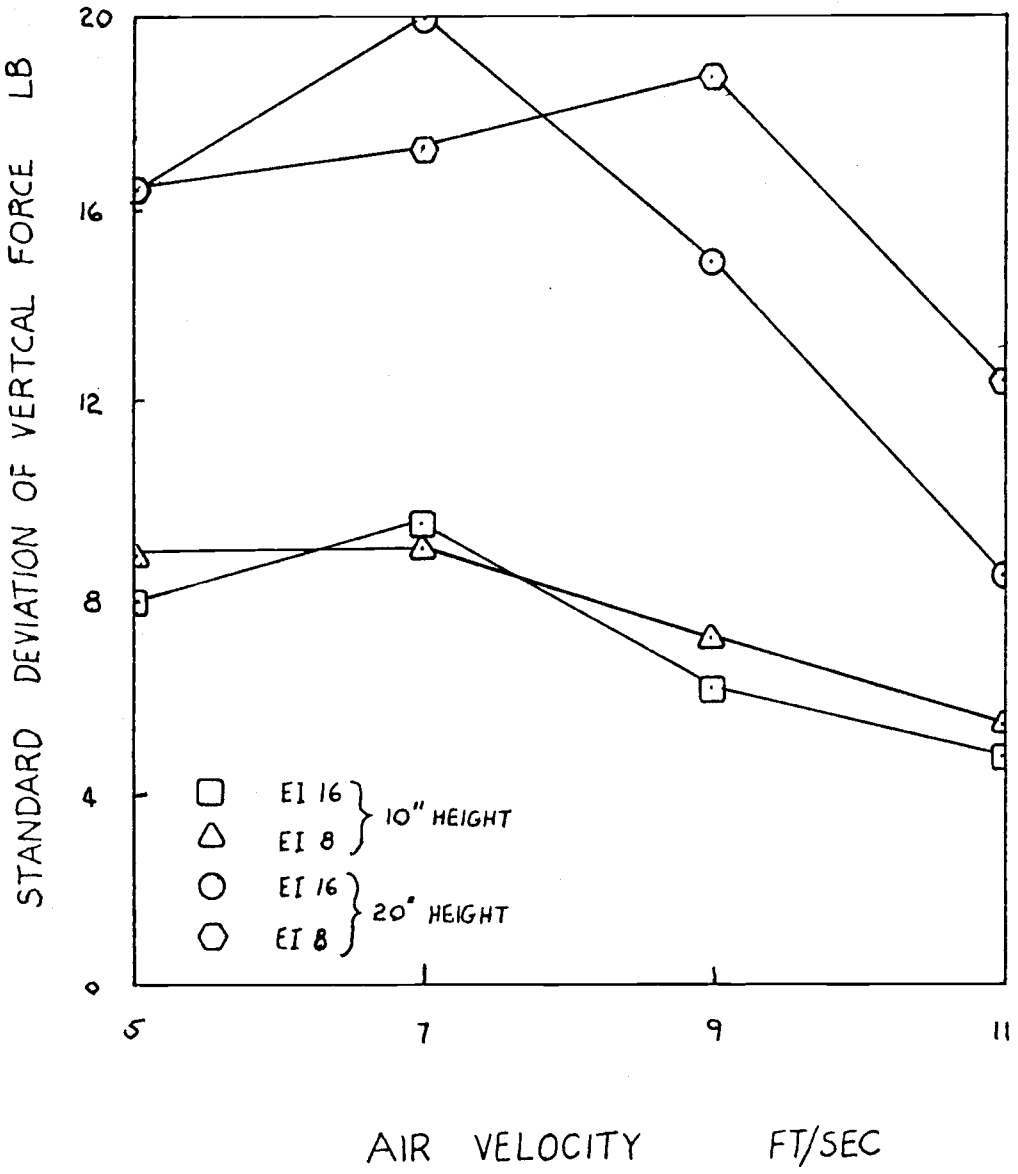


Figure 22. Standard deviation of vertical force vs air velocity on a 10-tube array with 4" tube spacing.

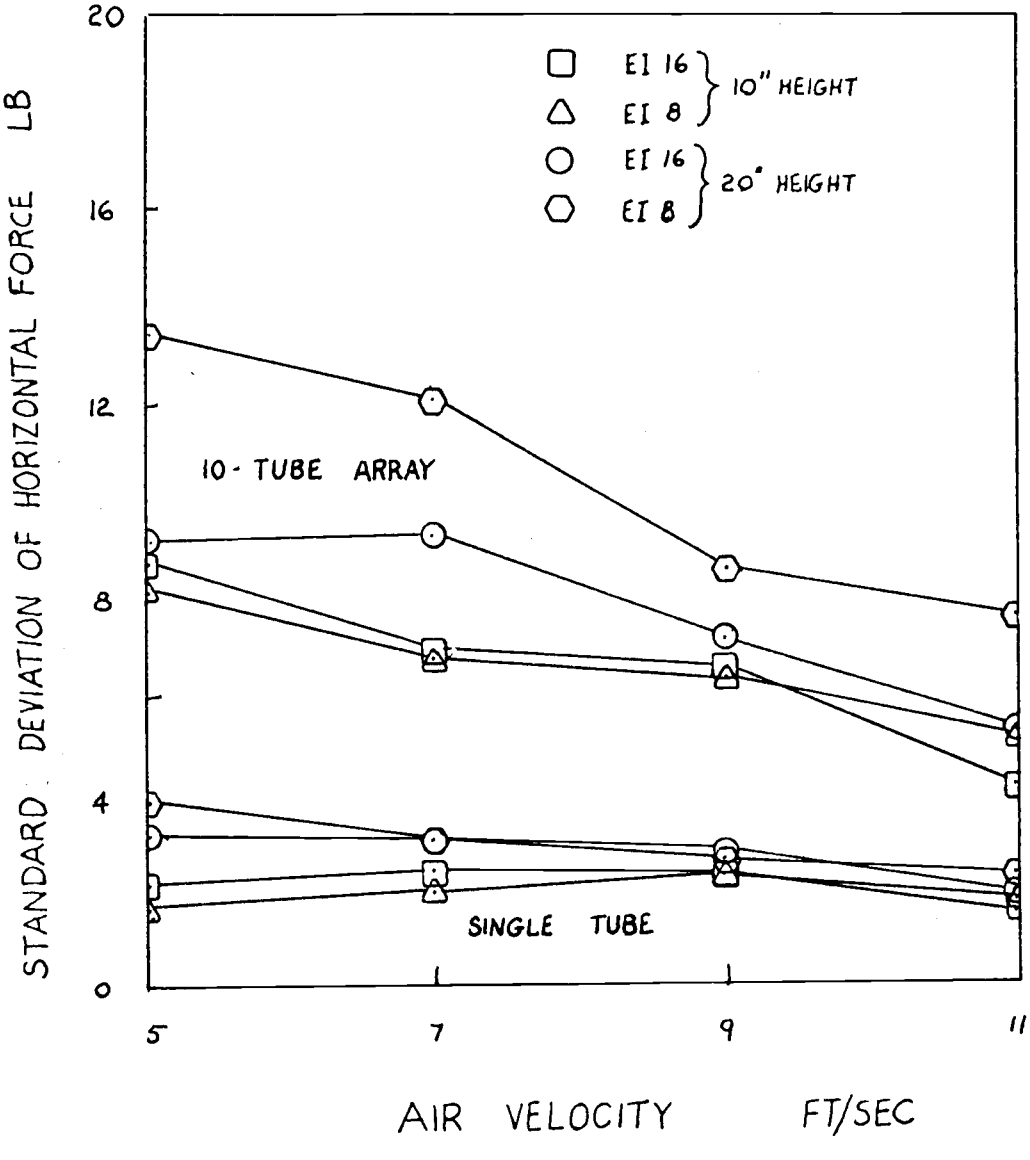


Figure 23. Standard deviation of horizontal force vs air velocity for 4" tube spacing.

the mean vertical force, however the standard deviation of the horizontal force for the 10-tube array, Figure 23, decreased or stayed nearly constant as air velocities were increased from 5 ft/sec to 11 ft/sec. The standard deviation of horizontal force for the single (bottom) tube stayed fairly constant throughout all of the air velocities studied.

## The Array with Six-inch Tube Spacing

Tests on the array with six-inch tube spacing between centers indicated that the most severe loads were not always on the bottom tube. When the array was mounted at the 20" height above the distributor plate, the bottom tube did experience the most severe loading. However when the array was mounted at the lower height, 10", the tubes near the middle of the array experienced the most severe loading. At this height, the magnitude of the forces on the tubes in the middle of the array were double the magnitude of the forces on the tubes at the bottom of the array. The tubes at the top of the array experienced loads varying from near zero at lower velocities to about half as severe as the forces on tubes near the middle of the array at higher velocities. At the 20" array height, forces on tubes near the middle of the array were only slightly less severe than the forces on the bottom tube; and the upper tubes received noticeably less severe loading as the height of the individual tube increased, with the top tube experiencing nearly zero load at all of the studied air velocities.

Typical peak vertical loads on a single tube at the bottom of the array at the 20" array height were in the range of 60 to 80 lbs (270 to 360 N) with an occasional spike over 140 lbs (620 N). At the 10" array height, the peak vertical loads on a single tube near the middle of the array were around 40 to 60 lbs (180 to 270 N). Peak vertical loads on the total instrumented array were observed to be over 200 lbs (890 N) at times. In each case, the magnitude of the horizontal components of the loads was less than half the magnitude of their respective vertical components.

The force-time histories of the vertical and horizontal forces on a single tube in the array with six-inch tube spacing, Figures 24 and 25, are very similar in shape to the force-time histories for the array with four-inch tube spacing. In between peaks, which occur approximately every half second, the force is nearly zero for vertical loading on a single tube. The horizontal forces on a single tube are less than half as severe as vertical forces on the same tube with horizontal peak forces in both directions. The power spectral density curves in Figures 24 and 25 are also very similar in shape to the previous power spectral density curves in Figures 15 and 16; however, the magnitude of these curves is approximately three times greater than the magnitude of the previous curves. The peak power spectral density for the load on a single tube occurs at about 2 to 3 Hz as before.

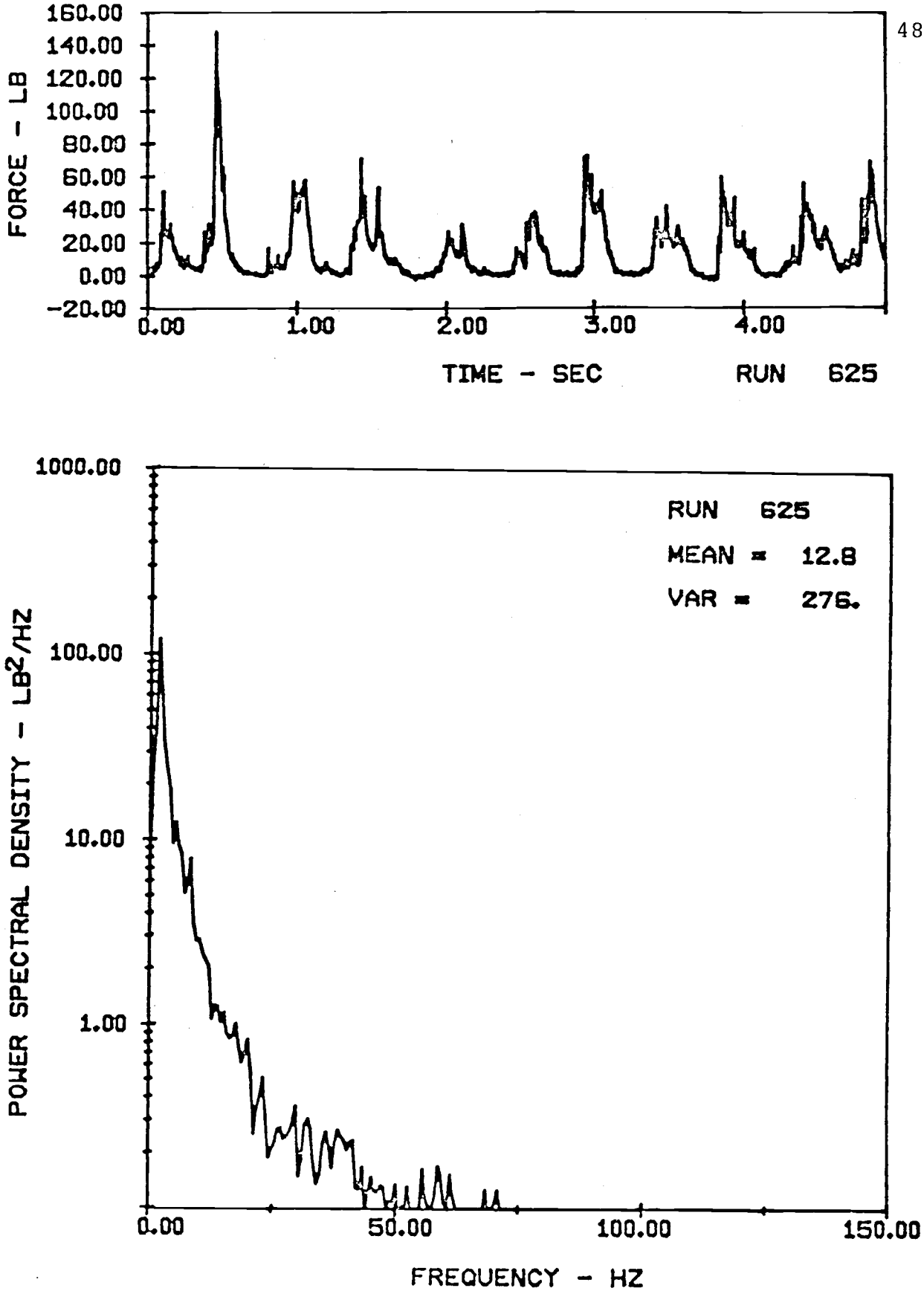


Figure 24. Vertical forces on a single tube (v = 9 ft/sec) in EI 16 sand with 20" array height and 6" tube spacing.

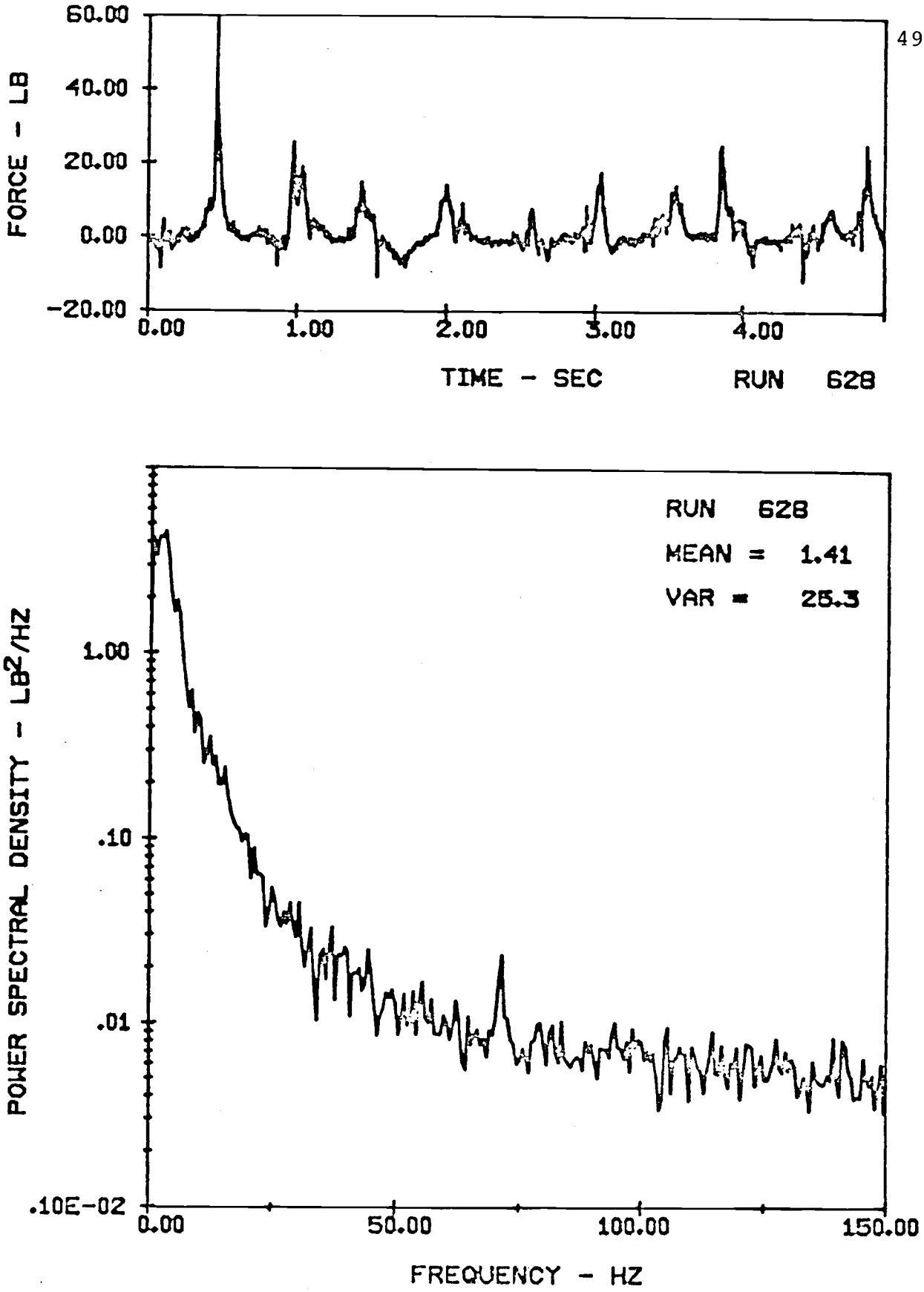


Figure 25. Horizontal forces on a single tube (V = 9 ft/sec) in EI 16 sand with 20" array height and 6" tube spacing.

The force-time histories of the loads on the entire instrumented array with six-inch tube spacing, Figures 26 and 27, are also very similar to the force-time histories of the loads on the entire instrumented array with four-inch tube spacing, Figures 17 and 18. The only noticeable difference between the case with four-inch tube spacing and the case with six-inch tube spacing is the magnitude of the loads on the array. The array with six-inch tube spacing had a magnitude of peak loads up to twice the magnitude of peak loads on the array with four-inch tube spacing.

Except for the magnitude, the power spectral density curves for the load on the entire instrumented array with six-inch tube spacing is very similar to the load on the entire instrumented array with four-inch tube spacing. Both of the power spectral density curves for the vertical and horizontal loads for the eight-tube array with six-inch tube spacing have the major peak near 1 Hz and most of the spectrum below 25 Hz. However, the magnitude of these power spectral density curves are about three to five times larger than the magnitude of the power spectral density curves in Figures 17 and 18. Similar plots for different values of the parameters are given in Appendix C.

In Figures 28 - 30, the statistical data is plotted as a function of air velocity. The mean vertical force, Figure 28, was nearly constant over all of the air velocities

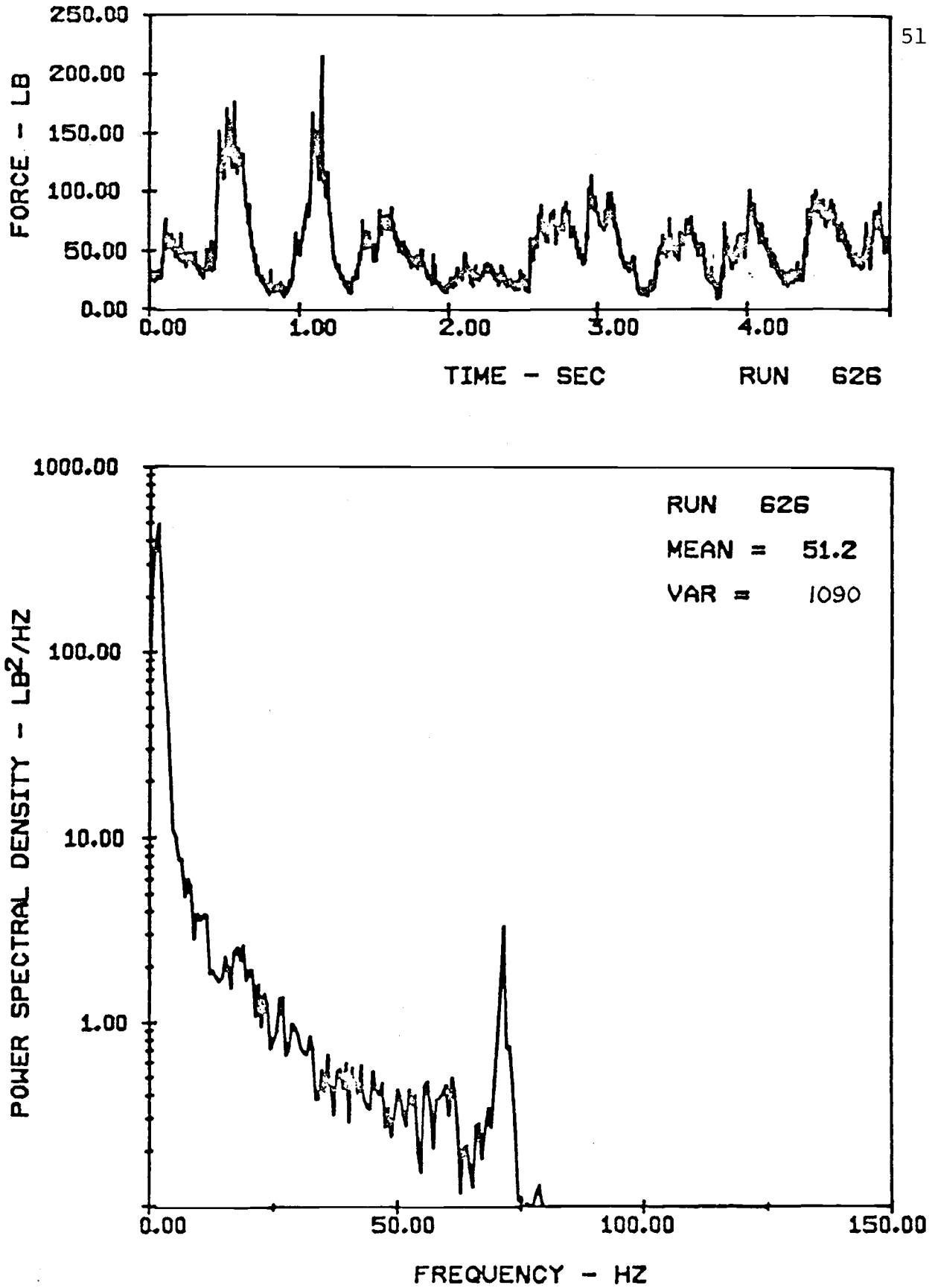


Figure 26. Vertical forces on an 8-tube array (V - 9 ft/sec) in EI 16 sand with 20" array height and 6" tube spacing.

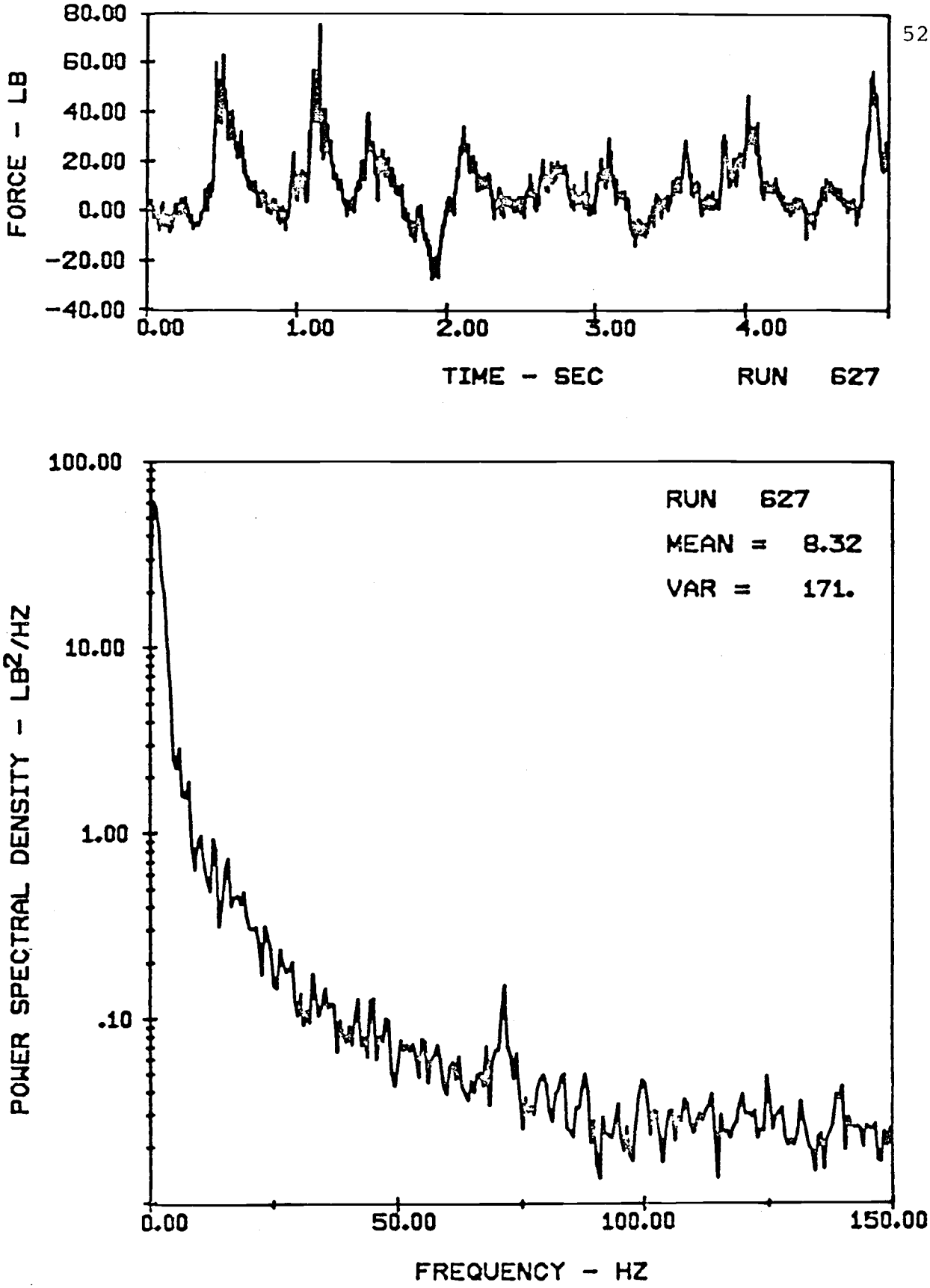


Figure 27. Horizontal forces on an 8-tube array (V = 9 ft/sec) in EI 16 sand with 20" array height and 6" tube spacing.

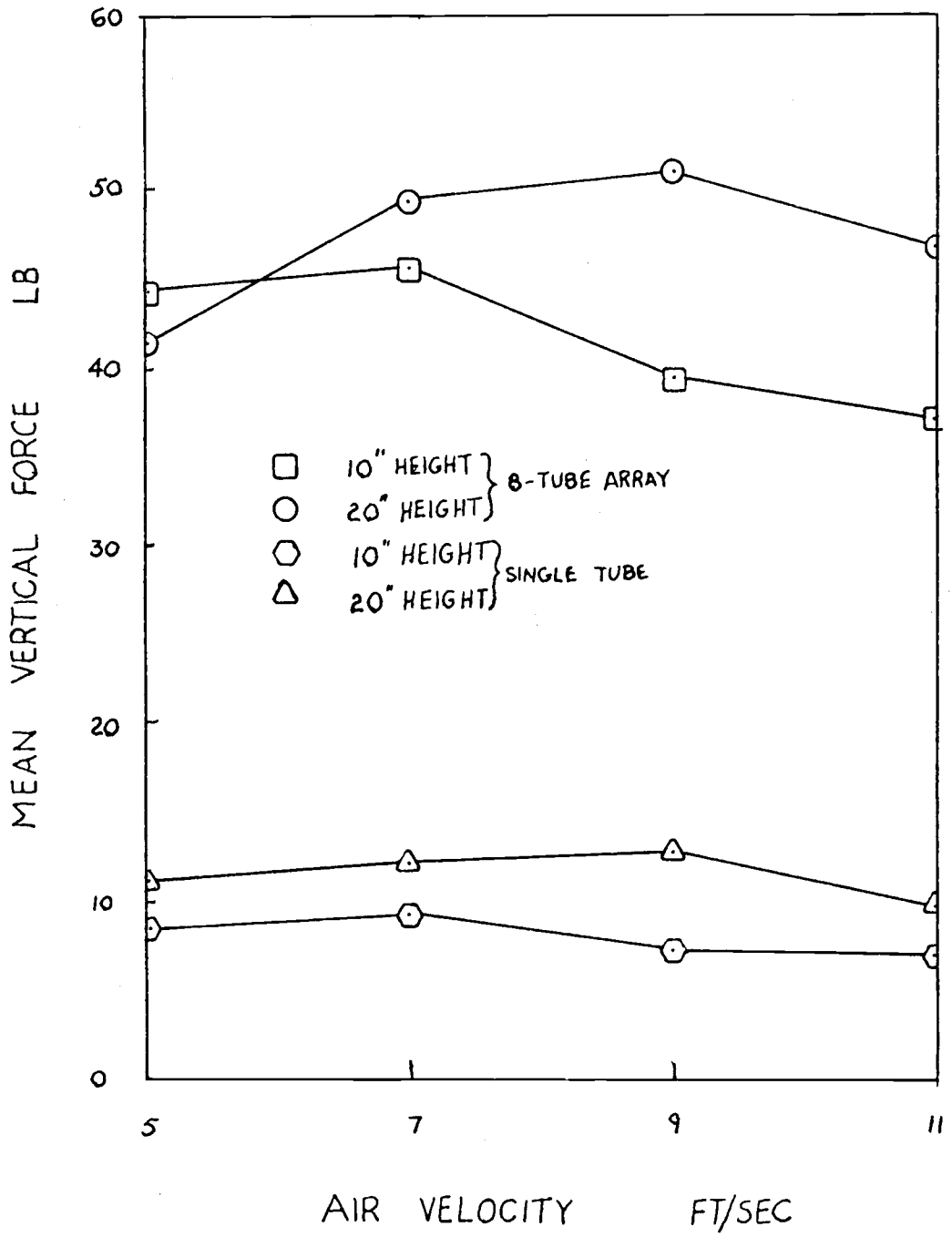


Figure 28. Mean vertical force vs air velocity for 6" tube spacing.

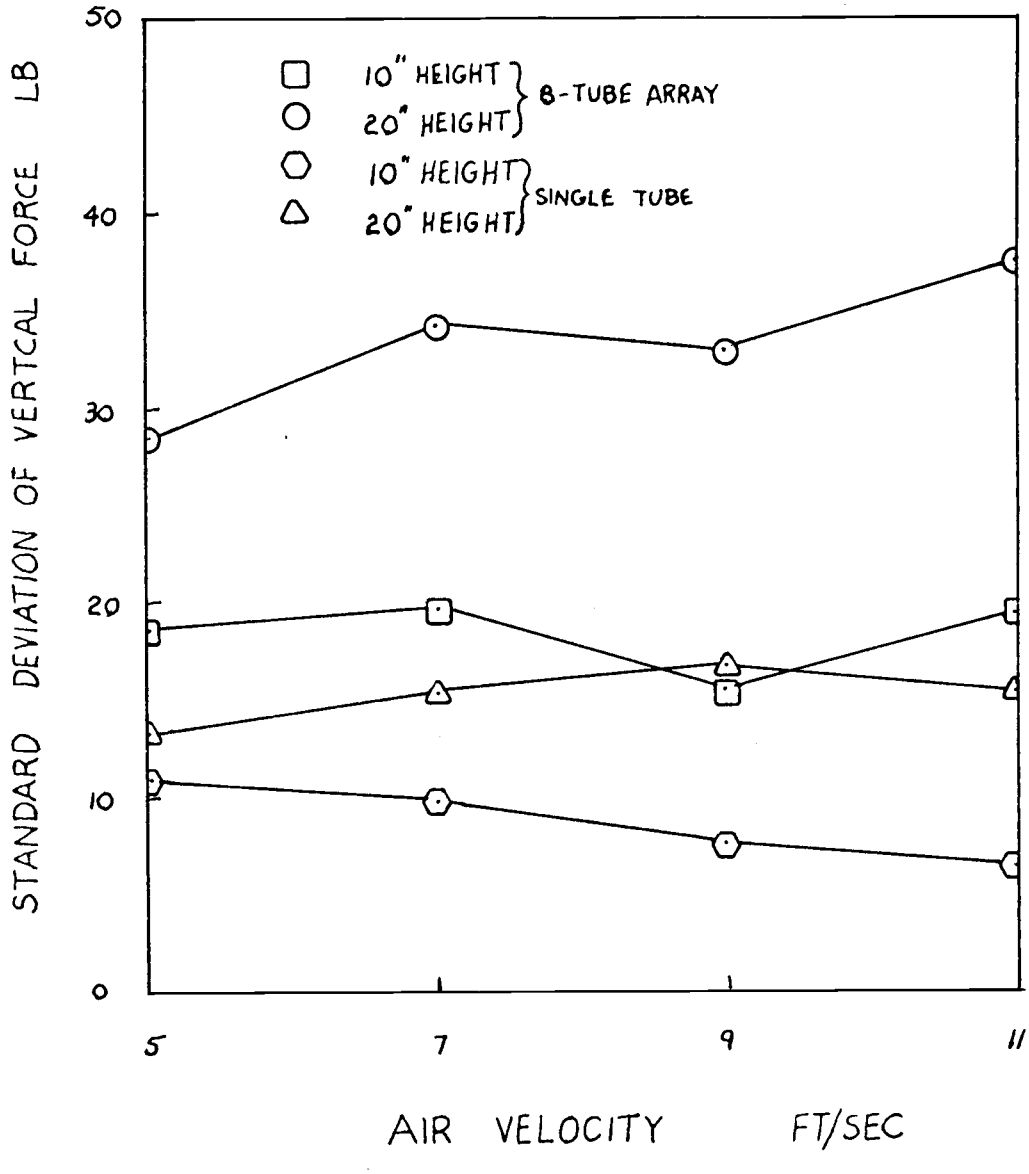


Figure 29. Standard deviation of vertical force vs air velocity for 6" tube spacing.

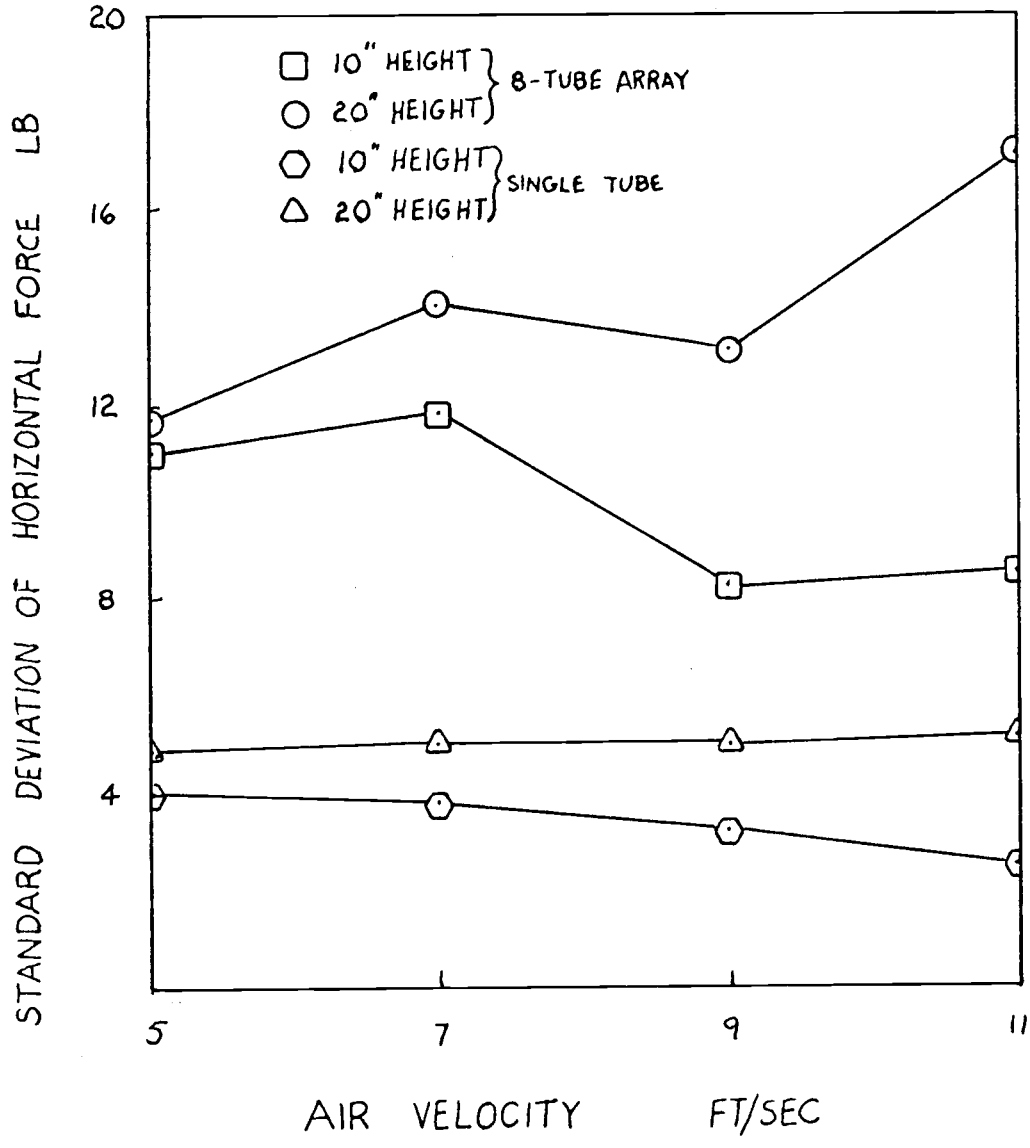


Figure 30. Standard deviation of horizontal force vs air velocity for 6" tube spacing.

studied for a single tube. However, for the eight-tube array, the mean vertical load varied somewhat with changes in air velocity, increasing for air velocities from 5 ft/sec to 7 or 9 ft/sec, then decreasing for air velocities increasing to 11 ft/sec. On the average, the mean vertical load was greater when the array was at the 20" height than at the 10" height. The standard deviation of forces in both the vertical and horizontal directions, Figures 29 and 30, on a single tube was nearly constant over the range of air velocities studied. However, for the eight-tube array it varied slightly with changes in air velocity. In each case for the eight-tube array, the standard deviation, for both vertical and horizonal loads, increased when the air velocity was increased from 5 ft/sec to 7 ft/sec and decreased when the air velocity was raised to 9 ft/sec, but for some unexplained reason increased again when the air velocity was further raised to 11 ft/sec. The standard deviation of force on the array with four-inch tube spacing always decreased when the air velocity was increased from 9 ft/sec to 11 ft/sec; yet for the eight-tube array with six-inch tube spacing, it increased. Both figures 29 and 30 indicate that the 20" array height had forces with higher standard deviations than the 10" array height, given that the other parameters did not change.

# IV. CONCLUSIONS AND RECOMMENDATIONS

## Conclusions

### Comparison of the Two Arrays

Both of the arrays, with four-inch tube spacing and with six-inch tube spacing, exhibited many similar characteristics. The force-time histories were very similar in shape, however the array with six-inch tube spacing experienced slightly higher peak loads than the array with four-inch tube spacing. In both cases the horizontal forces were only one-third to one-half as severe as the vertical forces. The power spectral density curves also showed very similar characteristics with the peak around 1 to 3 Hz and the magnitude of the power spectral density down by a factor of between 100 and 1000 from the peak power spectral density at the frequency of 25 Hz. Generally, the magnitude of the curve was the only noticeable difference between the power spectral density curves.

The major difference between the two arrays is in how the load is distributed through the array. The array with four-inch tube spacing received the most severe loading on the bottom tube while the array with six-inch tube spacing experienced a more even distribution of loads among the tubes located in the lower half of the array, with the most severe loads occuring on tubes in the middle of the array for the 10" array height and on the bottom tube for the

20" array height. Lockwood [5] observed gas by-passing for close spacing of tubes with high air velocities, where solid particles were blown out of the tube array section due to high local air velocities caused by the reduced air flow area in the tube array. Unfortunately, visual observation of the solids flow within the tube array was impossible in this test facility. Gas by-passing is a possible explanation for the difference in the distribution of the loads within each array. Gas by-passing would also be a possible explanation of why the array with four-inch tube spacing always experienced less severe loads when the air velocity was increased from 9 ft/sec to 11 ft/sec while the array with six-inch tube spacing experienced more severe loads when the air velocity was increased to 11 ft/sec.

Summary

The following observations have been made concerning forces on tubes immersed in a fluidized bed.

1. Peak vertical loads can be in excess of 140 lbs (620 N) on a single tube and in excess of 200 lbs (890 N) on an eight-tube array with six-inch tube spacing.
2. The magnitude of horizontal loads are less than half the magnitude of the vertical loads.
3. The loading is least severe on the tubes near the top of the array.

4. The loading was most severe on the tube at the bottom of the array, except when the array with six-inch tube spacing was mounted at the 10" array height, which showed the most severe loads on the tubes near the middle of the array.
5. The frequency composition of the loads is primarily in the 0 to 25 Hz range with the peak in the 1 to 3 Hz range.
6. The severity of load decreased as the air velocity was increased when the array with four-inch tube spacing was tested, while the severity of load on the array with six-inch tube spacing did not change appreciably when the air velocity was increased, until the air velocity was increased from 9 ft/sec to 11 ft/sec in which case the severity of the load on the entire instrumented array increased.
7. The severity of the load is higher when the tube array is 20" above the distributor plate than when it is 10" above the distributor plate.
8. The severity of loads on a single tube as well as the loads on the total instrumented array is higher in the array with six-inch tube spacing than the array with four-inch tube spacing.
9. The loads propagate up through the array at a rate of 2 to 5 ft/sec (0.6 to 1.5 m/s).
10. The difference in severity of loads in a bed with EI 16 sand and EI 8 sand is small.

## Recommendations

Research concerning the forces on heat exchange tubes immersed within a fluidized bed is only begun with this project. Limitations due to the equipment used and the time allotted only allowed us to study a few of the parameters related to the forces on immersed tubes. Some of the following unanswered questions could be possible topics of further study in this field.

1. Would varying the amount of bed material make a difference in the forces on the immersed tubes? This study only used 2000 lbs (900 kgs) of nearly one size of sand in all of the performed tests.
2. Was gas by-passing the reason for the difference in how the forces were distributed in each of the two arrays? Perhaps there is a critical spacing between the tubes which would allow the loads to be the most evenly distributed among the tubes. This critical spacing might be a function of the other parameters such as air velocity or the distance between the distributor plate and the array of tubes.
3. Would changing the particle size by more than the difference in size between EI 16 and EI 8 sands make a difference in the forces on the immersed tubes?
4. Will the results apply to a larger fluidized bed?

Flow of solids in this study behaved somewhat like a fountain in that the solids flowed up the center of the column and slowly sank down along the edges. Flow in larger facilities may vary from this observed phenomenum.

5. Will the results apply to a hot fluidized bed? Changing the temperature will change the ratio of densities between the air and solids as well as other properties such as viscosity. Perhaps these changes would have a significant effect on the forces on the tubes.

It is evident from looking at these questions that scaled experiments and a dimensional analysis should be considered in further research of this field. The ability to be able to statistically model the forces on the tubes as a function of significant physical parameters would be very helpful in providing a basis for the design of tubes and support systems.

# BIBLIOGRAPHY

1. Crandall, S. H., and Mark, W. D. Random Vibration in Mechanical Systems, Academic Press, New York, 1973, p.p. 112-126.

2. Donlevy, B. T., "Measuring Solids Movement in a Large Particle Fluidized Bed: Two Methods", MS Thesis, Oregon State University, 1977.

3. Fitzgerald, T. J., "Investigation of Fluidized Bed with Immersed Heat Exchange Tubes", Final Report RP 315-1, Oregon State University, p.p. 61-67.

4. Lin, Y. K., Probabilistic Theory of Structural Dynamics, McGraw Hill Book Company, New York, 1967, p.p. 293-338.

5. Lockwood, D. N., "An Investigation of the Effects of Immersed Heat Exchange Tube Spacing and Arrangement on the quality of Fluidization in a Cold Phase Two-Dimensional Fluidized Bed", MS Thesis, Oregon State University. 1976.

6. Loveland, W. D., "Proceedings: Conference on Magnitude and Deployment Schedule of Energy Resources", Oregon State University, 1975.

7. Wirsching, P. H. and Haugen, E. B., "Probabilistic design for Random Fatigue Loads", Journal of the Engineering Mechanics Division, ASCE, Dec., 1973, p.p. 1165-1179.

8. Wirsching, P. H. and Haugen, E. B., "A General Statistical Model for Random Fatigue", Journal of Engineering Materials and Technology, Trans. ASME, Jan., 1974,

9. Wirsching, P. H. and Shehata, A. M., "Fatigue Under Wide Band Random Stresses Using the Rain-Flow Method", Journal of Engineering Materials and Technology. Trans. ASME, July, 1977, p.p. 205-211.

10. Yaverbaum, Lee, Fluidized Bed Combustion of Coal and Waste Materials, Noyes Data Corporation, New Jersey, 1977.

# APPENDICES

# APPENDIX A

## Dynamic Calibration of the Tube-Load Cell System

A tube, identical to the tubes used in the instrumented array, was mounted between two load cells which were in turn mounted rigidly to a shaker table. The shaker table with the tube-load cell system was then harmonically oscillated with constant peak acceleration while sweeping, at a constant rate, through all of the frequencies from 10 to 500 Hz. The amplification factor of the output verses frequency is shown in the figure on the following page.

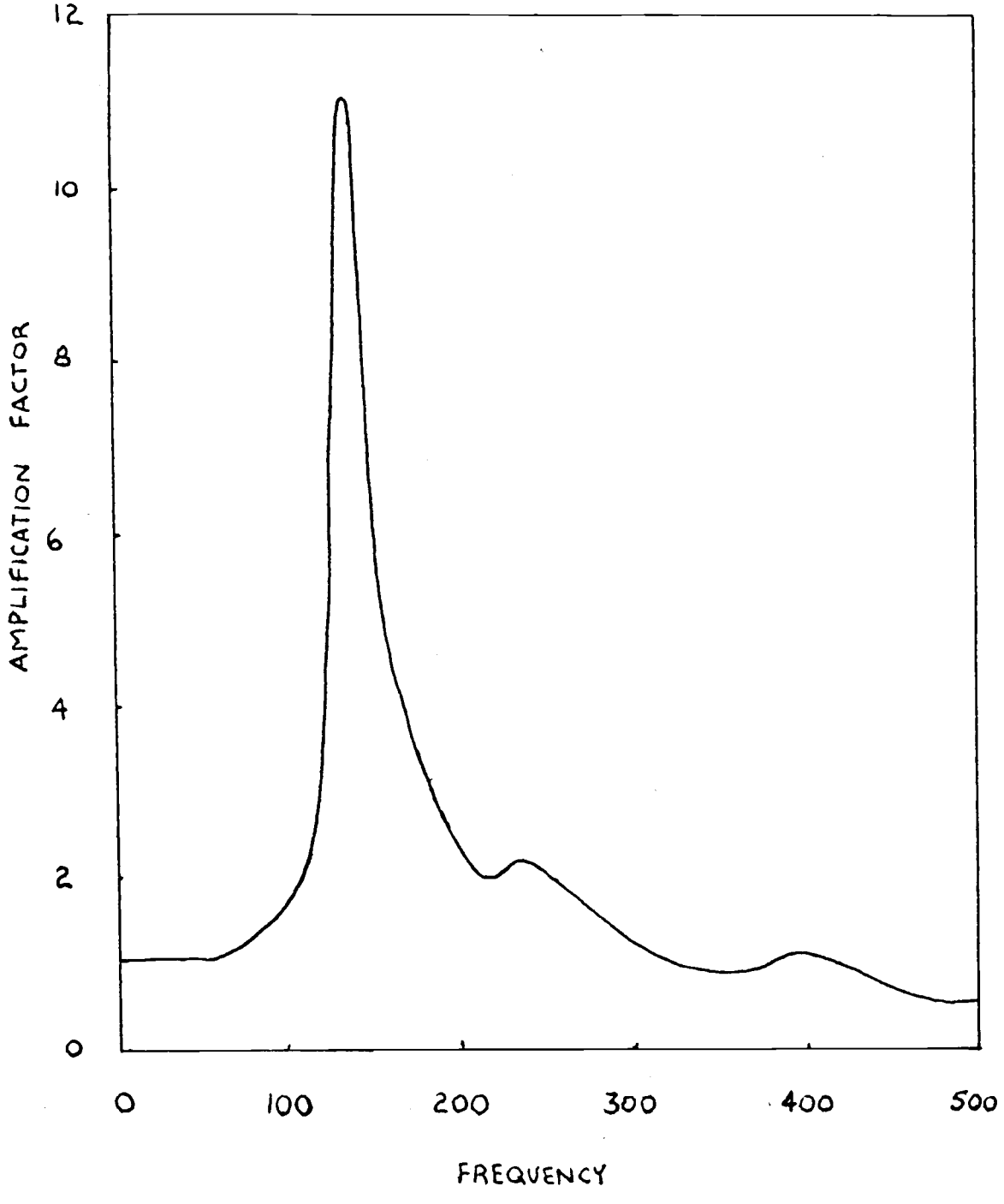
12
10
8
6
4
2
0
AMPLIFICATION FACTOR
0
100
200
300
400
500
FREQUENCY

APPENDIX A

# APPENDIX B

## Computer Parameters

The data was collected by the use of a high speed data acquisition program on the Nova minicomputer, and was analyzed on the Cyber computer with the use of a fast fourier transform subroutine (FTFFT1) in the IMSL library which is accessible from a fortran program. The documentation for FTFFT1 is on the following pages and the parameters used in it are listed below. The output is an array of power spectral densities, PSX(I), at the frequencies, F(I), found by the equation: $F(I) = \frac{I-1}{L\,\Delta t}$ where $I = 1, 2, \ldots, (\frac{L}{2} + 1)$

| Parameter | Description | 4" Tube Spacing | 6" Tube Spacing |
|---|---|---|---|
| | Number of instrumented tubes | 10 | 8 |
| | Number of data channels | 40 | 32 |
| | Number of Samples/sec per channel | 247 | 310 |
| $\Delta t$ | Time interval (sec) | 0.00405 | 0.00323 |
| N | Total samples per channel | 8192 | 8192 |
| L | Segment Length | 512 | 512 |

```
      SUBROUTINE FTFFT1 (X,Y,N,L,IND,PSX,PSY,XPS,IWK,WK,IER)              FTFF0010
C                                                                         FTFF0020
C-FTFFT1--------S-------LIBRARY 3-----------------------------------------FTFF0030
C                                                                         FTFF0040
C   FUNCTION              - FAST FOURIER TRANSFORM ESTIMATES OF POWER      FTFF0050
C                             SPECTRA AND CROSS-SPECTRA OF TIME SERIES.   FTFF0060
C   USAGE                 - CALL FTFFT1 (X,Y,N,L,IND,PSX,PSY,XPS,IWK,WK,  FTFF0070
C                             IER)                                        FTFF0080
C   PARAMETERS   X        - INPUT VECTOR OF LENGTH N CONTAINING THE FIRST FTFF0090
C                             TIME SERIES.  SEE PROGRAMMING NOTES.        FTFF0100
C                Y        - INPUT VECTOR OF LENGTH N CONTAINING THE       FTFF0110
C                             SECOND TIME SERIES.  DEFINED ONLY FOR       FTFF0120
C                             POSITIVE IND.                               FTFF0130
C                N        - INPUT LENGTH OF THE TIME SERIES.  N MUST BE   FTFF0140
C                             DIVISIBLE EVENLY BY L.                      FTFF0150
C                L        - INPUT PARAMETER THAT MUST BE A POWER OF 2,    FTFF0160
C                             USED TO SEGMENT THE TIME SERIES.  SPECTRAL  FTFF0170
C                             COMPUTATIONS ARE AT (L/2)+1 FREQUENCIES.    FTFF0180
C                IND      - INPUT CONTROL PARAMETER.  IND POSITIVE IN-    FTFF0190
C                             DICATES TWO TIME SERIES ARE INPUT AND THAT  FTFF0200
C                             PSX,PSY,AND XPS ARE OUTPUT.  IND NONPOSITIVEFTFF0210
C                             INDICATES ONLY ONE TIME SERIES IS INPUT AND FTFF0220
C                             PSX IS THE OUTPUT.                          FTFF0230
C                PSX      - OUTPUT VECTOR OF LENGTH (L/2)+1 CONTAINING    FTFF0240
C                             THE SPECTRAL ESTIMATES OF X.  SEE PRO-      FTFF0250
C                             GRAMMING NOTES.                             FTFF0260
C                PSY      - OUTPUT VECTOR OF LENGTH (L/2)+1 CONTAINING    FTFF0270
C                             THE SPECTRAL ESTIMATES OF Y, DEFINED FOR    FTFF0280
C                             POSITIVE IND.                               FTFF0290
C                XPS      - OUTPUT VECTOR OF LENGTH L+2, DEFINED FOR IND  FTFF0300
C                             POSITIVE. THE FIRST (L/2)+1 LOCATIONS CON-  FTFF0310
C                             TAIN THE MAGNITUDE OF THE CROSS-SPECTRUM,   FTFF0320
C                             AND THE LAST (L/2)+1 LOCATIONS CONTAIN THE  FTFF0330
C                             PHASE OF THE CROSS-SPECTRUM, GIVEN IN       FTFF0340
C                             FRACTIONS OF A CIRCLE, I.E., ON THE CLOSED  FTFF0350
C                             INTERVAL (0,1).                             FTFF0360
C                IWK      - WORK AREA OF LENGTH LOG BASE 2 OF L.          FTFF0370
C                             I.E., OF LENGTH M IF L = 2**M .             FTFF0380
C                WK       - WORK AREA OF LENGTH L/2.                      FTFF0390
C                IER      - ERROR PARAMETER.  IER=0 IMPLIES NO ERROR.     FTFF0400
C                           TERMINAL ERROR = 128+N.                       FTFF0410
C                             N=1 INDICATES L DOES NOT DIVIDE N EVENLY.   FTFF0420
C   PRECISION             - SINGLE                                        FTFF0430
C   REQD. IMSL ROUTINES   - FERROR2,FFTP,FFTN,FFT2,UERTST                 FTFF0440
C   LANGUAGE              - FORTRAN                                       FTFF0450
C-----------------------------------------------------------------------FTFF0460
```

CALL FTFFT1(X,Y,N,L,IND,PSX,PSY,XPS,IWK,WK,IER)

Purpose

Using fast Fourier transform techniques, spectral estimates are obtained for time series with cross-spectral estimates available. The computational technique is designed for fast computation with large sample sizes.

Algorithm

First a symmetric data window is calculated.

$$W(j) = 1 - \left| \frac{j - \frac{L-1}{2}}{\frac{L+1}{2}} \right| \qquad j = 0,1,\ldots,L-1$$

This is approximately the Parzen spectral window. The data window is applied to each segment of length L of the time series (of total length N). Then IMSL routine FFTR is called to give the fast Fourier transform of that segment, from which spectral estimates may be made for that segment. The estimates for the N/L segments are averaged and scaled.

For the cross-spectral calculations, the cross-spectrum is calculated for each segment and averaged, then the following are calculated:

a. magnitude of cross-spectrum $\equiv$ $|\text{cross-spectrum}|^2$

b. phase of cross-spectrum $\equiv$ argument of cross-spectrum on circle $(0,2\pi)$, scaled down to $(0,1)$.

See references: Welch, Peter D., "The use of fast Fourier transform for the estimation of power spectra: A method based on time averaging over short, modified periodograms", I.E.E.E. Transactions on Audio and Electroacoustics, Vol. AU-15, No. 2, June 1967.

Otnes, Robert K. and Enochson, Loren, Digital Time and Series Analysis. John Wiley & Sons, New York, 1972.

Jenkins, Gwilym M. and Watts, Donald G., Spectral Analysis And Its Applications, Holden-Day, San Francisco, 1969. (used for testing).

Programming Notes

1. The stability of the estimates depends on the averaging process; i.e. the greater the number of segments N/L, the more stable the resulting estimates are. N/L greater than 15 is appropriate. Otherwise, IMSL routine FTFREQ is recommended.
2. L is usually taken to be 16, 32, 64, or 128.
3. Prior to calling FTFFT1, the means of time series X and Y should be removed from their respective series and the resultant series padded with zeros as follows:
   a. Compute the means $\overline{X}$ and $\overline{Y}$ of X and Y, respectively. Center each time series by subtracting $\overline{X}$ and $\overline{Y}$ from each element of X and Y, respectively.
   b. Given L (an integer power of 2), the length of the time series (call it NP) is usually not divisible evenly by L. The centered time series should be padded with zeros on the right to a length N, where N is the first integer greater than or equal to NP that is evenly divisible by L. N may be computed according to the formula

$$N = NP + L - (NP \text{ modulo } L).$$

4. The resulting spectral estimates are taken to be at the following frequencies:

$$f_i = \frac{i-1}{L} \quad , \quad i = 1,2,\ldots,\left(\frac{L}{2}\right)+1$$

   or more generally, $f_i = \frac{i-1}{L\Delta t}$, where $\Delta t$ is the period of sampling of the time series.

6. Input time series X and Y are destroyed on output.

Example

Input: X = (1.4696, -0.085540, 0.50465, 0.24784, 0.95925, -1.4027, 1.3512, 0.75327, 1.4586, 0.24690, -2.2006, -1.0595, -0.73718, -1.5057, 0.0, 0.0)
Y = not defined
N = 16 = (time series of length 14 + 2 padding zeros)
L = 4
IND = 0
IWK(M), where $M \geq \log_2 L=2$
WK(K), where $K \geq \frac{L}{2} = 2$

Output: PSX = (1.0645, 1.8736, 1.4772)

Note: a. The input vector X has zero mean, before 2 padding zeros adjoined.
b. The output spectrum vector is at frequencies 0, 1/4, and 1/2, respectively.

# APPENDIX C

The following pages contain the sets of results for all of the combinations of parameters tested during the course of this research. Each page contains a short force-time history of the load on a tube or array of tubes as well as the mean and variance of the complete force-time history and a power spectral density verses frequency curve.

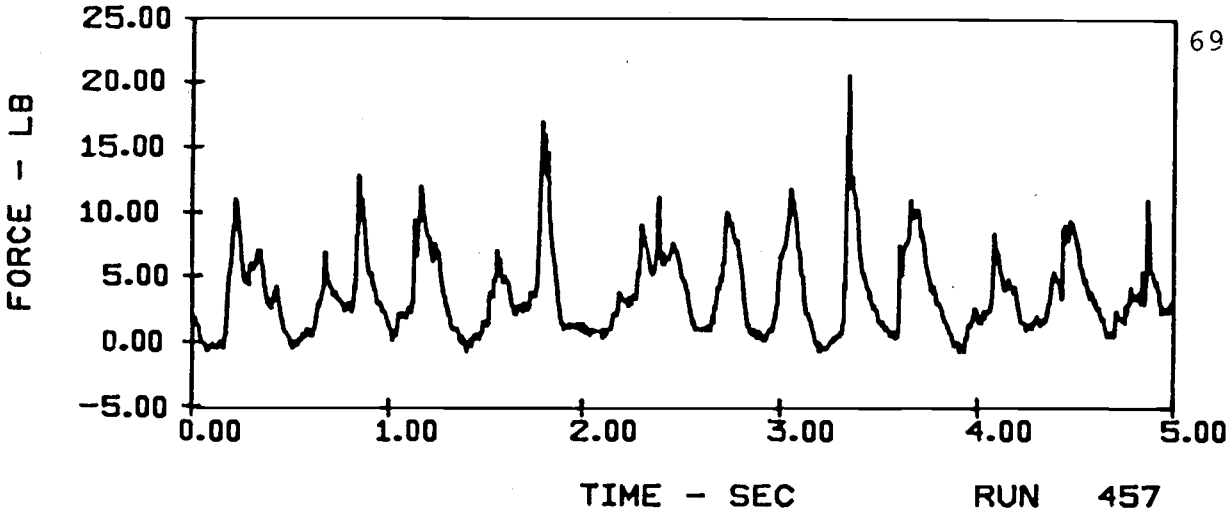


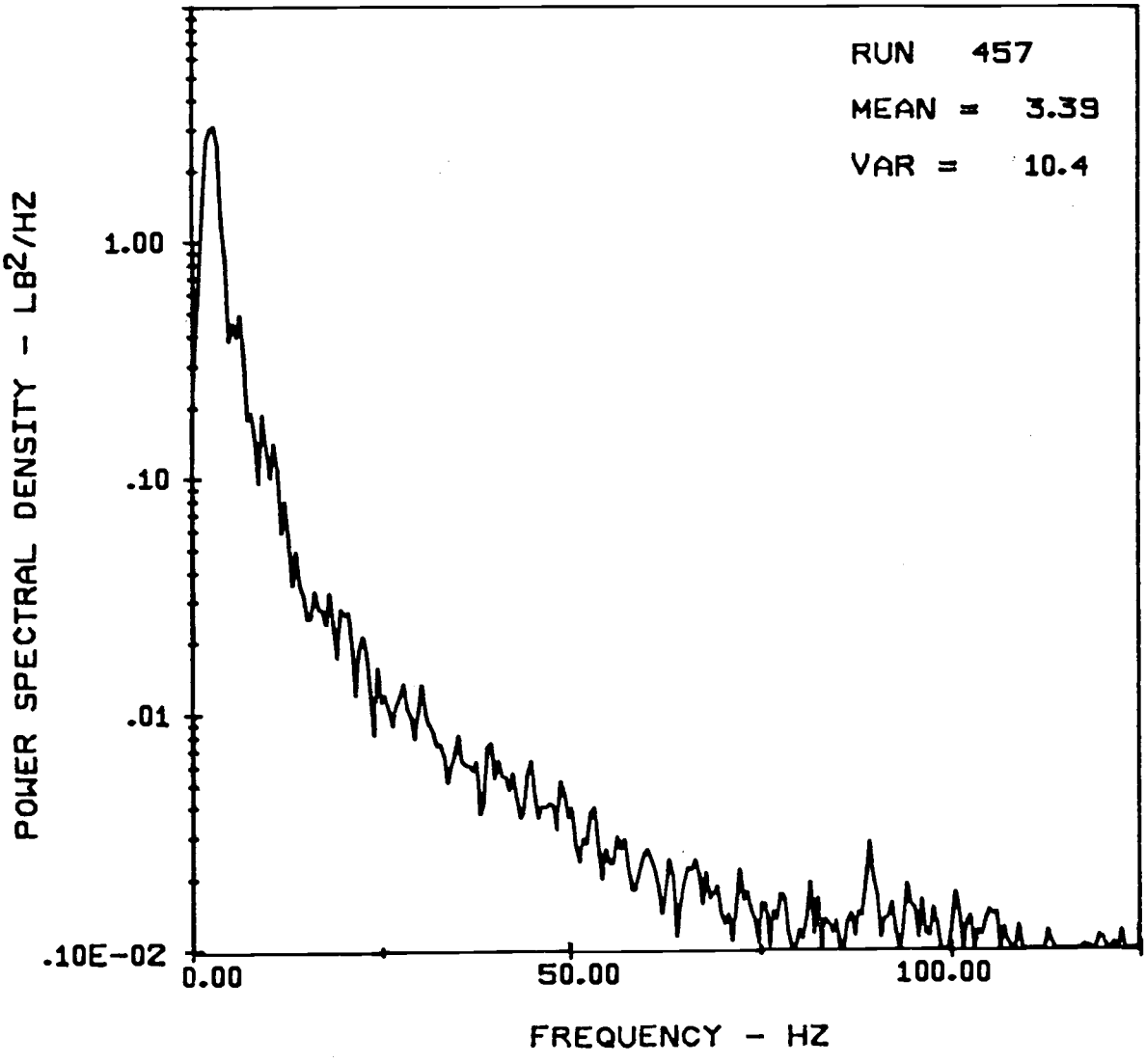


VERTICAL FORCES ON A SINGLE TUBE (V = 5 ft/sec)
IN E116 SAND WITH 10" ARRAY HEIGHT AND 4" TUBE SPACING

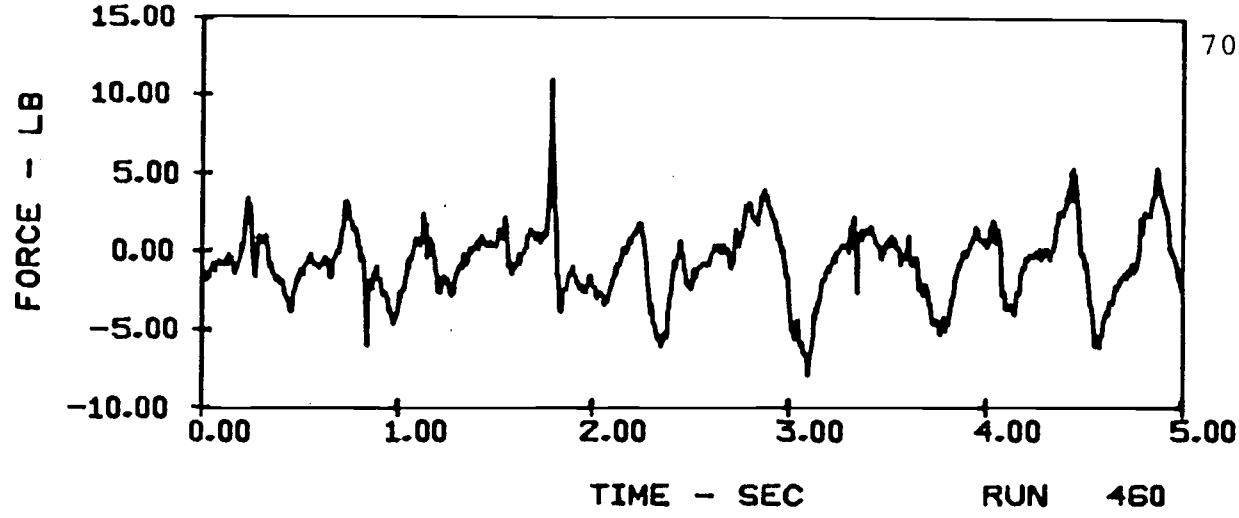


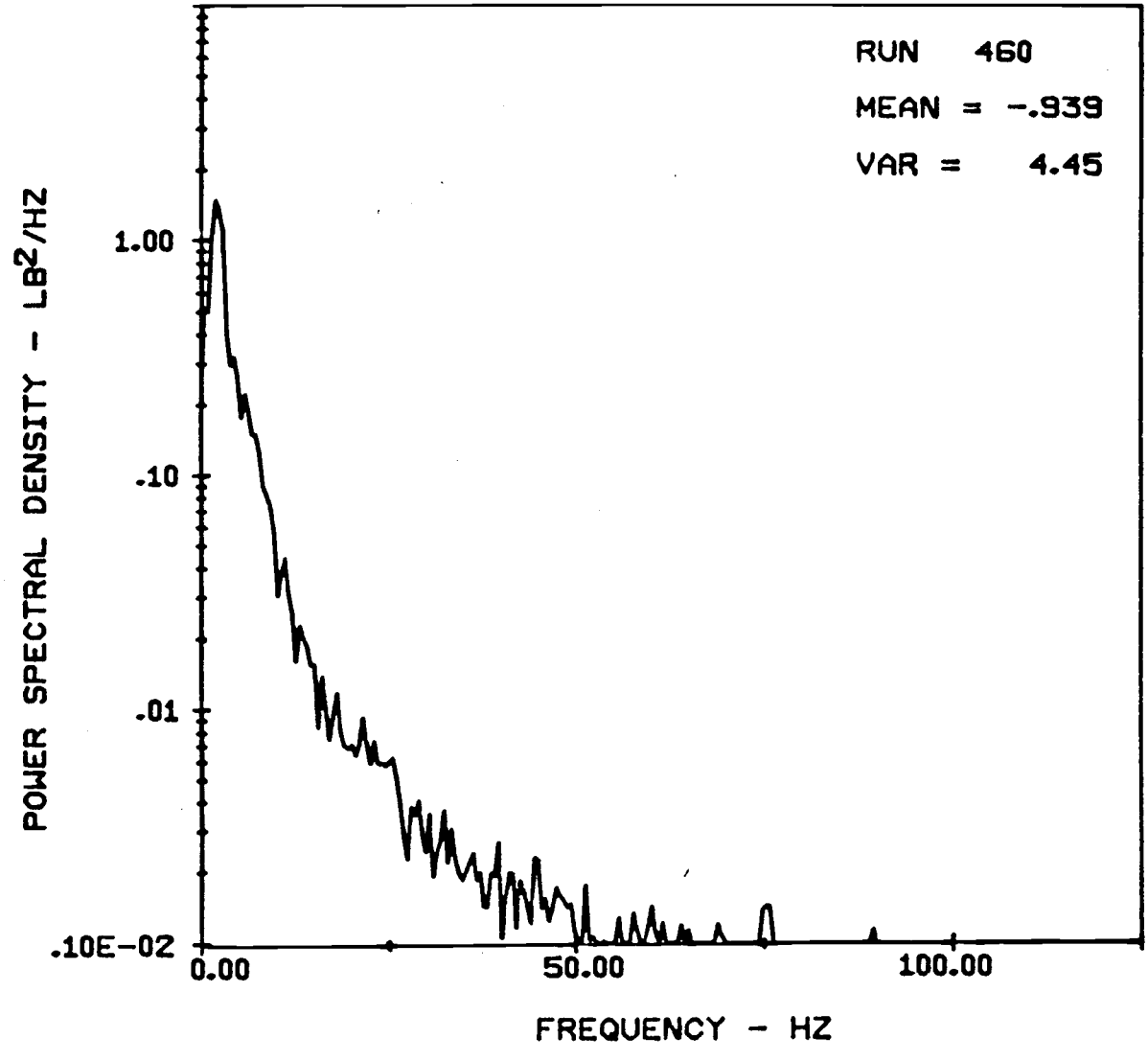


HORIZONTAL FORCES ON A SINGLE TUBE (V = 5 ft/sec)
IN E116 SAND WITH 10" ARRAY HEIGHT AND 4" TUBE SPACING

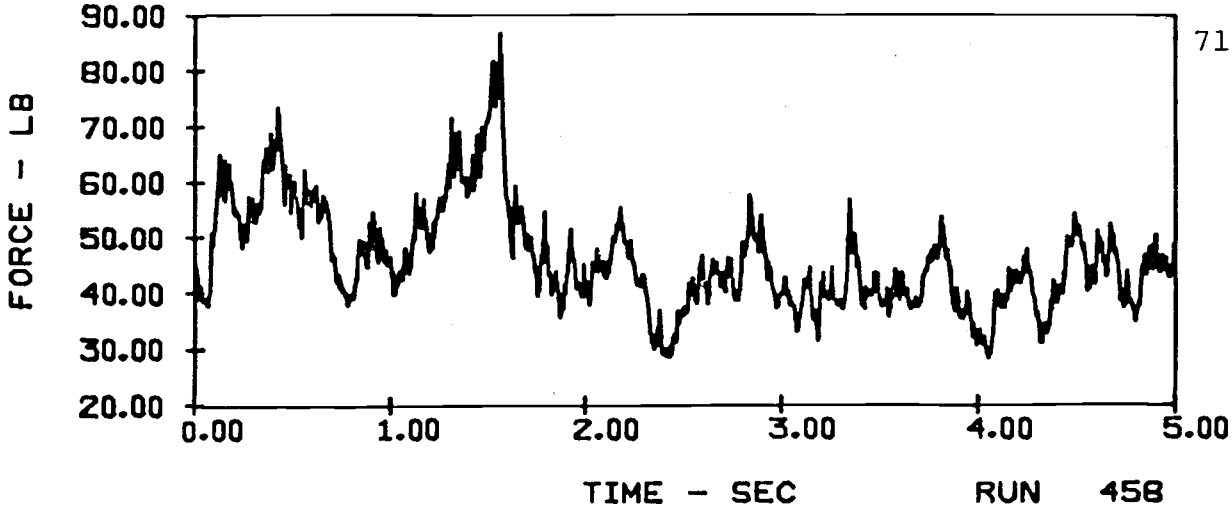


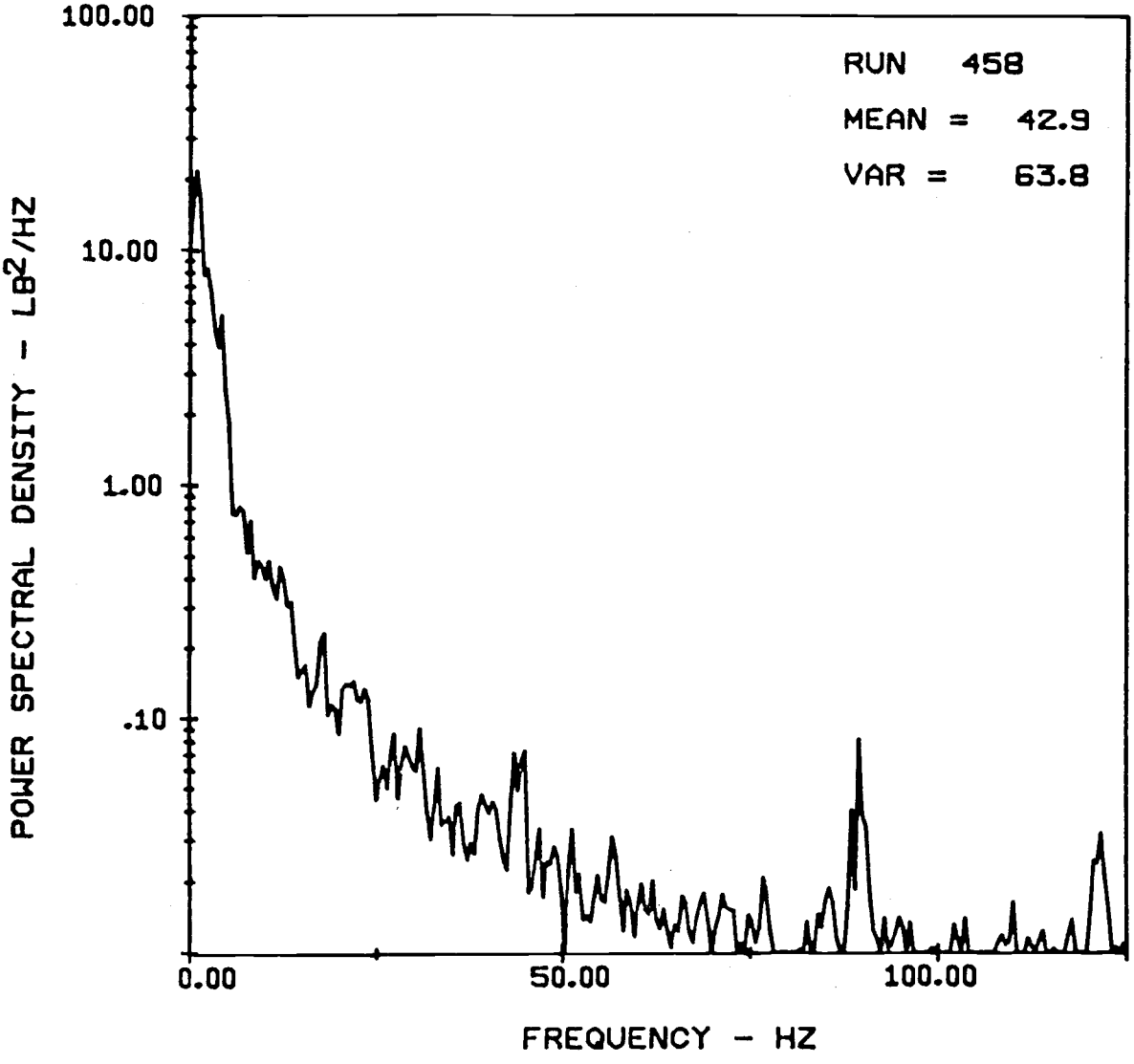


VERTICAL FORCES ON A 10-TUBE ARRAY (V = 5ft/sec)
IN E116 SAND WITH 10" ARRAY HEIGHT AND 4" TUBE SPACING

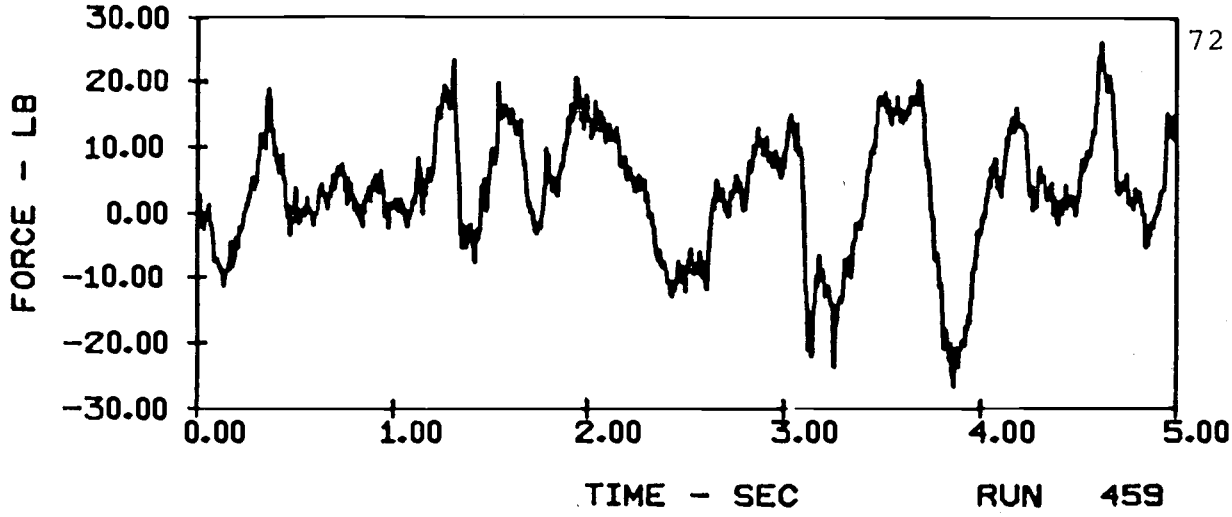


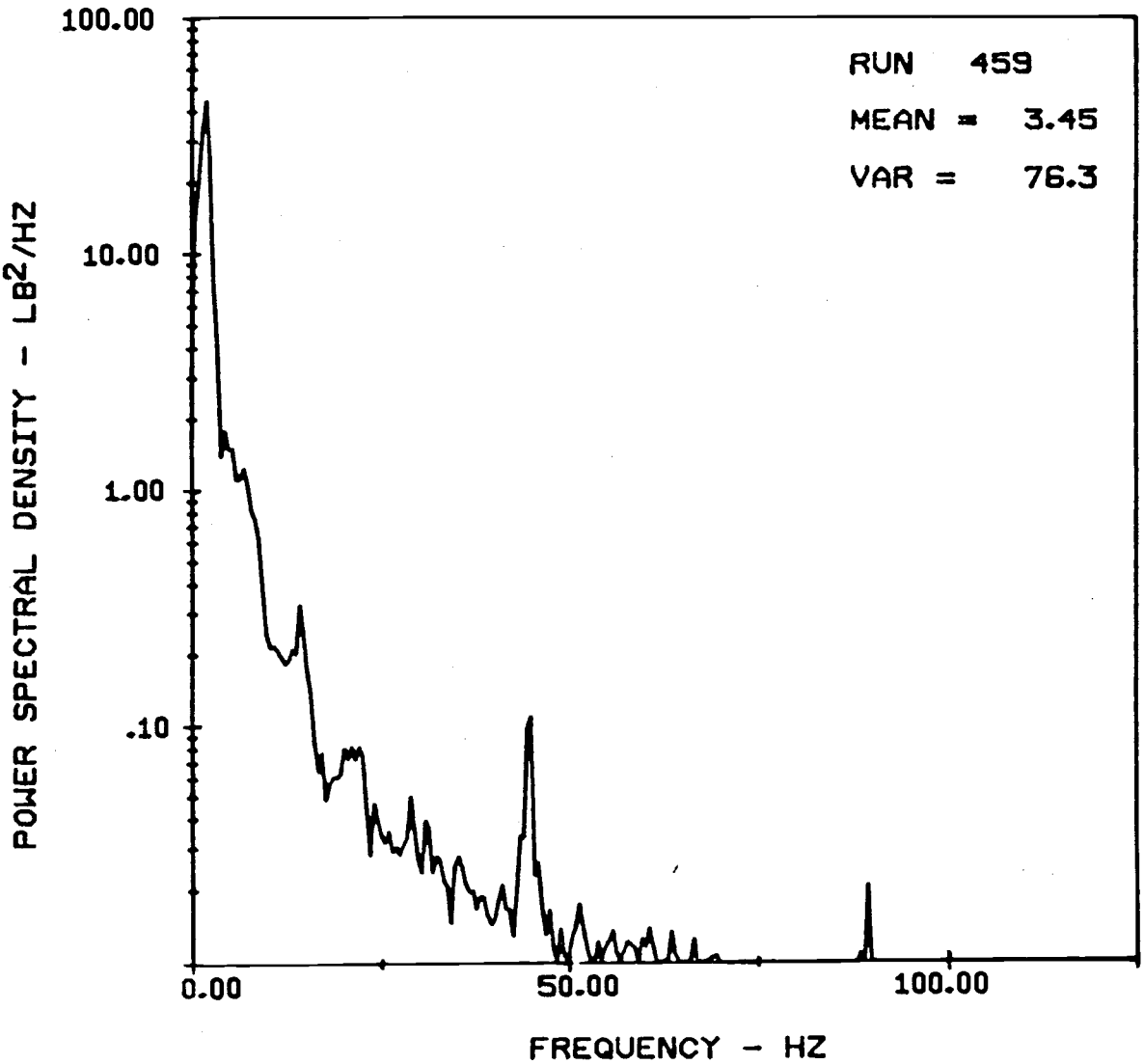


HORIZONTAL FORCES ON A 10-TUBE ARRAY (V = 5 ft/sec)
IN E116 SAND WITH 10" ARRAY HEIGHT AND 4" TUBE SPACING

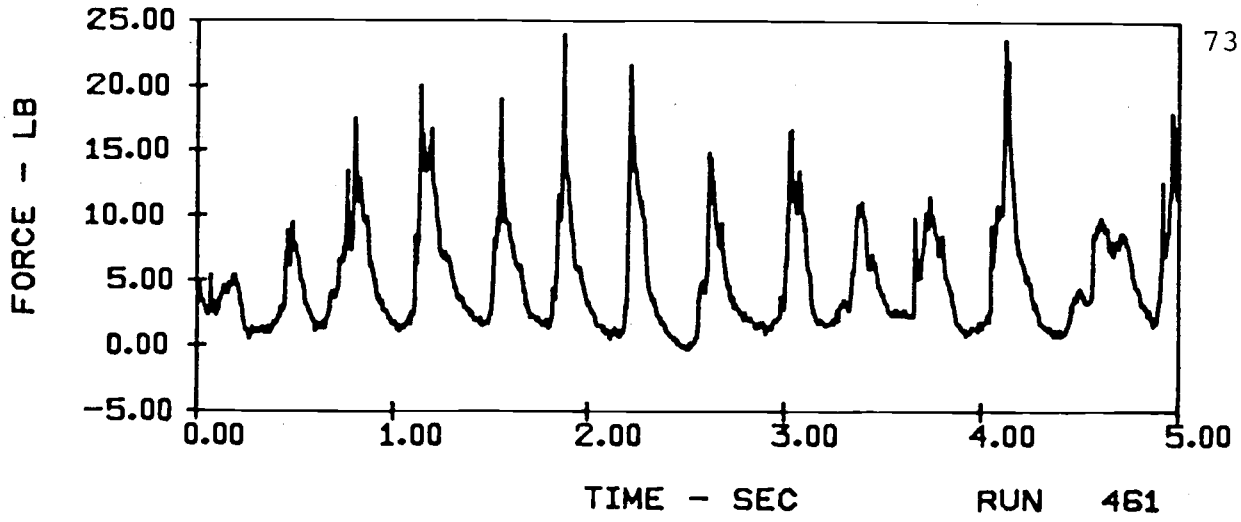


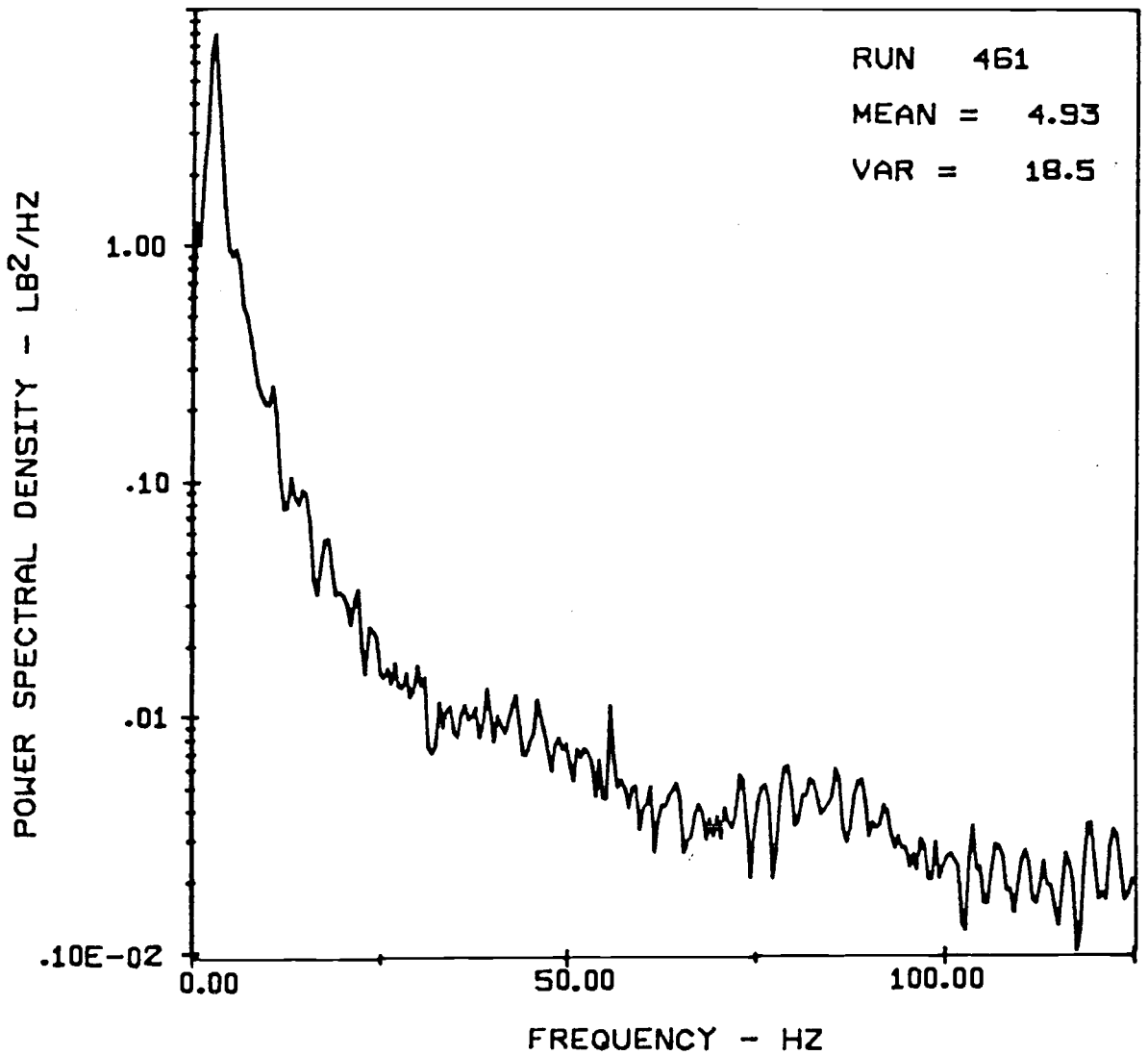


VERTICAL FORCES ON A SINGLE TUBE (V = 7 ft/sec)
IN E116 SAND WITH 10" ARRAY HEIGHT AND 4" TUBE SPACING

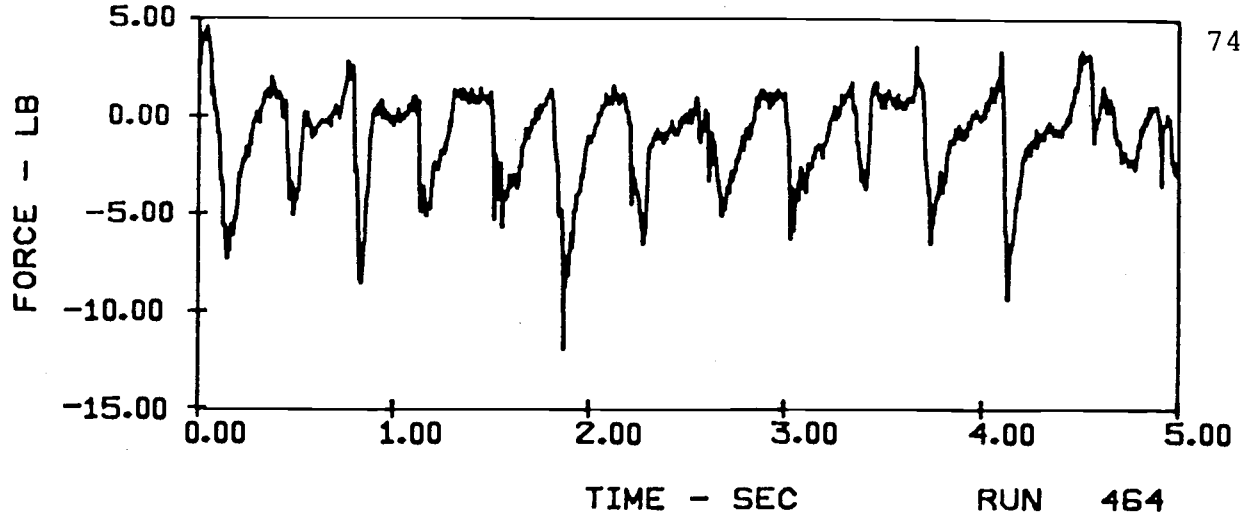


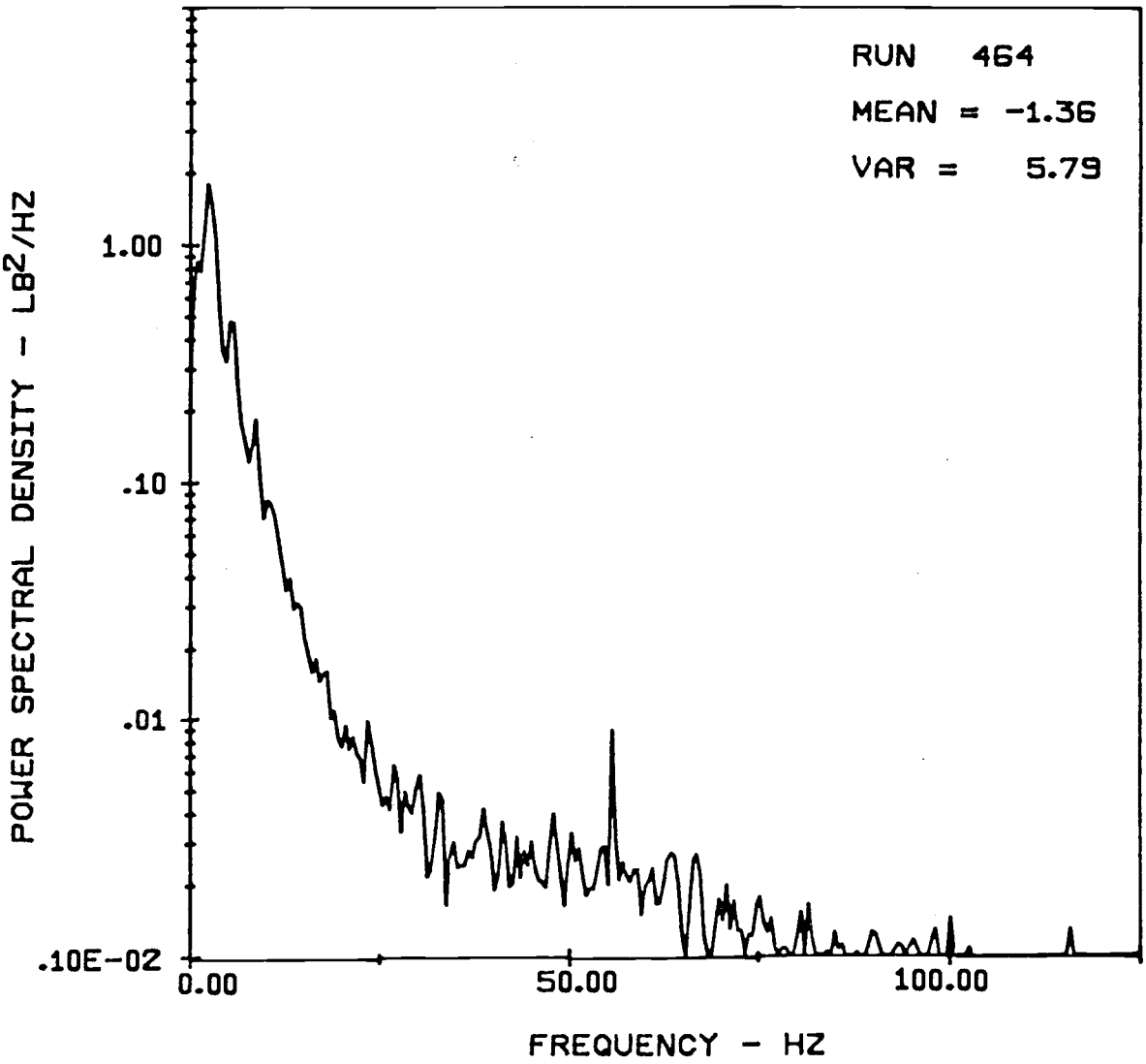


HORIZONTAL FORCES ON A SINGLE TUBE (V = 7 ft/sec)
IN E116 SAND WITH 10" ARRAY HEIGHT AND 4" TUBE SPACING

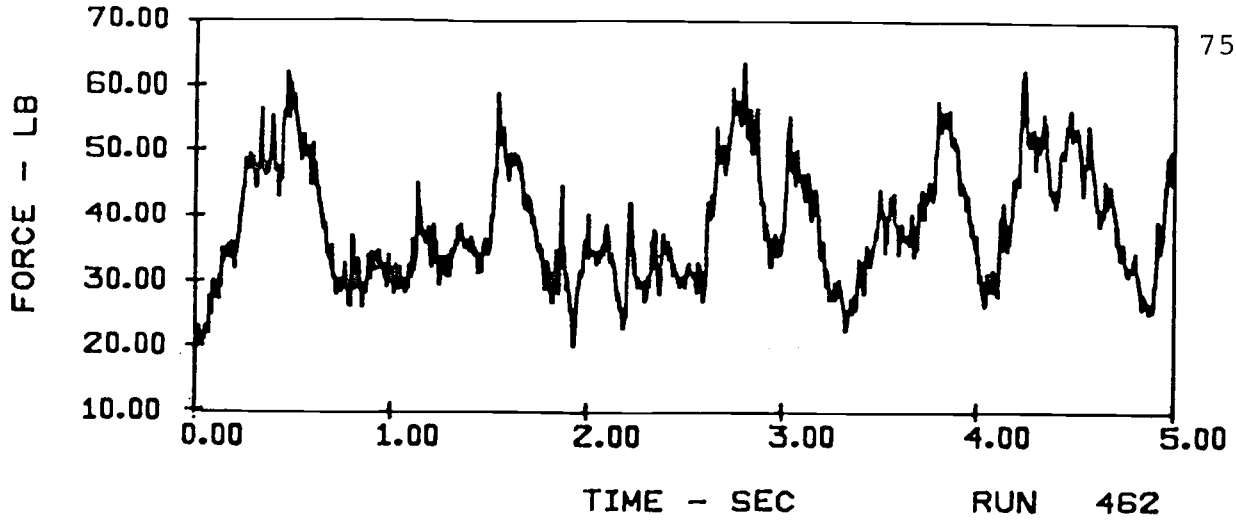


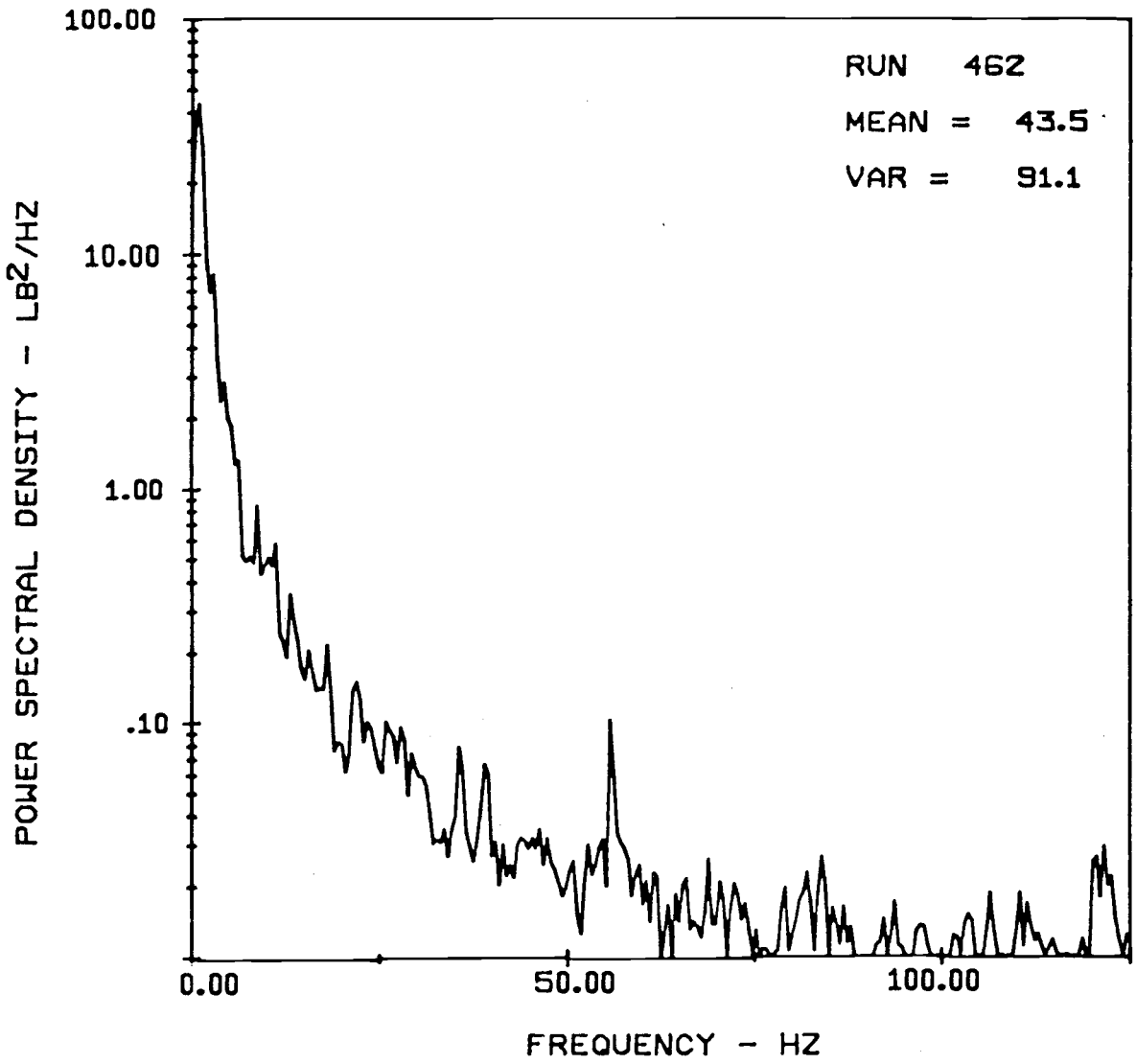


VERTICAL FORCES ON A 10-TUBE ARRAY (V = 7ft/sec)
IN E116 SAND WITH 10" ARRAY HEIGHT AND 4" TUBE SPACING

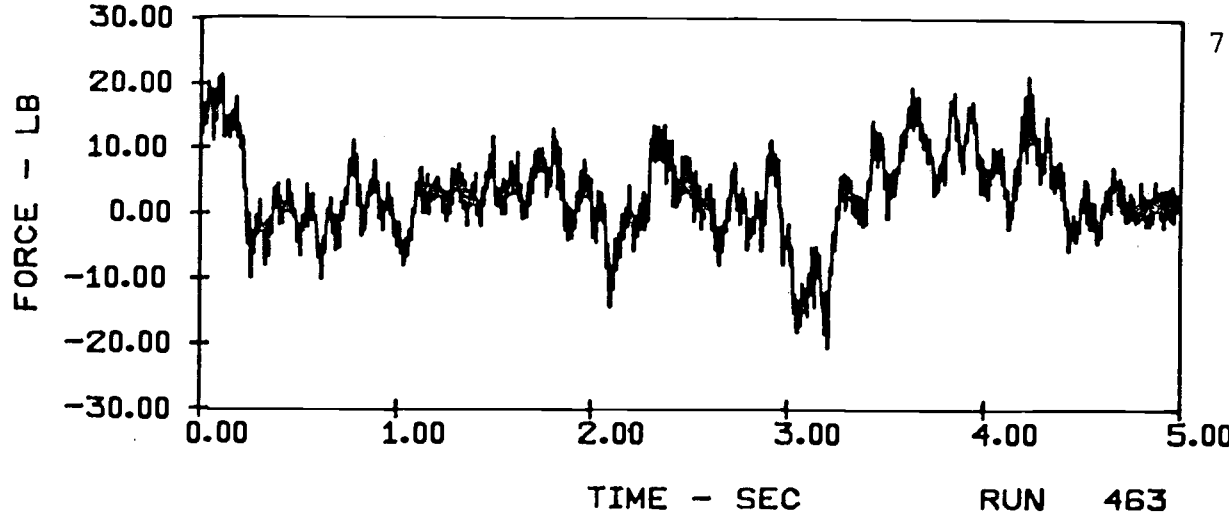


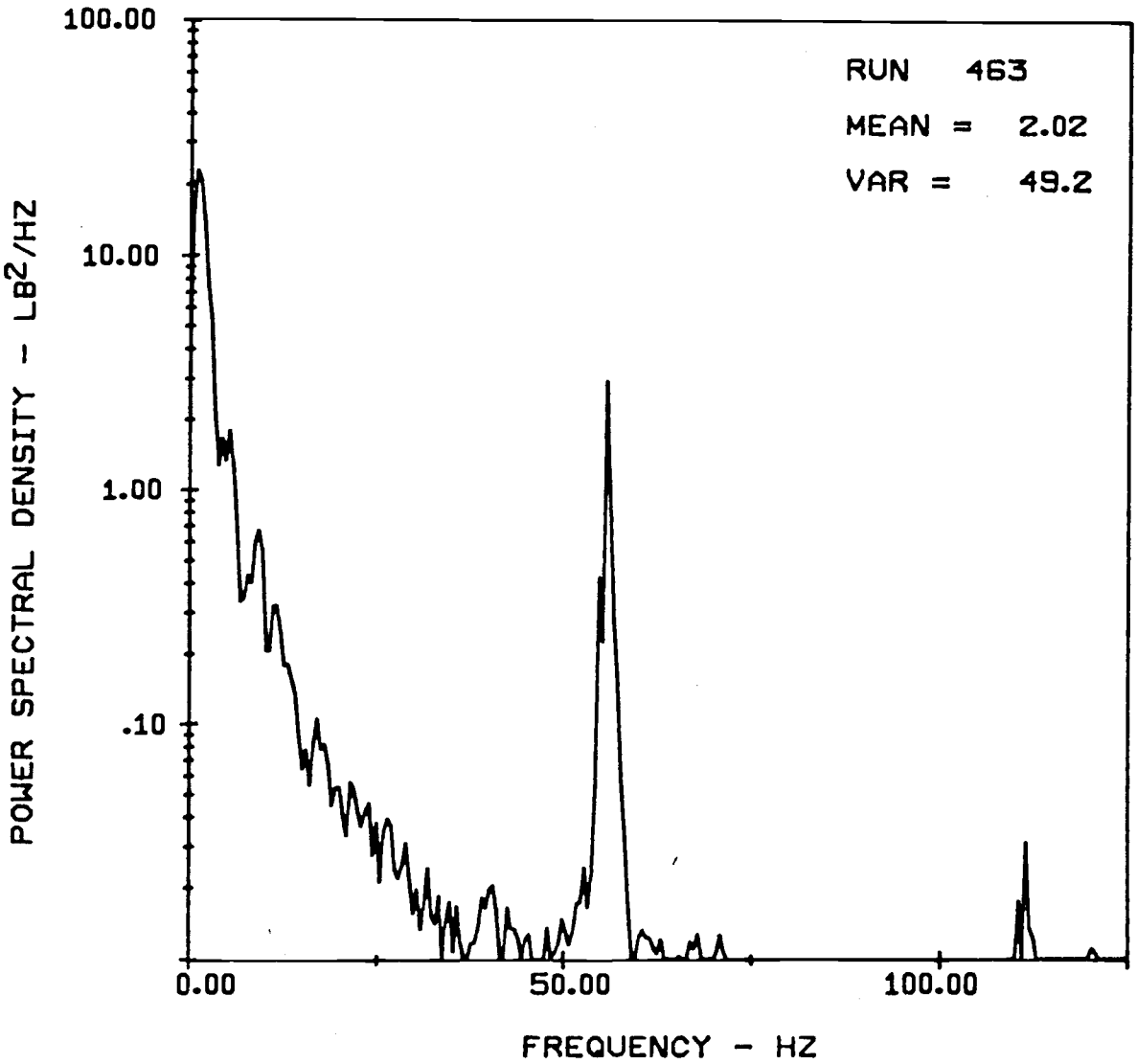


HORIZONTAL FORCES ON A 10-TUBE ARRAY (V = 7 ft/sec)
IN E116 SAND WITH 10" ARRAY HEIGHT AND 4" TUBE SPACING

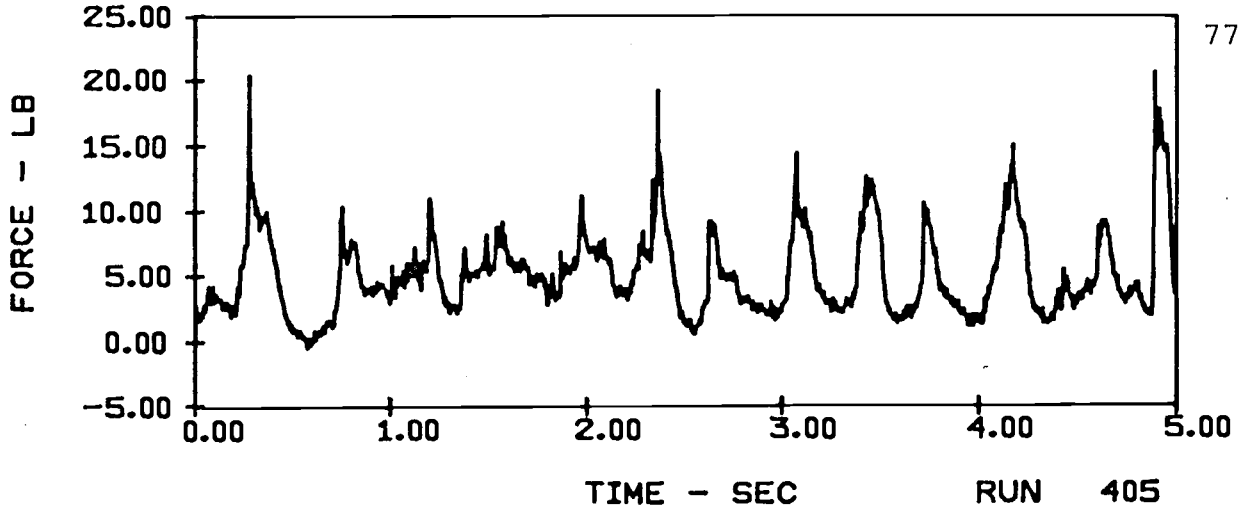


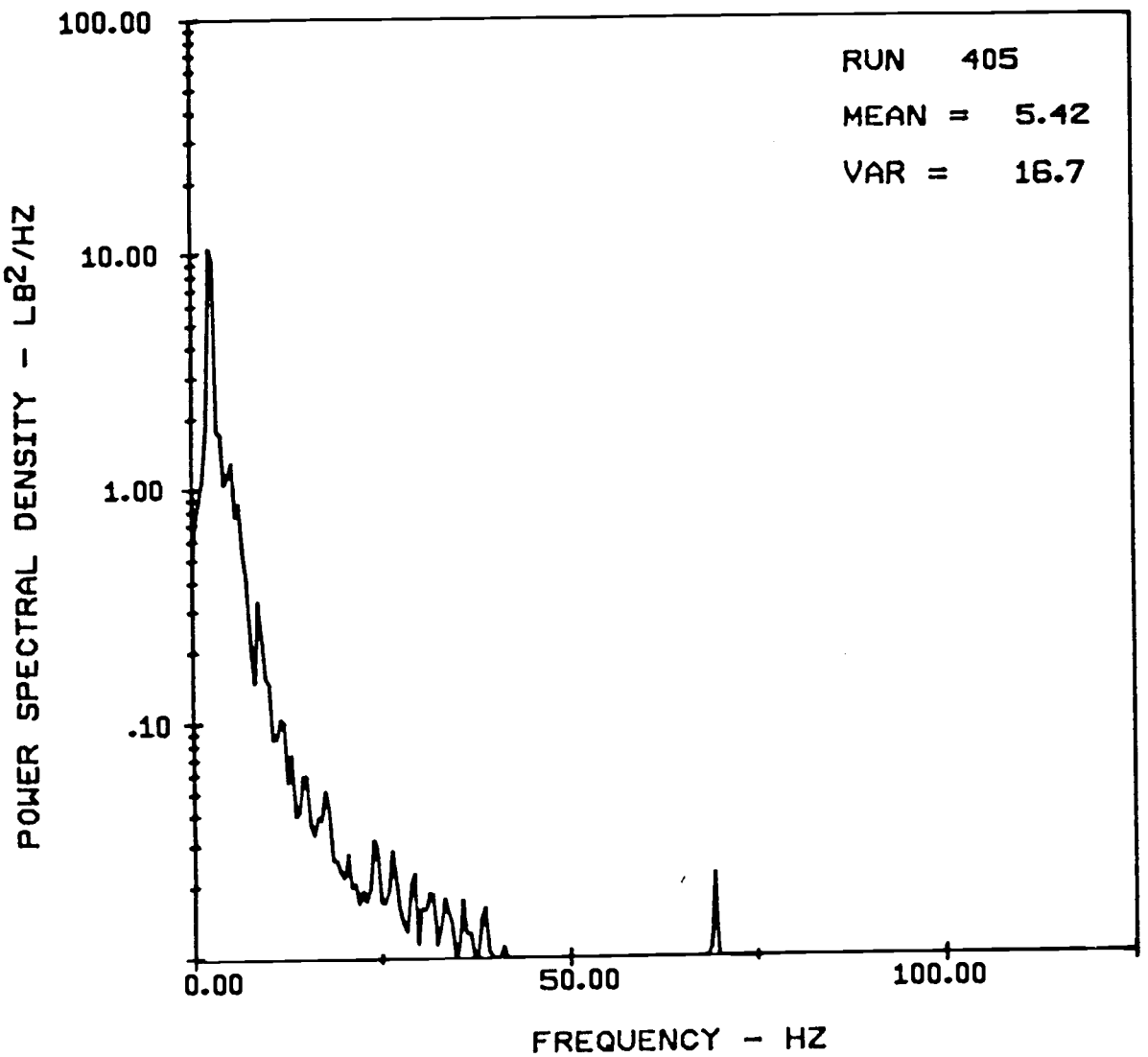


VERTICAL FORCES ON A SINGLE TUBE (V = 9 ft/sec)
IN E116 SAND WITH 10" ARRAY HEIGHT AND 4" TUBE SPACING

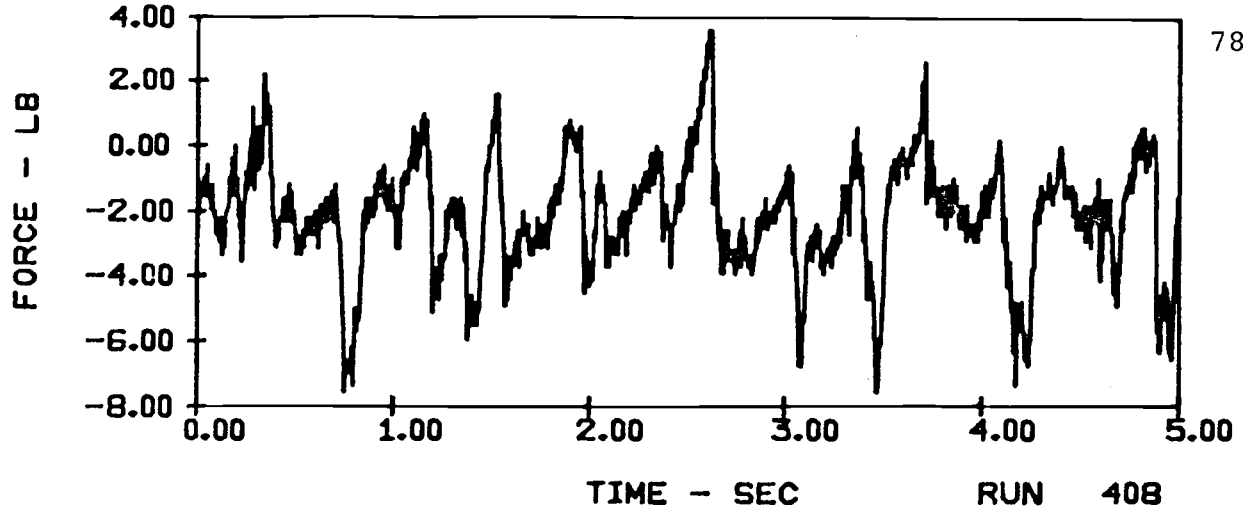


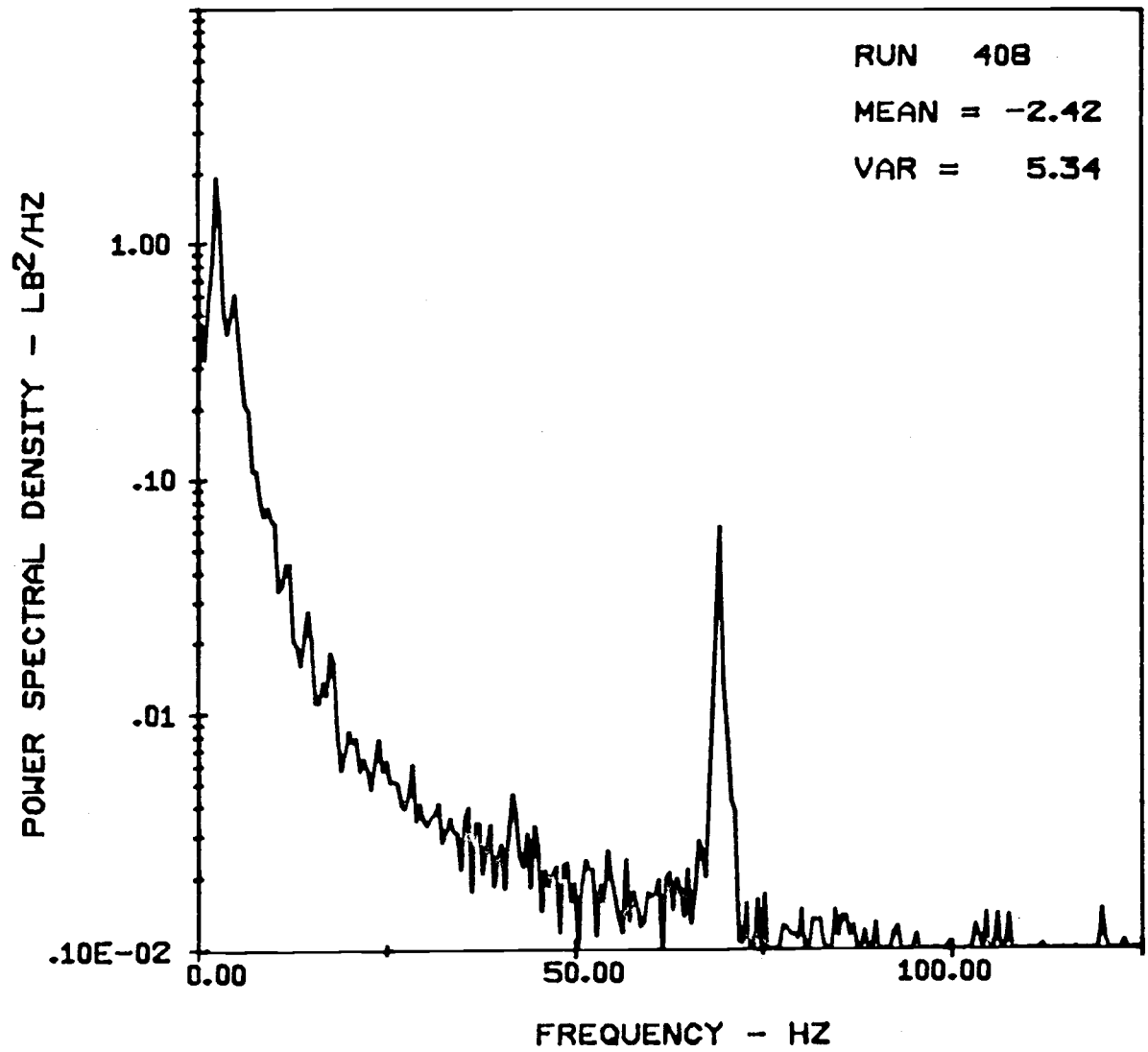


HORIZONTAL FORCES ON A SINGLE TUBE (V = 9 ft/sec)
IN E116 SAND WITH 10" ARRAY HEIGHT AND 4" TUBE SPACING

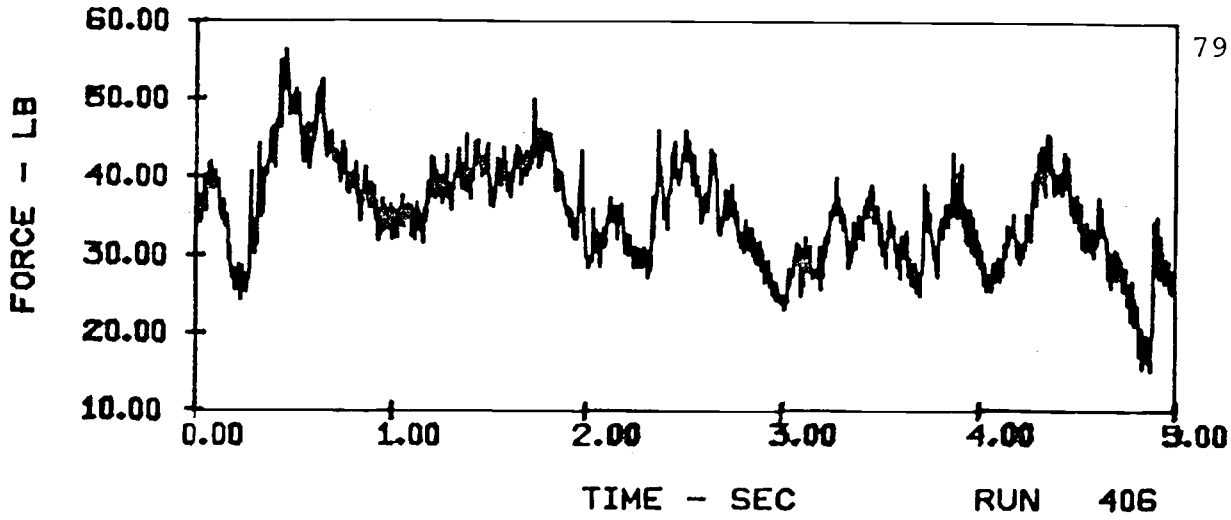


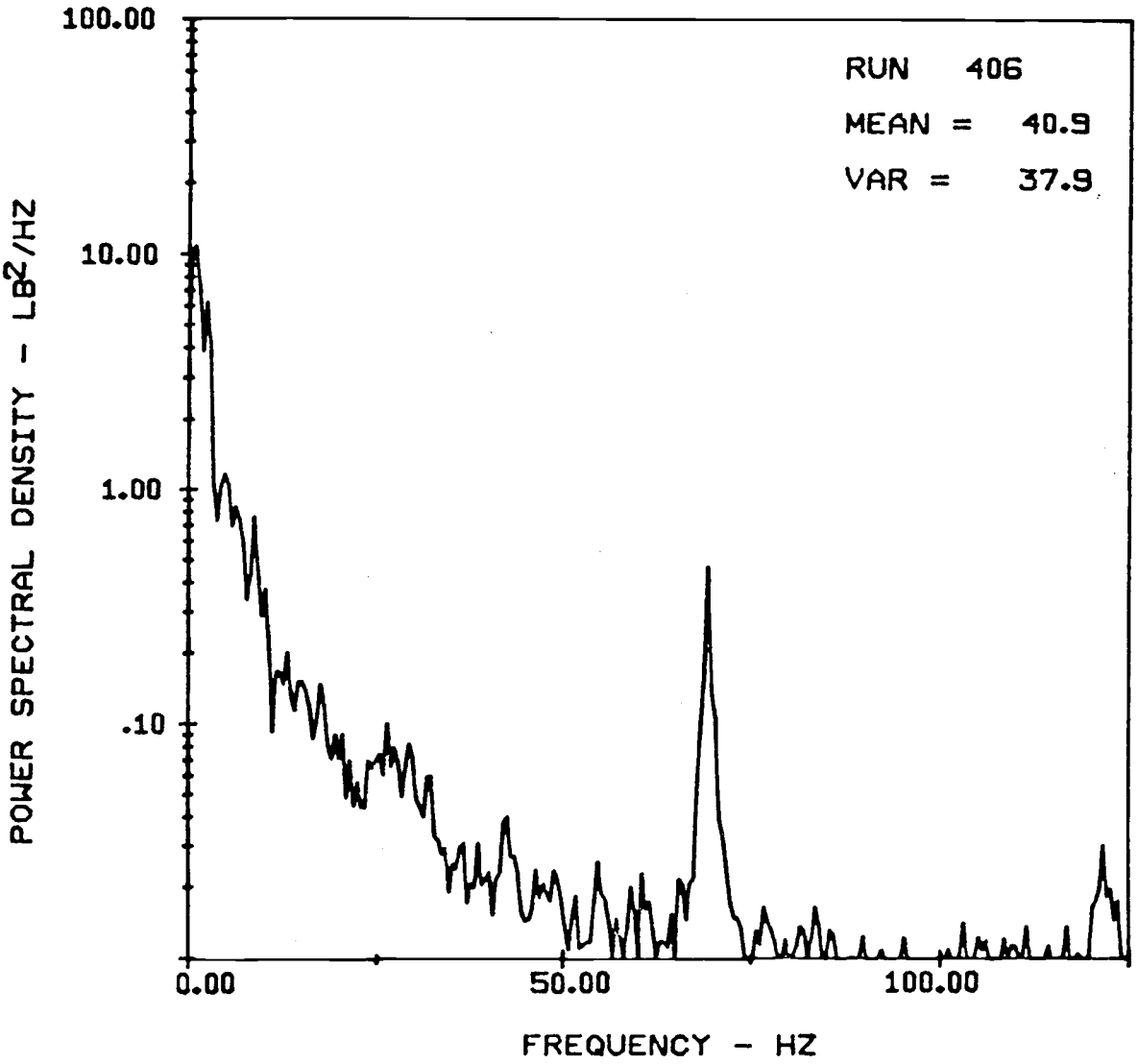


VERTICAL FORCES ON A 10-TUBE ARRAY (V = 9ft/sec)
IN E116 SAND WITH 10" ARRAY HEIGHT AND 4" TUBE SPACING

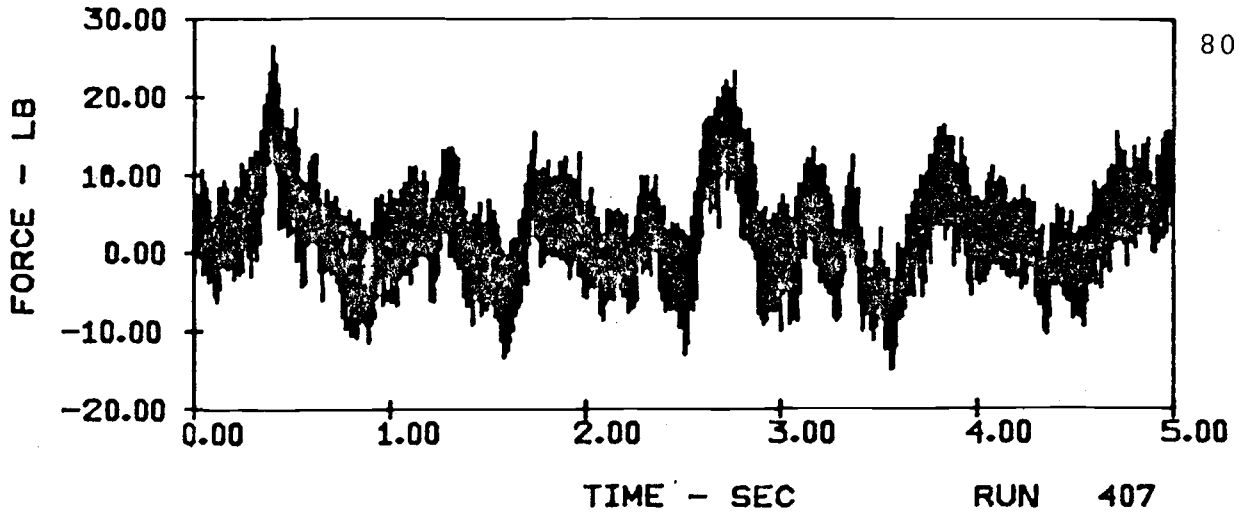


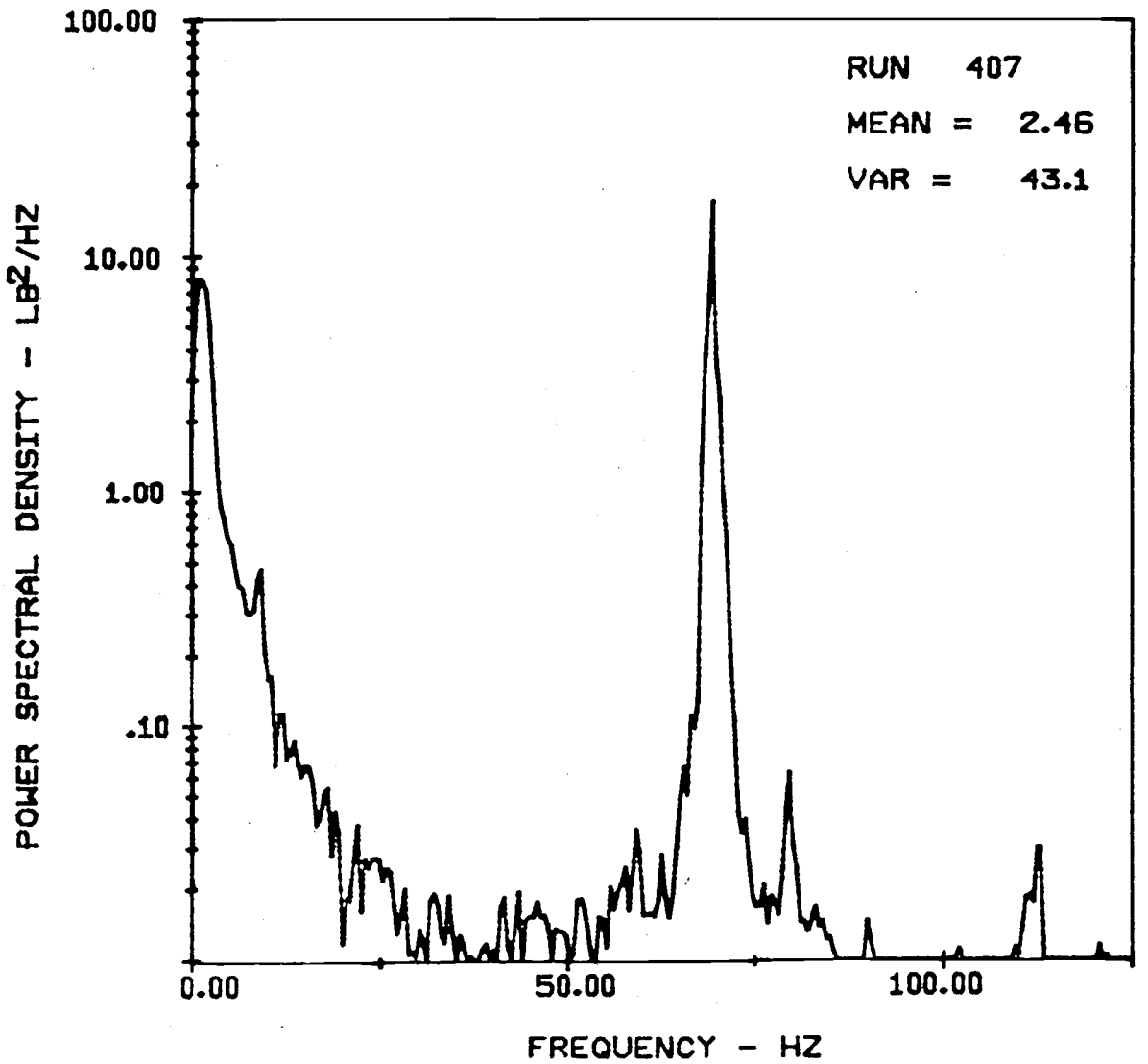


HORIZONTAL FORCES ON A 10-TUBE ARRAY (V = 9 ft/sec)
IN E116 SAND WITH 10" ARRAY HEIGHT AND 4" TUBE SPACING

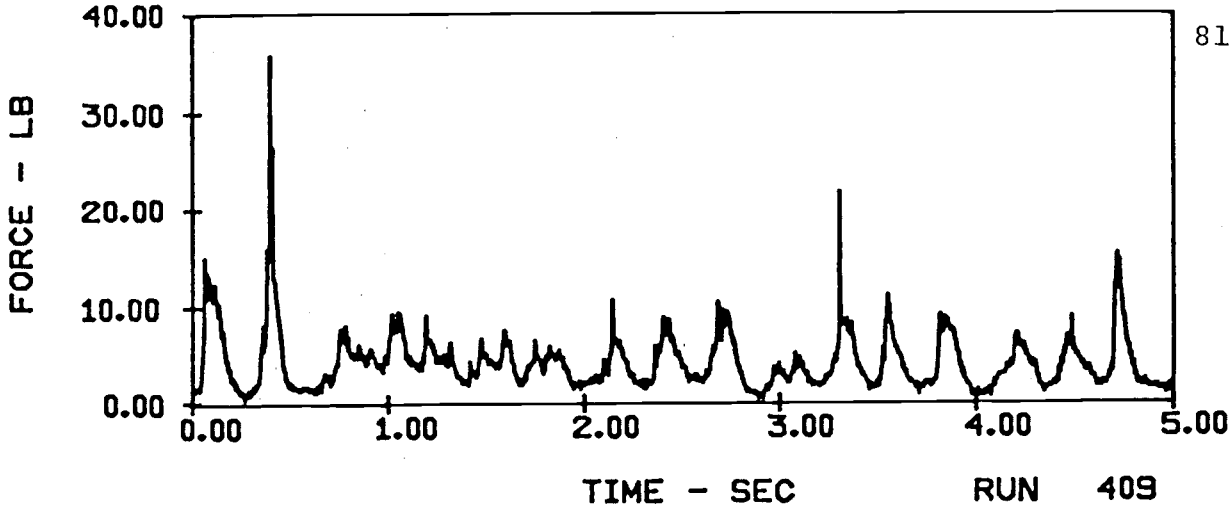


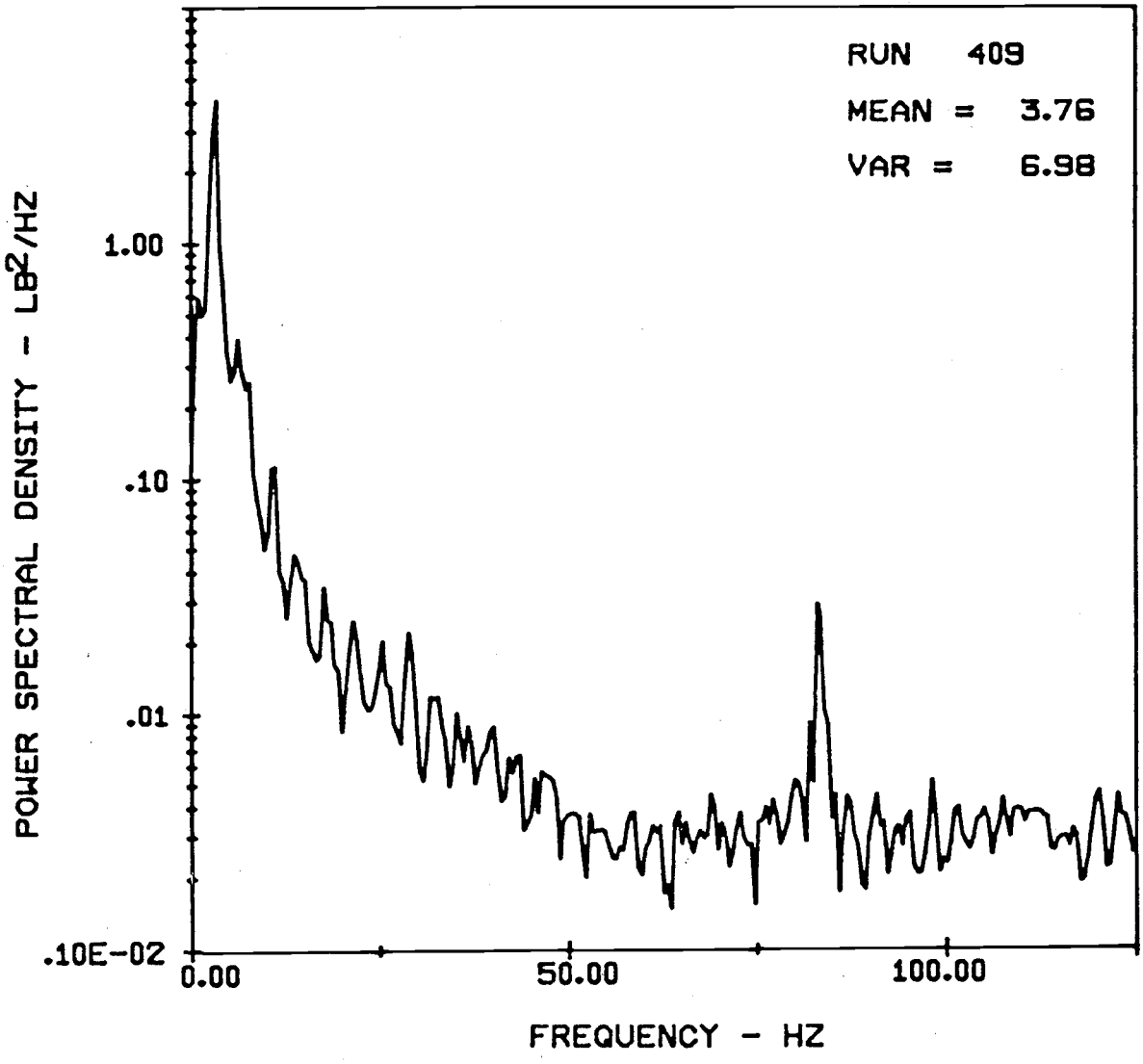


VERTICAL FORCES ON A SINGLE TUBE (V = 11 ft/sec)
IN E116 SAND WITH 10" ARRAY HEIGHT AND 4" TUBE SPACING

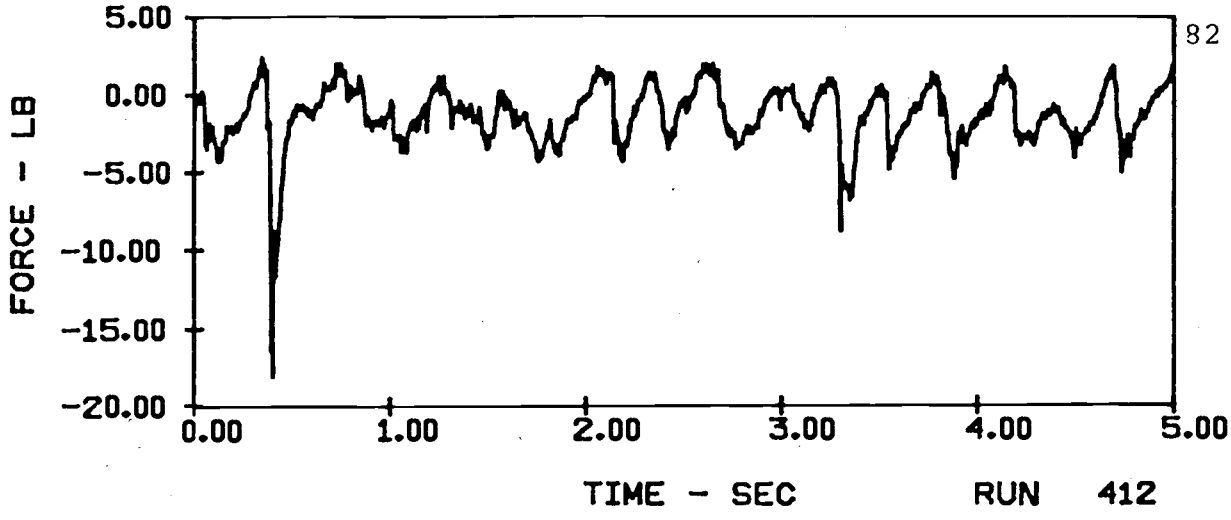


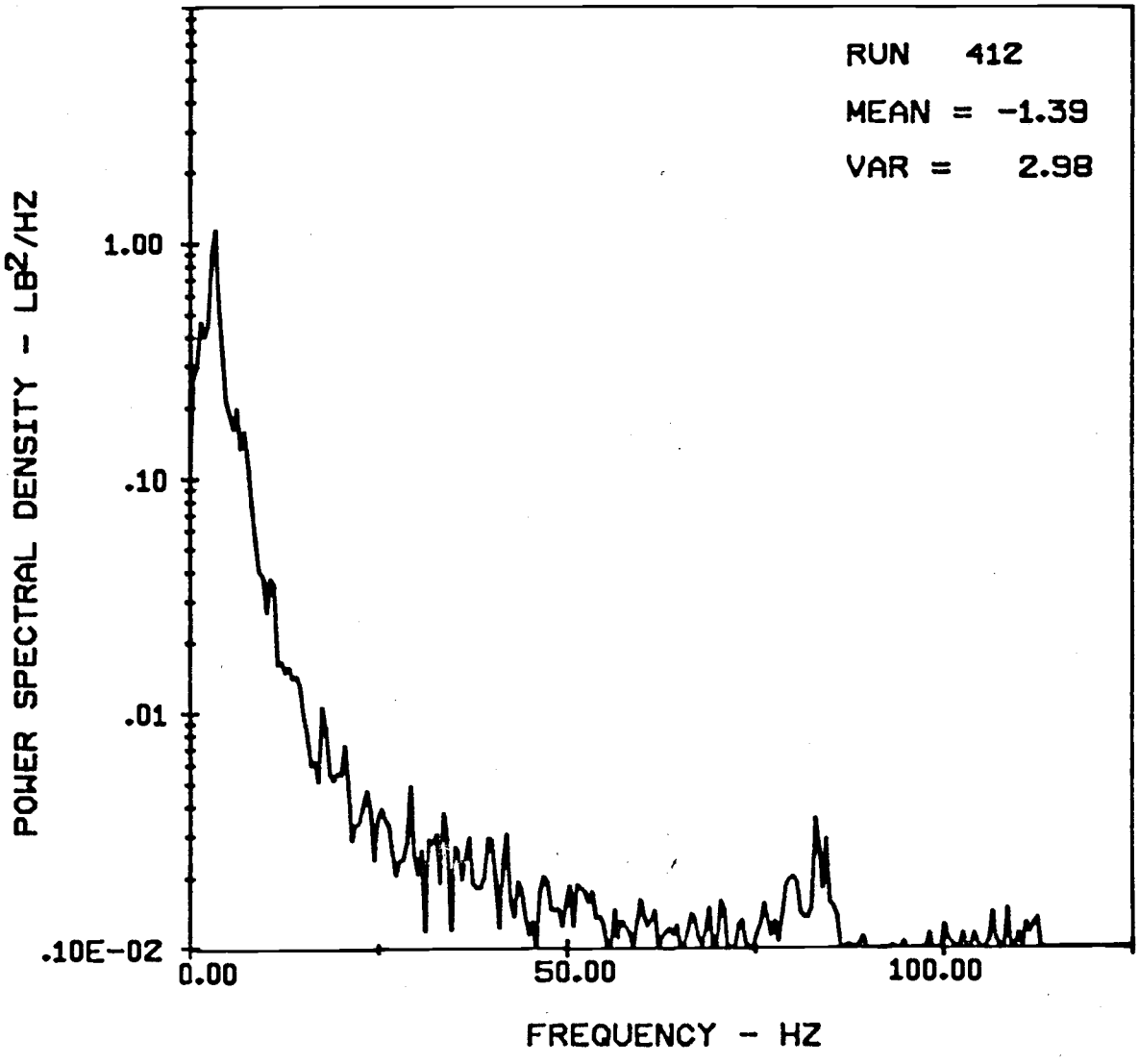


HORIZONTAL FORCES ON A SINGLE TUBE (V = 11 ft/sec)
IN E116 SAND WITH 10" ARRAY HEIGHT AND 4" TUBE SPACING

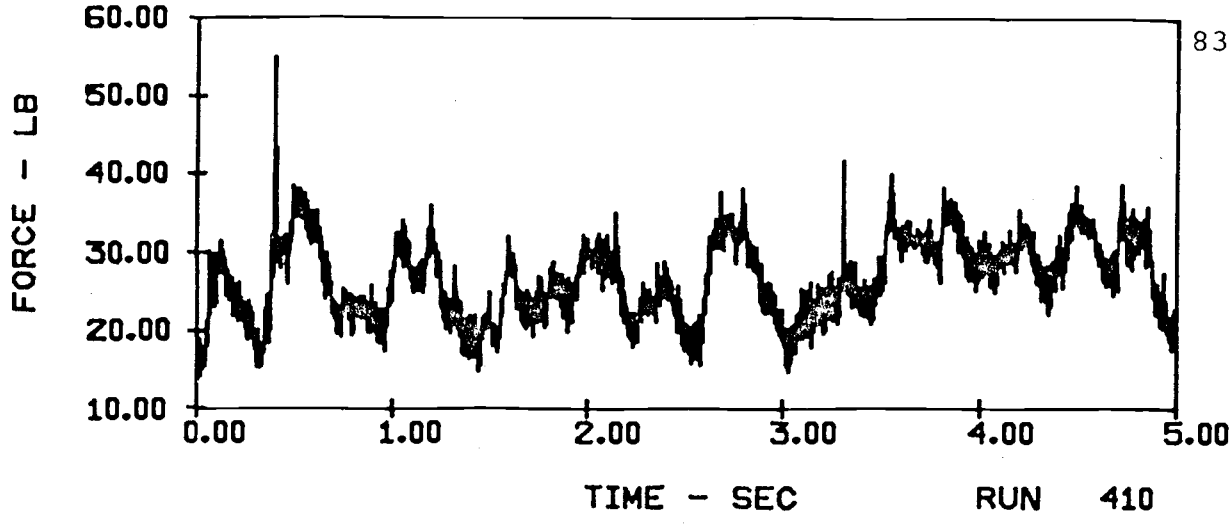


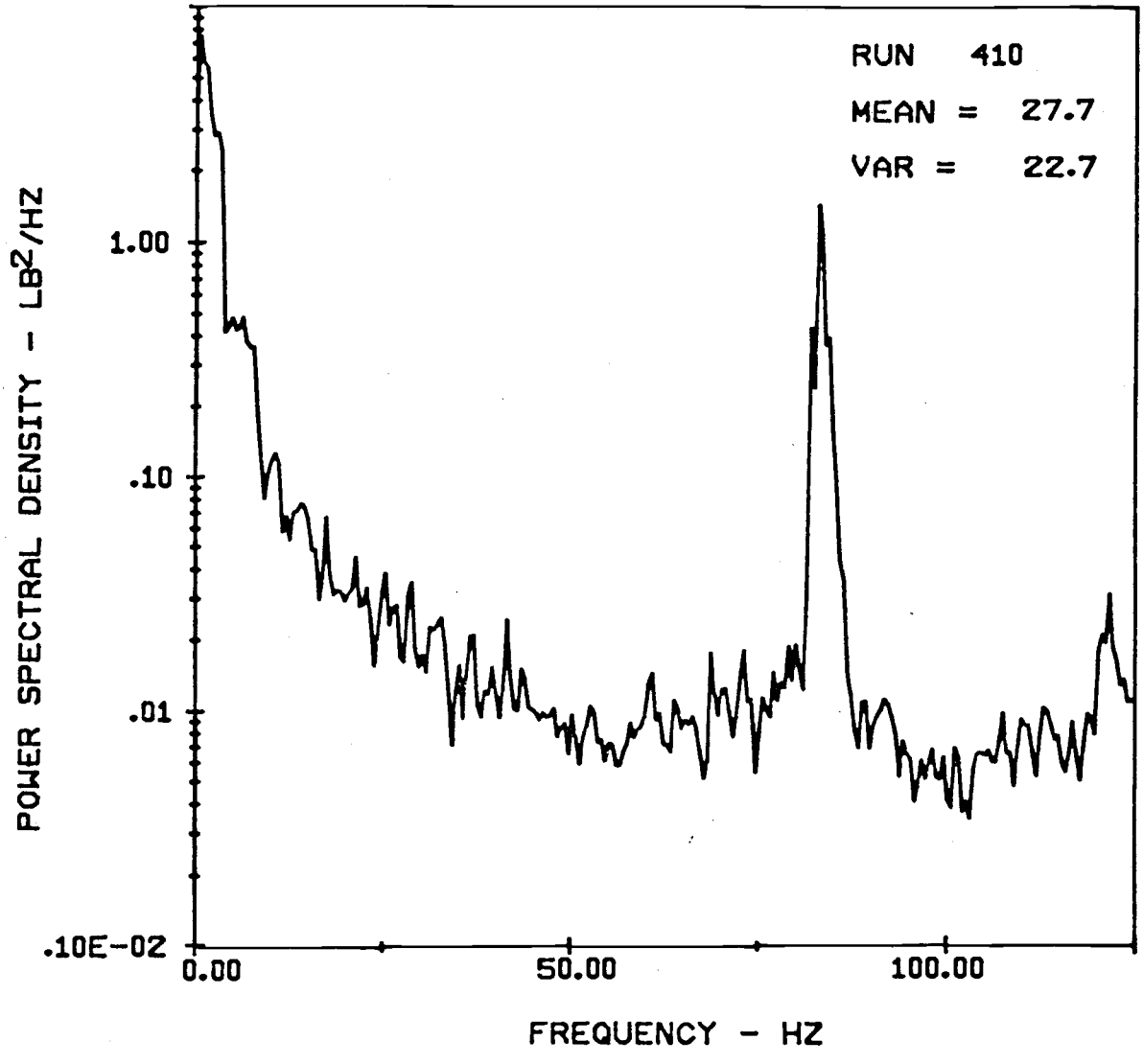


VERTICAL FORCES ON A 10-TUBE ARRAY (V = 11ft/sec)
IN E116 SAND WITH 10" ARRAY HEIGHT AND 4" TUBE SPACING

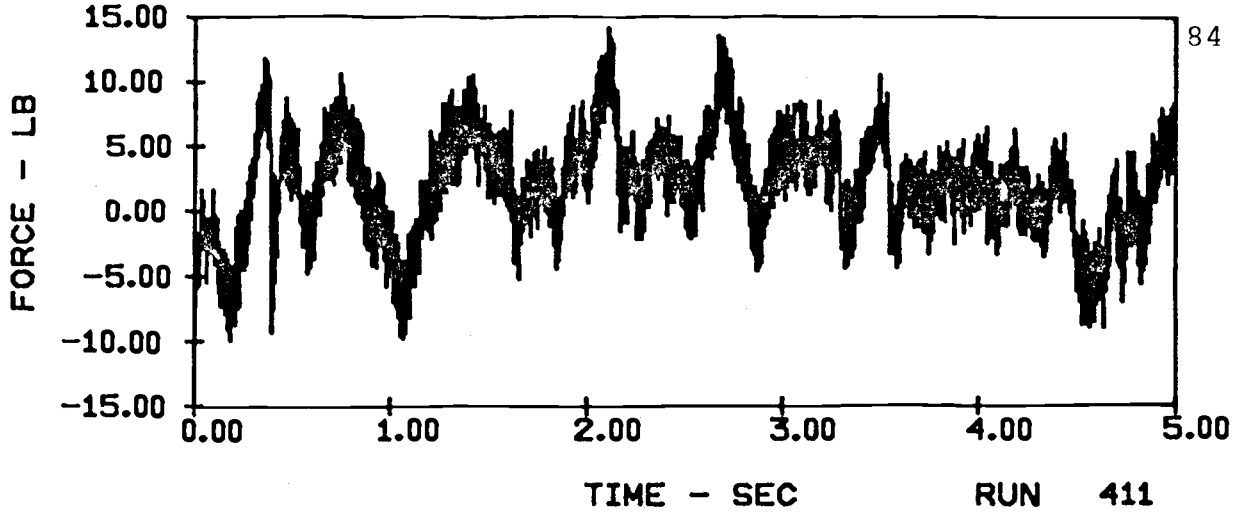


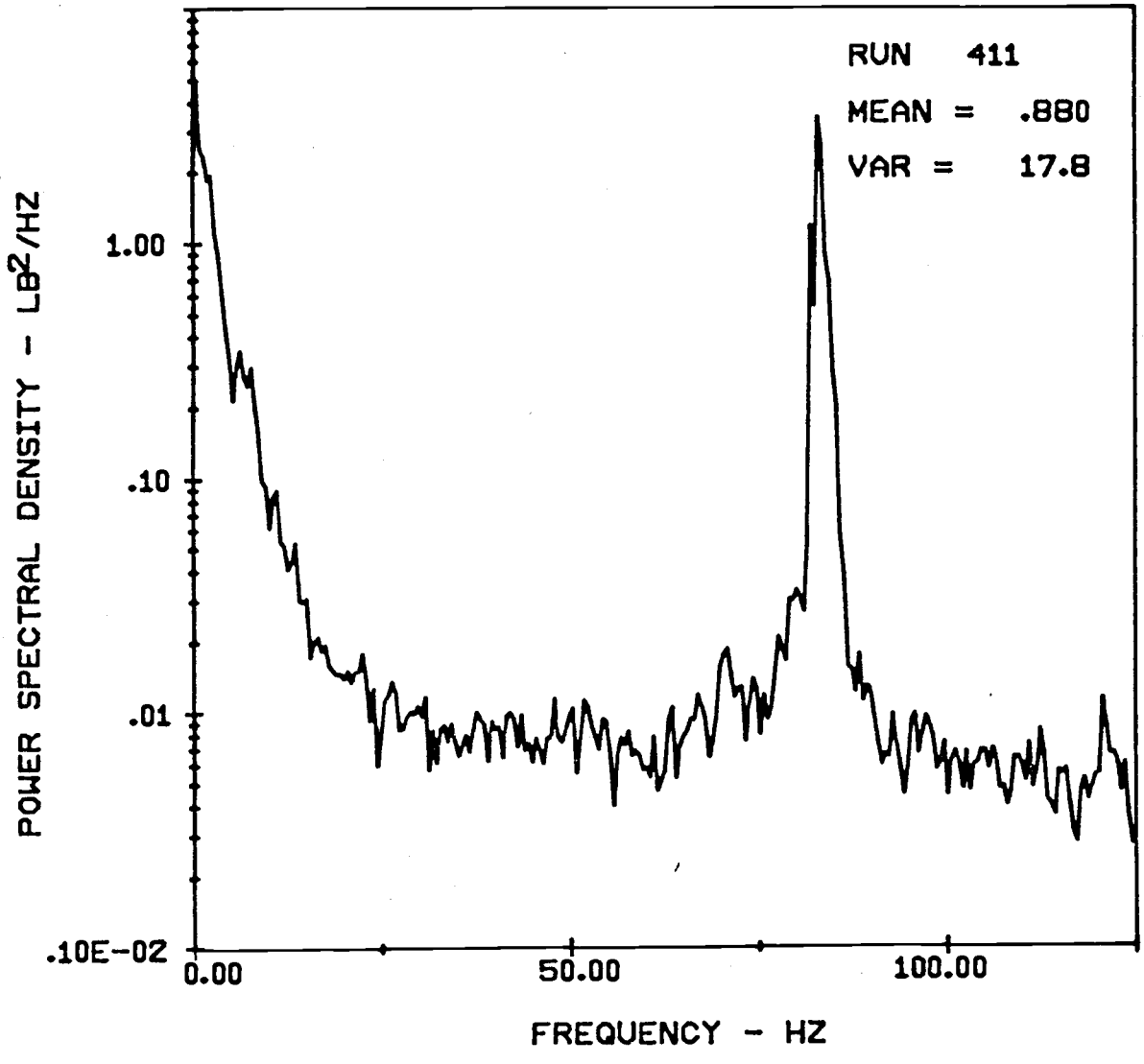


HORIZONTAL FORCES ON A 10-TUBE ARRAY (V = 11 ft/sec)
IN E116 SAND WITH 10" ARRAY HEIGHT AND 4" TUBE SPACING

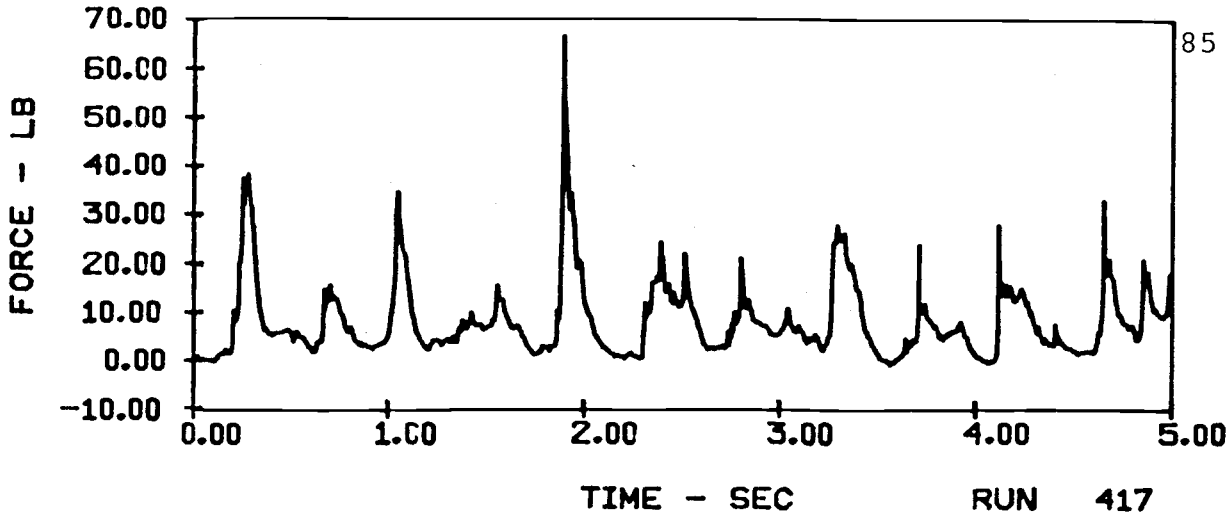


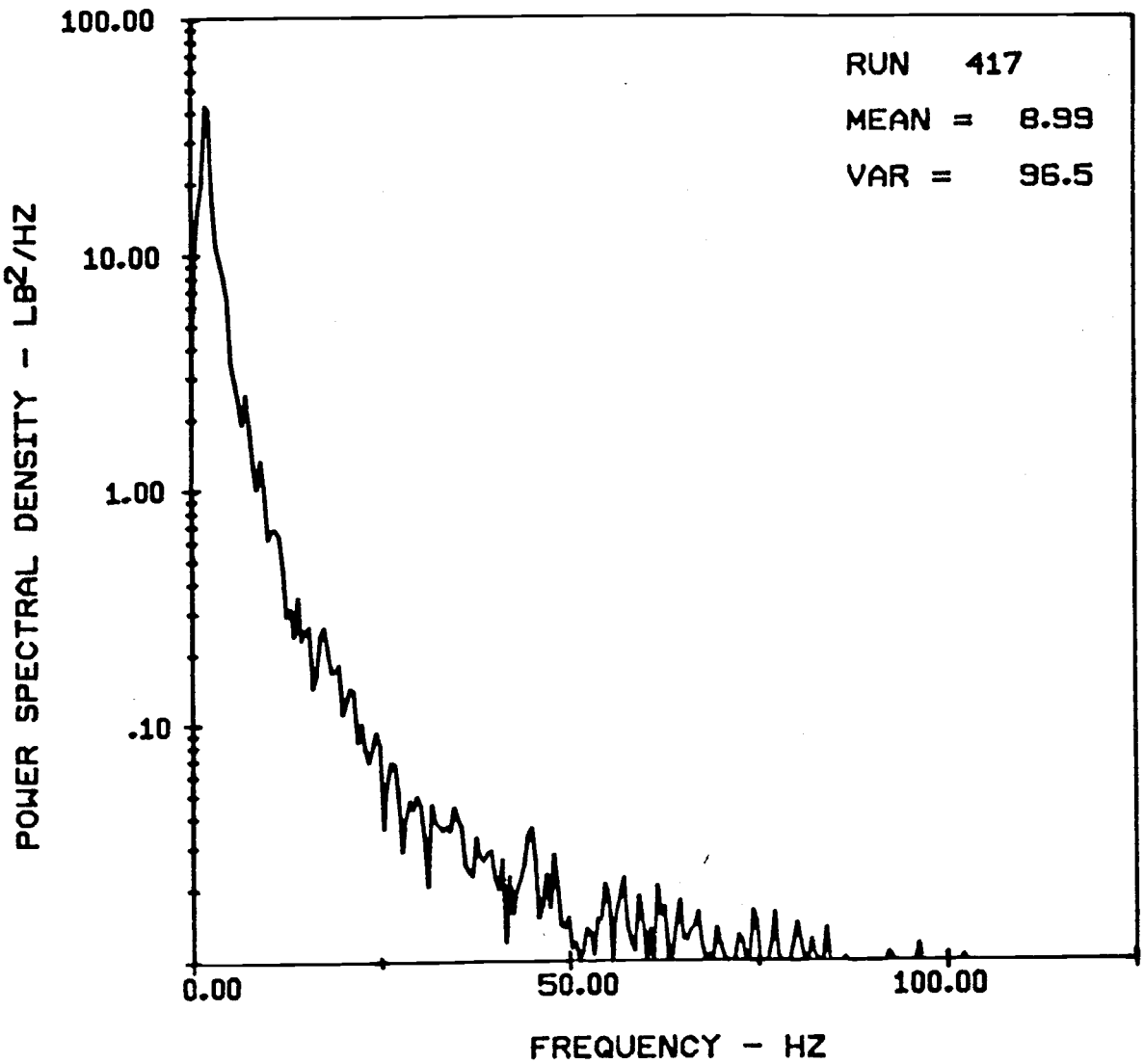


VERTICAL FORCES ON A SINGLE TUBE (V = 5 ft/sec)
IN E116 SAND WITH 20" ARRAY HEIGHT AND 4" TUBE SPACING

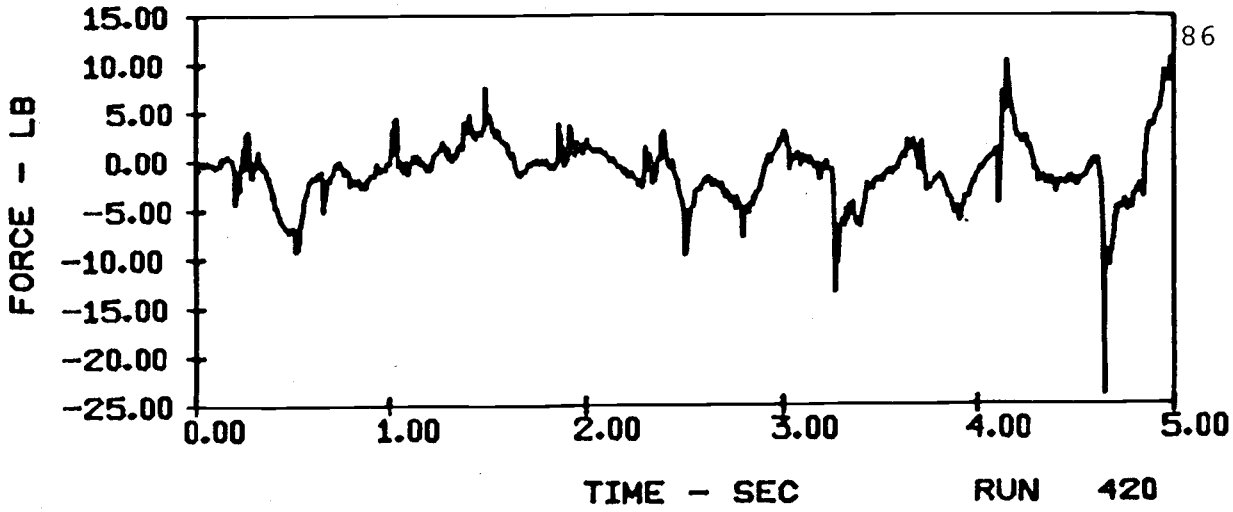


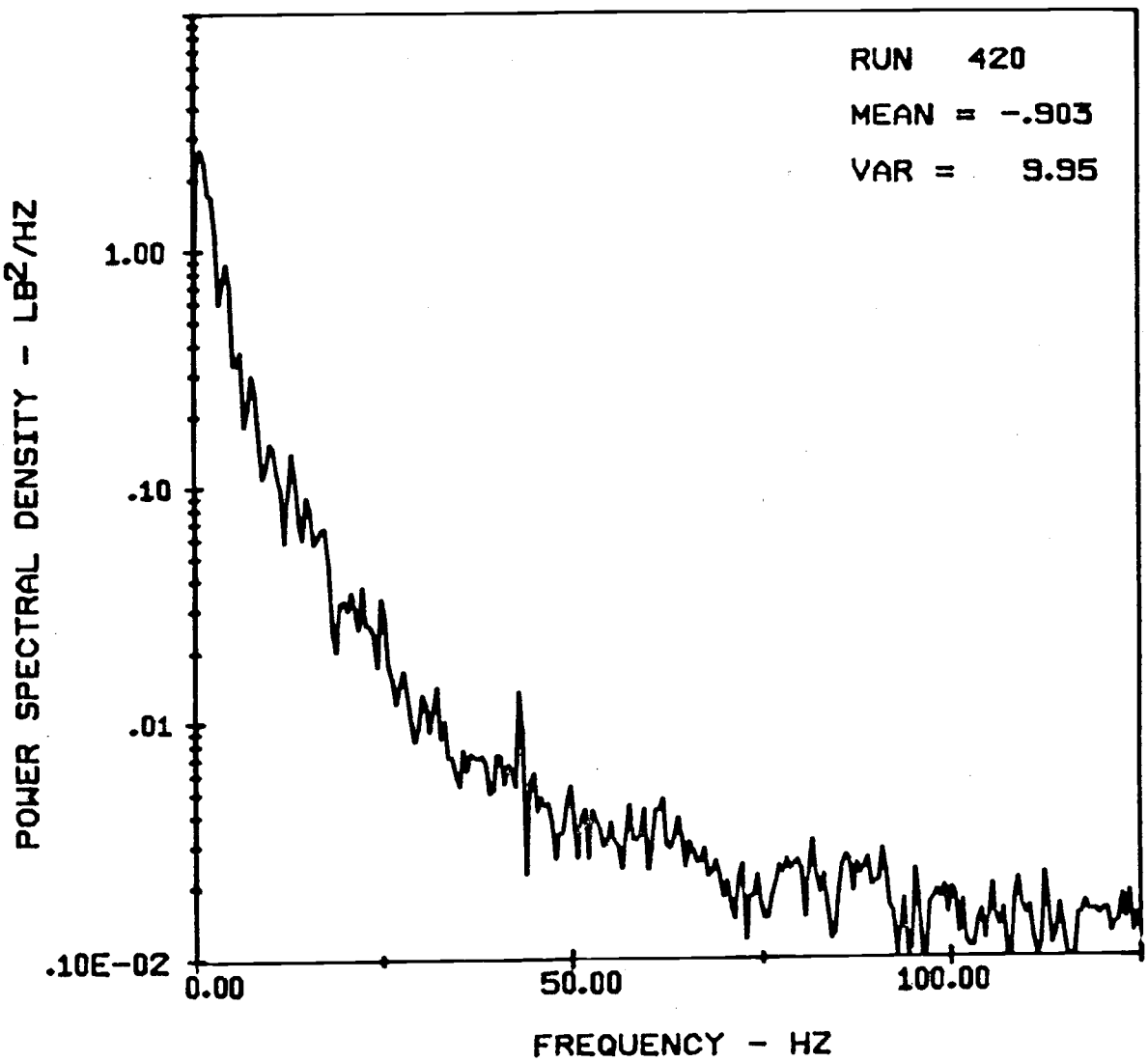


HORIZONTAL FORCES ON A SINGLE TUBE (V = 5 ft/sec)
IN E116 SAND WITH 20" ARRAY HEIGHT AND 4" TUBE SPACING

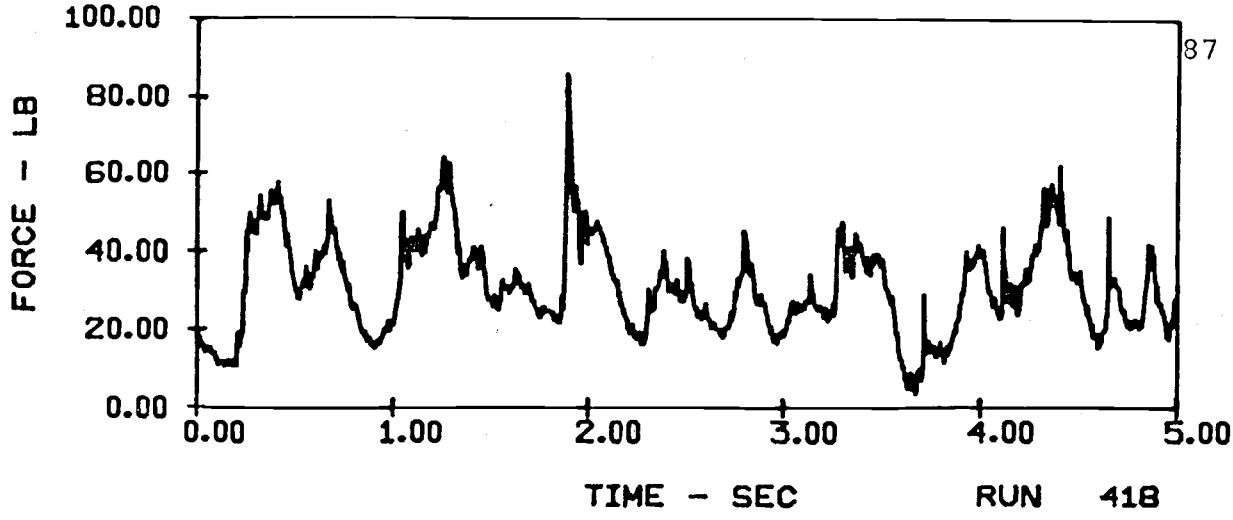


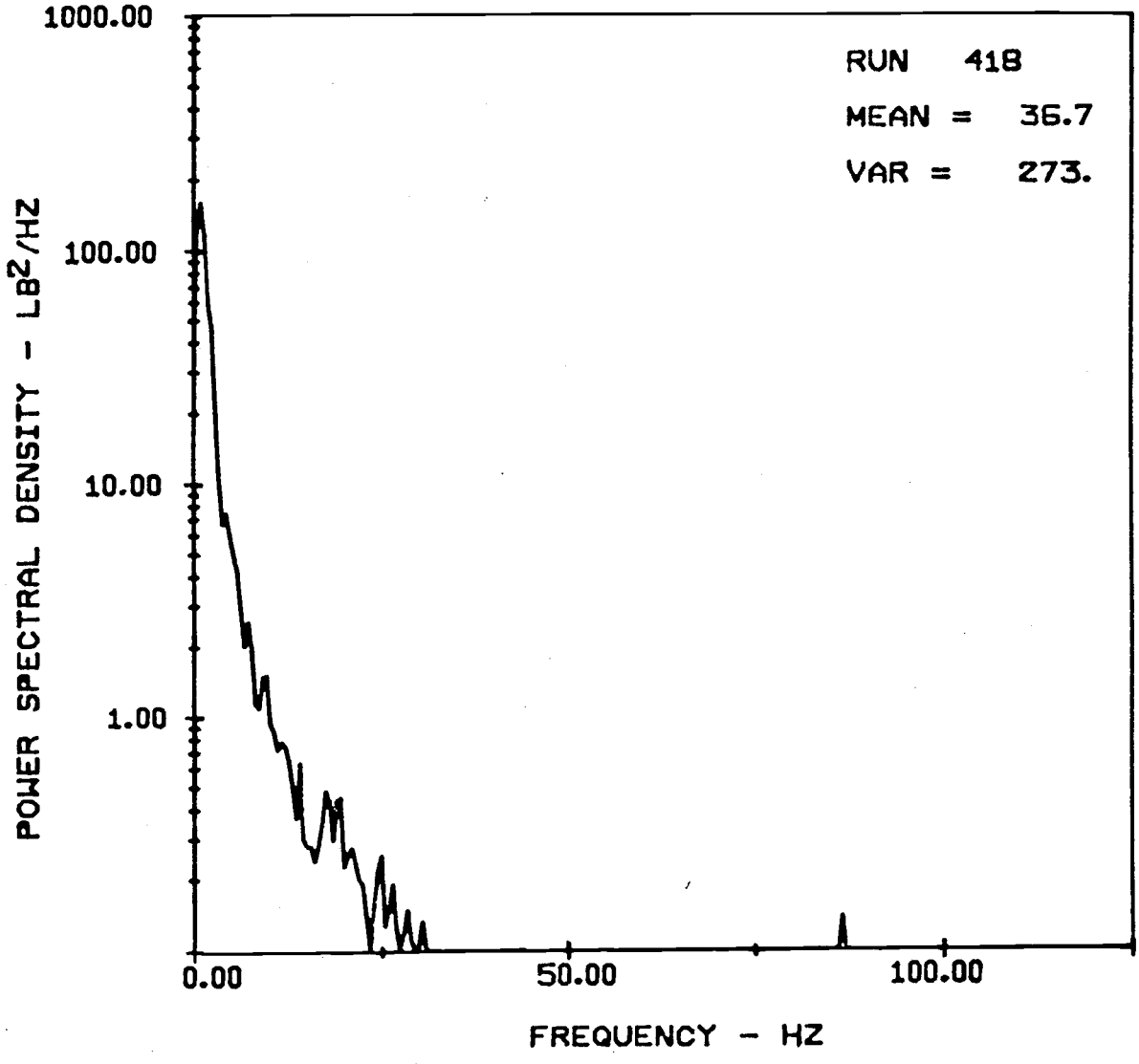


VERTICAL FORCES ON A 10-TUBE ARRAY (V = 5ft/sec)
IN E116 SAND WITH 20" ARRAY HEIGHT AND 4" TUBE SPACING

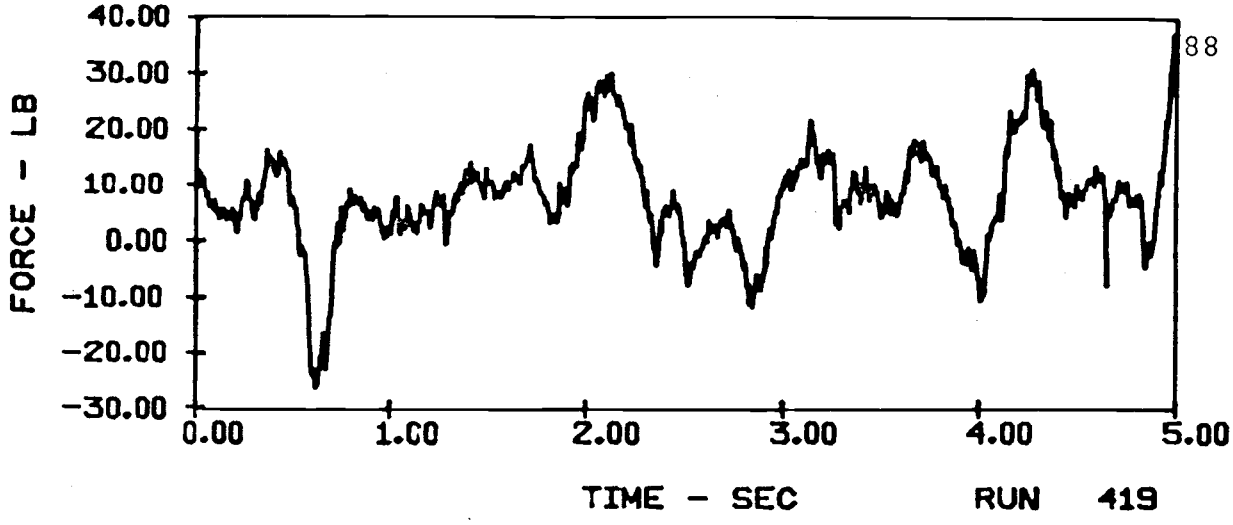


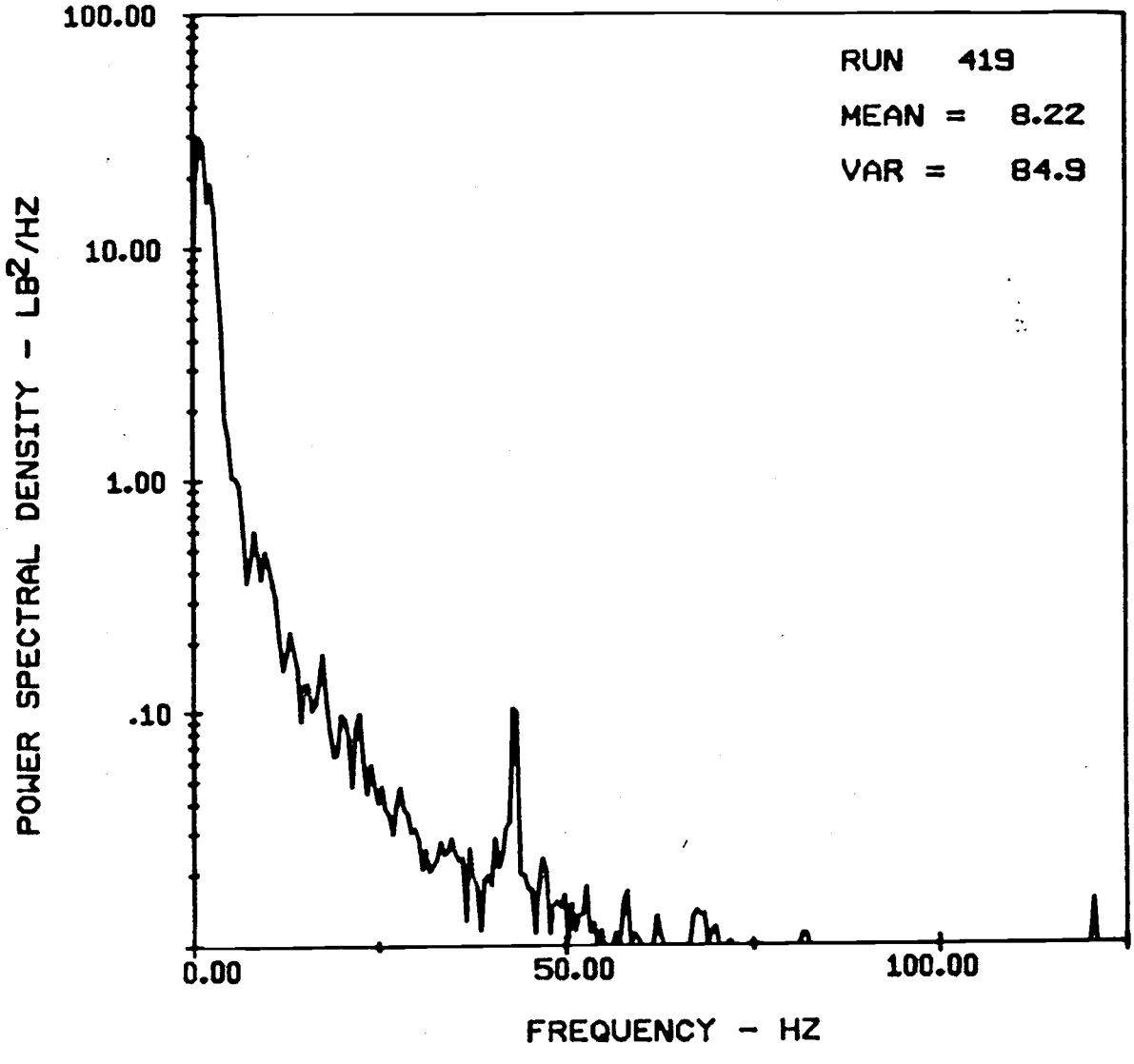


HORIZONTAL FORCES ON A 10-TUBE ARRAY (V = 5 ft/sec)
IN E116 SAND WITH 20" ARRAY HEIGHT AND 4" TUBE SPACING

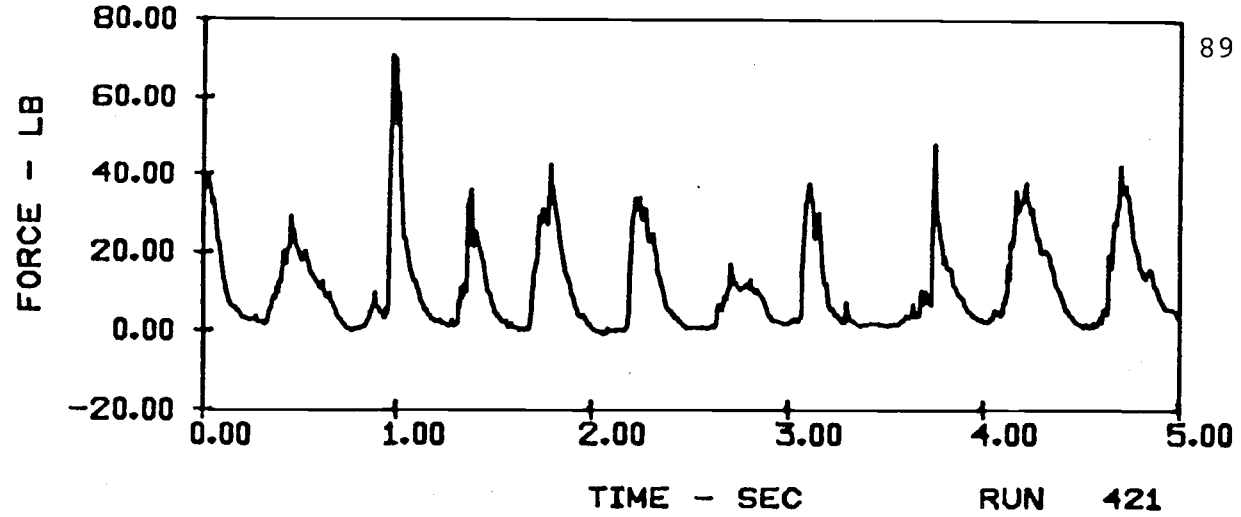


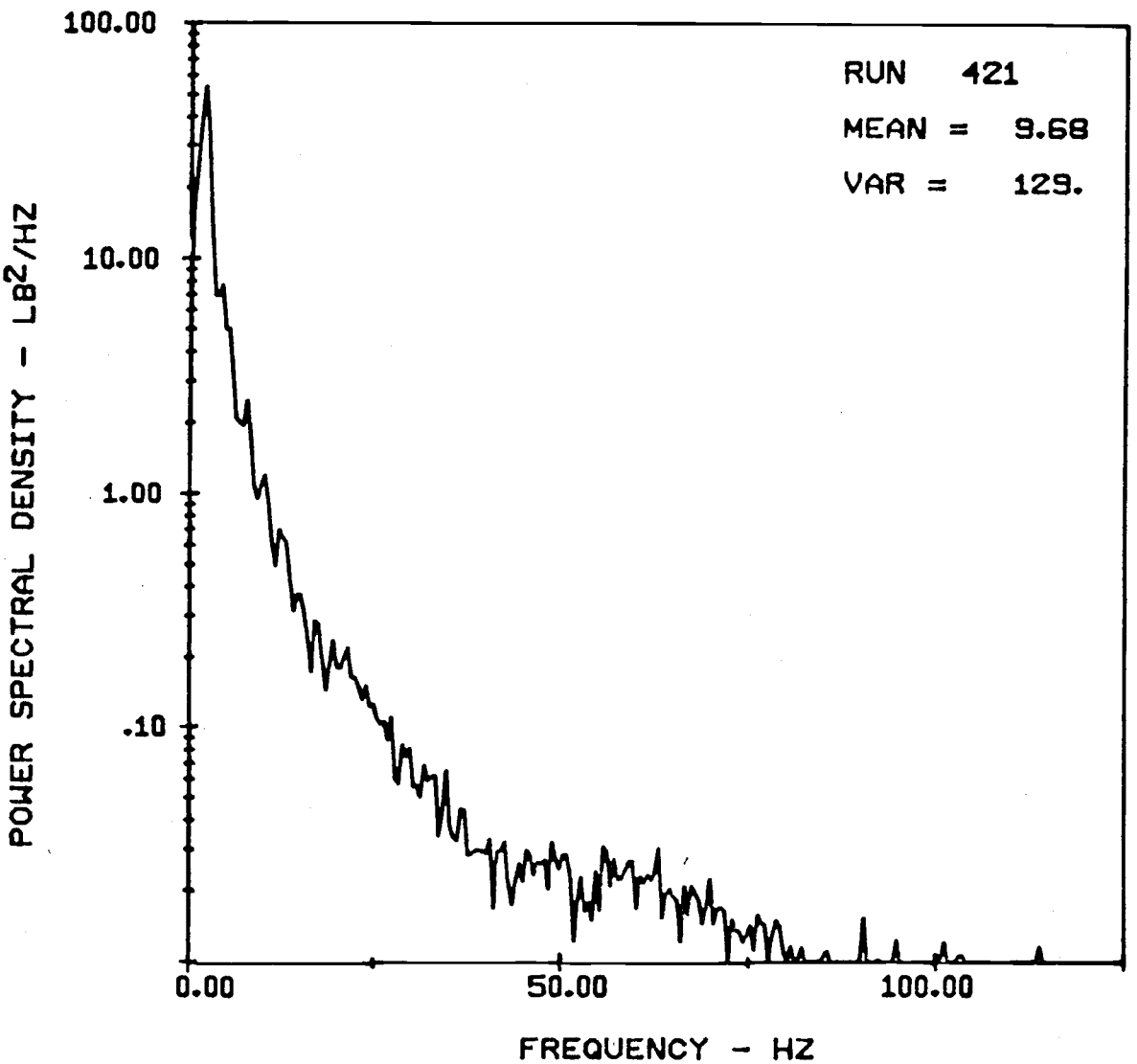


VERTICAL FORCES ON A SINGLE TUBE (V = 7 ft/sec)
IN E116 SAND WITH 20" ARRAY HEIGHT AND 4" TUBE SPACING

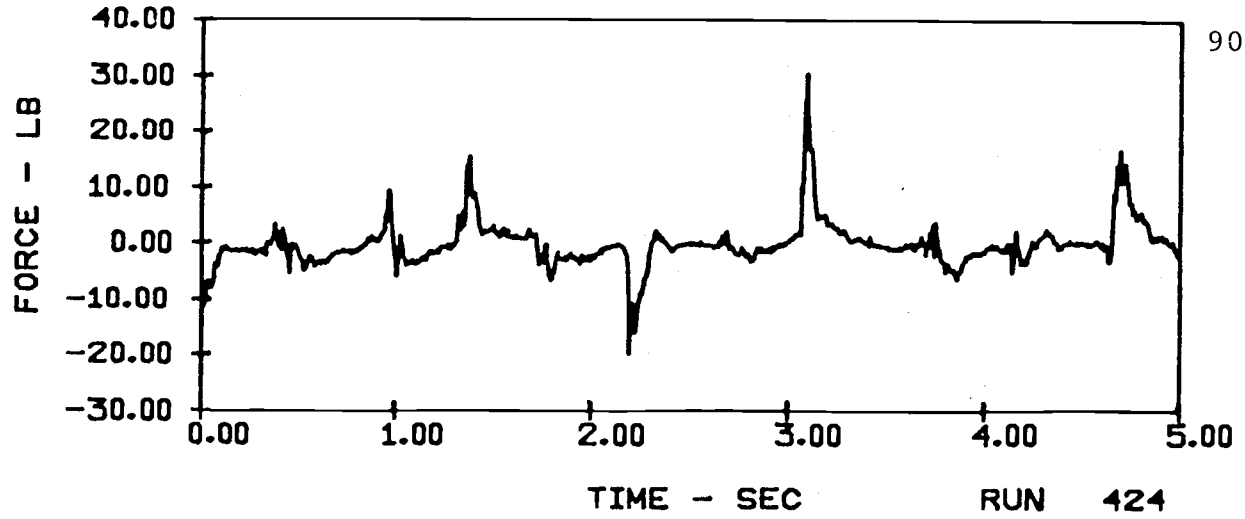


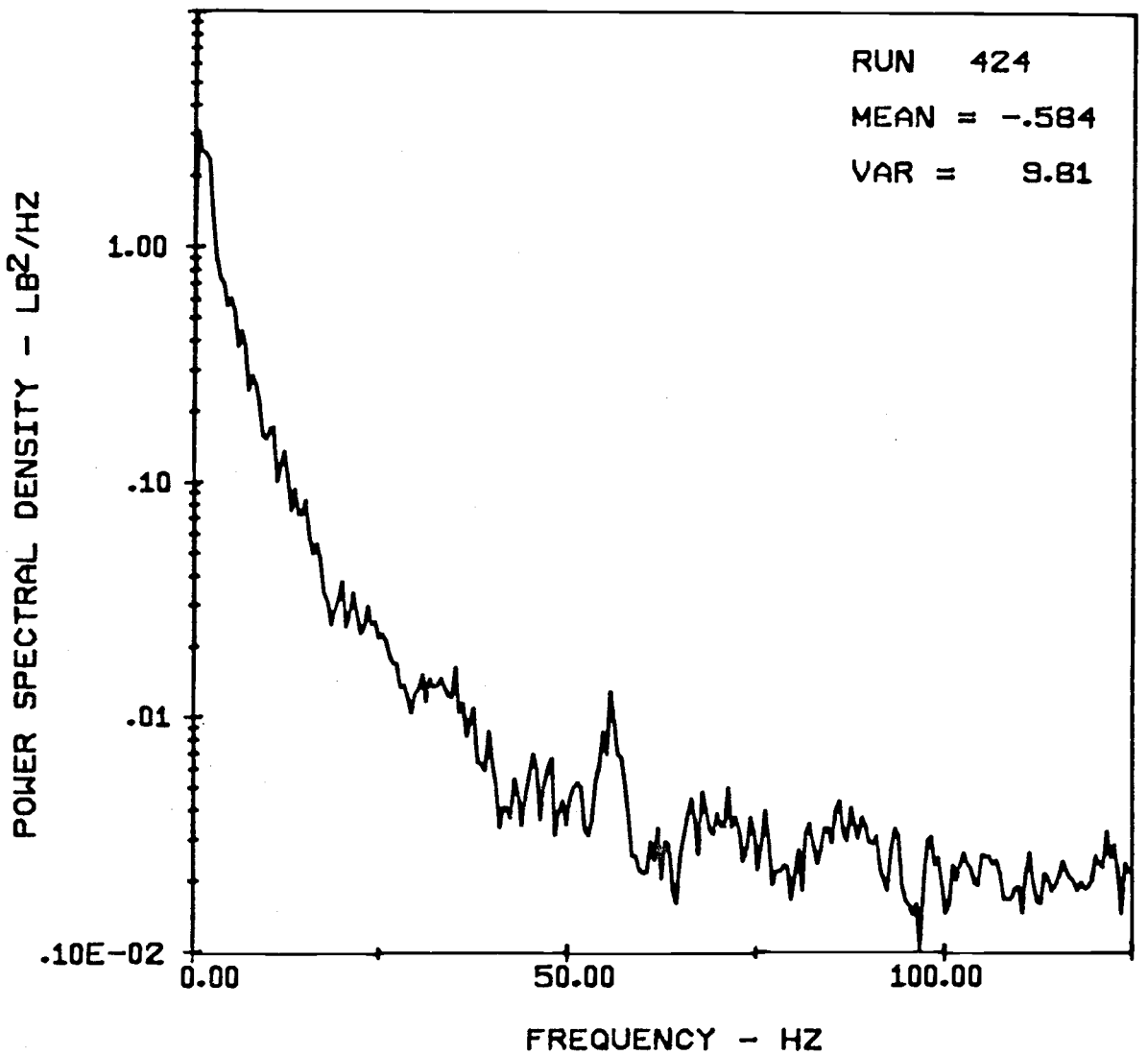


HORIZONTAL FORCES ON A SINGLE TUBE (V = 7 ft/sec)
IN E116 SAND WITH 20'' ARRAY HEIGHT AND 4'' TUBE SPACING

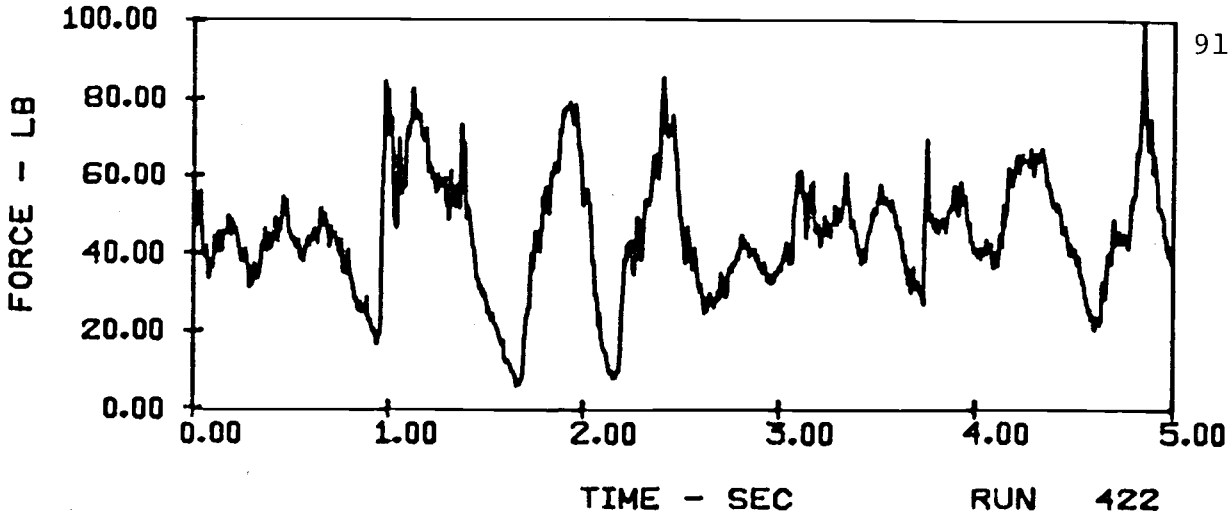


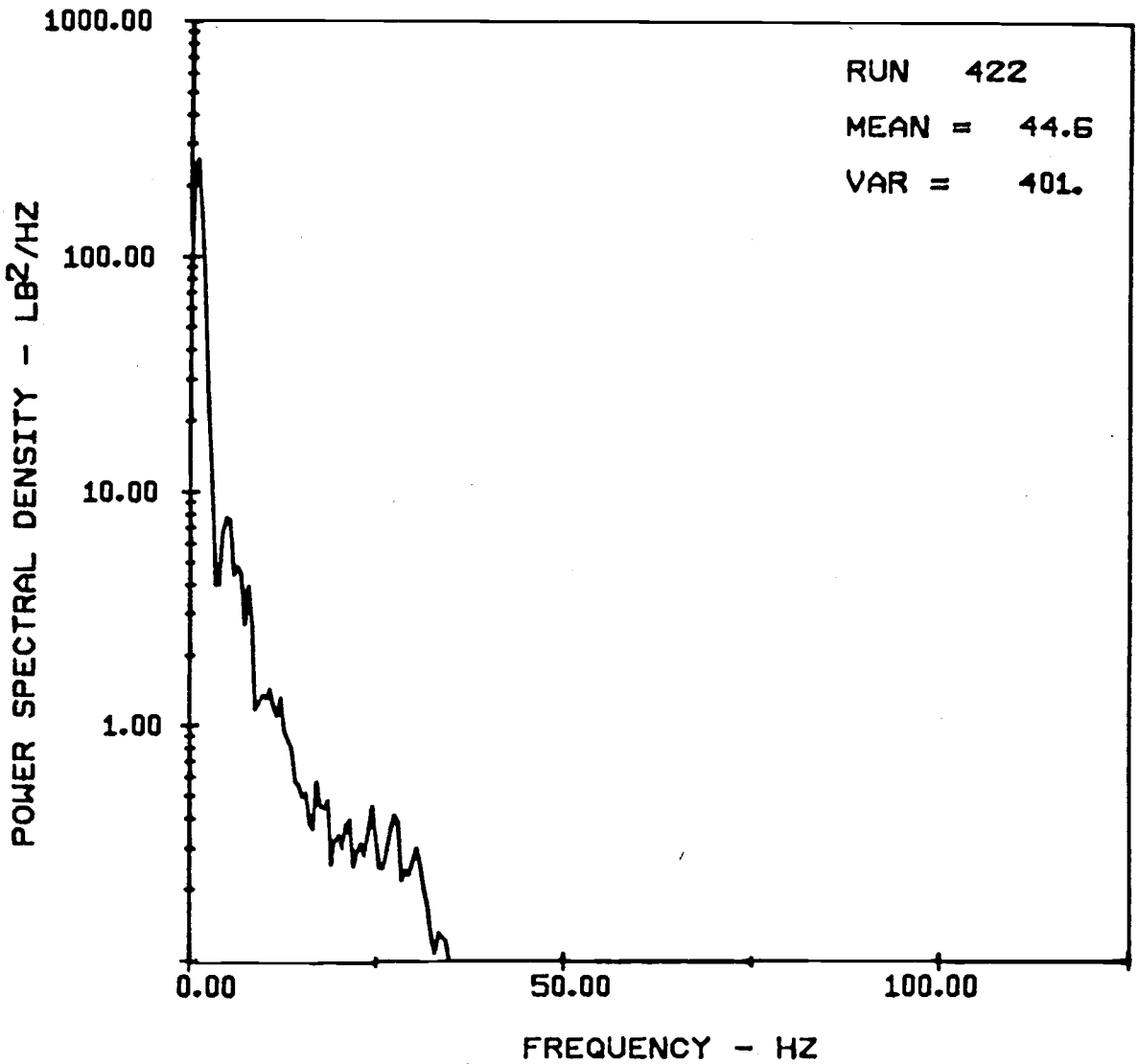


VERTICAL FORCES ON A 10-TUBE ARRAY (V = 7ft/sec)
IN E116 SAND WITH 20" ARRAY HEIGHT AND 4" TUBE SPACING

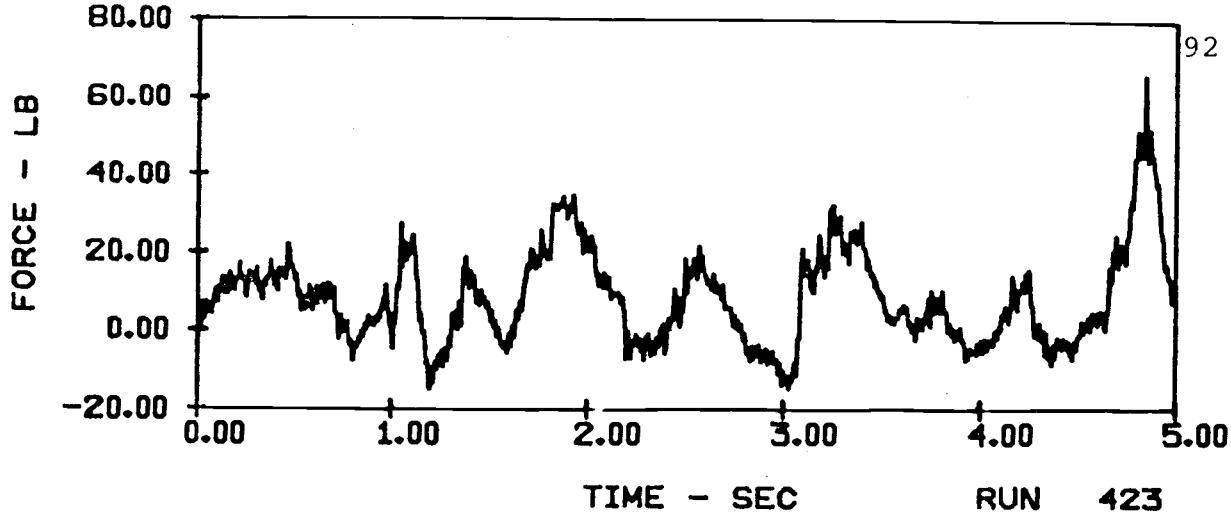


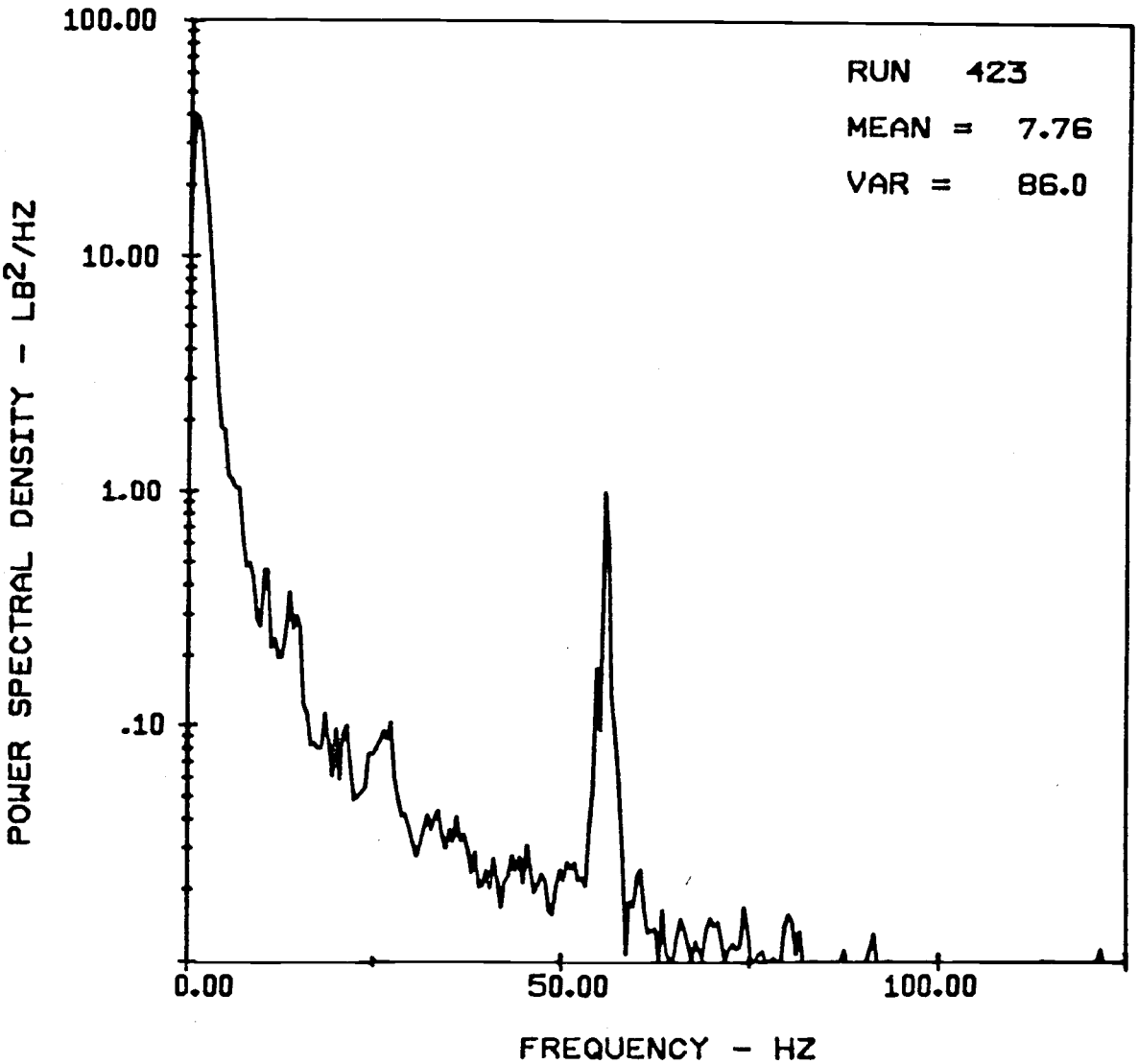


HORIZONTAL FORCES ON A 10-TUBE ARRAY (V = 7 ft/sec)
IN E116 SAND WITH 20" ARRAY HEIGHT AND 4" TUBE SPACING

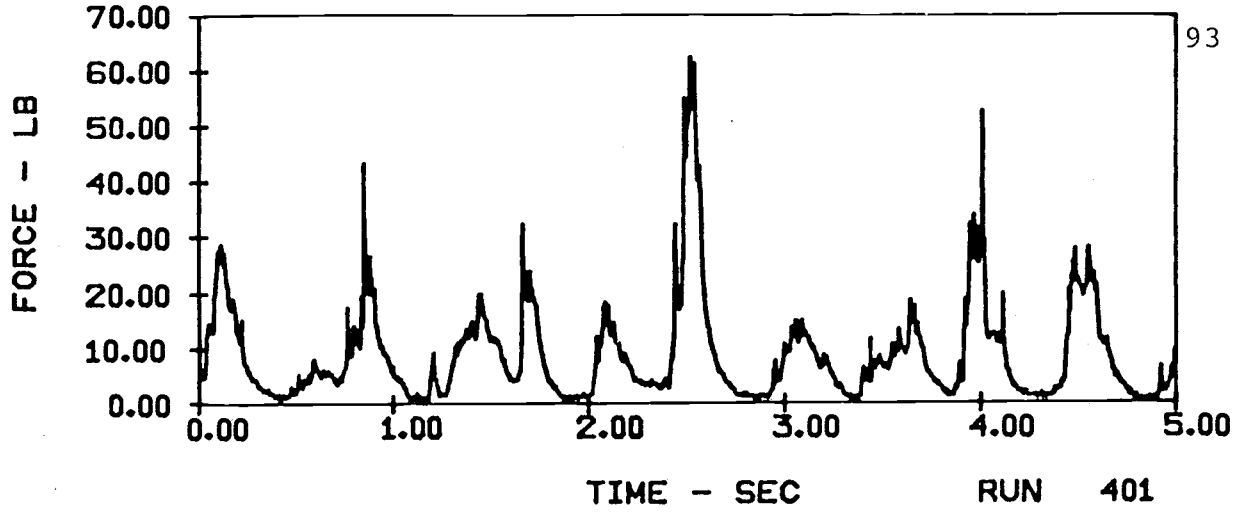


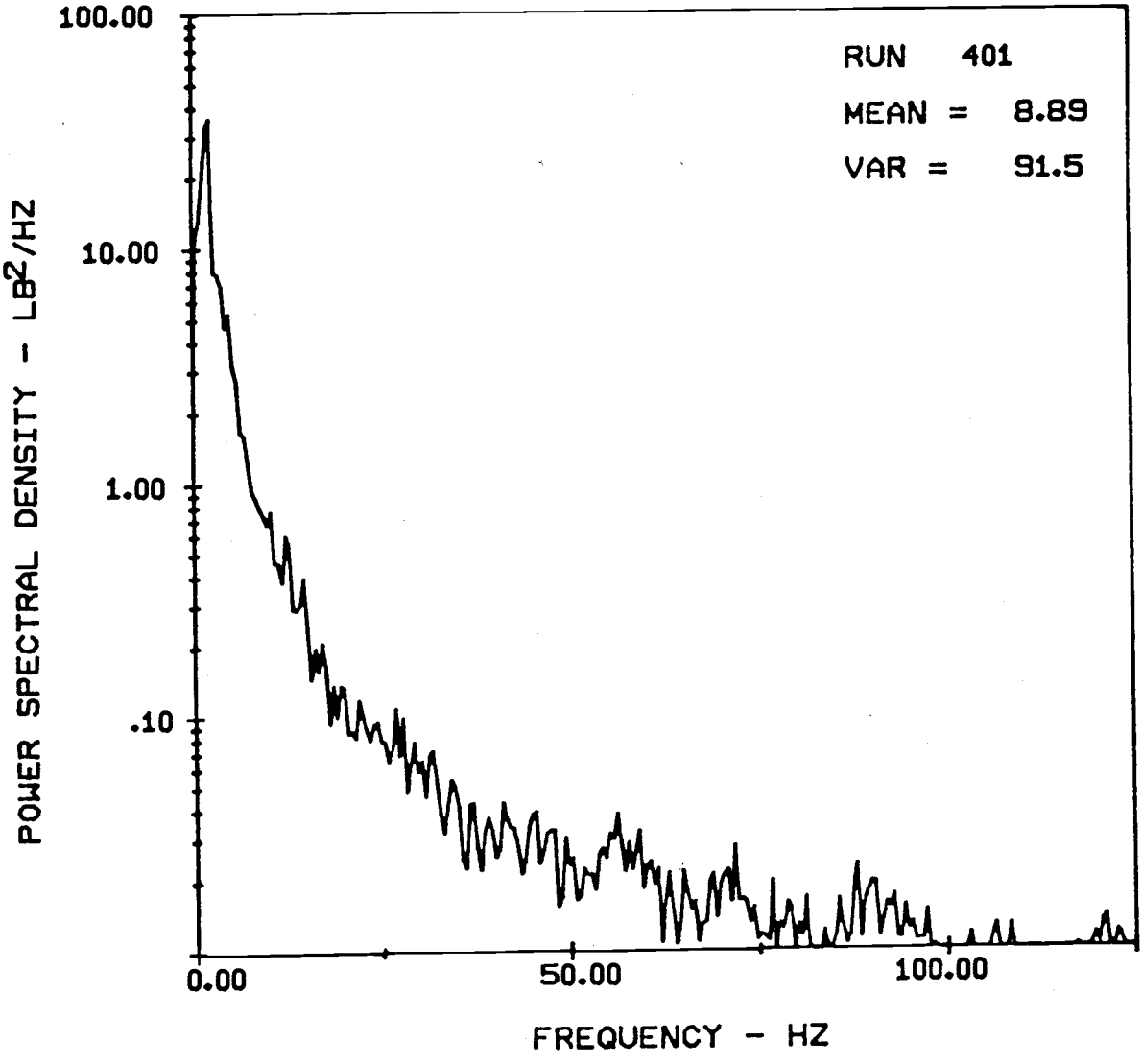


VERTICAL FORCES ON A SINGLE TUBE (V = 9 ft/sec)
IN E116 SAND WITH 20" ARRAY HEIGHT AND 4" TUBE SPACING

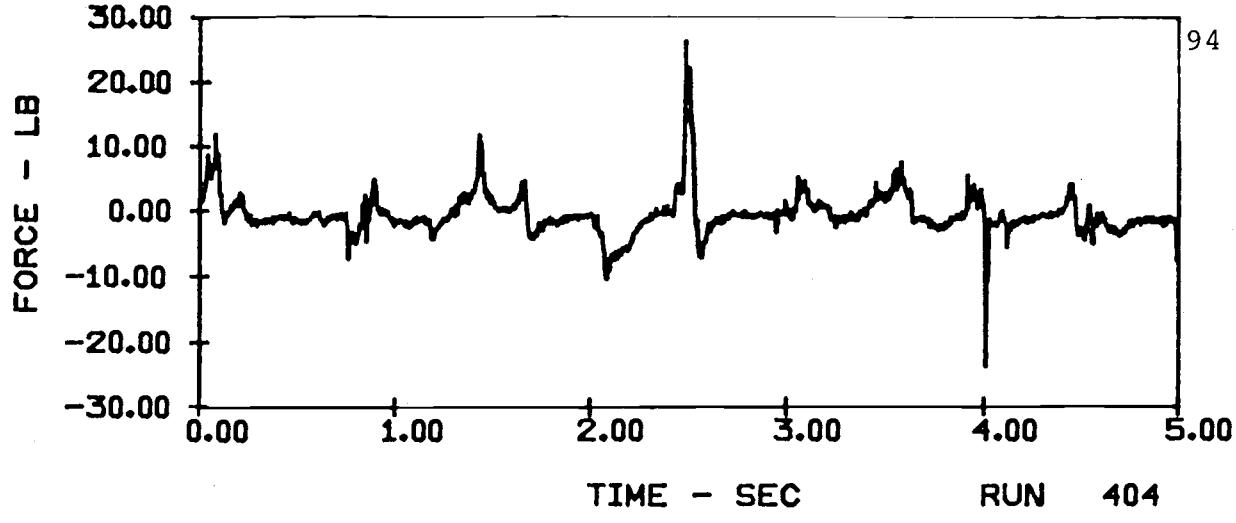


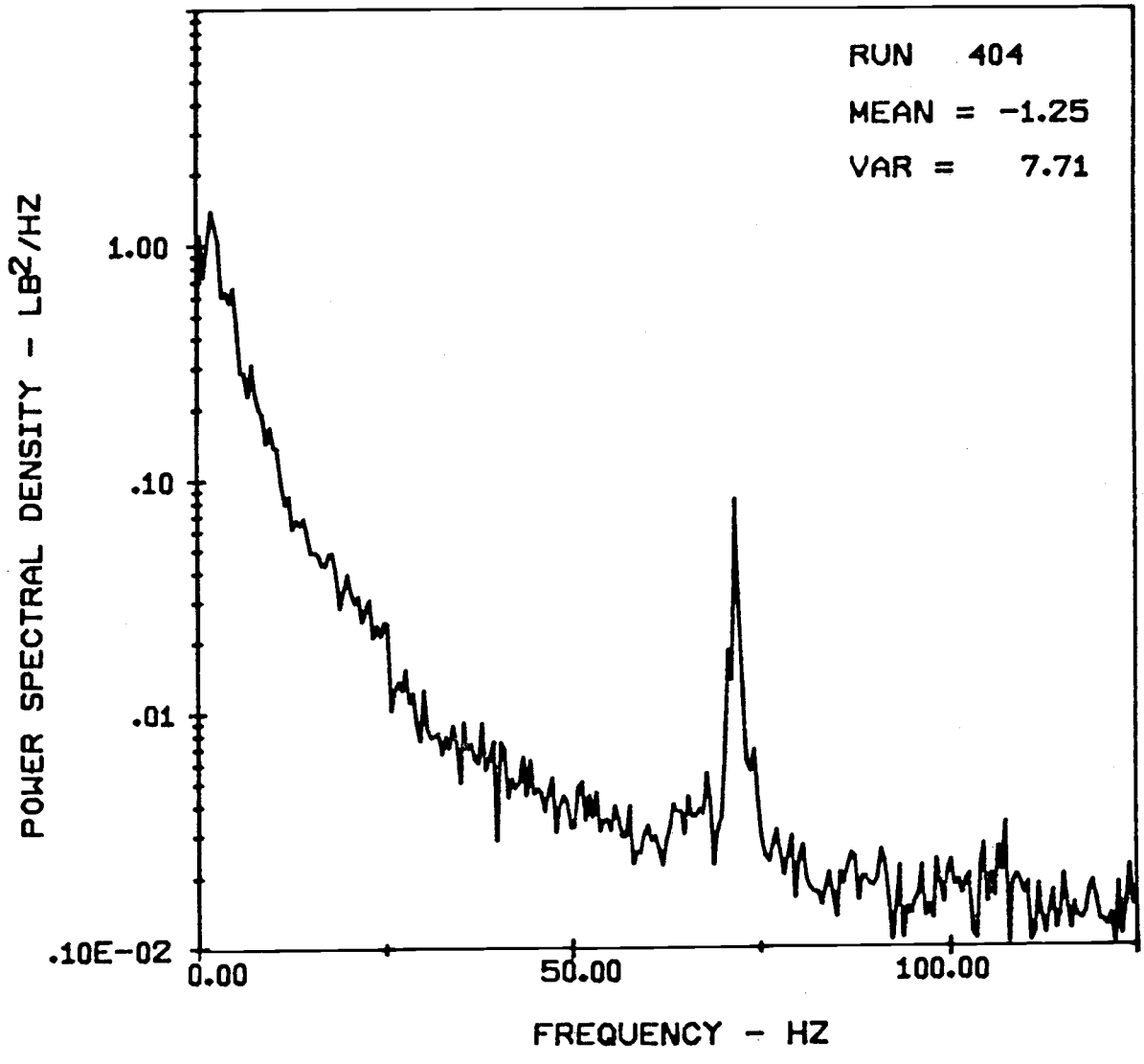


HORIZONTAL FORCES ON A SINGLE TUBE (V = 9 ft/sec)
IN E116 SAND WITH 20" ARRAY HEIGHT AND 4" TUBE SPACING

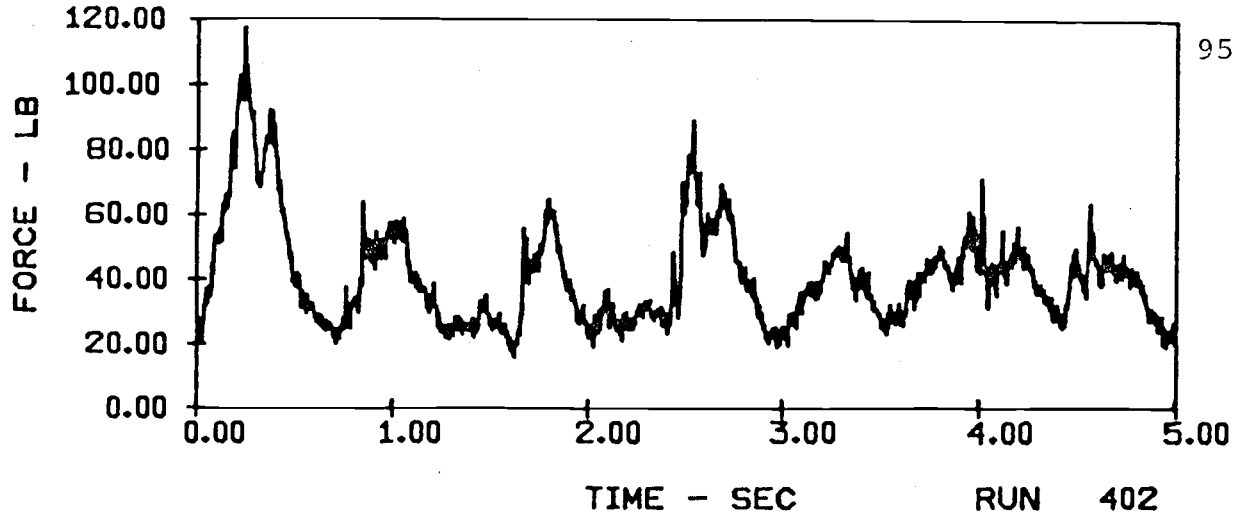


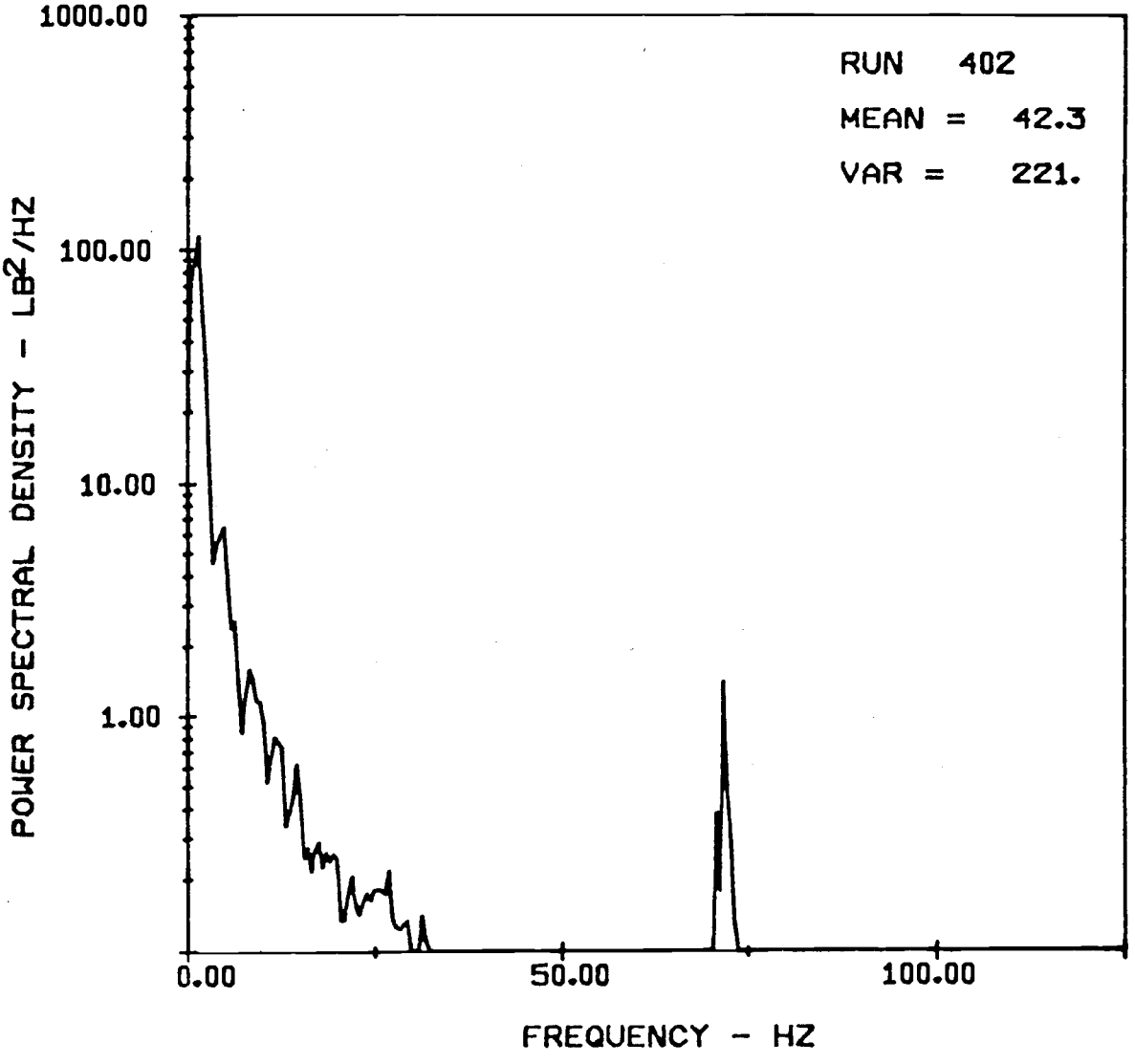


VERTICAL FORCES ON A 10-TUBE ARRAY (V = 9ft/sec)
IN E116 SAND WITH 20" ARRAY HEIGHT AND 4" TUBE SPACING

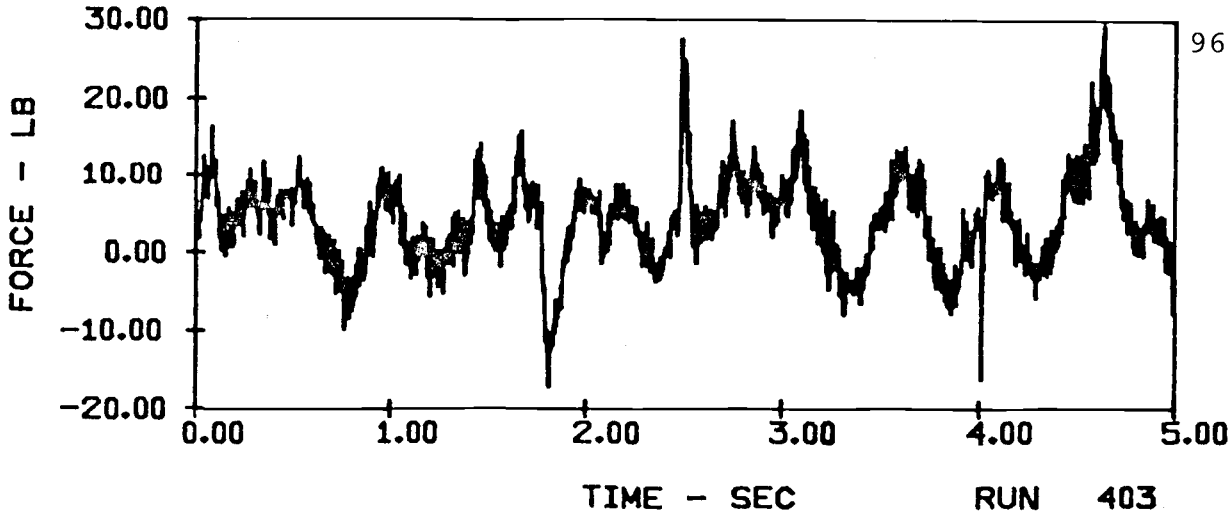


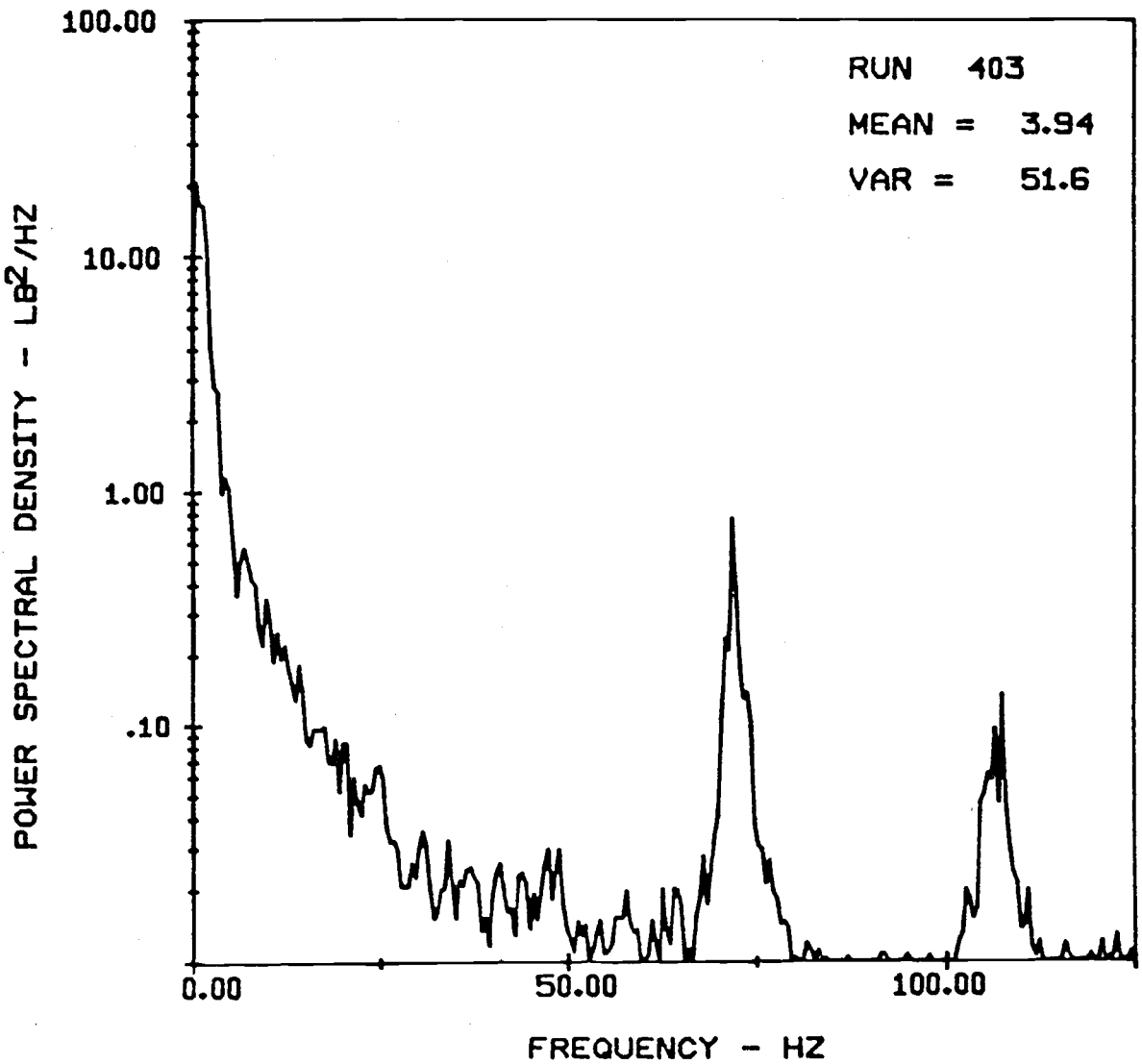


HORIZONTAL FORCES ON A 10-TUBE ARRAY (V = 9 ft/sec)
IN E116 SAND WITH 20" ARRAY HEIGHT AND 4" TUBE SPACING

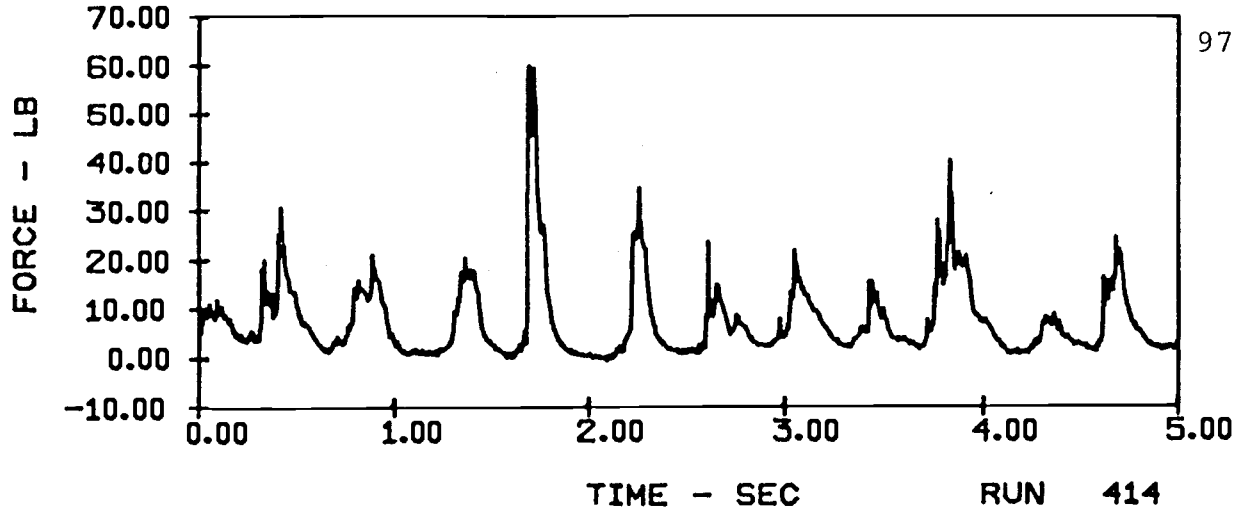


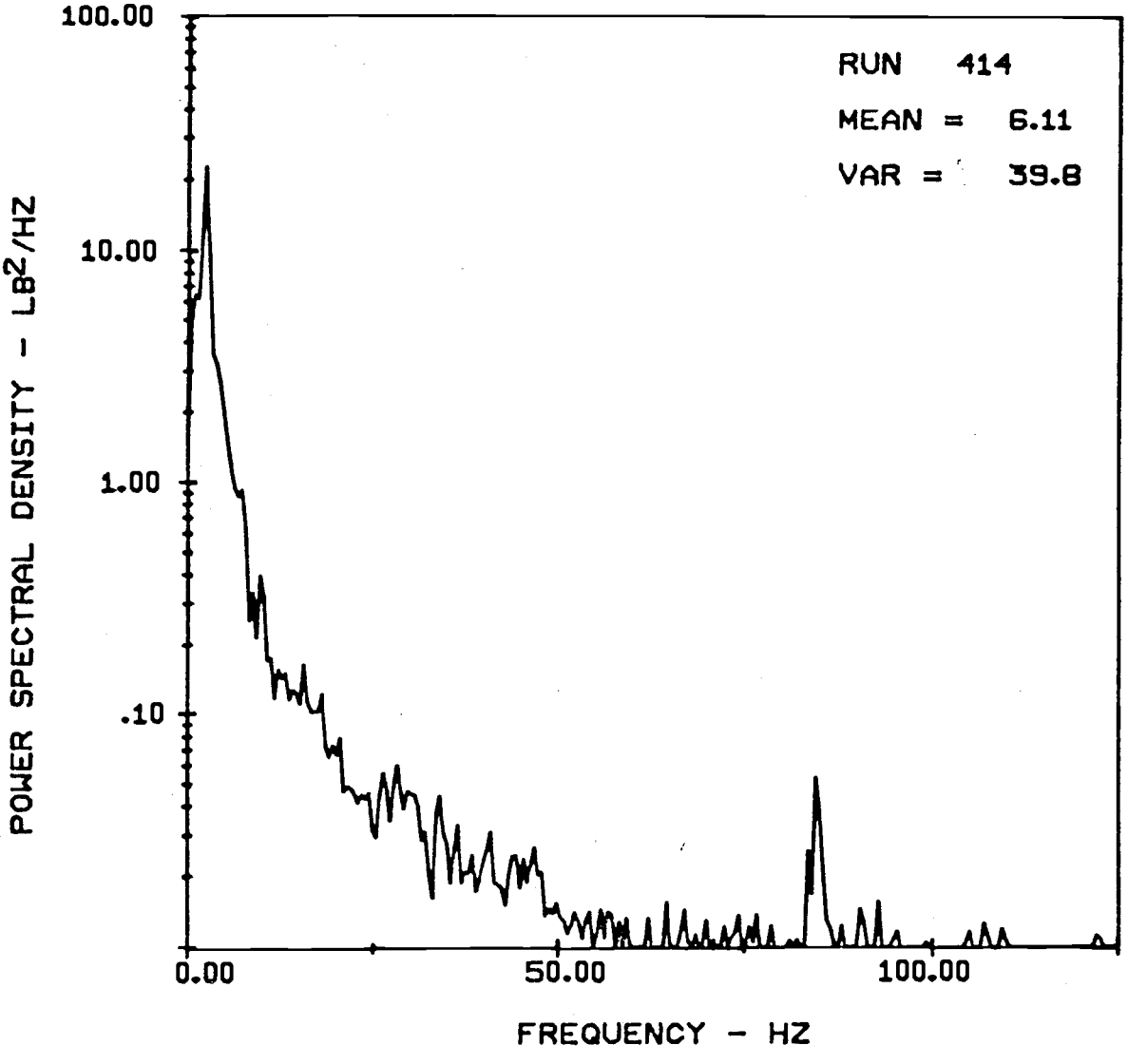


VERTICAL FORCES ON A SINGLE TUBE (V = 11 ft/sec)
IN E116 SAND WITH 20" ARRAY HEIGHT AND 4" TUBE SPACING

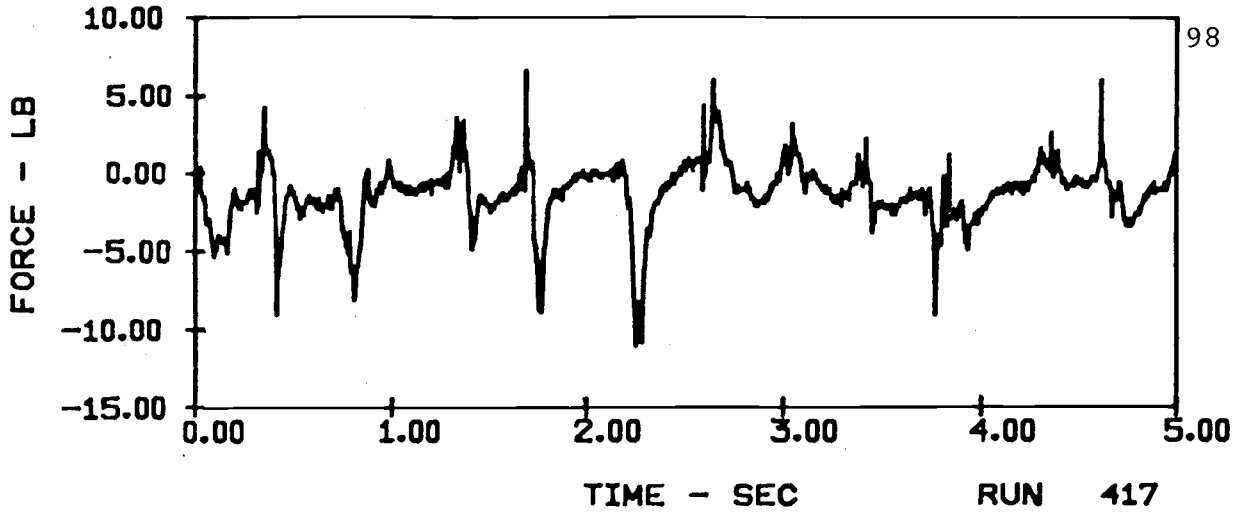


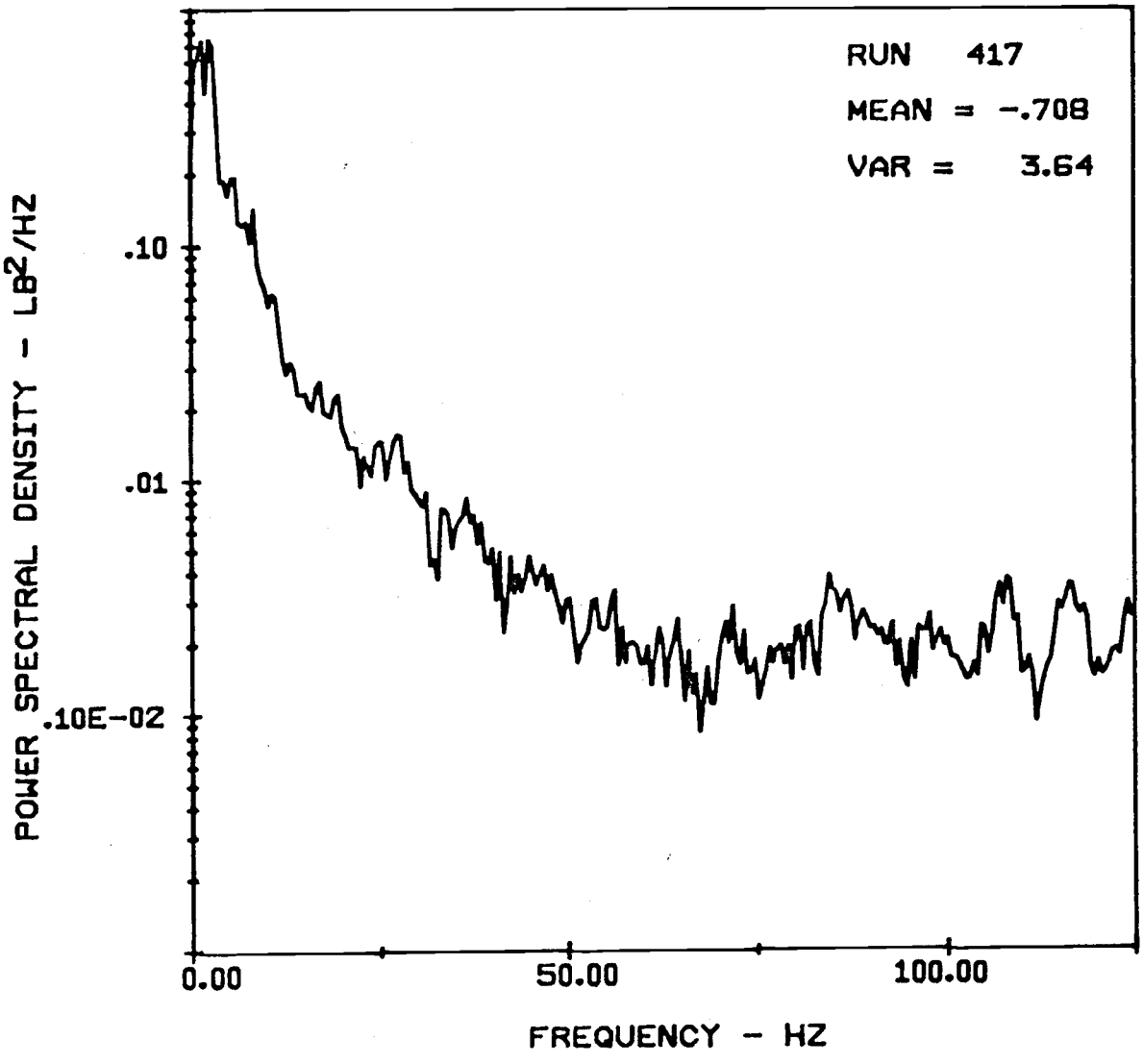


HORIZONTAL FORCES ON A SINGLE TUBE (V = 11 ft/sec)
IN E116 SAND WITH 20" ARRAY HEIGHT AND 4" TUBE SPACING

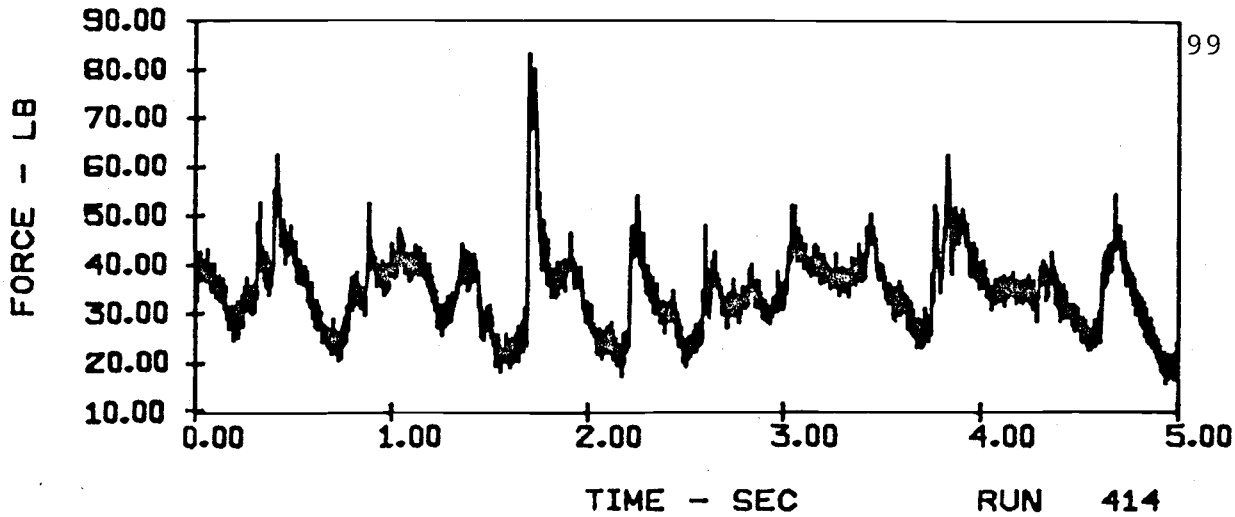


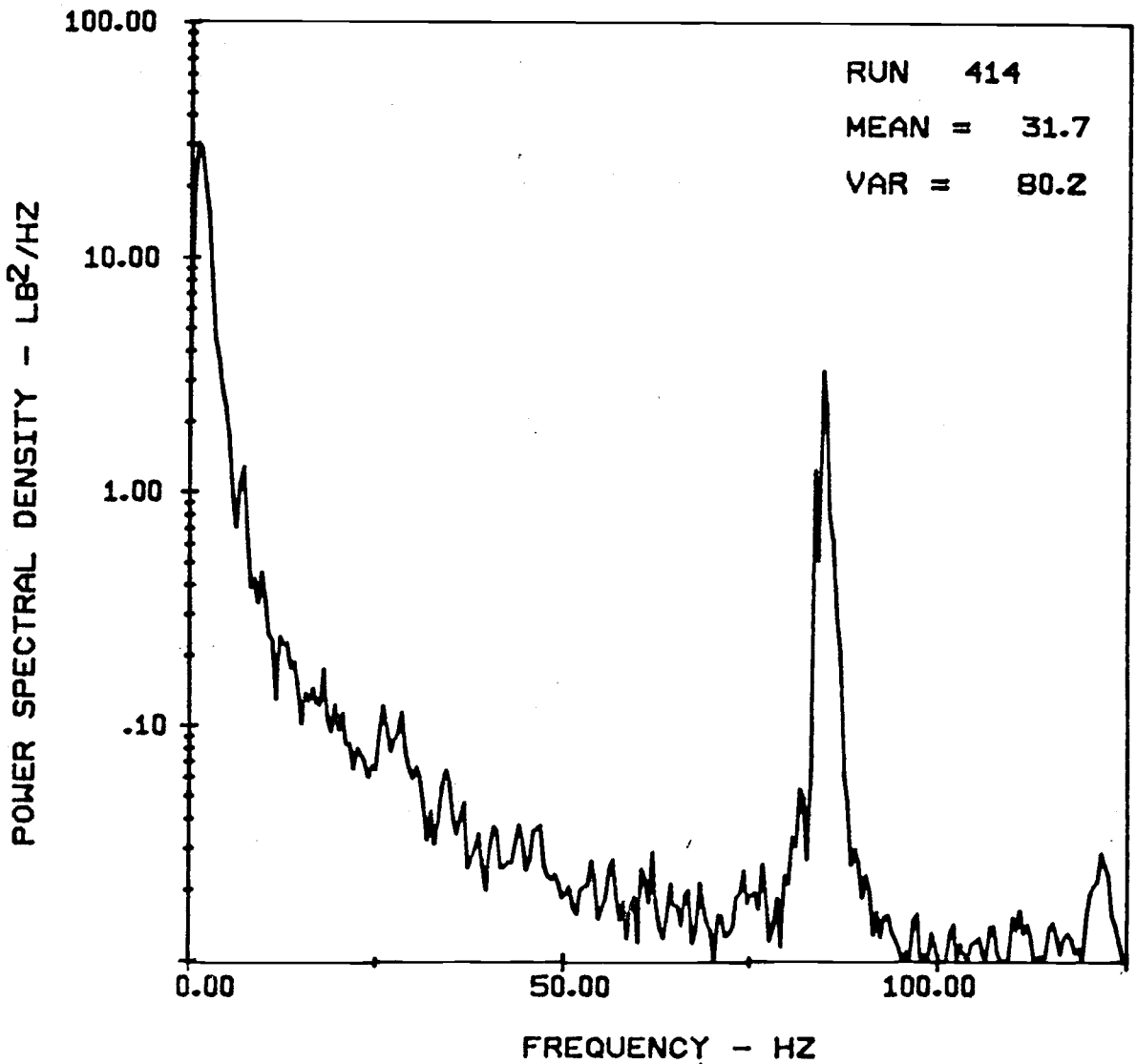


VERTICAL FORCES ON A 10-TUBE ARRAY (V = 11ft/sec)
IN E116 SAND WITH 20" ARRAY HEIGHT AND 4" TUBE SPACING

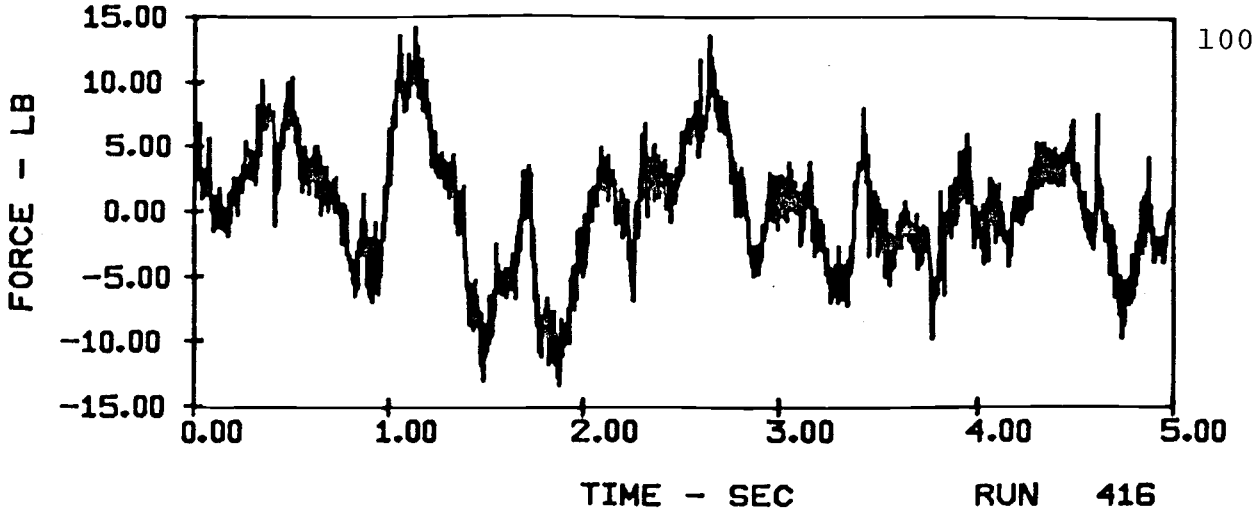


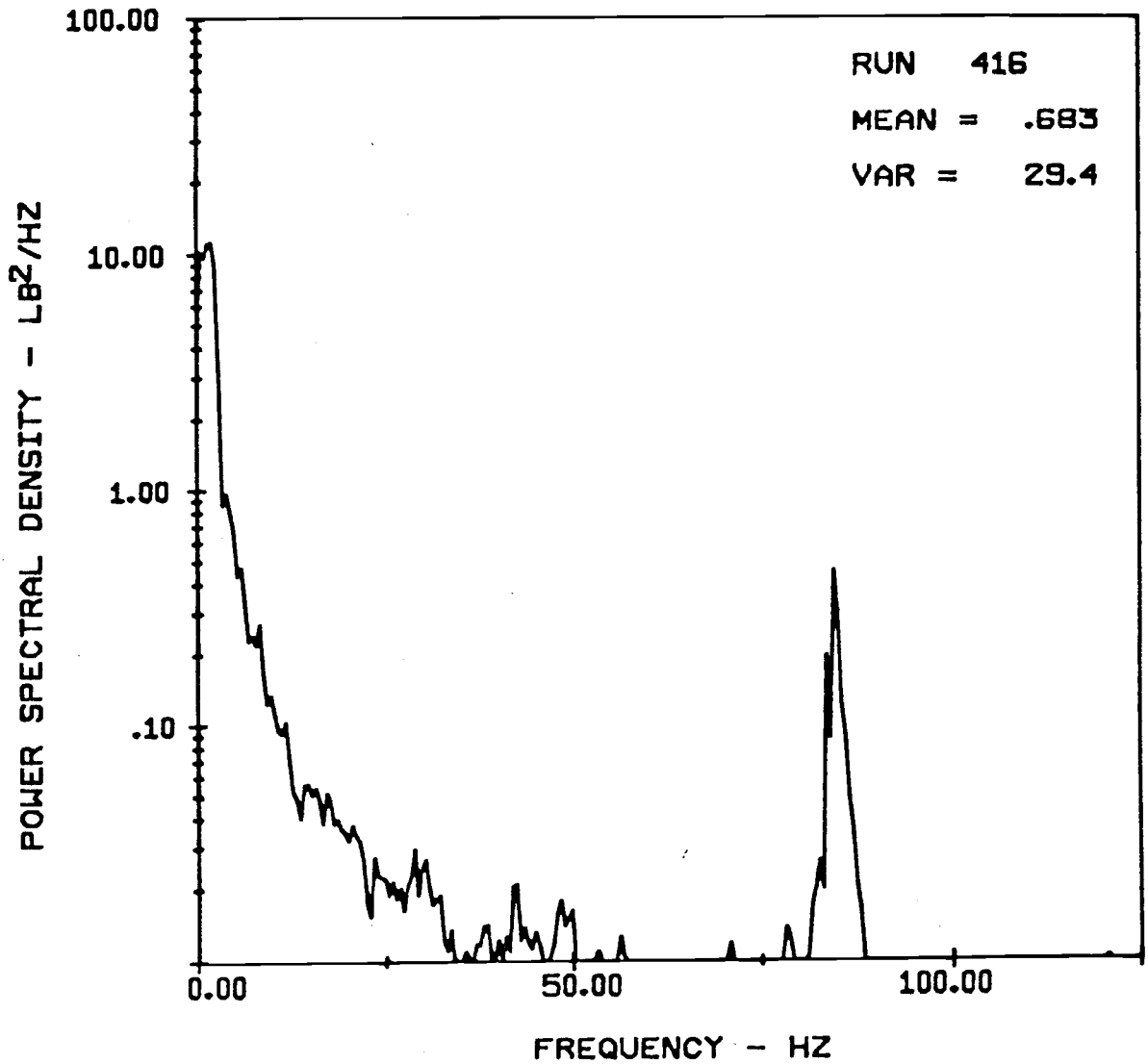


HORIZONTAL FORCES ON A 10-TUBE ARRAY (V = 11 ft/sec)
IN E116 SAND WITH 20" ARRAY HEIGHT AND 4" TUBE SPACING

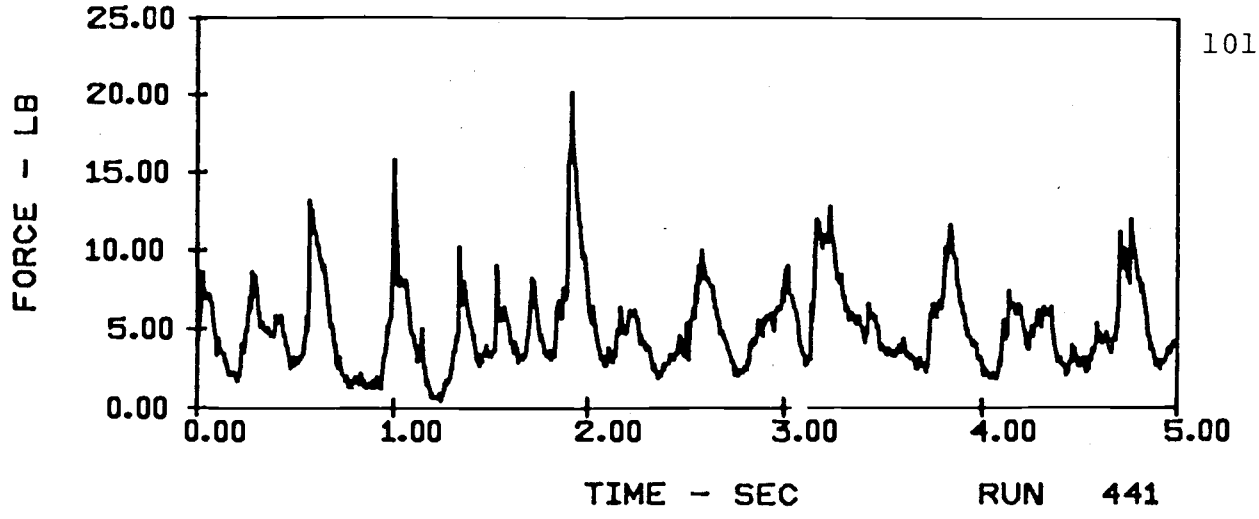


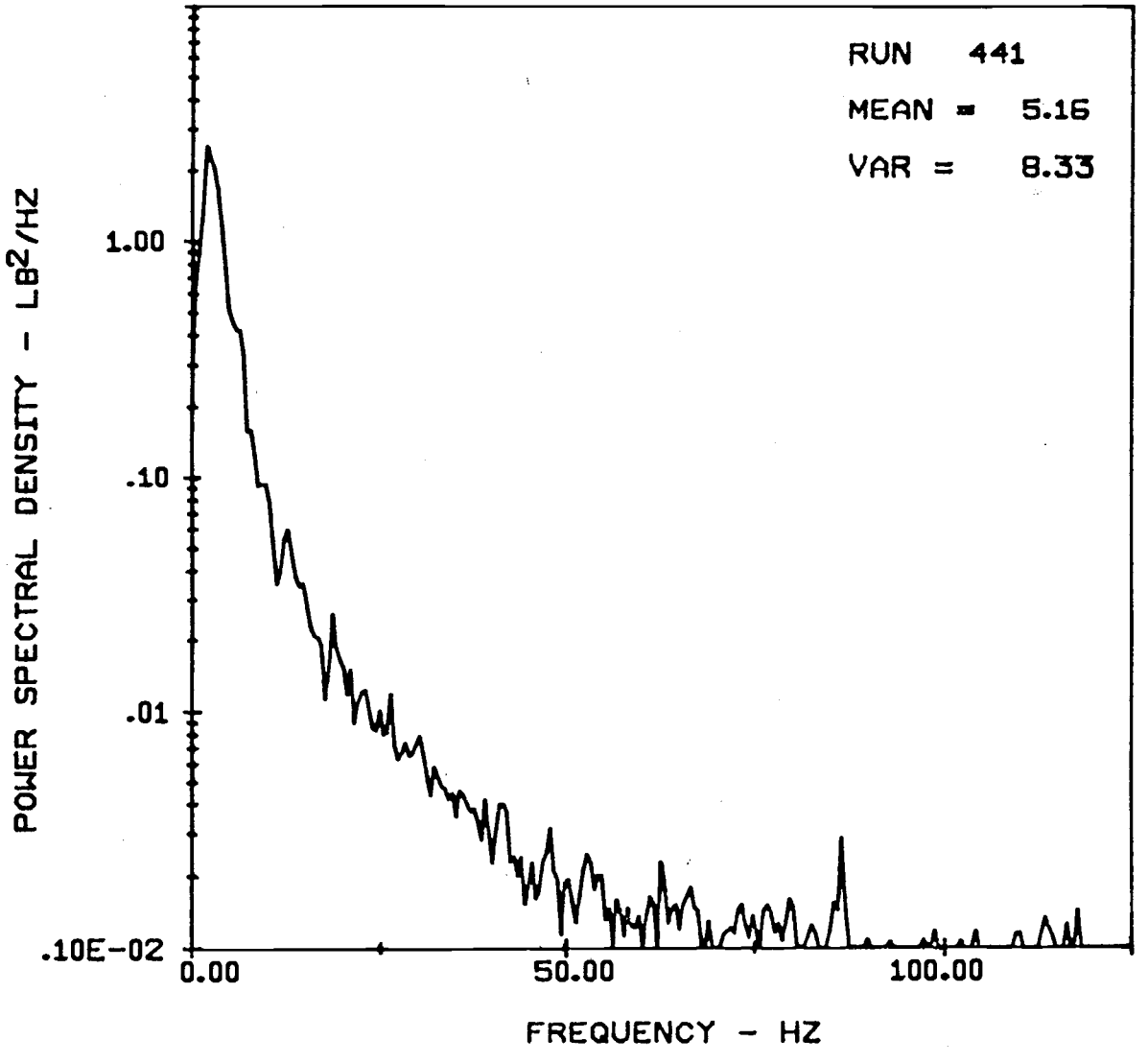


VERTICAL FORCES ON A SINGLE TUBE (V = 5 ft/sec)
IN E18 SAND WITH 10" ARRAY HEIGHT AND 4" TUBE SPACING

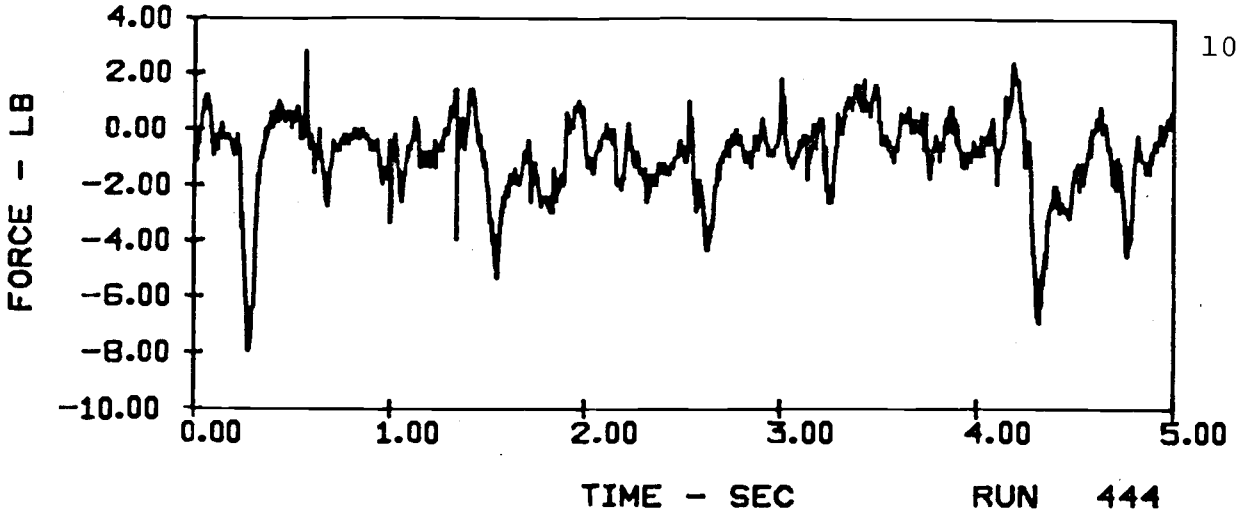


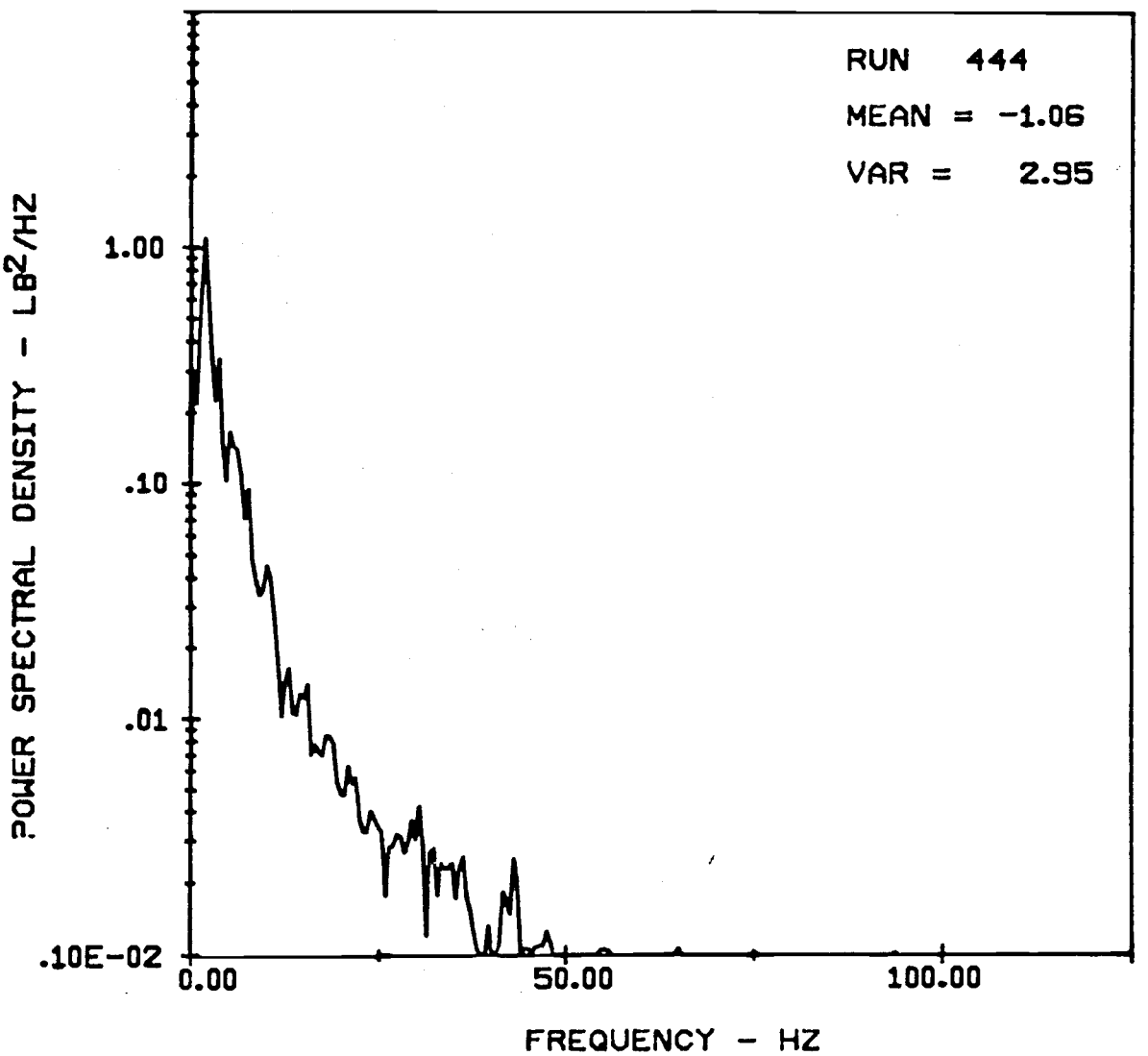


HORIZONTAL FORCES ON A SINGLE TUBE (V = 5 ft/sec)
IN E18 SAND WITH 10" ARRAY HEIGHT AND 4" TUBE SPACING

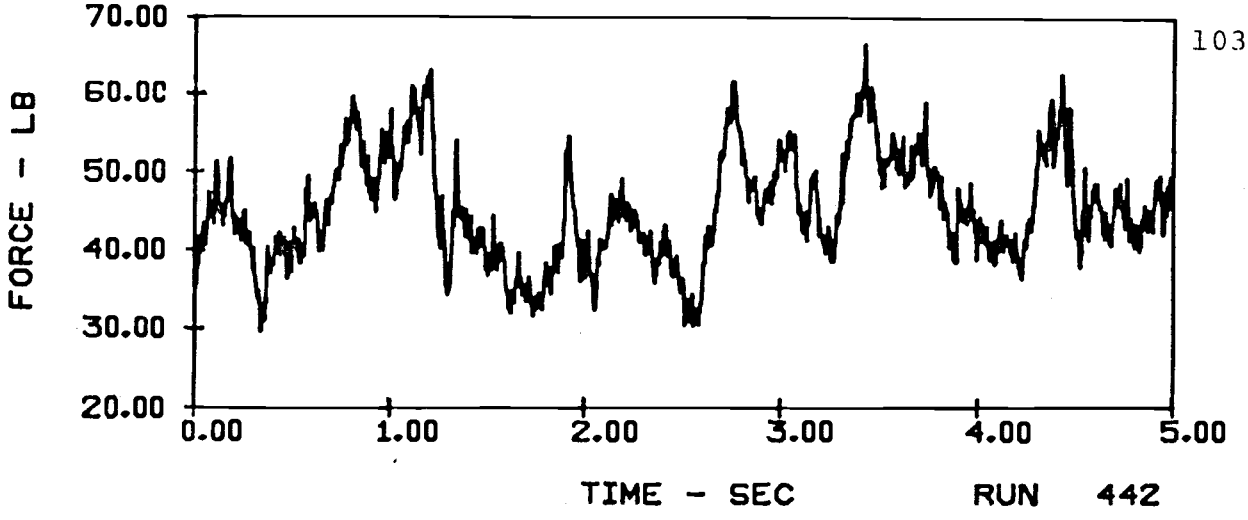


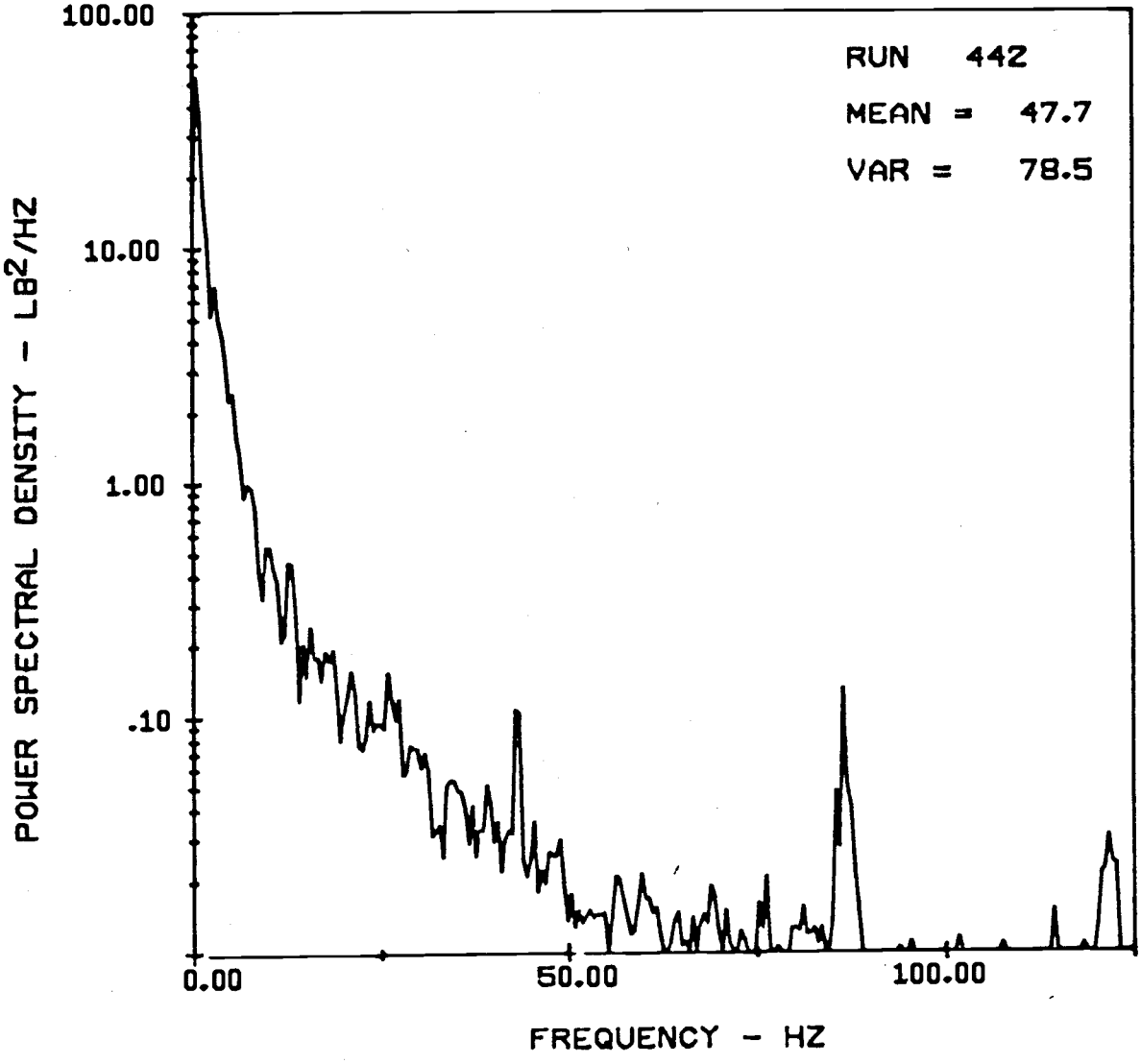


VERTICAL FORCES ON A 10-TUBE ARRAY (V = 5ft/sec)
IN E18 SAND WITH 10" ARRAY HEIGHT AND 4" TUBE SPACING

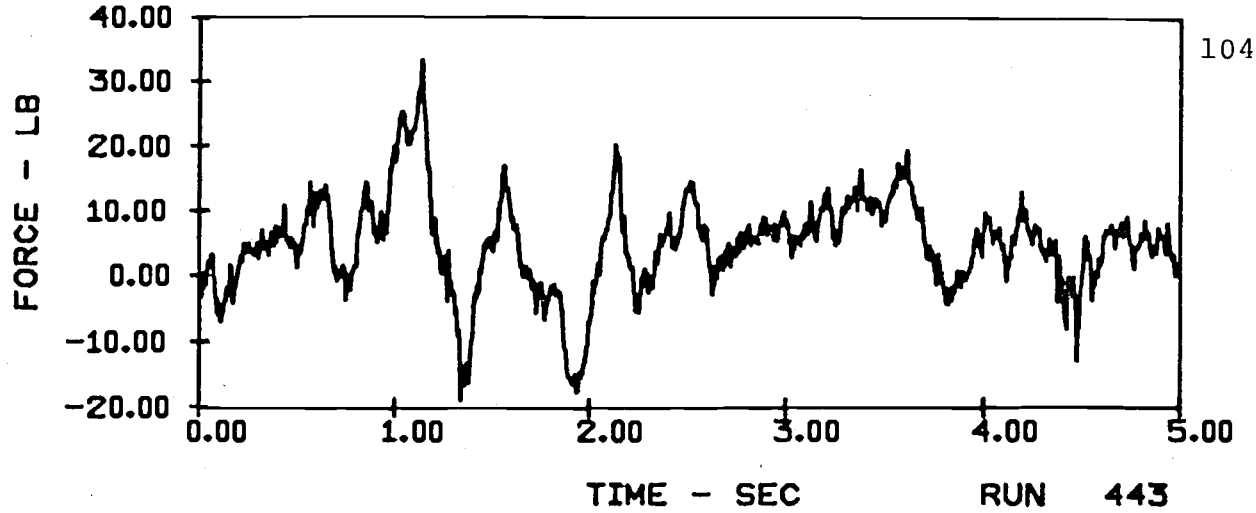


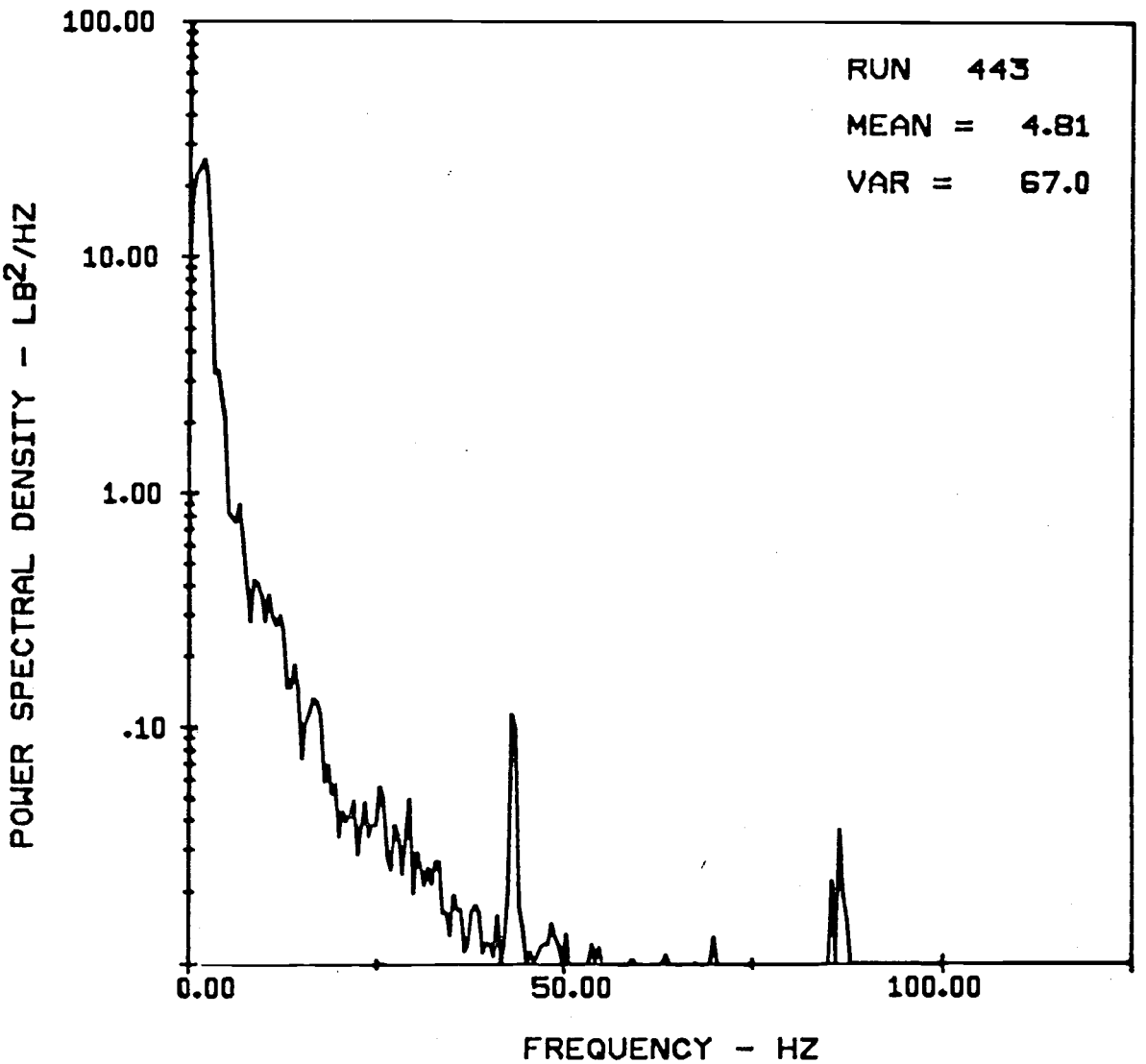


HORIZONTAL FORCES ON A 10-TUBE ARRAY (V = 5 ft/sec)
IN E18 SAND WITH 10" ARRAY HEIGHT AND 4" TUBE SPACING

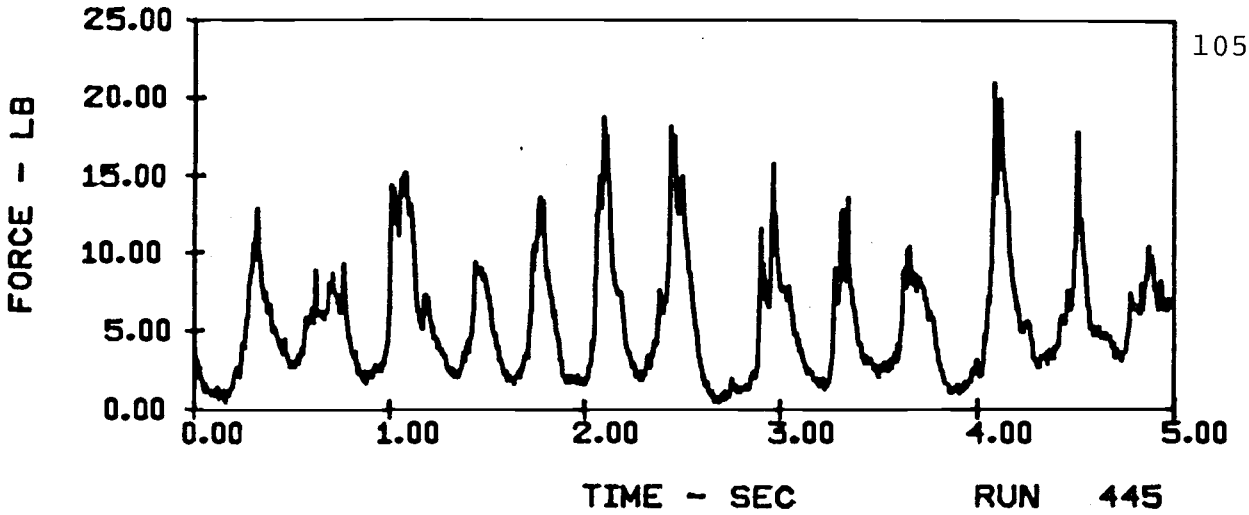


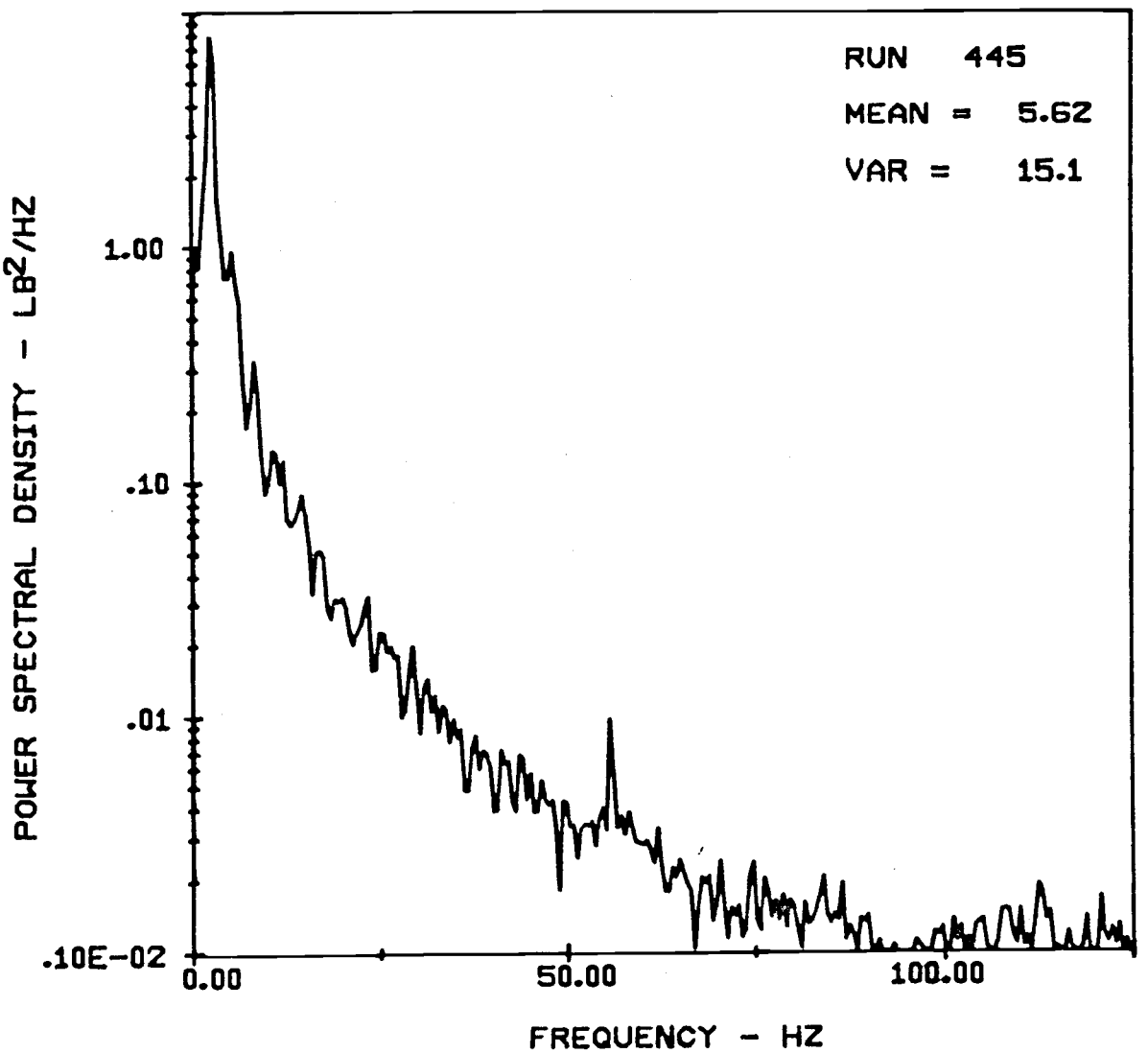


VERTICAL FORCES ON A SINGLE TUBE (V = 7 ft/sec)
IN E18 SAND WITH 10" ARRAY HEIGHT AND 4" TUBE SPACING

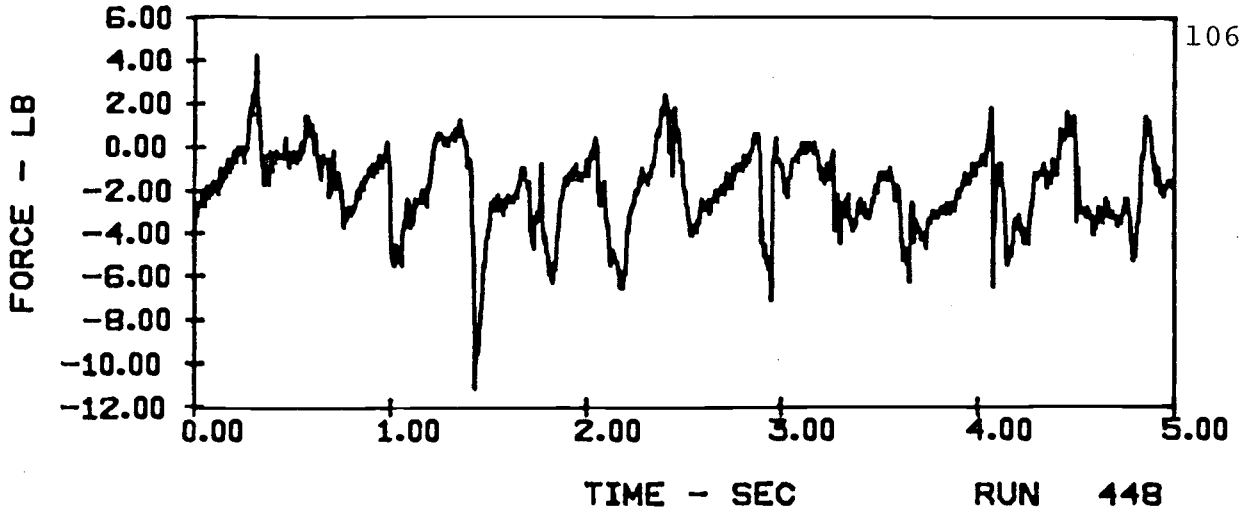


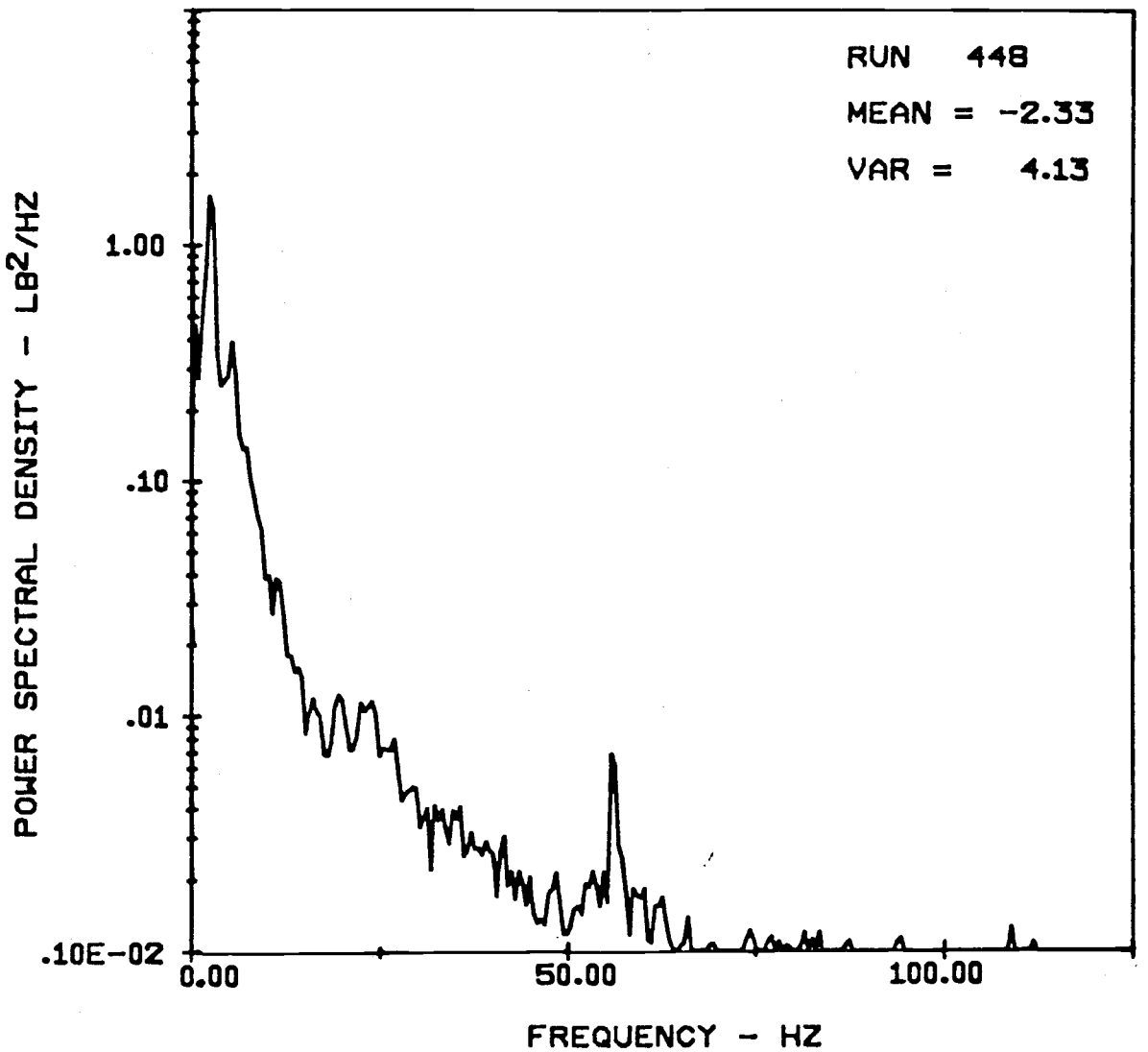


HORIZONTAL FORCES ON A SINGLE TUBE (V = 7 ft/sec)
IN E18 SAND WITH 10" ARRAY HEIGHT AND 4" TUBE SPACING

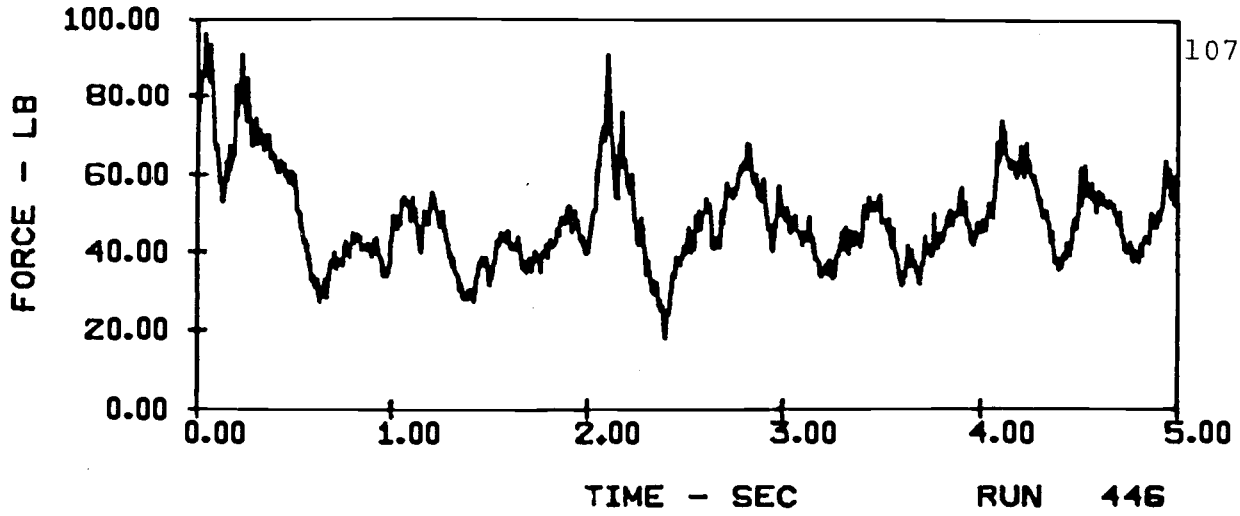


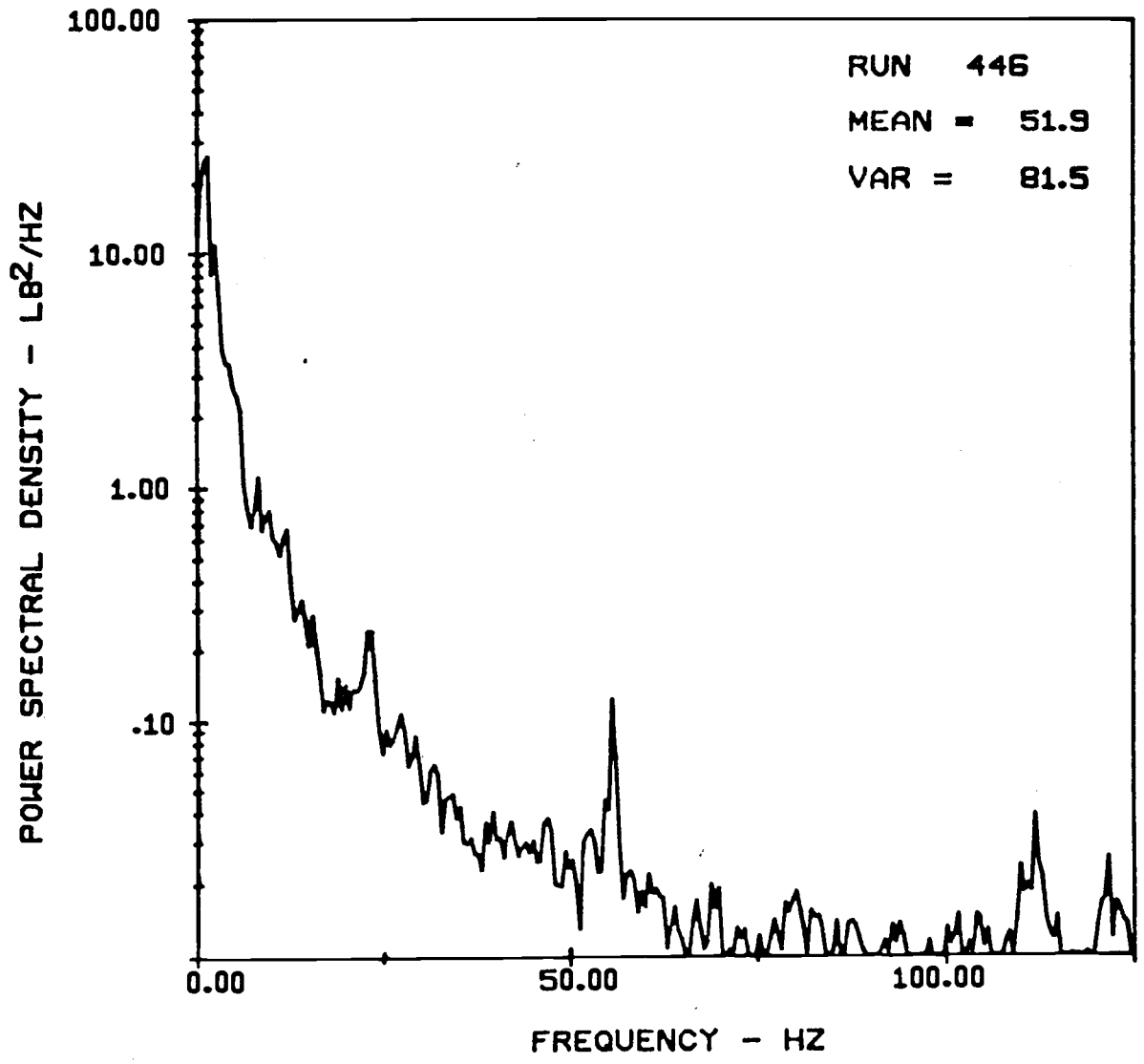


VERTICAL FORCES ON A 10-TUBE ARRAY (V = 7ft/sec)
IN E18 SAND WITH 10" ARRAY HEIGHT AND 4" TUBE SPACING

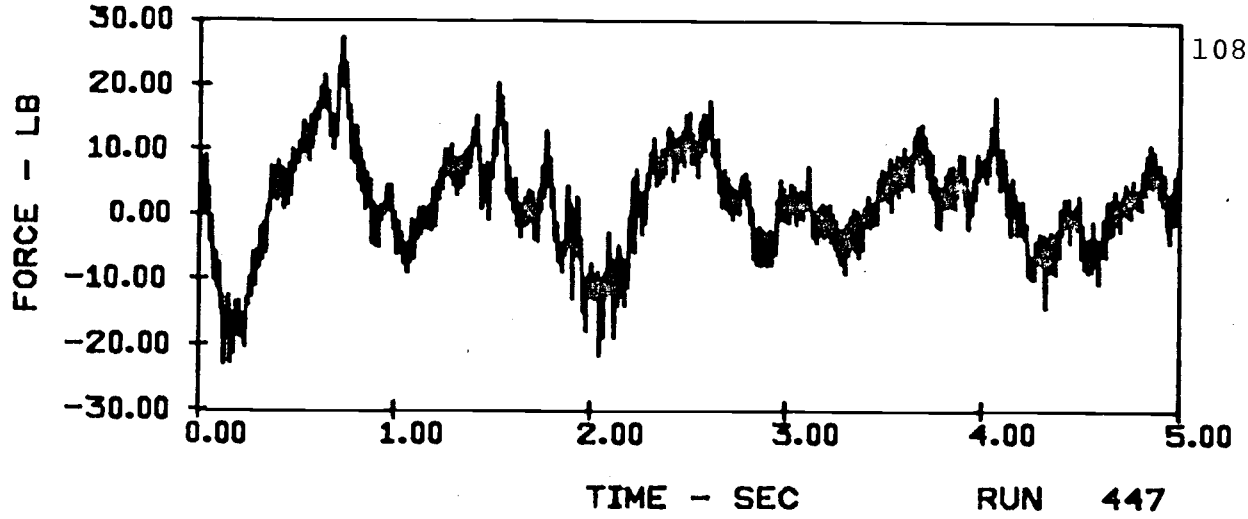


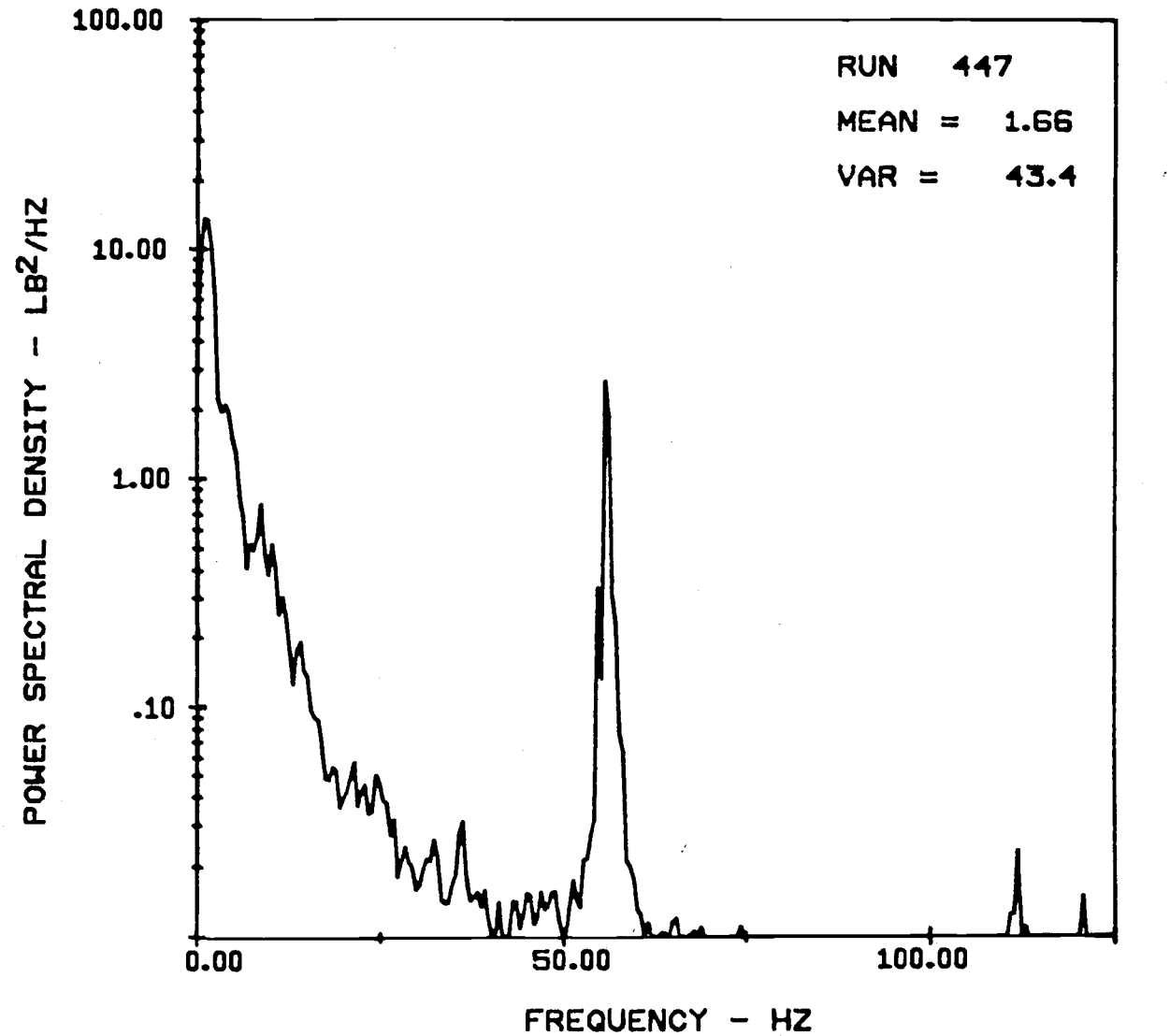


HORIZONTAL FORCES ON A 10-TUBE ARRAY (V = 7 ft/sec)
IN E18 SAND WITH 10" ARRAY HEIGHT AND 4" TUBE SPACING

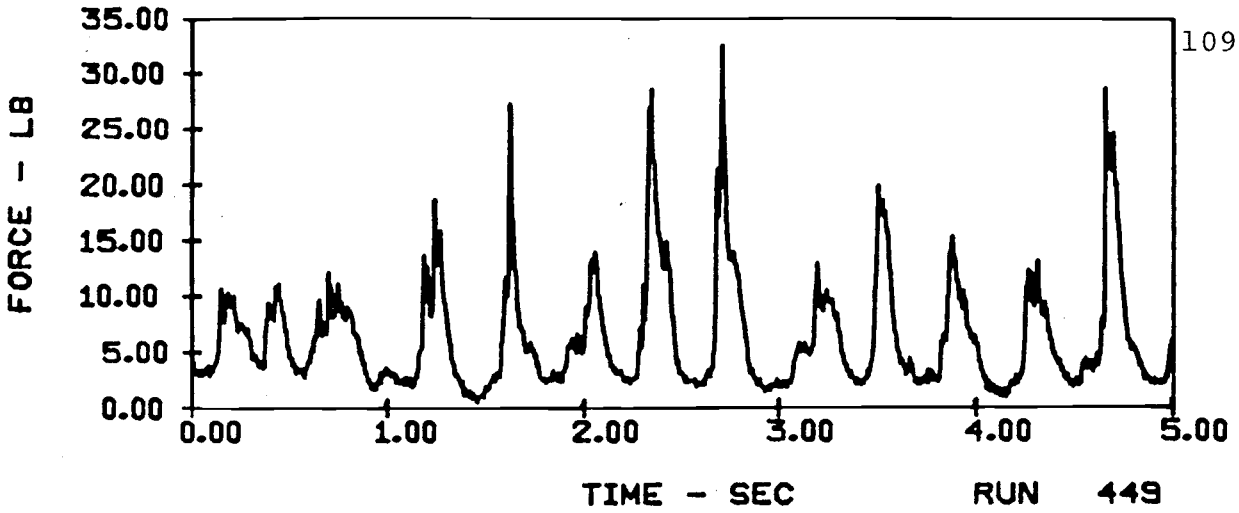


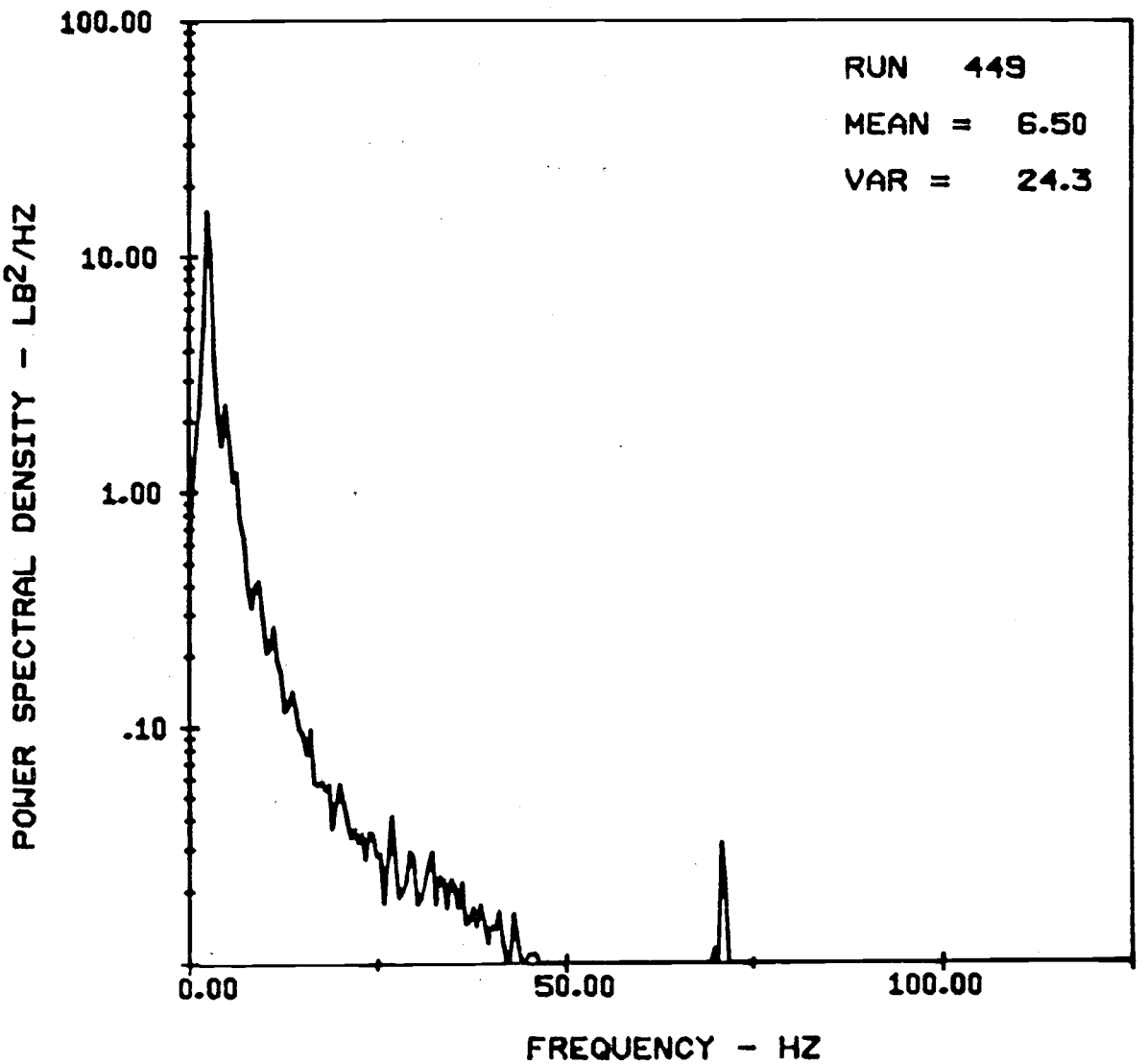


VERTICAL FORCES ON A SINGLE TUBE (V = 9 ft/sec)
IN E18 SAND WITH 10" ARRAY HEIGHT AND 4" TUBE SPACING

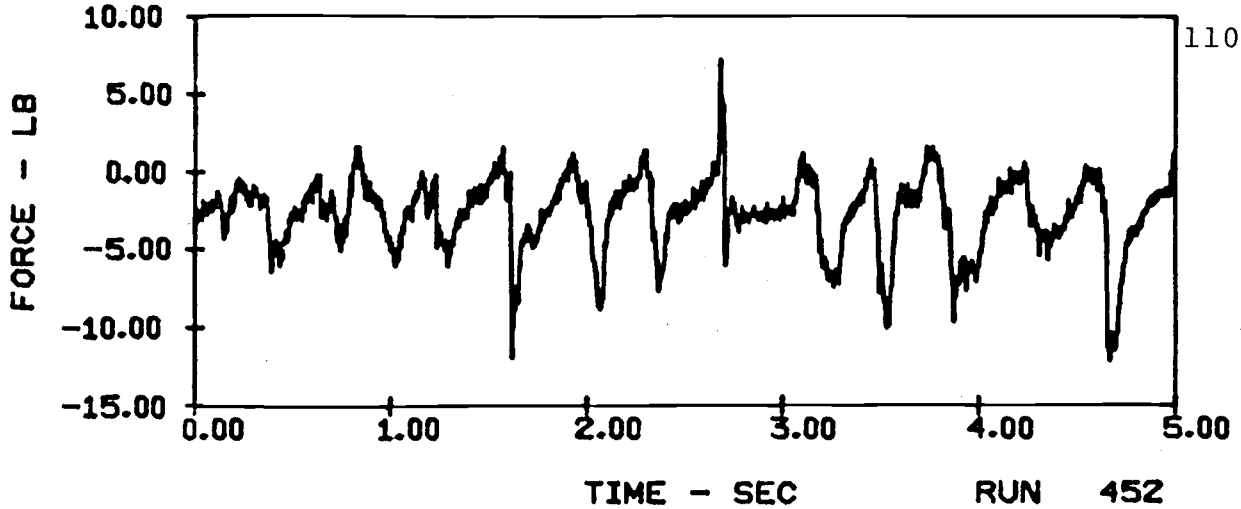


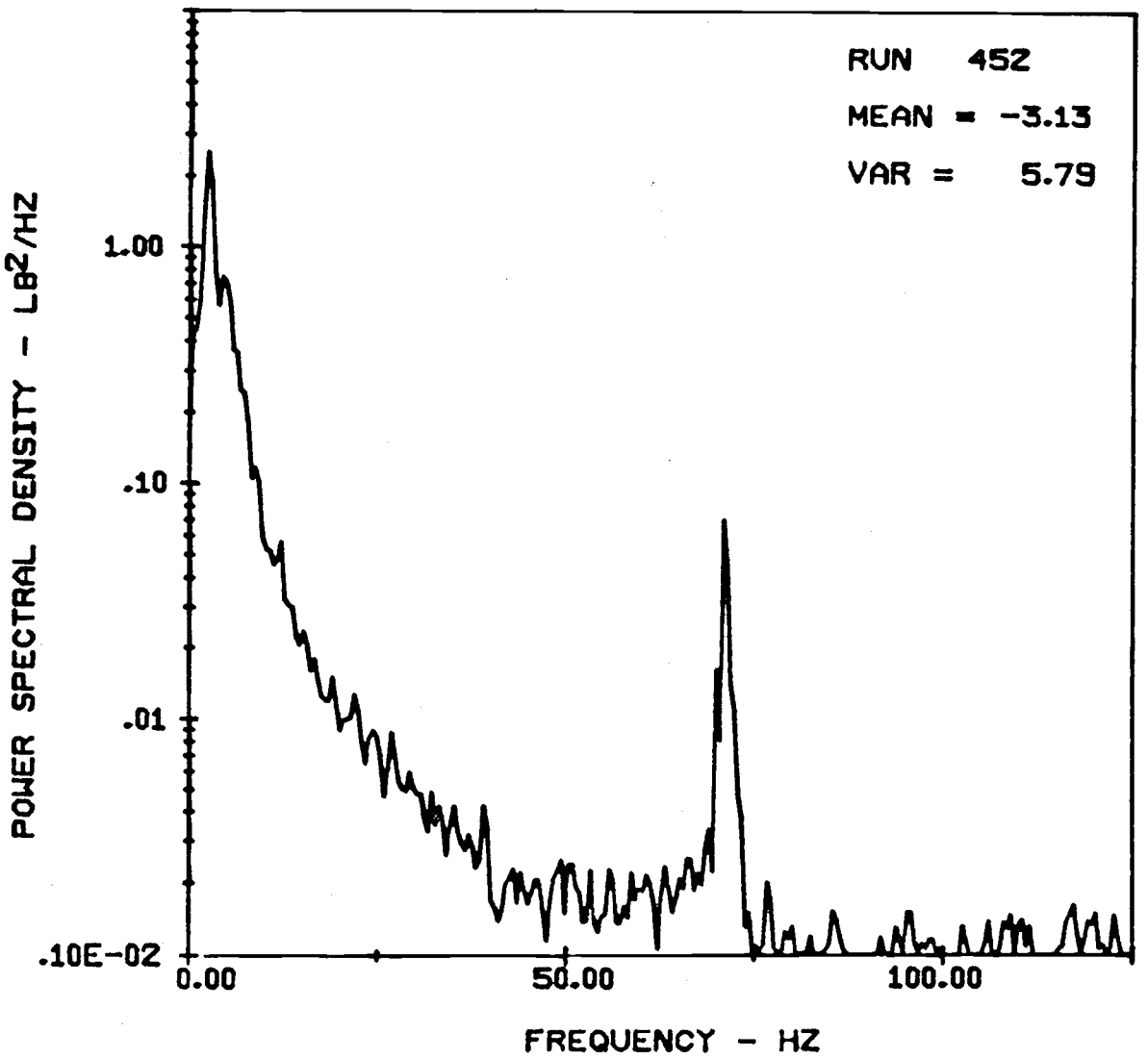


HORIZONTAL FORCES ON A SINGLE TUBE (V = 9 ft/sec)
IN E18 SAND WITH 10" ARRAY HEIGHT AND 4" TUBE SPACING

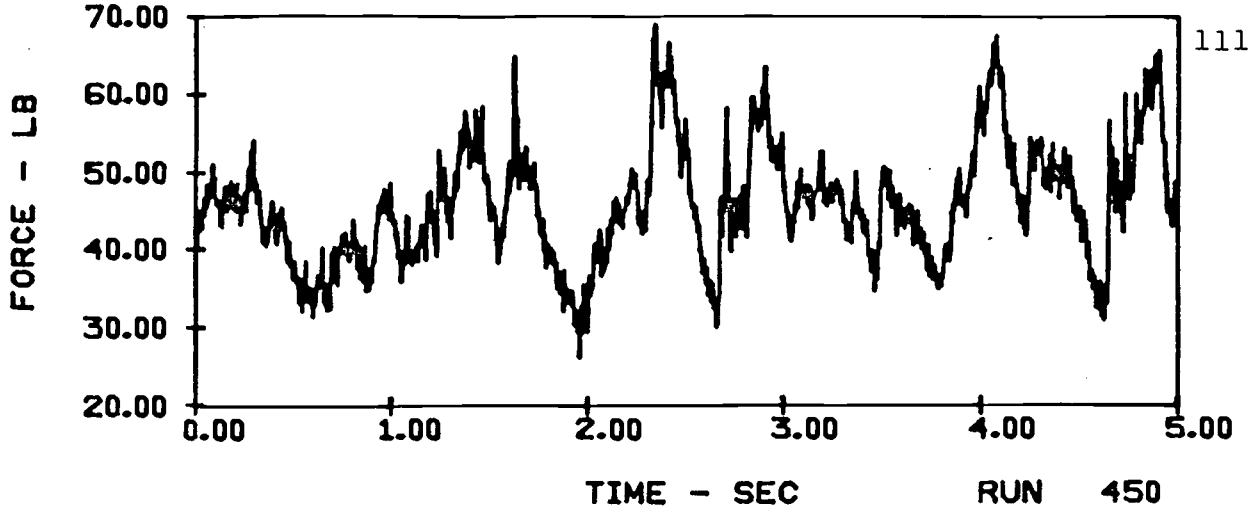


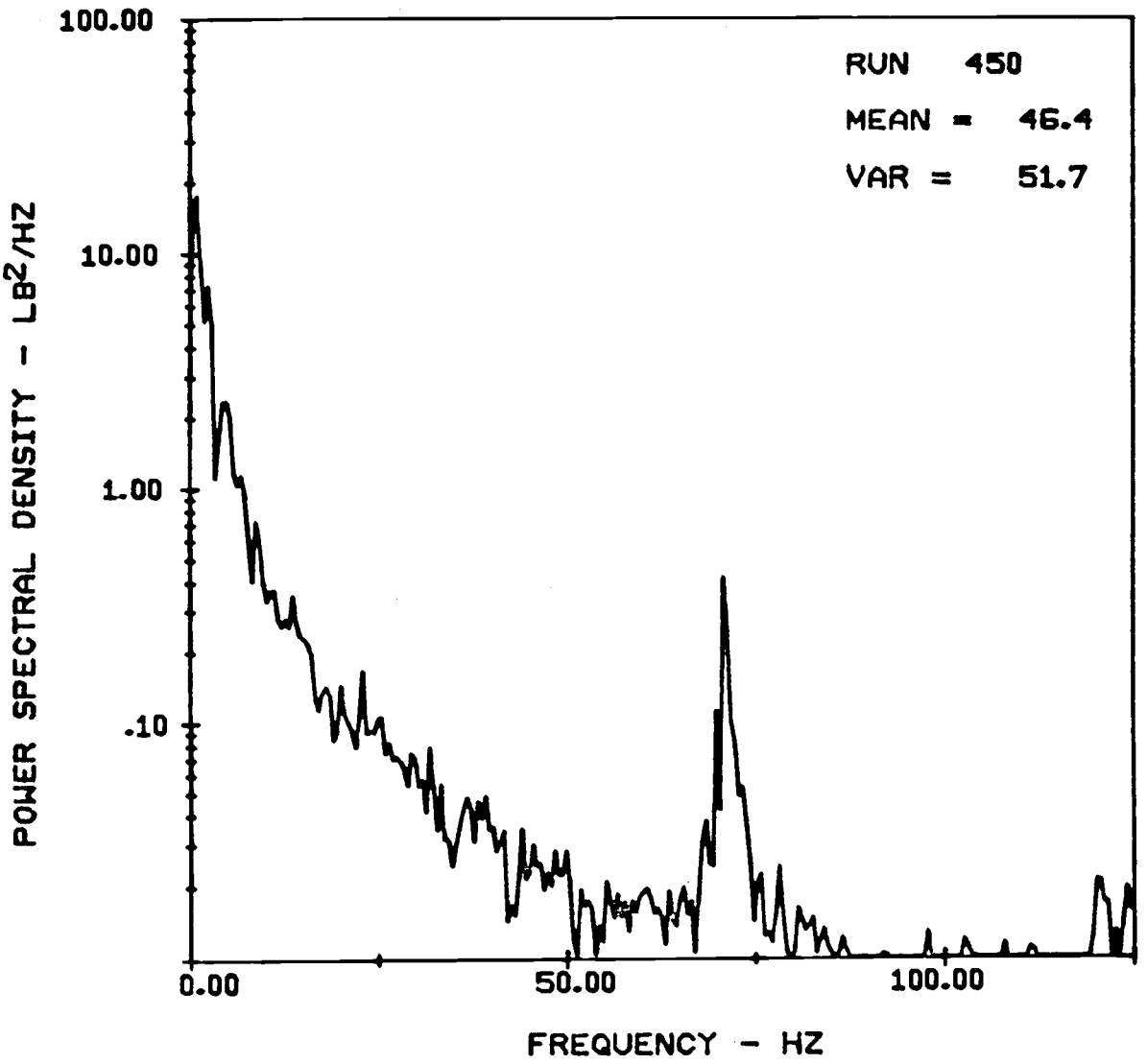


VERTICAL FORCES ON A 10-TUBE ARRAY (V = 9ft/sec)
IN E18 SAND WITH 10" ARRAY HEIGHT AND 4" TUBE SPACING

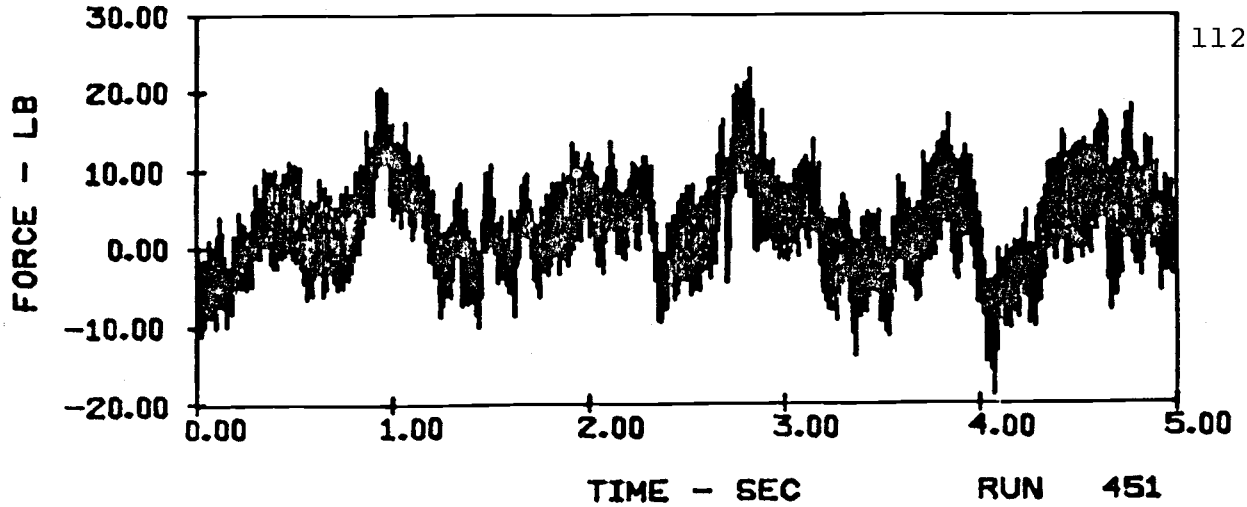


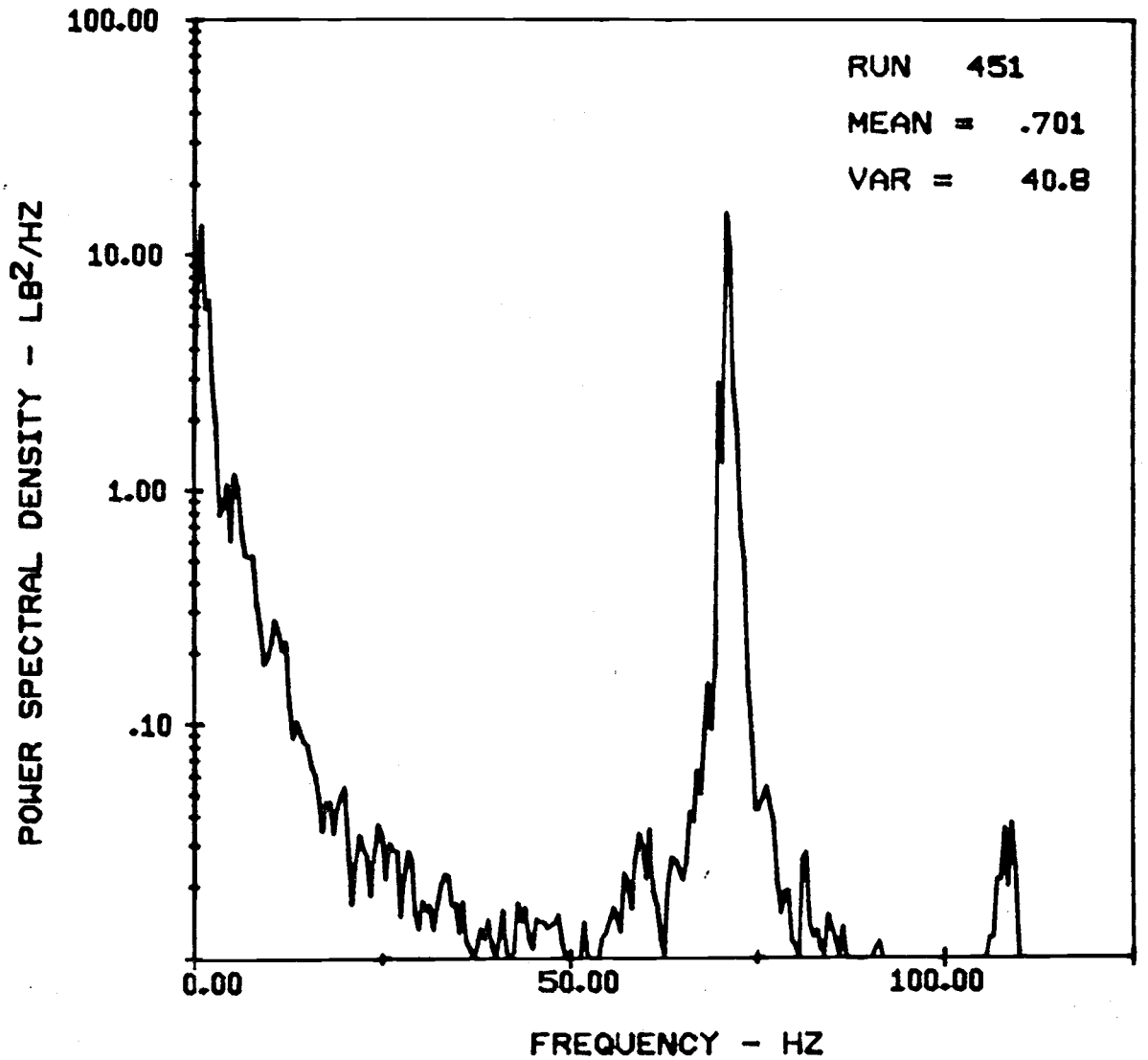


HORIZONTAL FORCES ON A 10-TUBE ARRAY (V = 9 ft/sec)
IN E18 SAND WITH 10" ARRAY HEIGHT AND 4" TUBE SPACING

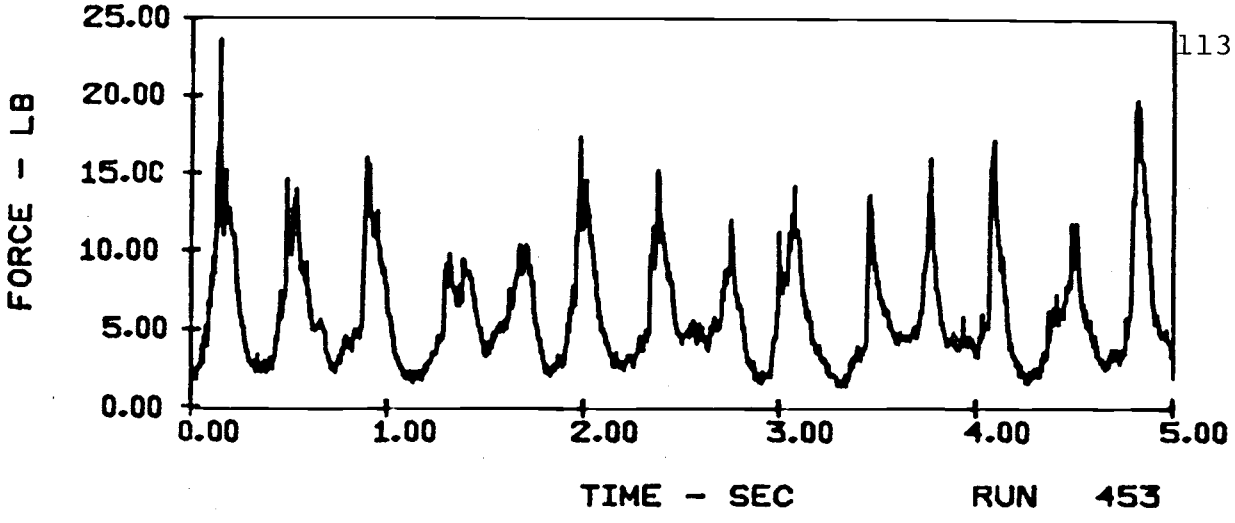


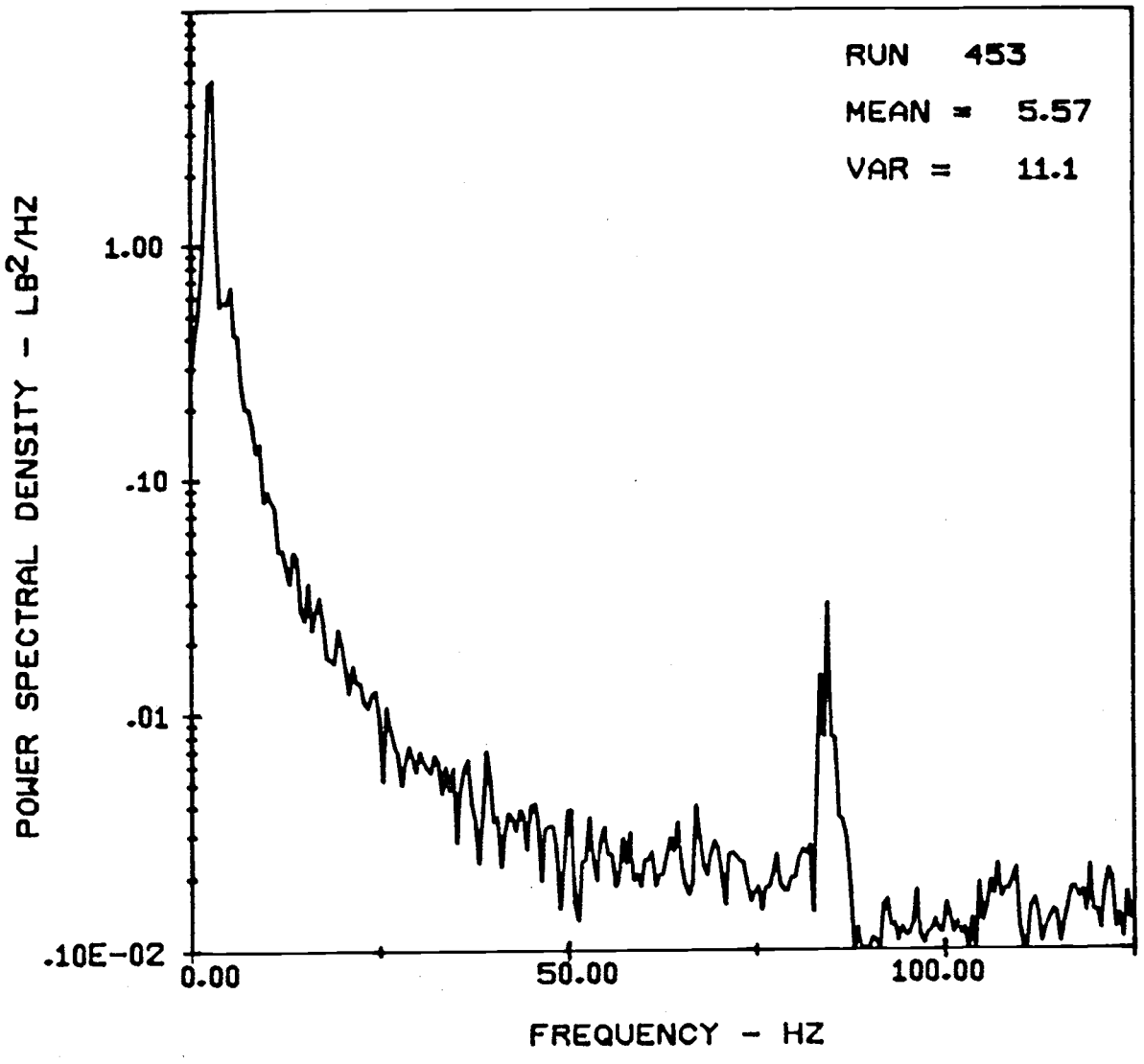


VERTICAL FORCES ON A SINGLE TUBE (V = 11 ft/sec)
IN E18 SAND WITH 10" ARRAY HEIGHT AND 4" TUBE SPACING

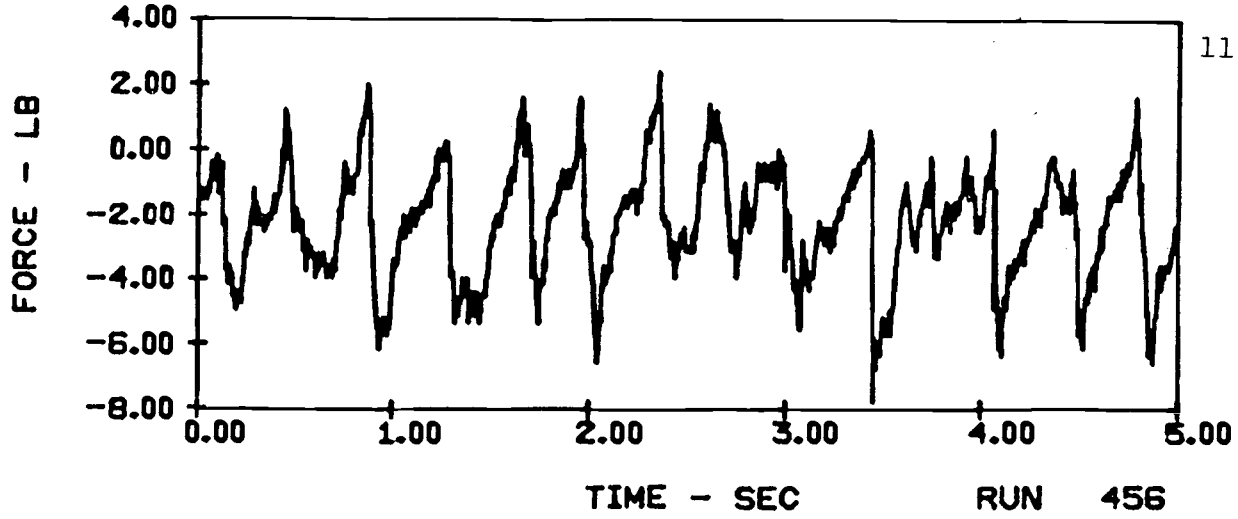


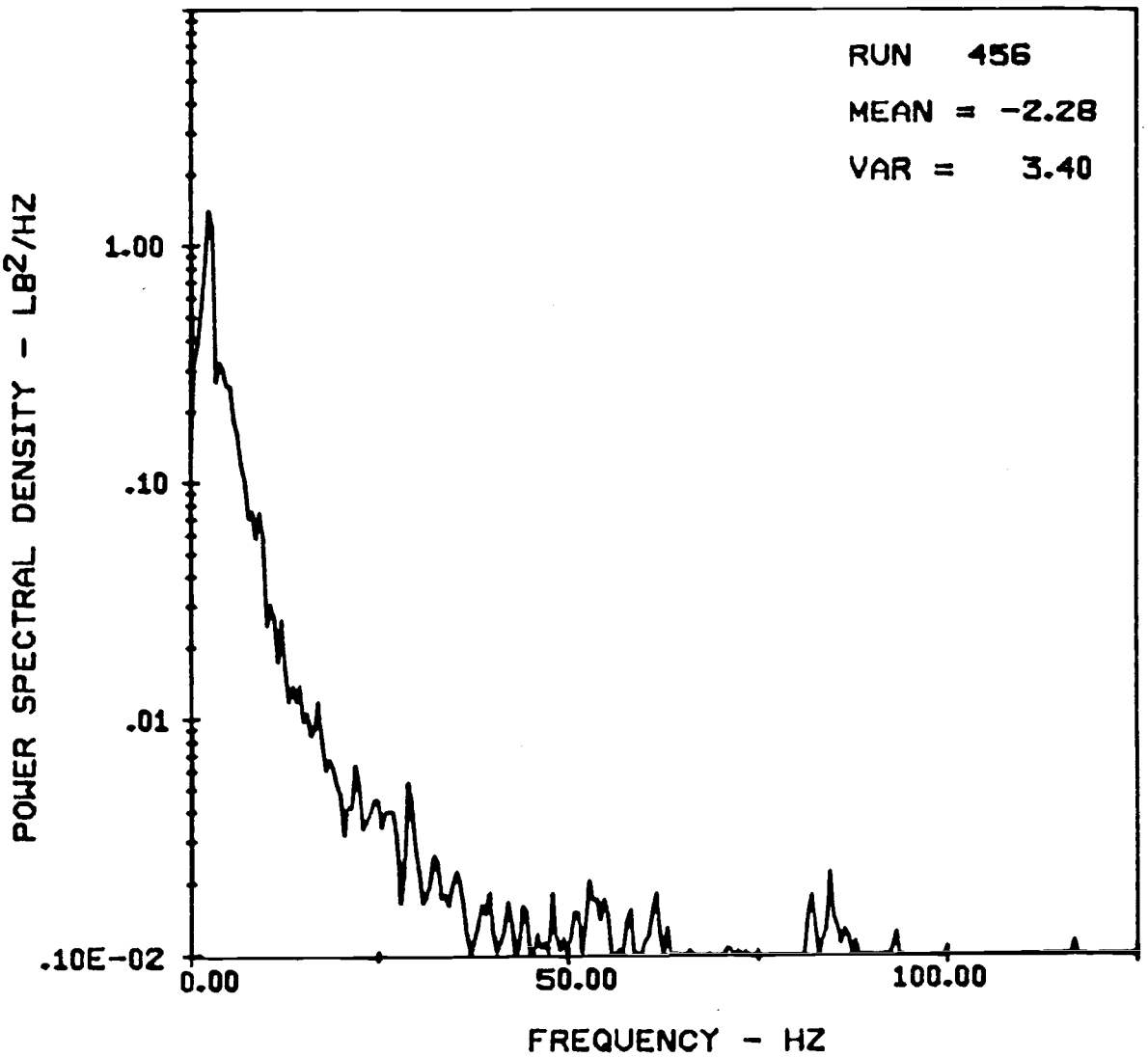


HORIZONTAL FORCES ON A SINGLE TUBE (V = 11 ft/sec)
IN E18 SAND WITH 10" ARRAY HEIGHT AND 4" TUBE SPACING

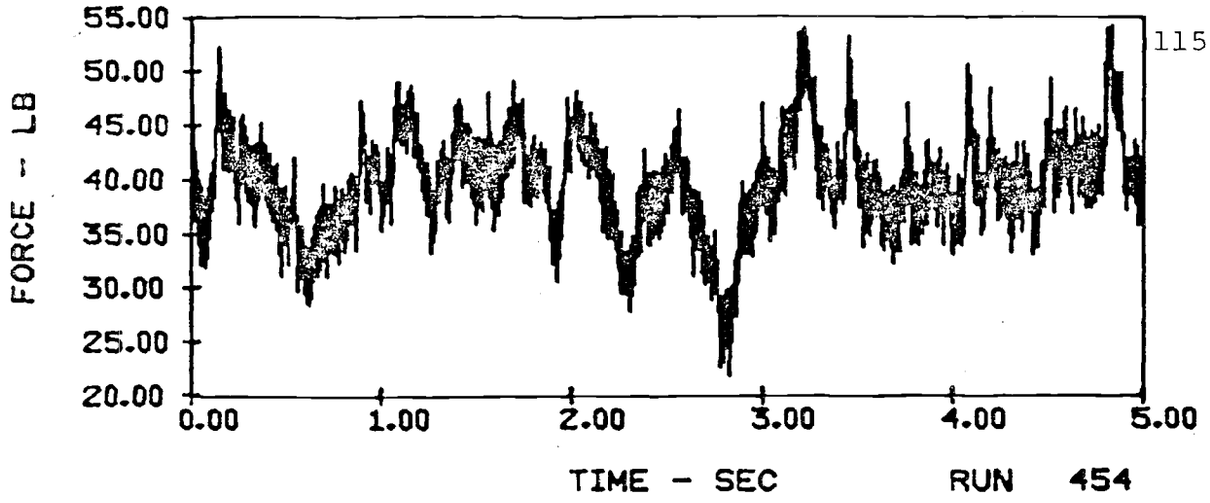


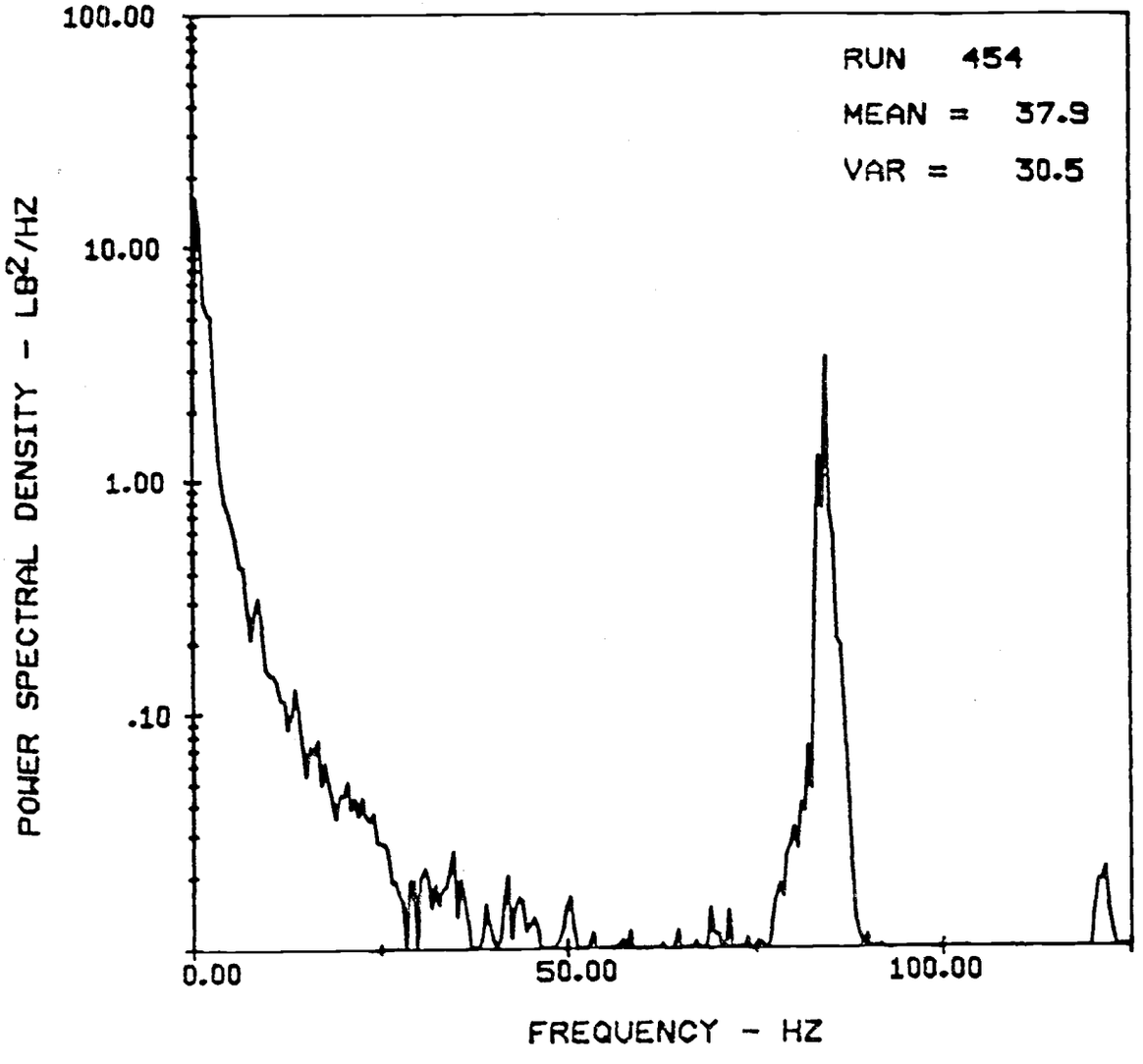


VERTICAL FORCES ON A 10-TUBE ARRAY (V = 11ft/sec)
IN E18 SAND WITH 10" ARRAY HEIGHT AND 4" TUBE SPACING

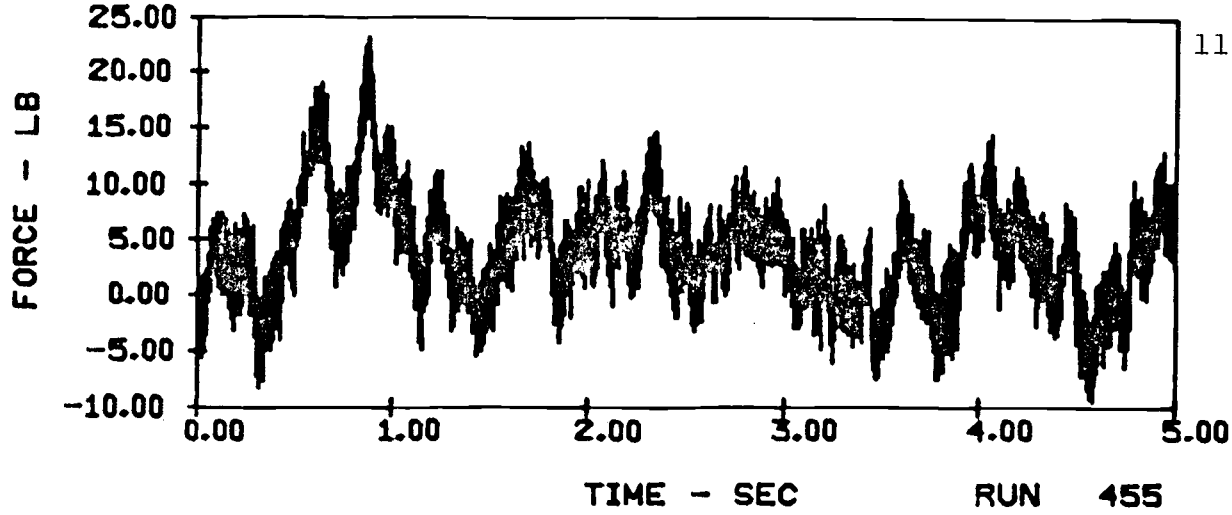


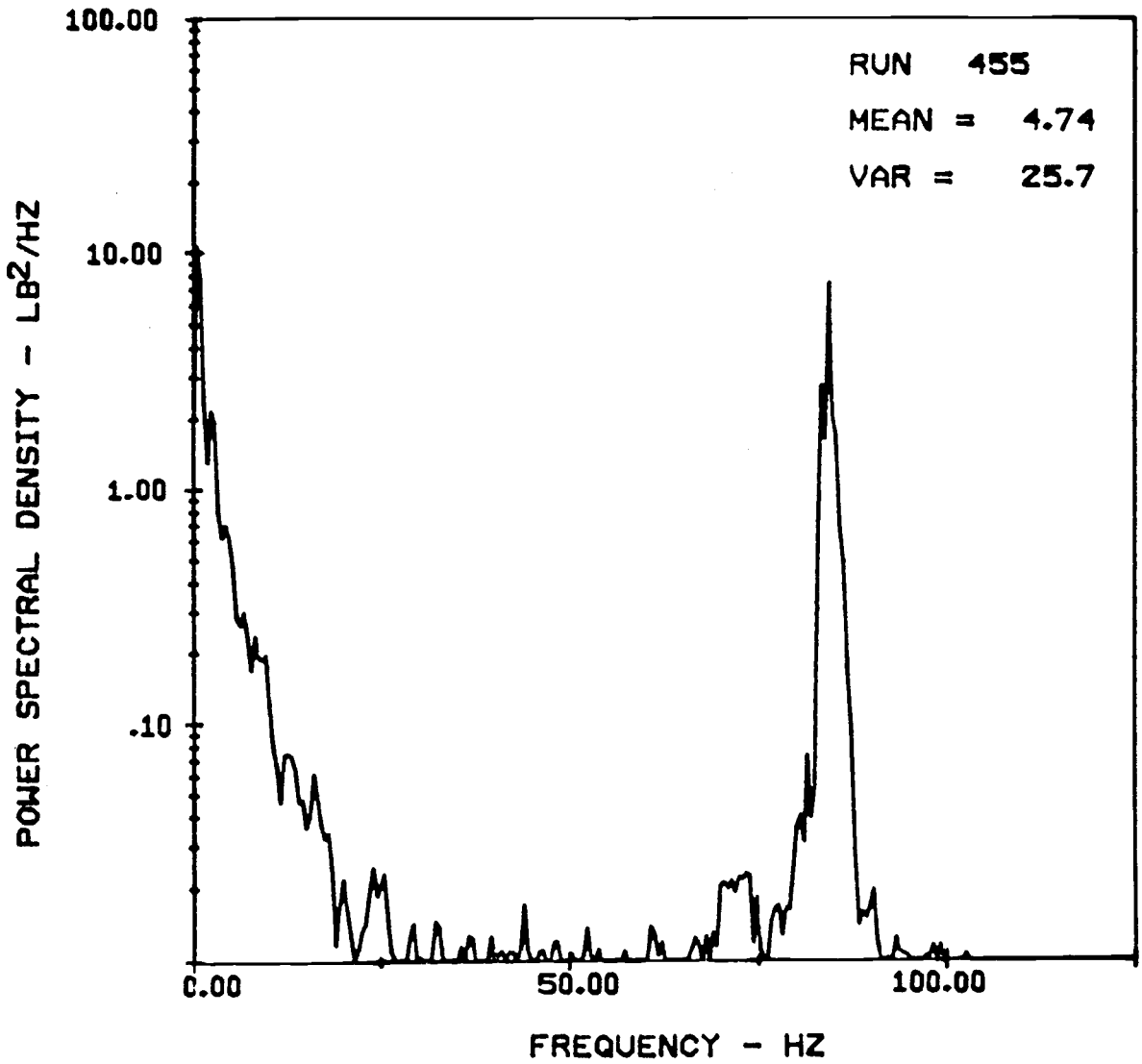


HORIZONTAL FORCES ON A 10-TUBE ARRAY (V = 11 ft/sec)
IN E18 SAND WITH 10" ARRAY HEIGHT AND 4" TUBE SPACING

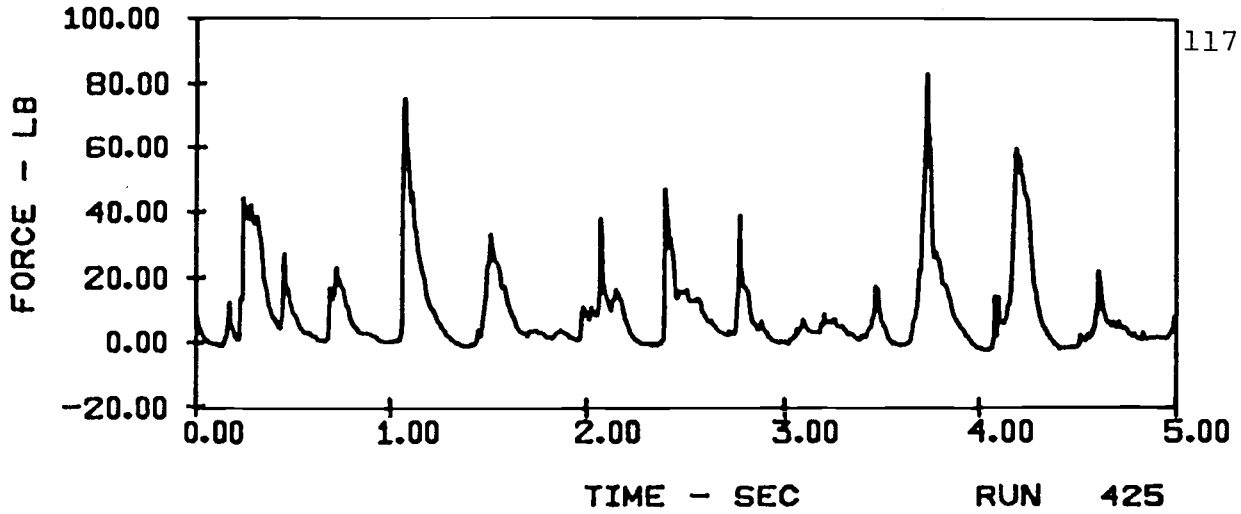


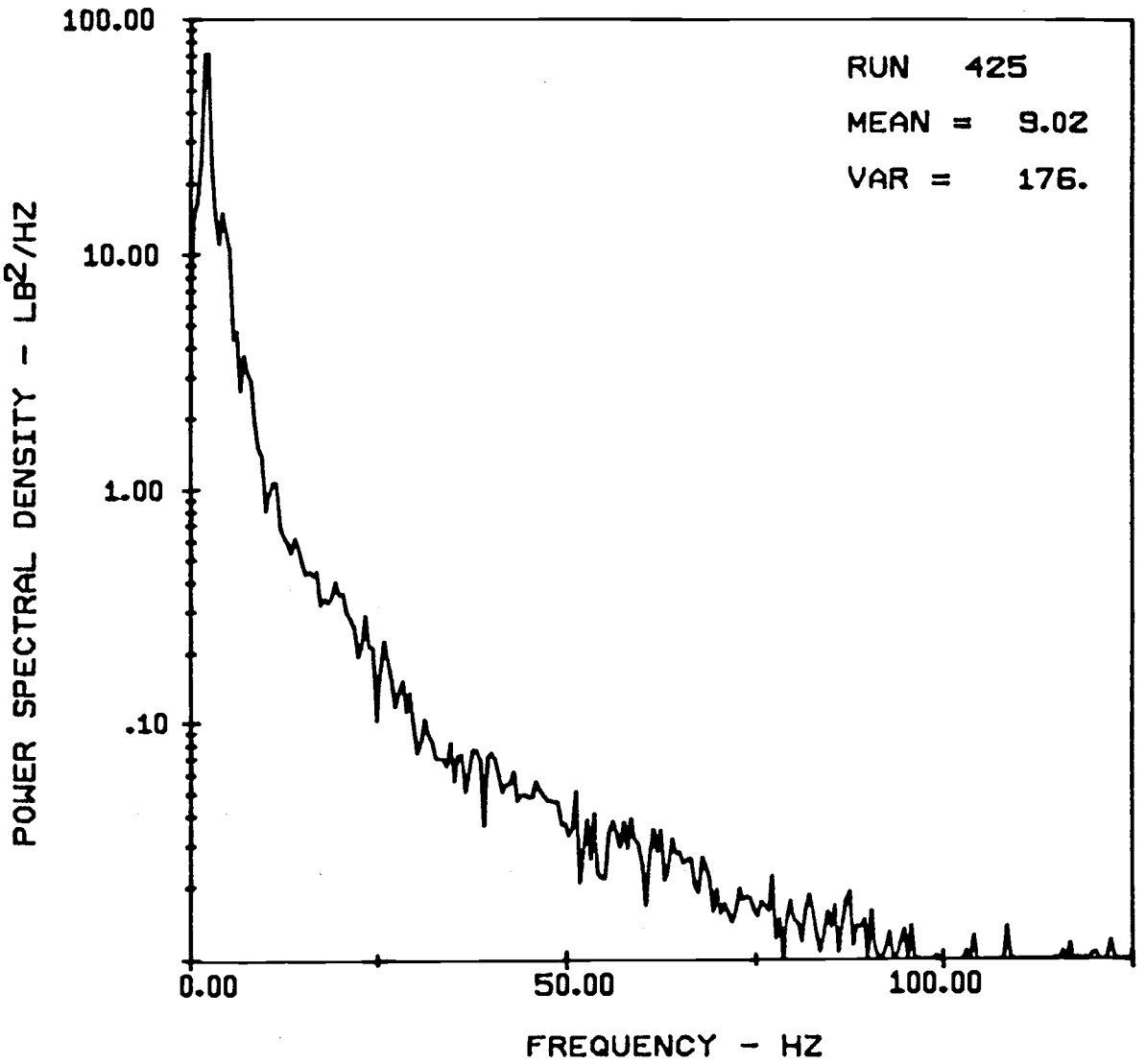


VERTICAL FORCES ON A SINGLE TUBE (V = 5 ft/sec)
IN E18 SAND WITH 20" ARRAY HEIGHT AND 4" TUBE SPACING

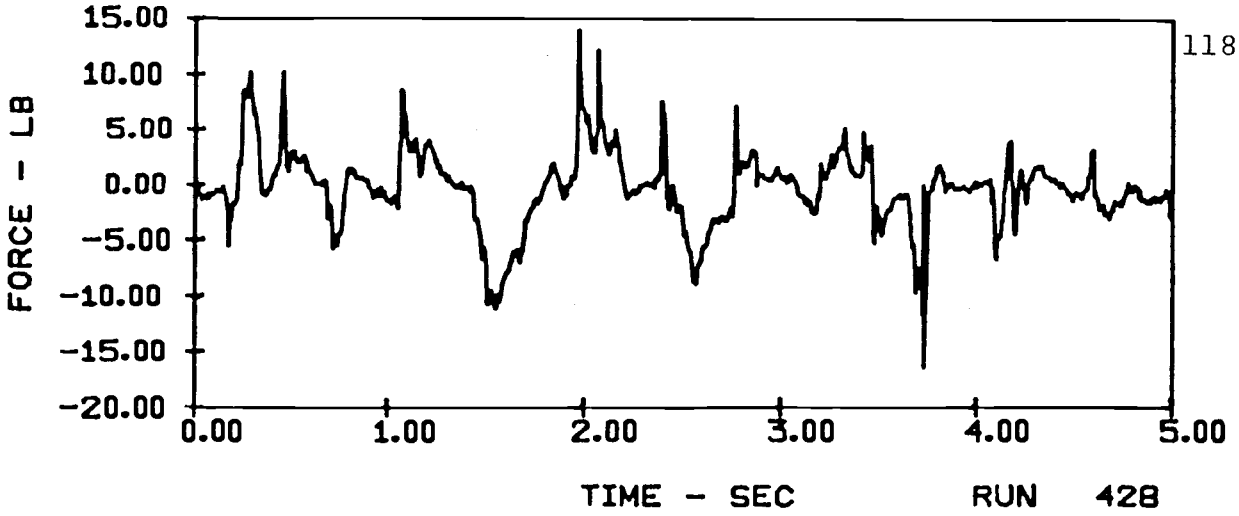


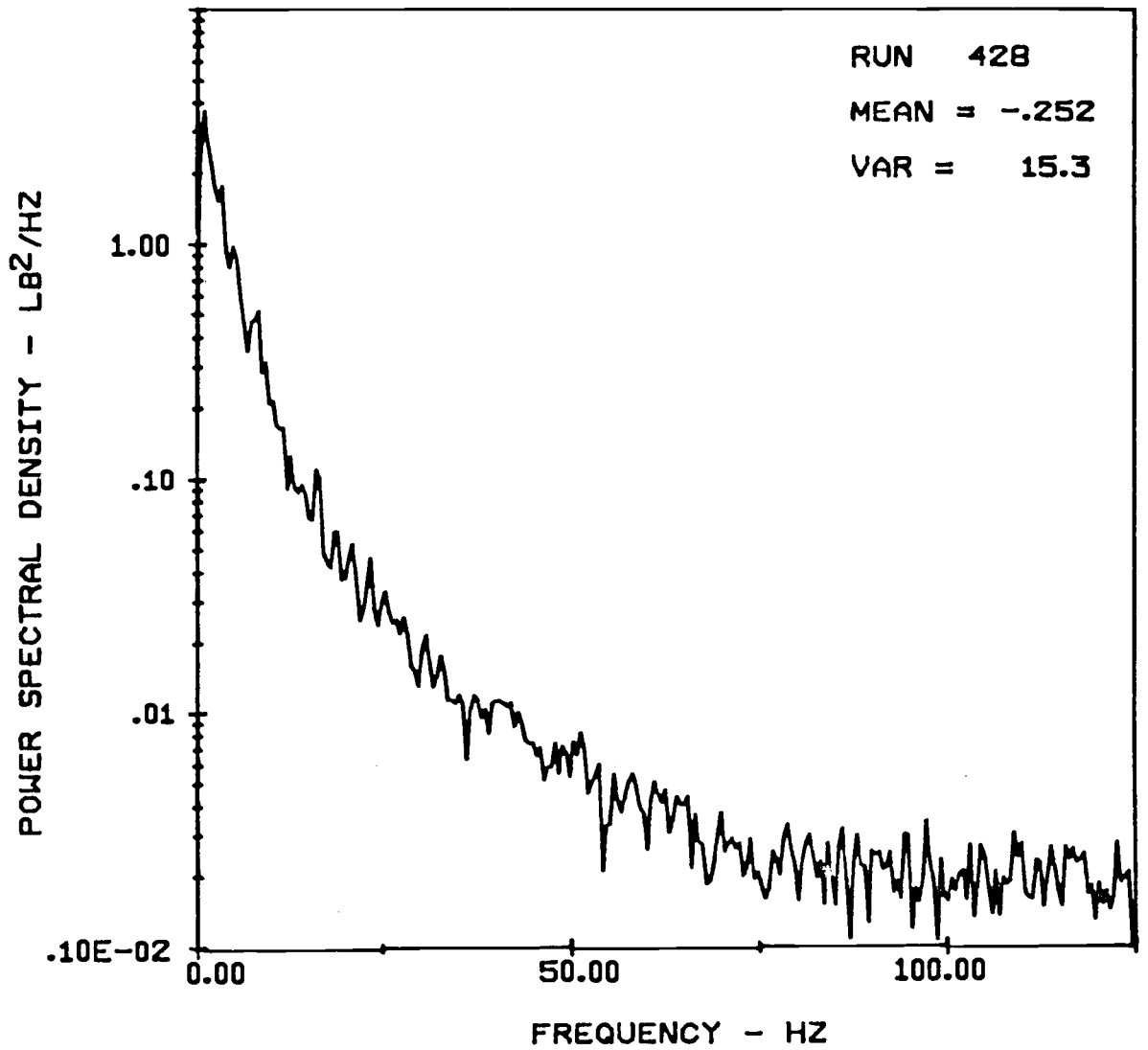


HORIZONTAL FORCES ON A SINGLE TUBE (V = 5 ft/sec)
IN E18 SAND WITH 20" ARRAY HEIGHT AND 4" TUBE SPACING

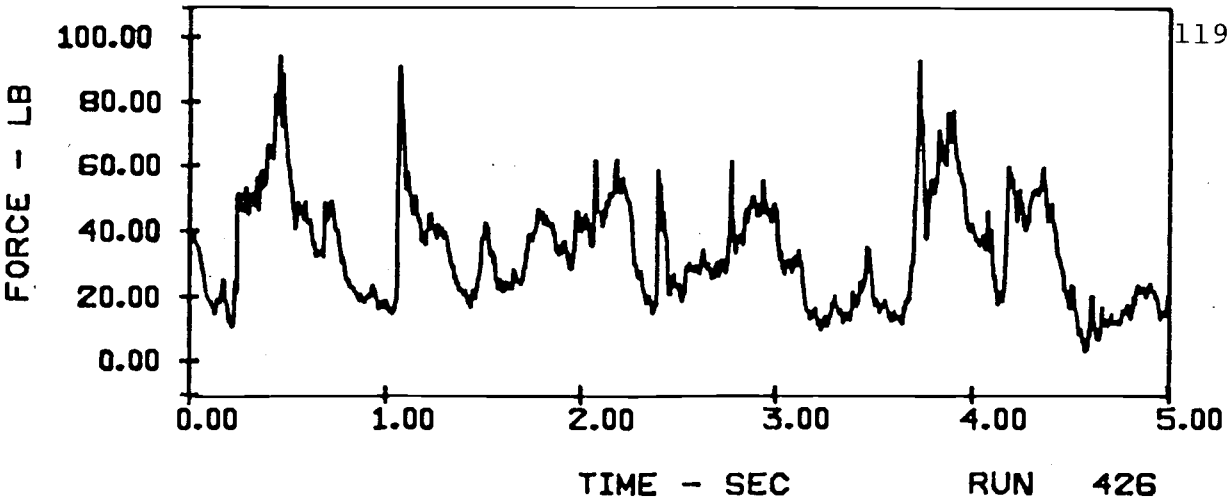


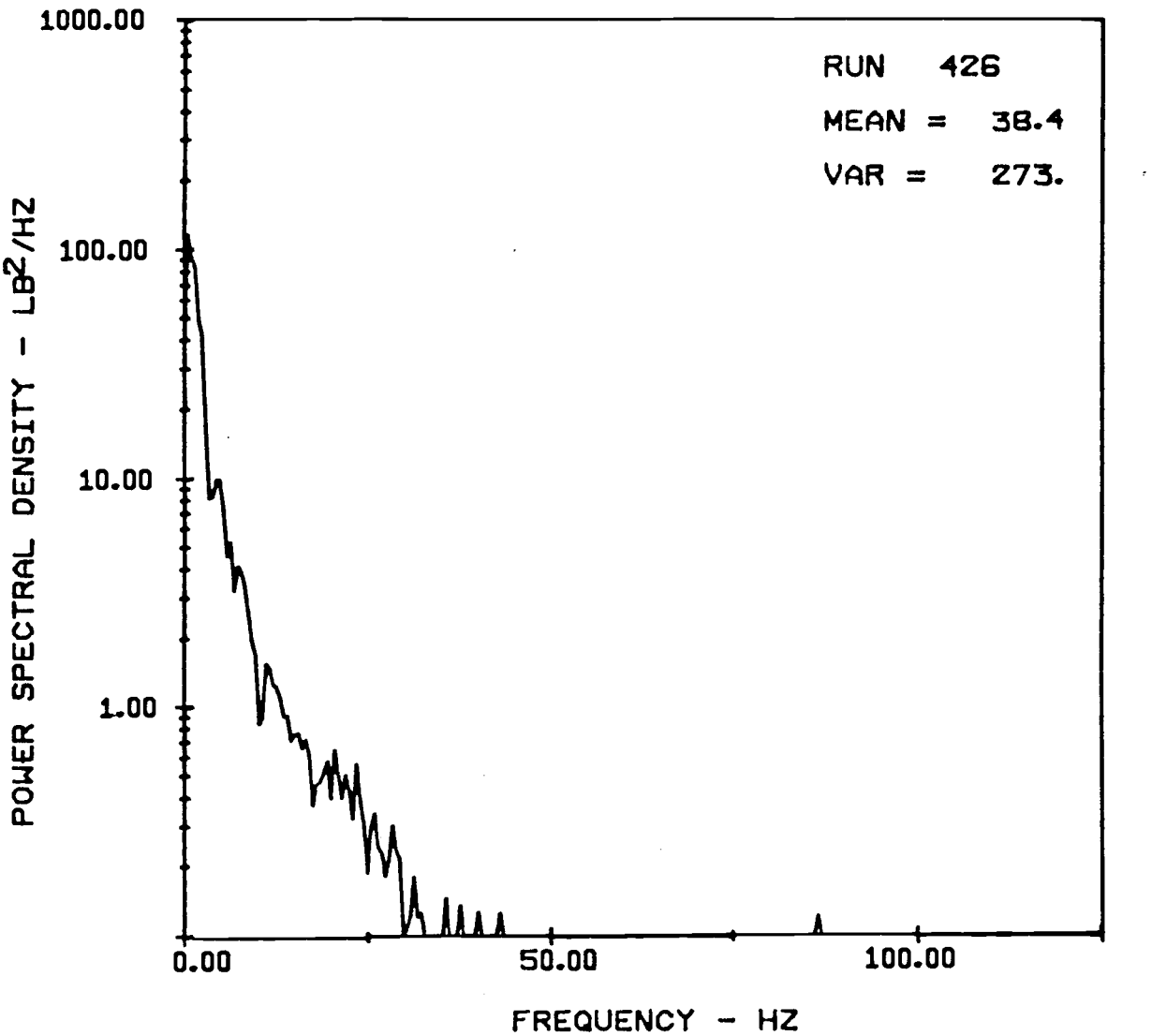


VERTICAL FORCES ON A 10-TUBE ARRAY (V = 5ft/sec)
IN E18 SAND WITH 20" ARRAY HEIGHT AND 4" TUBE SPACING

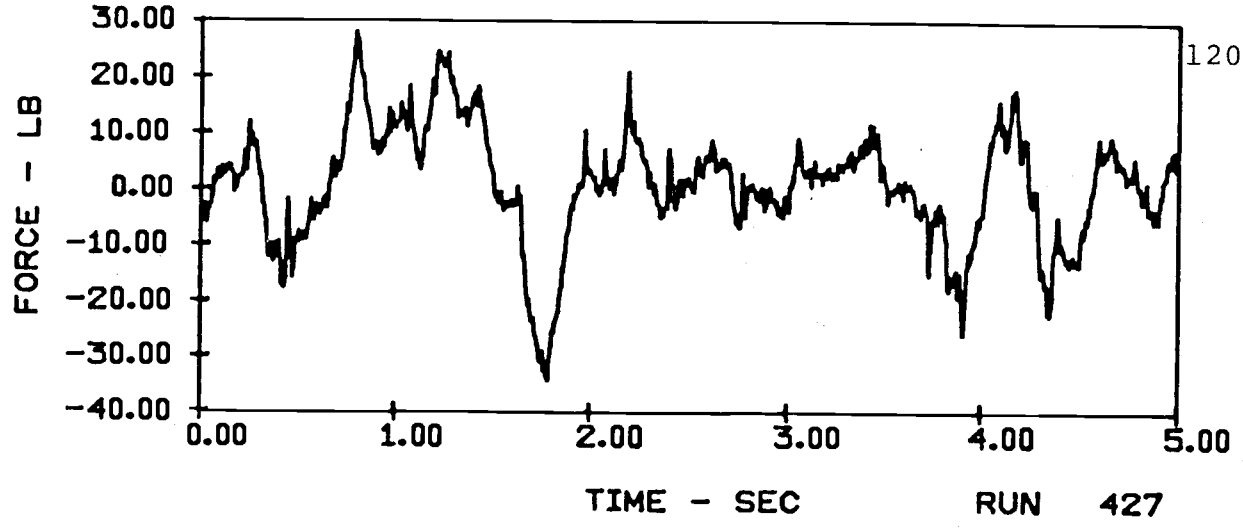


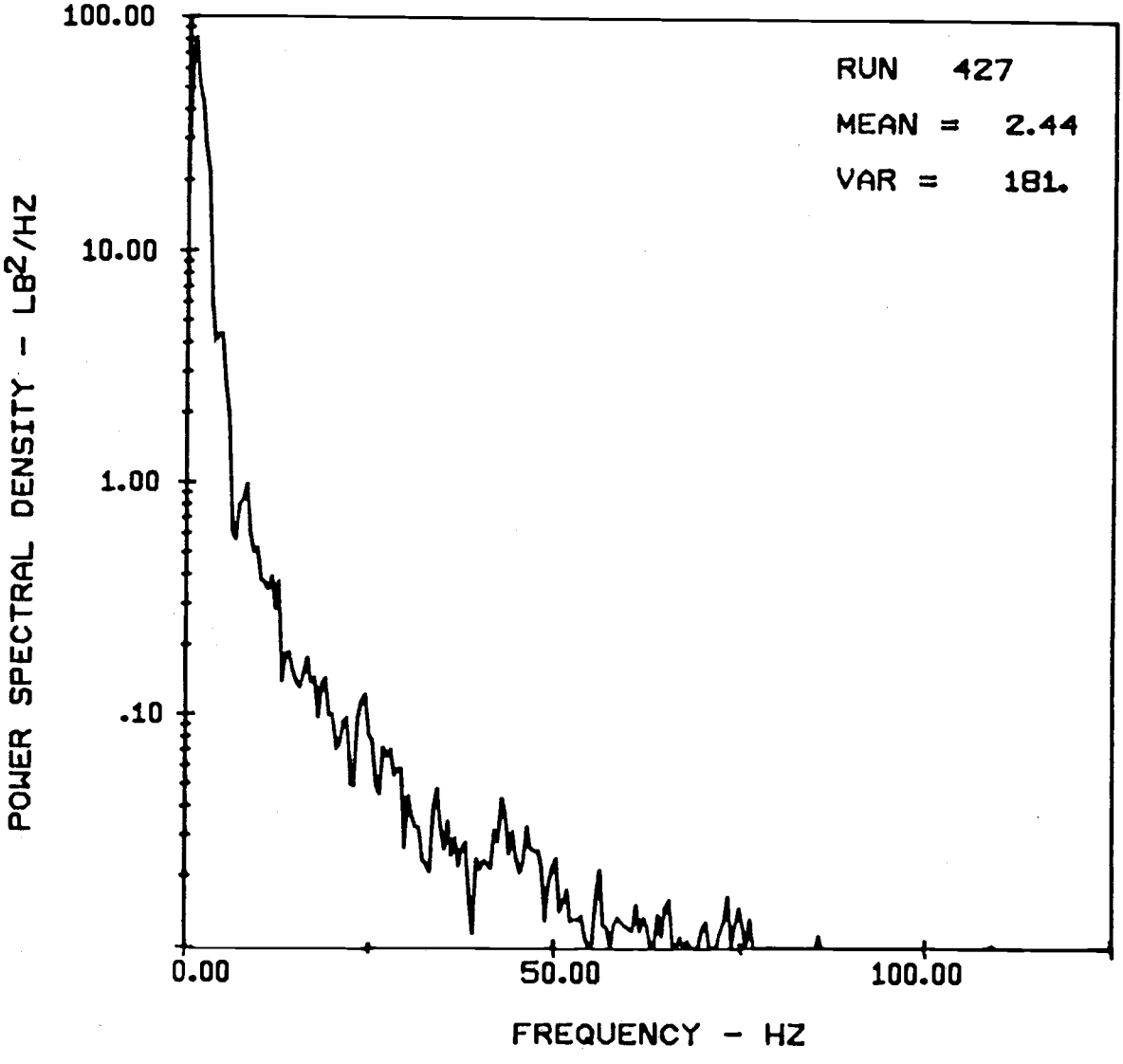


HORIZONTAL FORCES ON A 10-TUBE ARRAY (V = 5 ft/sec)
IN E18 SAND WITH 20" ARRAY HEIGHT AND 4" TUBE SPACING

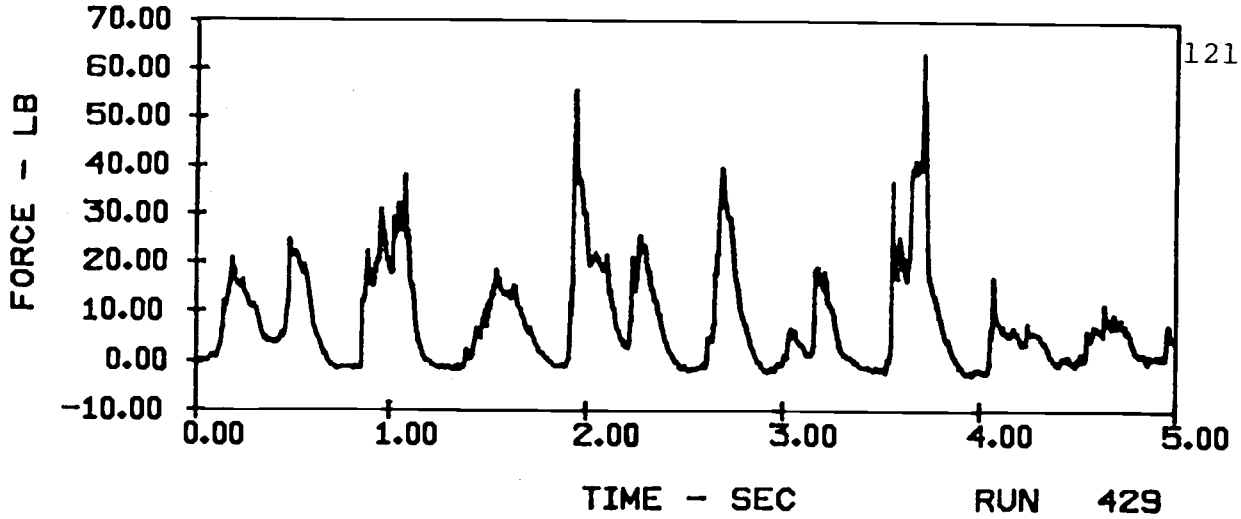


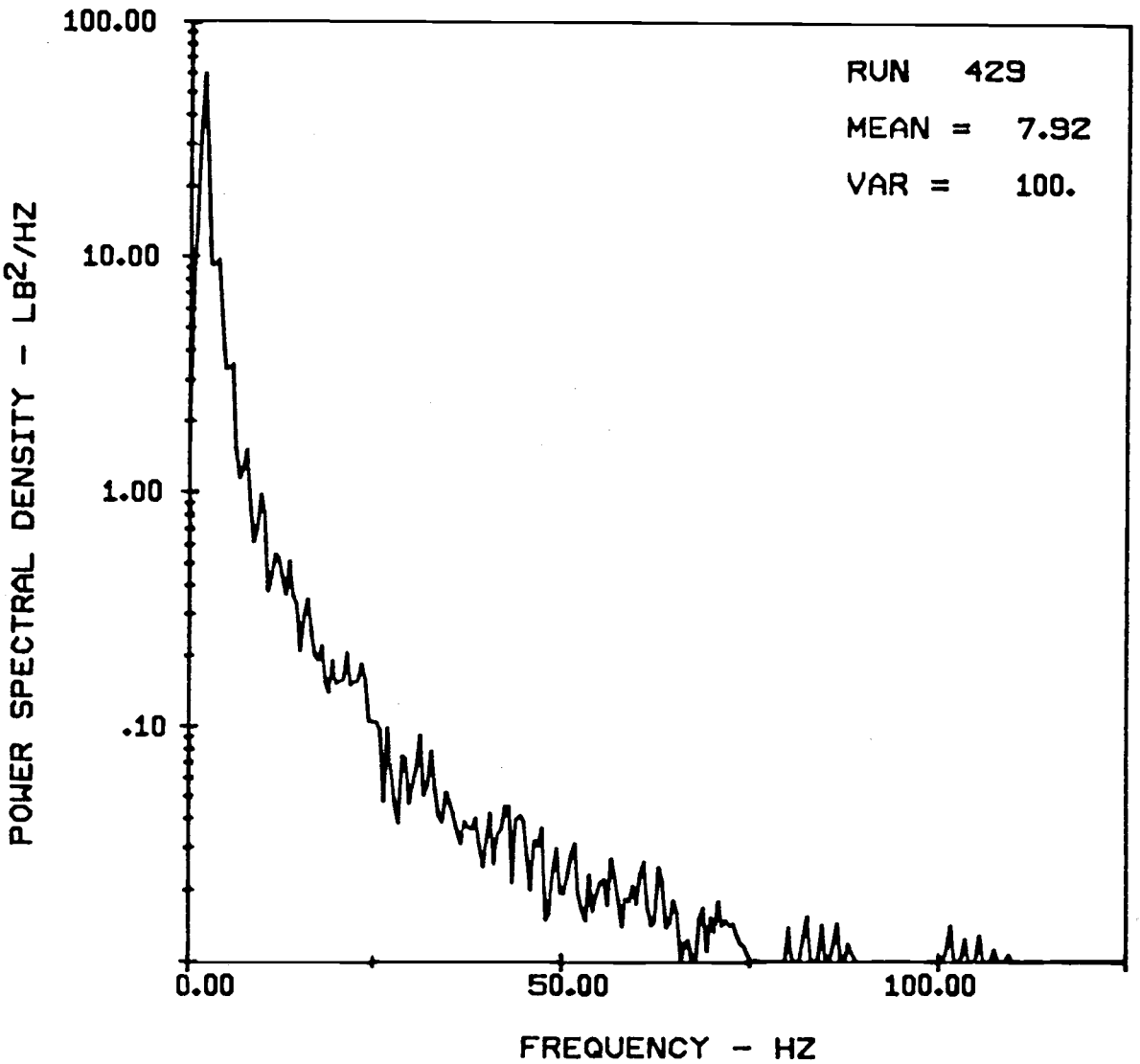


VERTICAL FORCES ON A SINGLE TUBE (V = 7 ft/sec)
IN E18 SAND WITH 20" ARRAY HEIGHT AND 4" TUBE SPACING

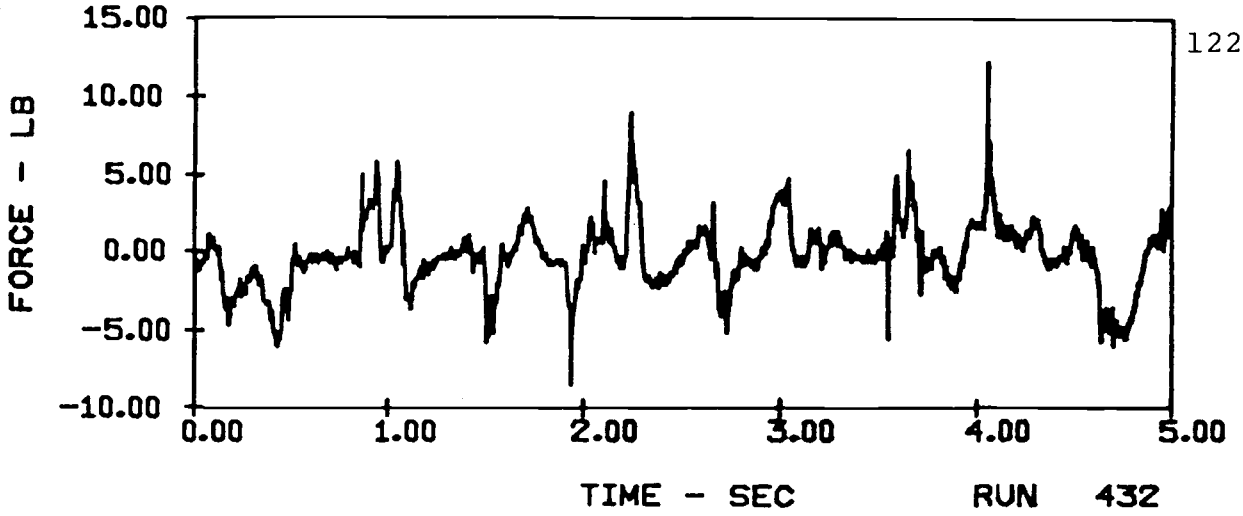


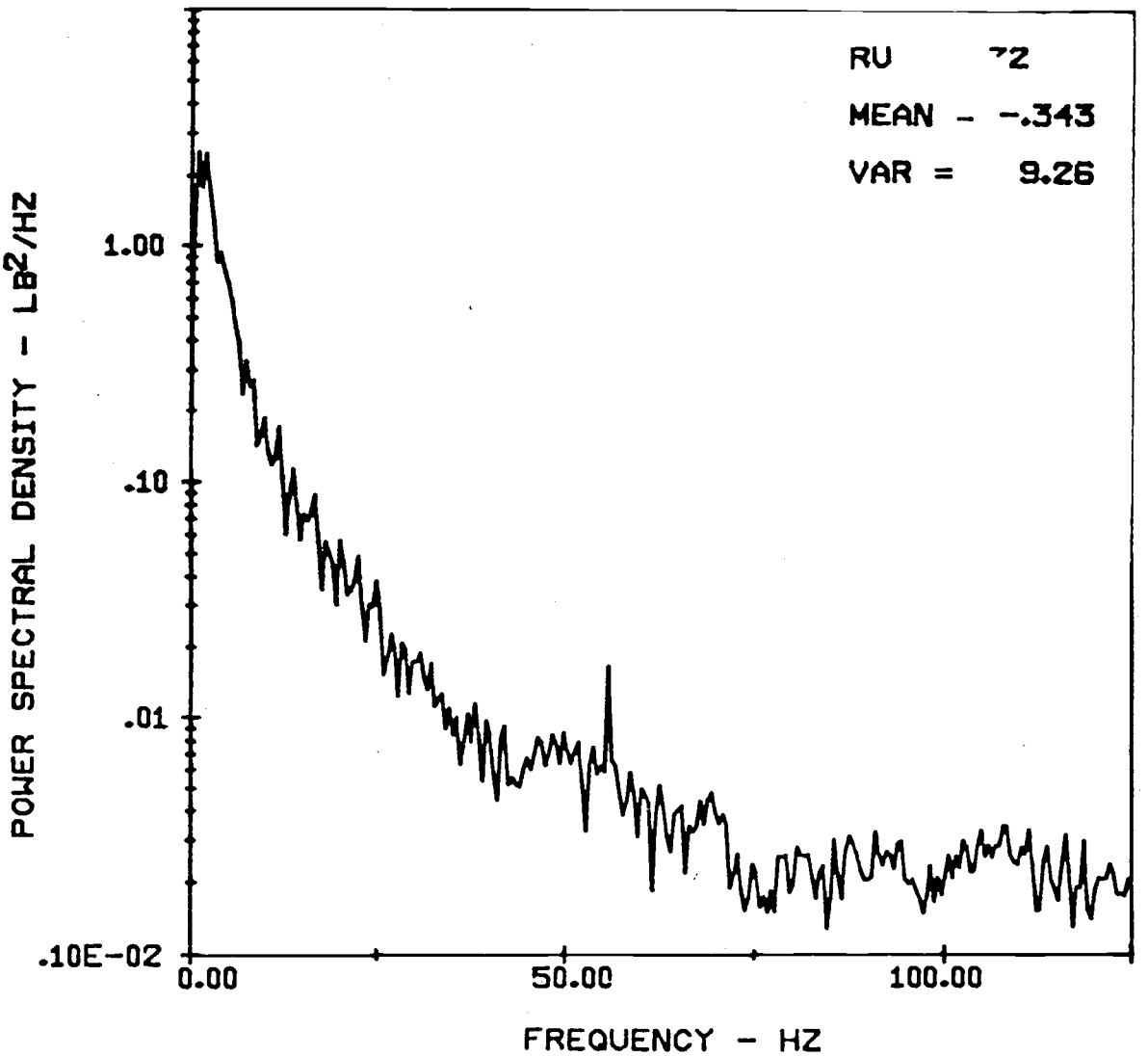


HORIZONTAL FORCES ON A SINGLE TUBE (V = 7 ft/sec)
IN E18 SAND WITH 20" ARRAY HEIGHT AND 4" TUBE SPACING

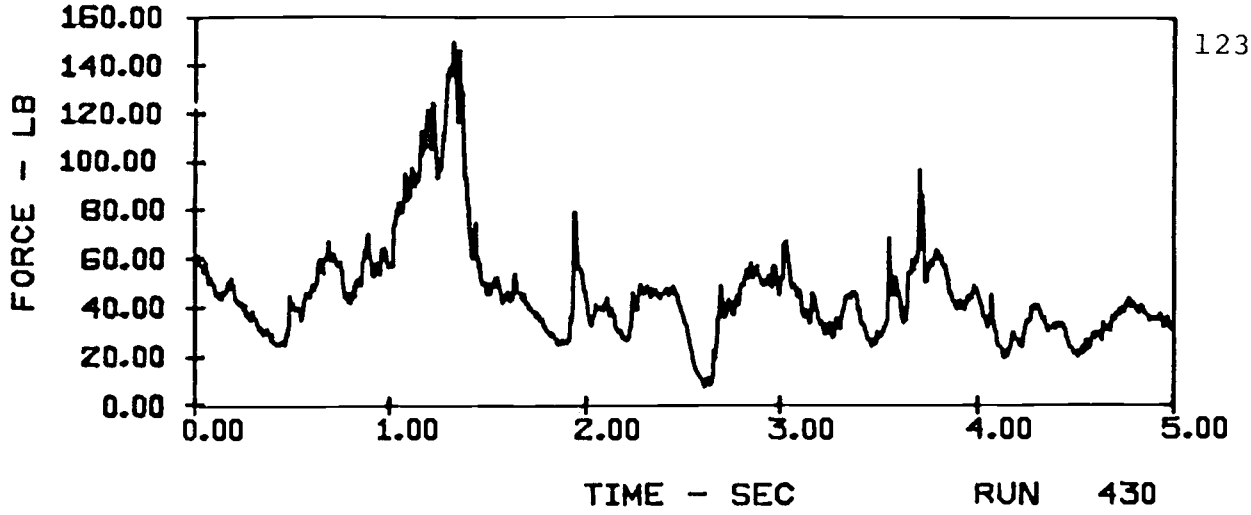


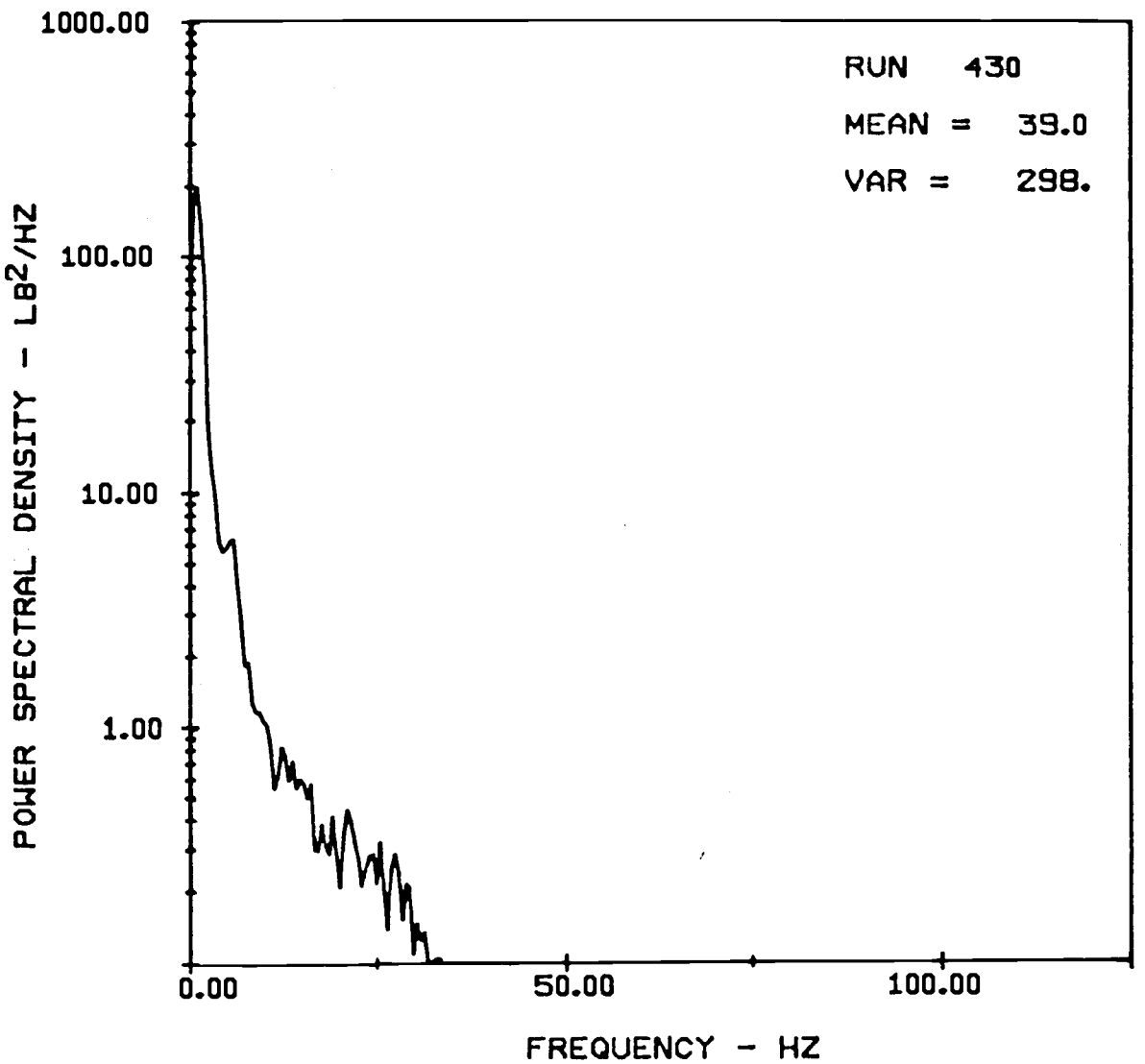


VERTICAL FORCES ON A 10-TUBE ARRAY (V = 7ft/sec)
IN E18 SAND WITH 20" ARRAY HEIGHT AND 4" TUBE SPACING

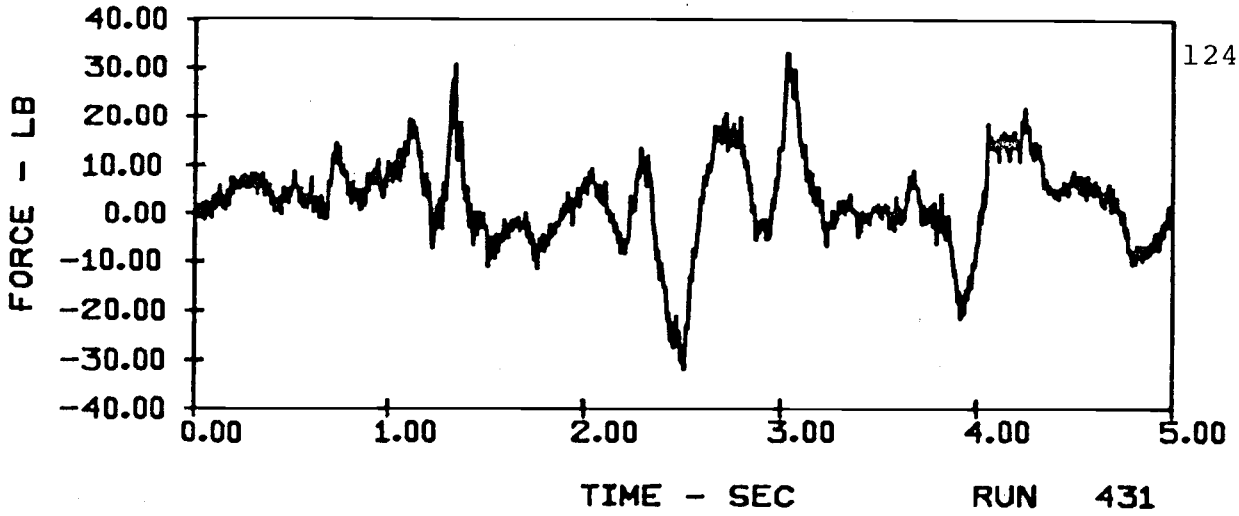


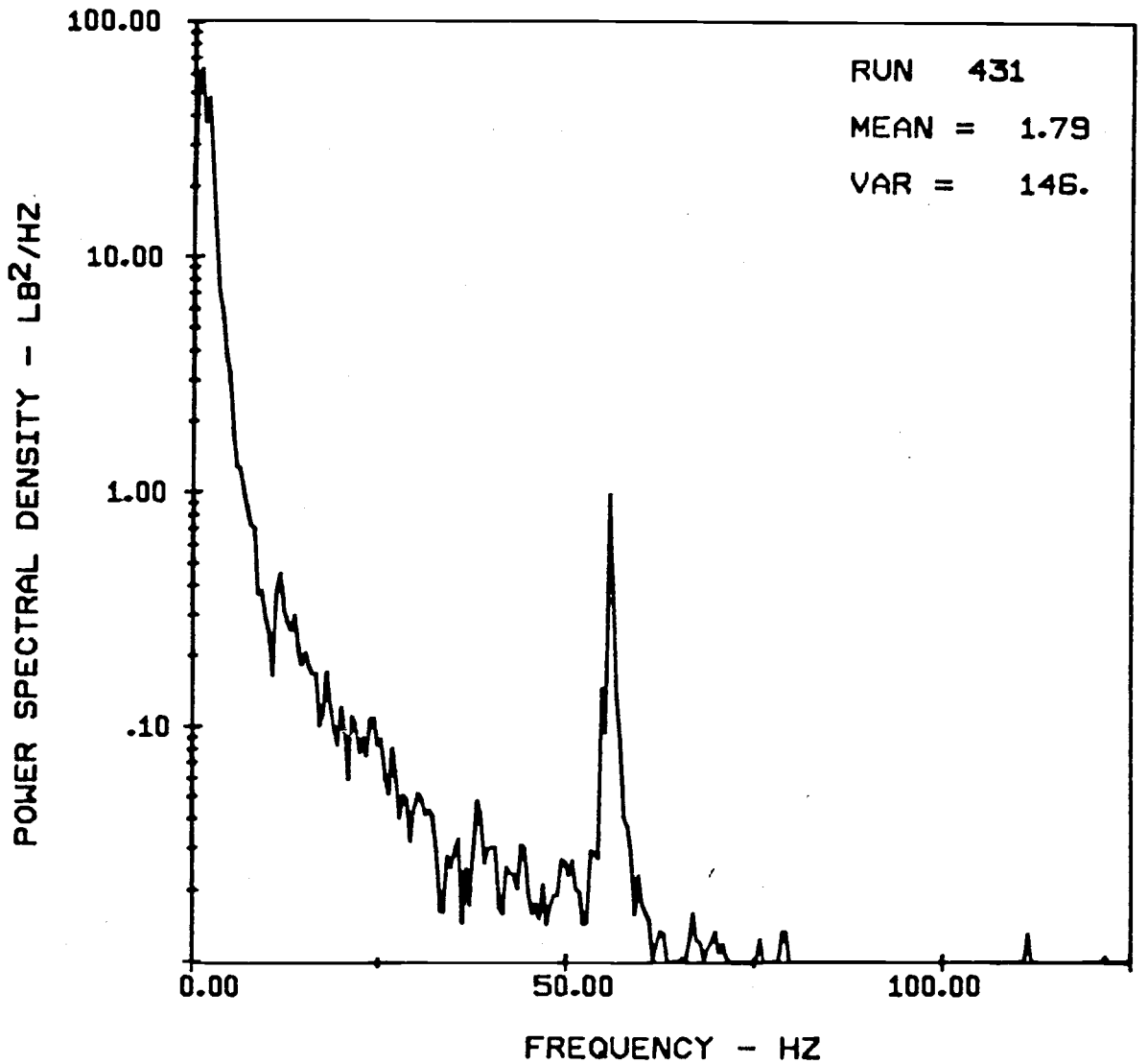


HORIZONTAL FORCES ON A 10-TUBE ARRAY (V = 7 ft/sec)
IN E18 SAND WITH 20'' ARRAY HEIGHT AND 4'' TUBE SPACING

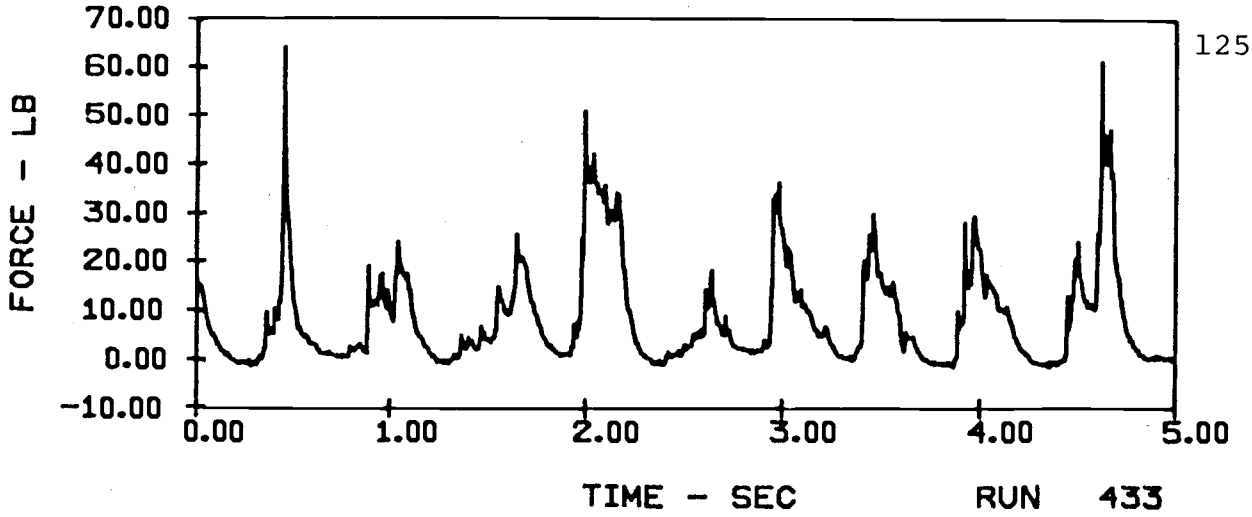


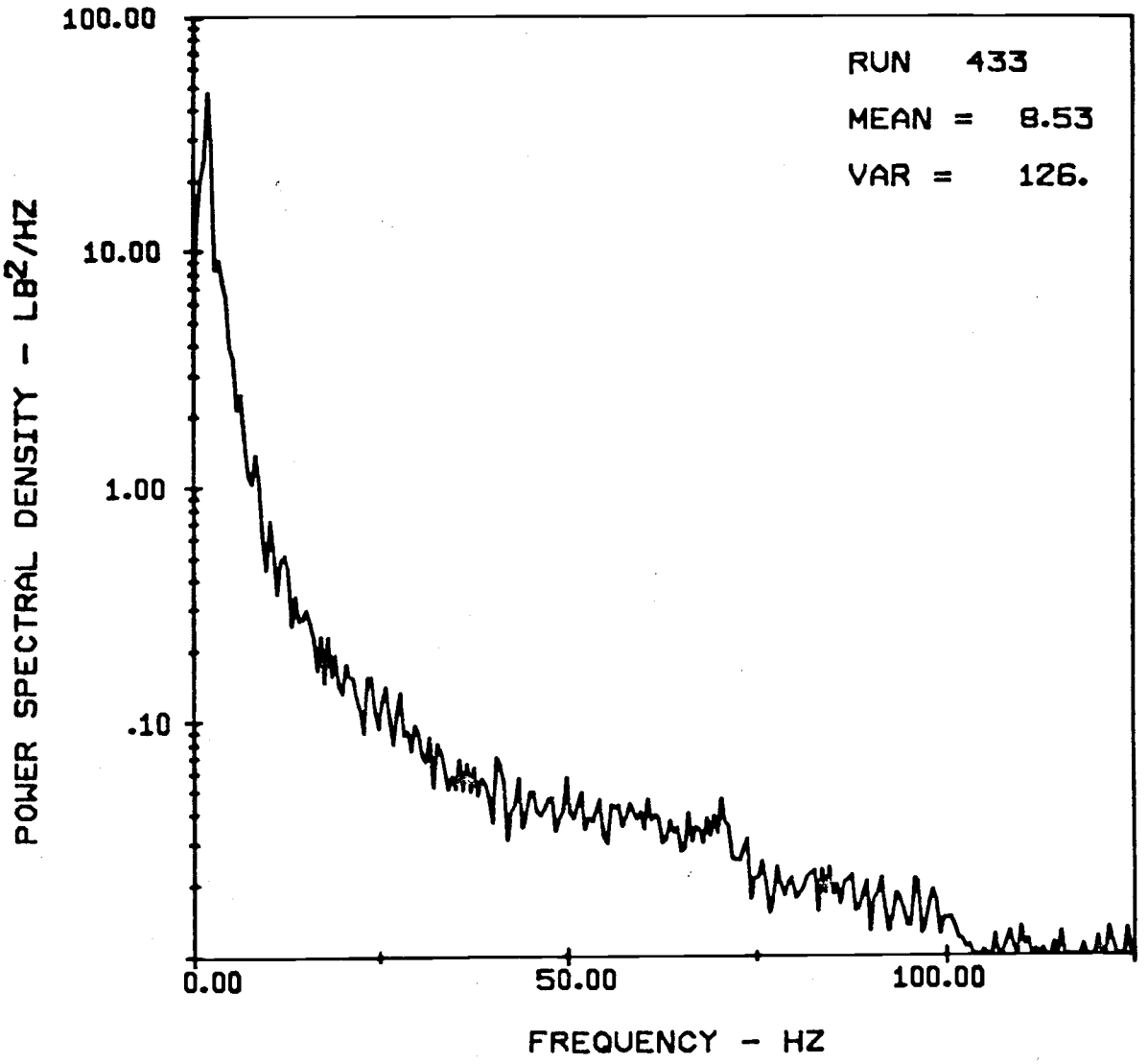


VERTICAL FORCES ON A SINGLE TUBE (V = 9 ft/sec)
IN E18 SAND WITH 20" ARRAY HEIGHT AND 4" TUBE SPACING

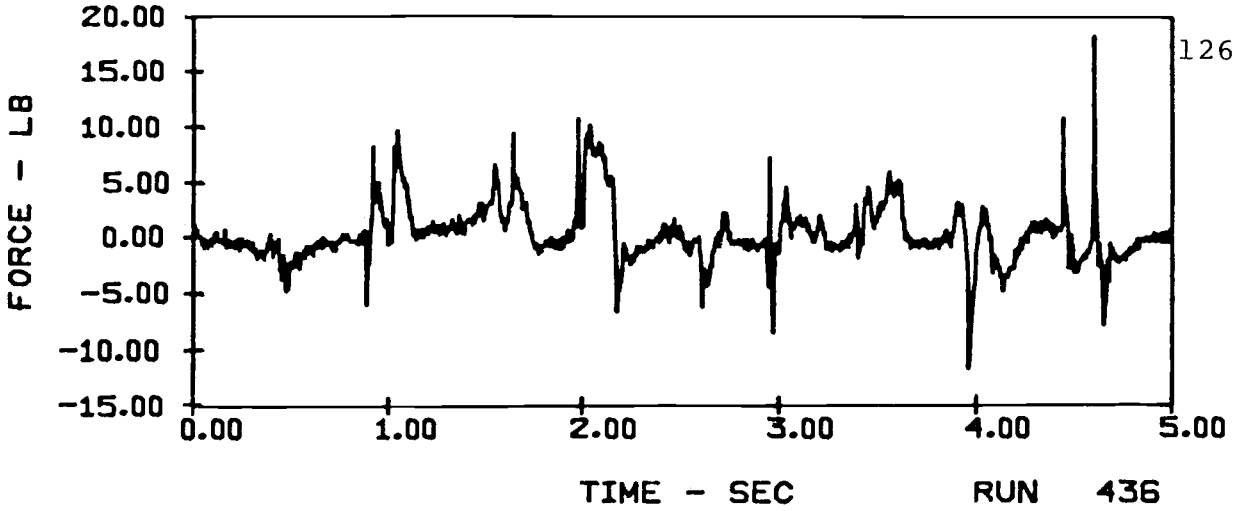


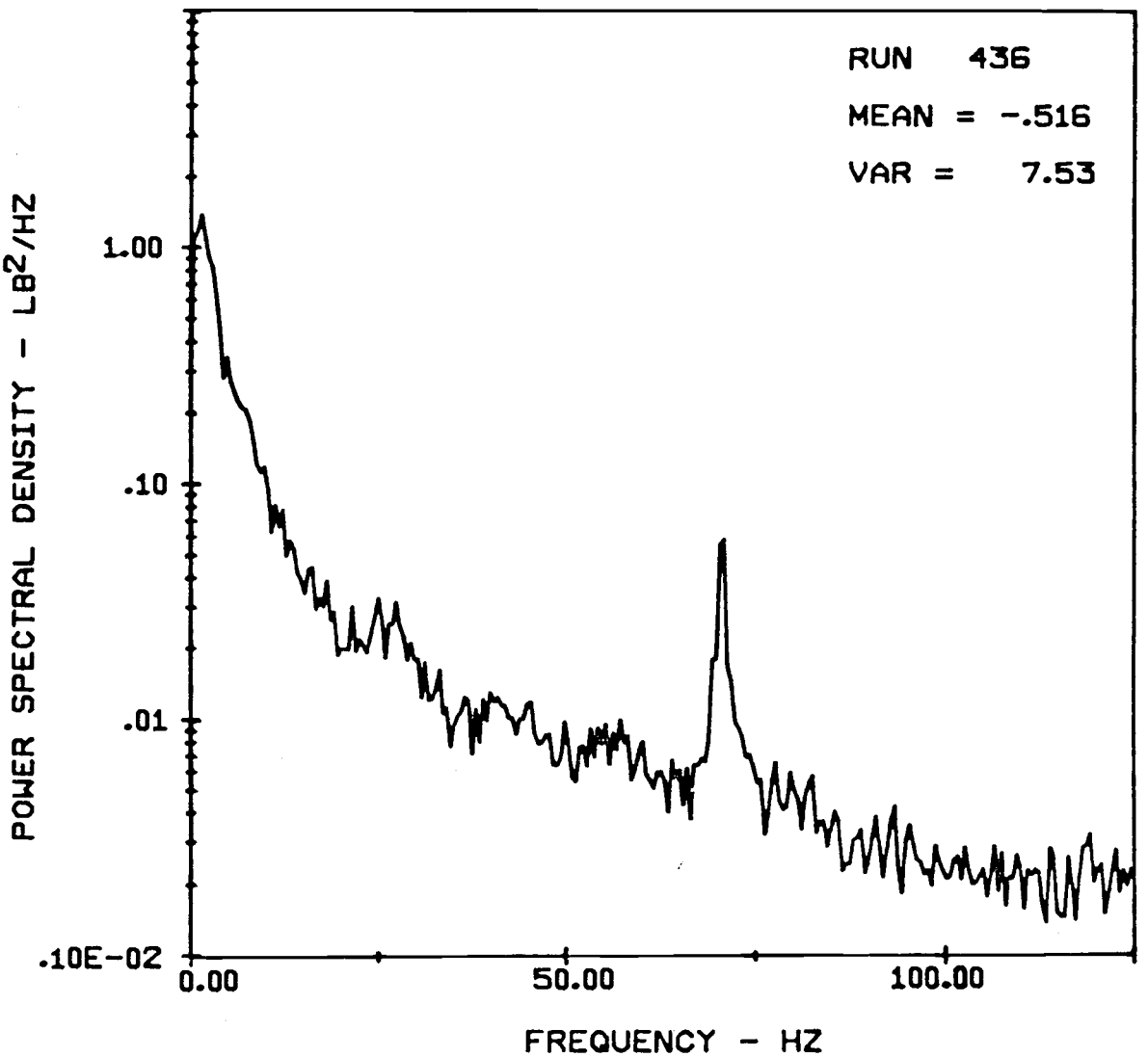


HORIZONTAL FORCES ON A SINGLE TUBE (V = 9 ft/sec)
IN E18 SAND WITH 20" ARRAY HEIGHT AND 4" TUBE SPACING

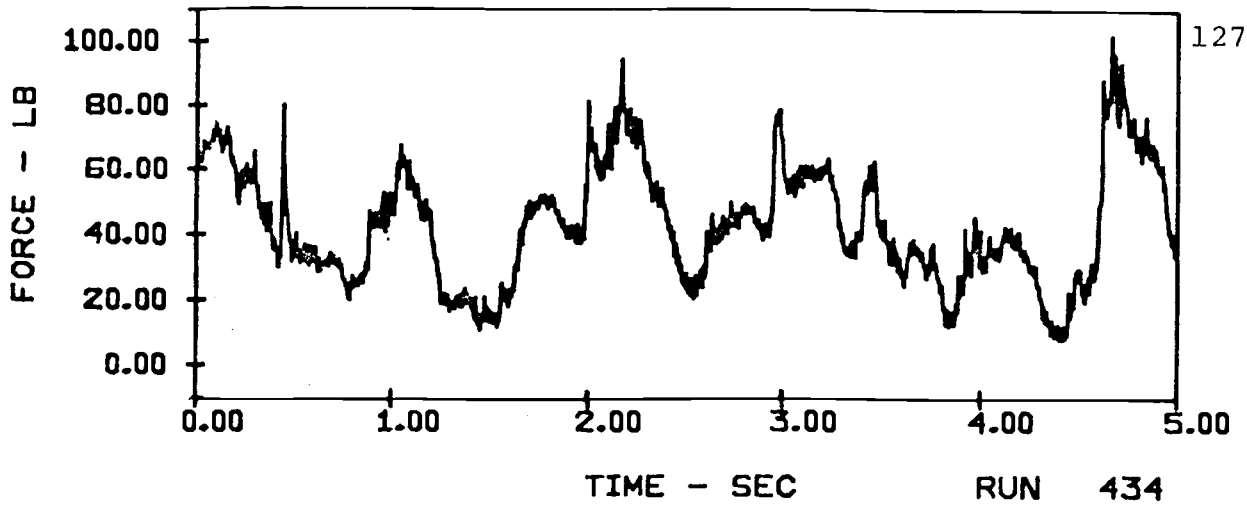


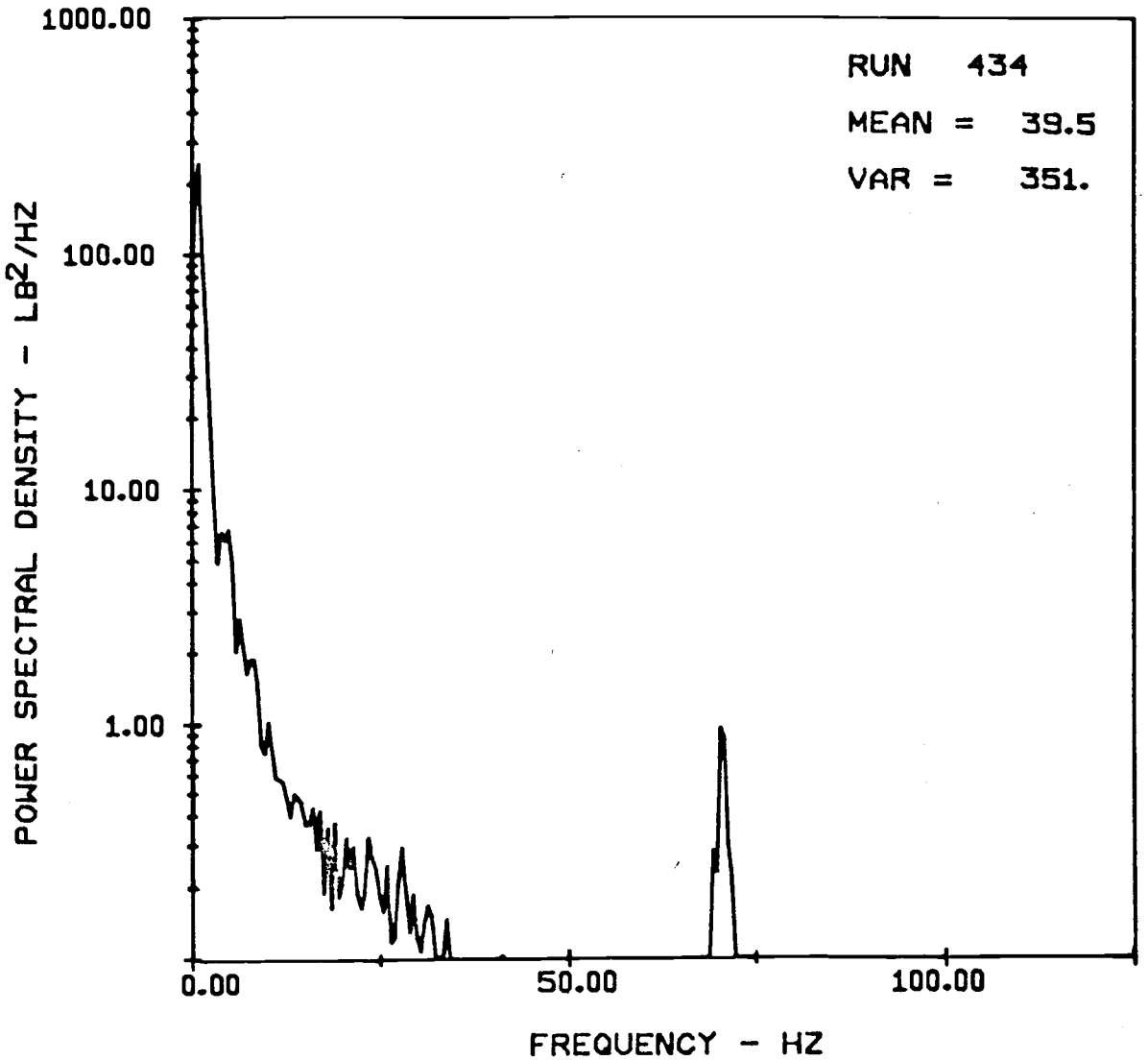


VERTICAL FORCES ON A 10-TUBE ARRAY (V = 9ft/sec)
IN E18 SAND WITH 20" ARRAY HEIGHT AND 4" TUBE SPACING

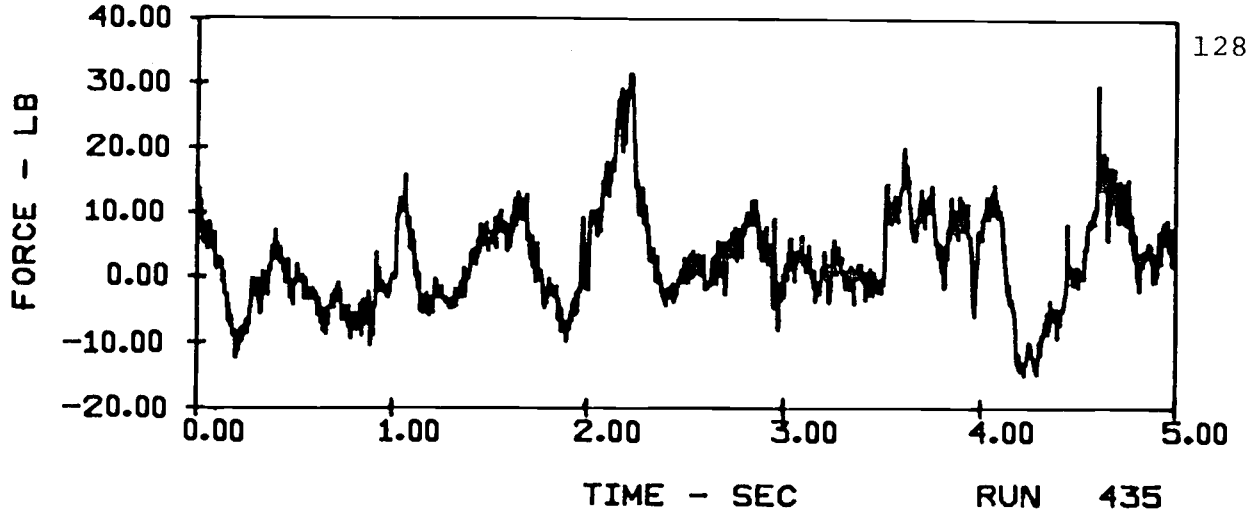


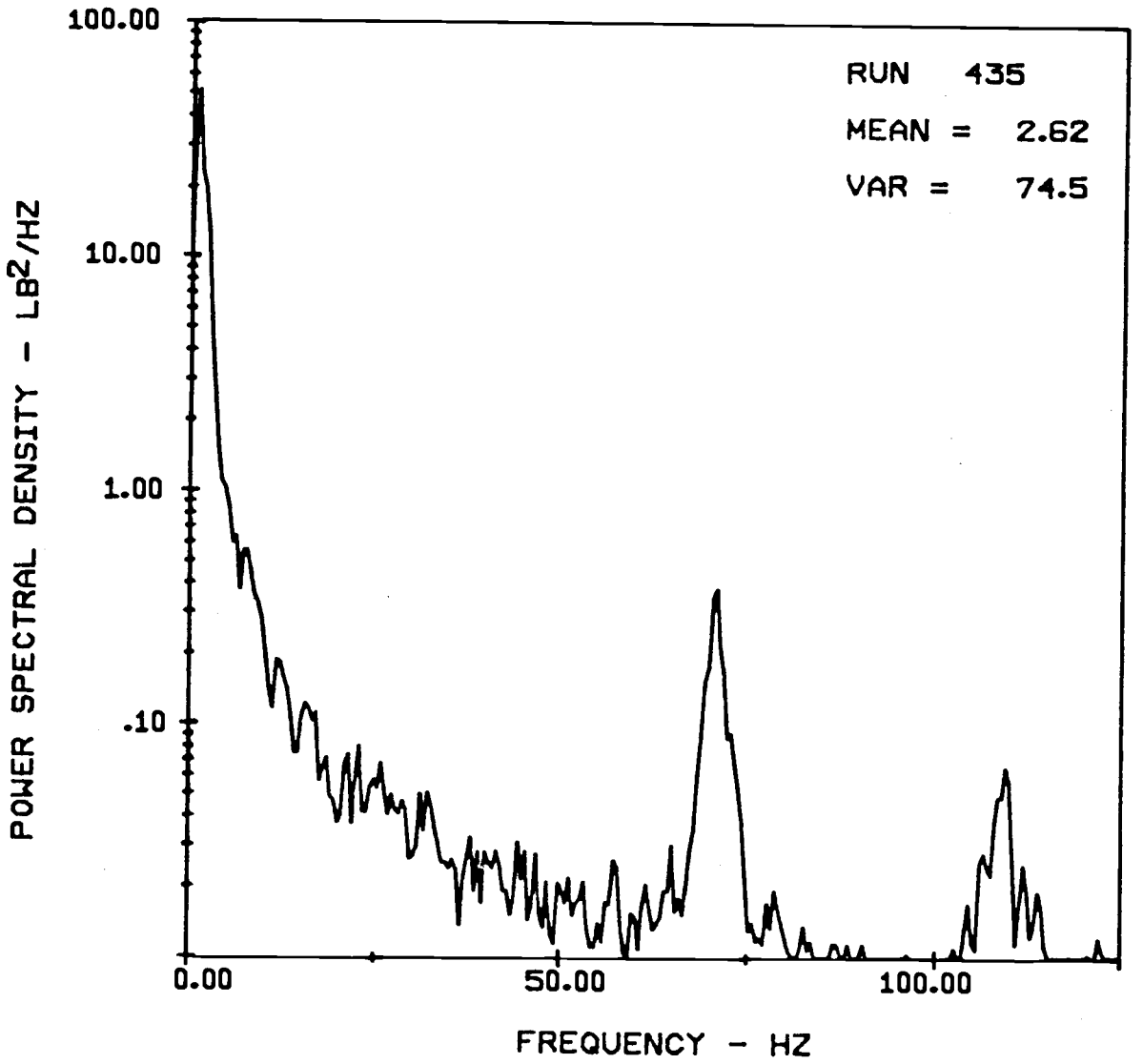


HORIZONTAL FORCES ON A 10-TUBE ARRAY (V = 9 ft/sec)
IN E18 SAND WITH 20" ARRAY HEIGHT AND 4" TUBE SPACING

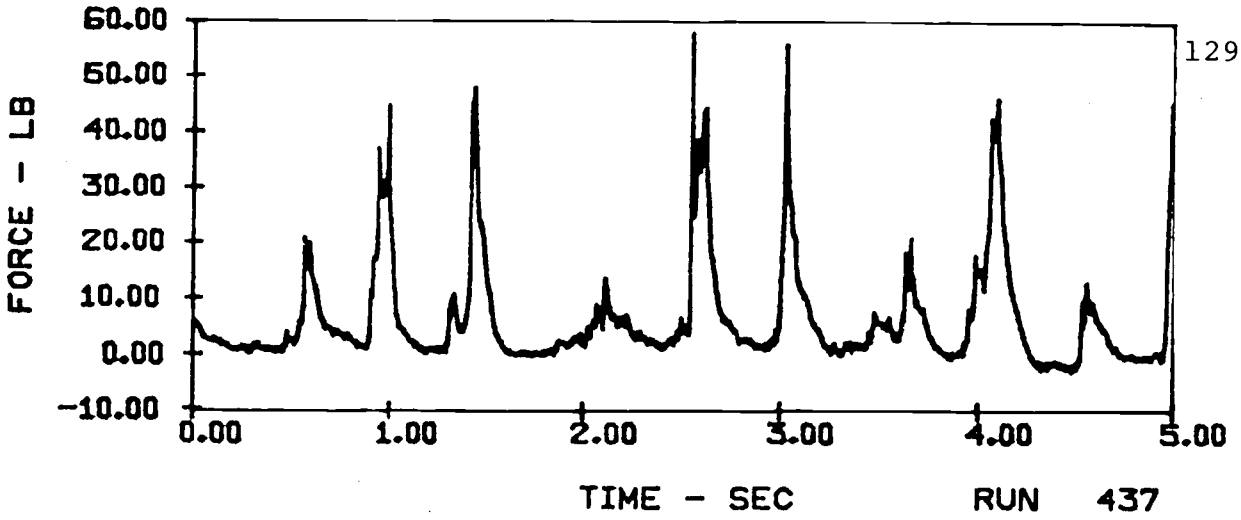


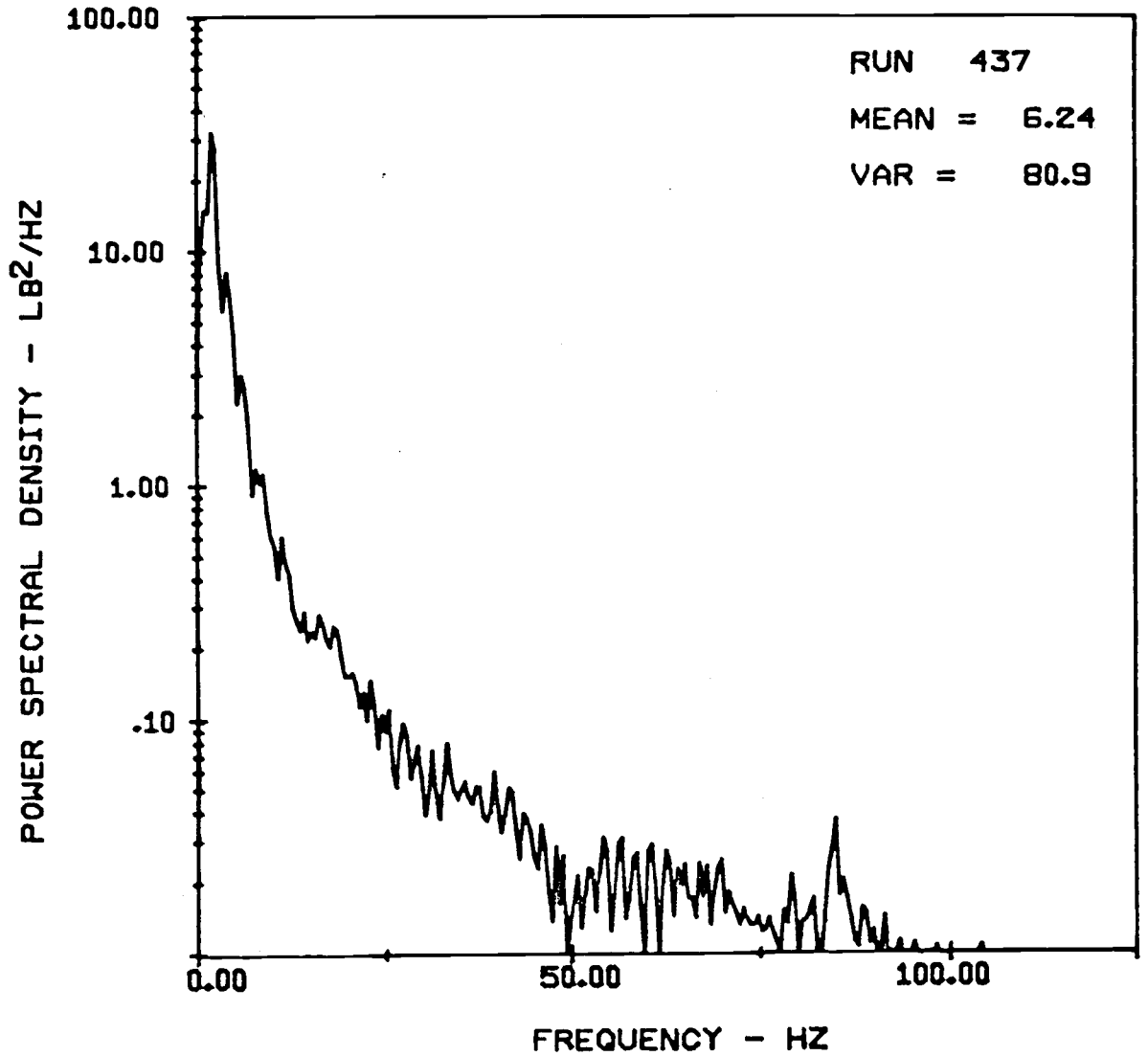


VERTICAL FORCES ON A SINGLE TUBE (V = 11 ft/sec)
IN E18 SAND WITH 20" ARRAY HEIGHT AND 4" TUBE SPACING

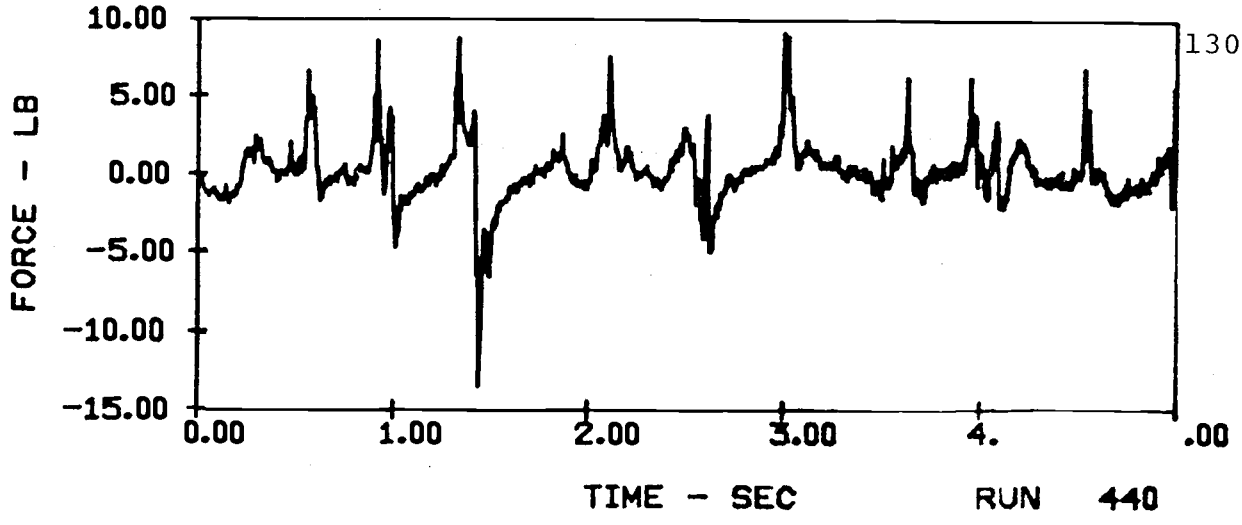


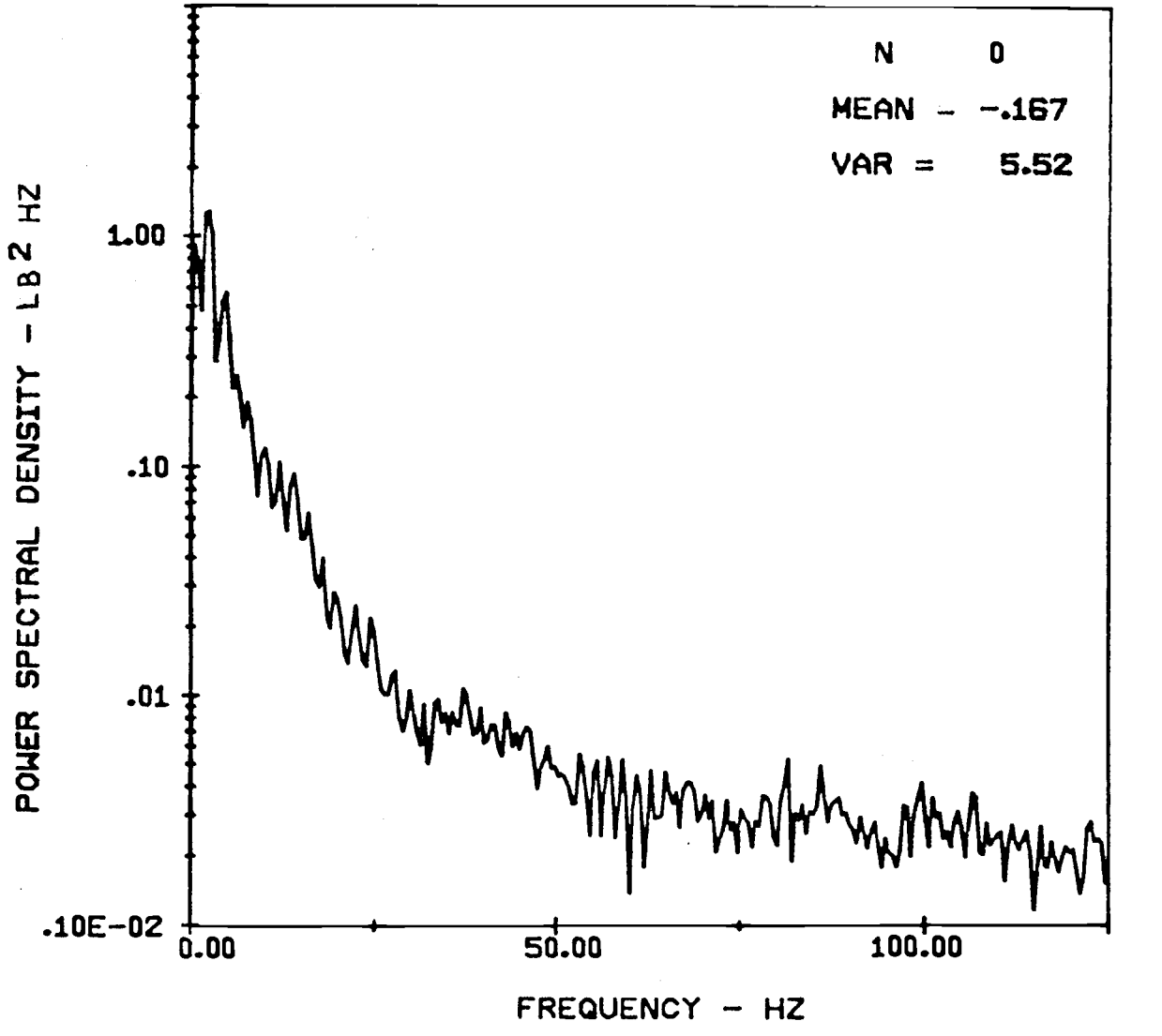


HORIZONTAL FORCES ON A SINGLE TUBE (V = 11 ft/sec)
IN E18 SAND WITH 20" ARRAY HEIGHT AND 4" TUBE SPACING

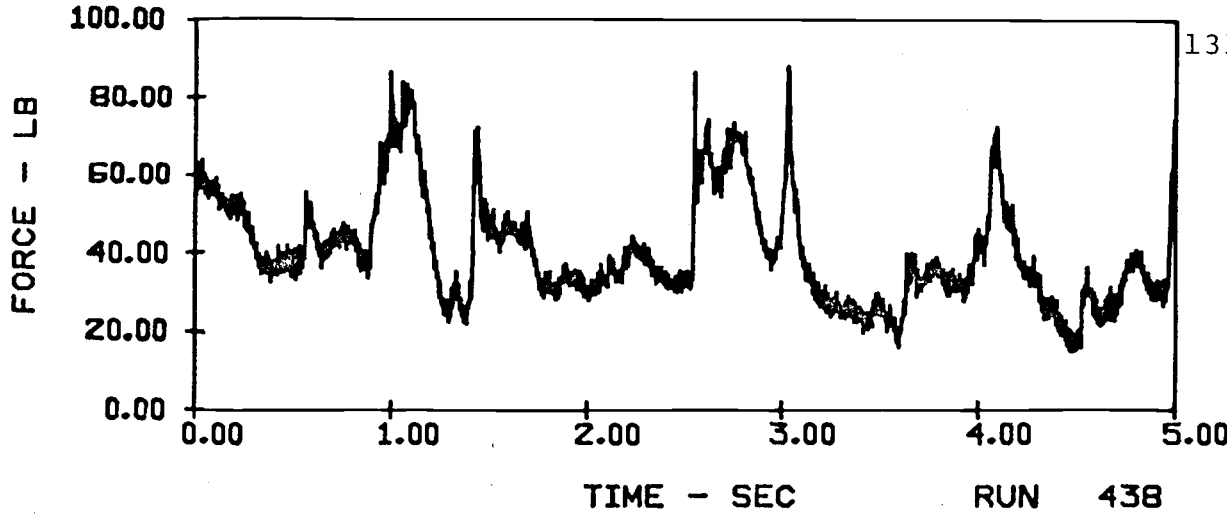


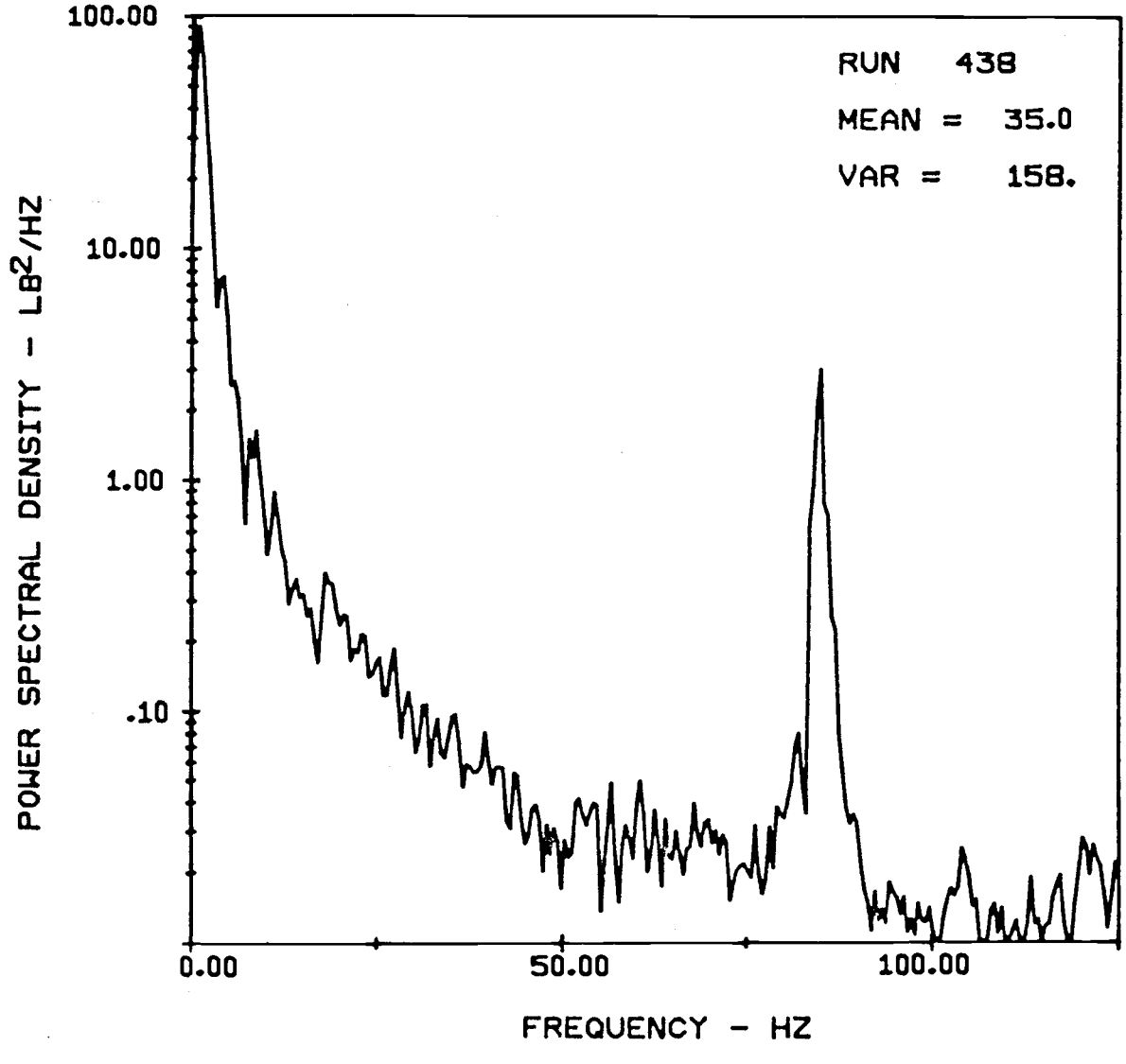


VERTICAL FORCES ON A 10-TUBE ARRAY (V = 11ft/sec)
IN E18 SAND WITH 20'' ARRAY HEIGHT AND 4'' TUBE SPACING

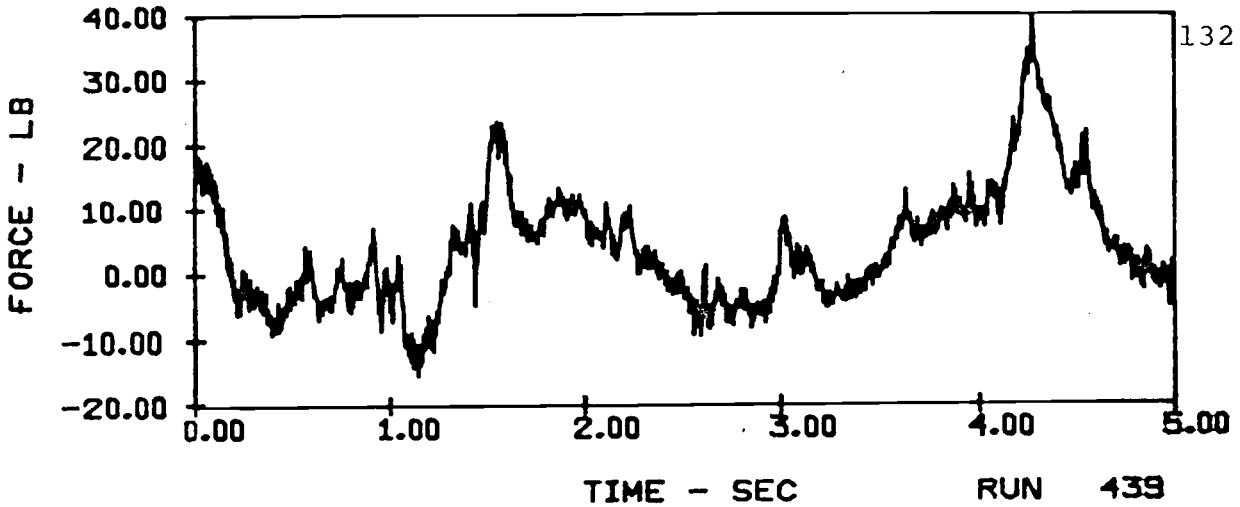


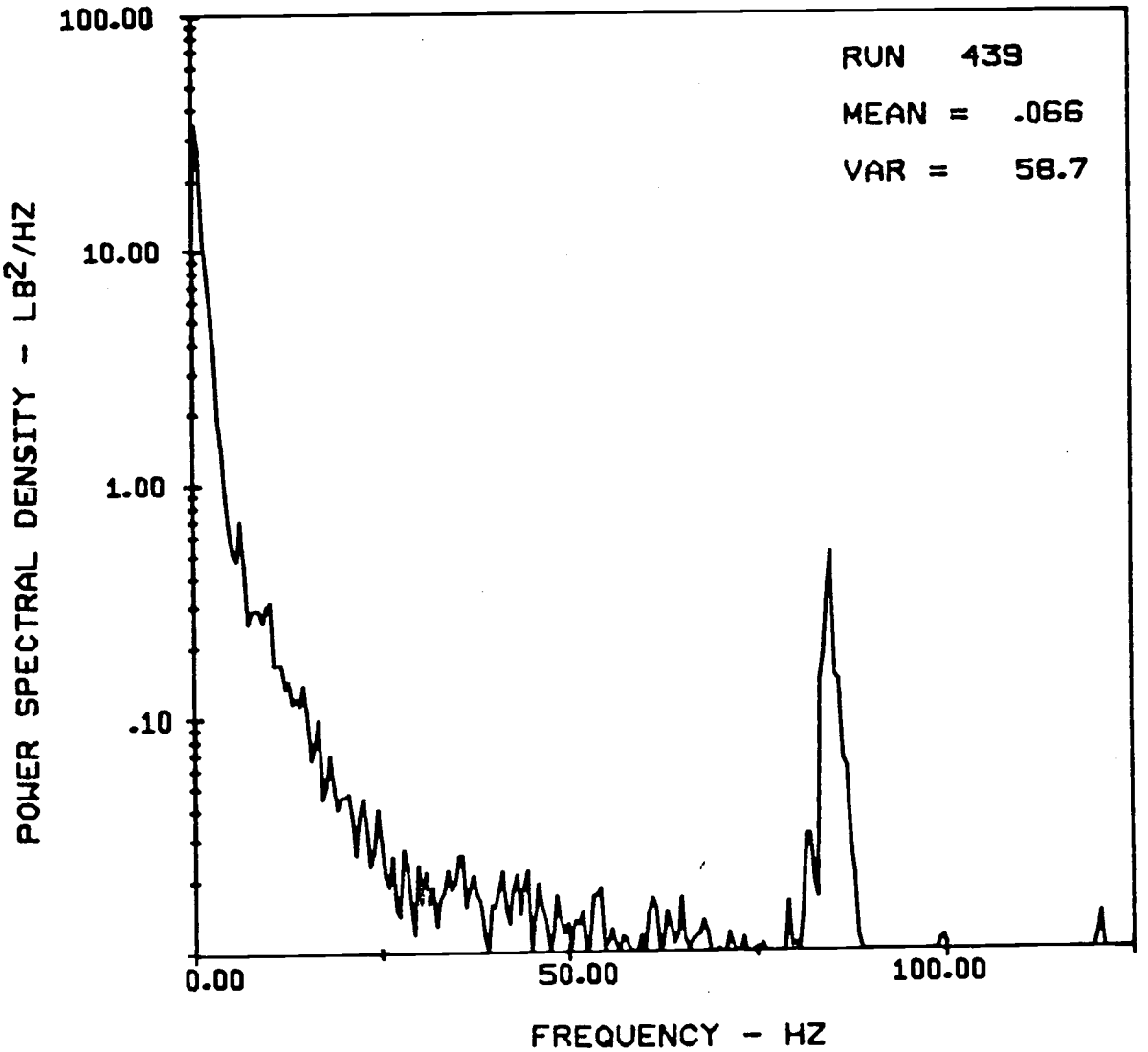


HORIZONTAL FORCES ON A 10-TUBE ARRAY (V = 11 ft/sec)
IN E18 SAND WITH 20'' ARRAY HEIGHT AND 4'' TUBE SPACING

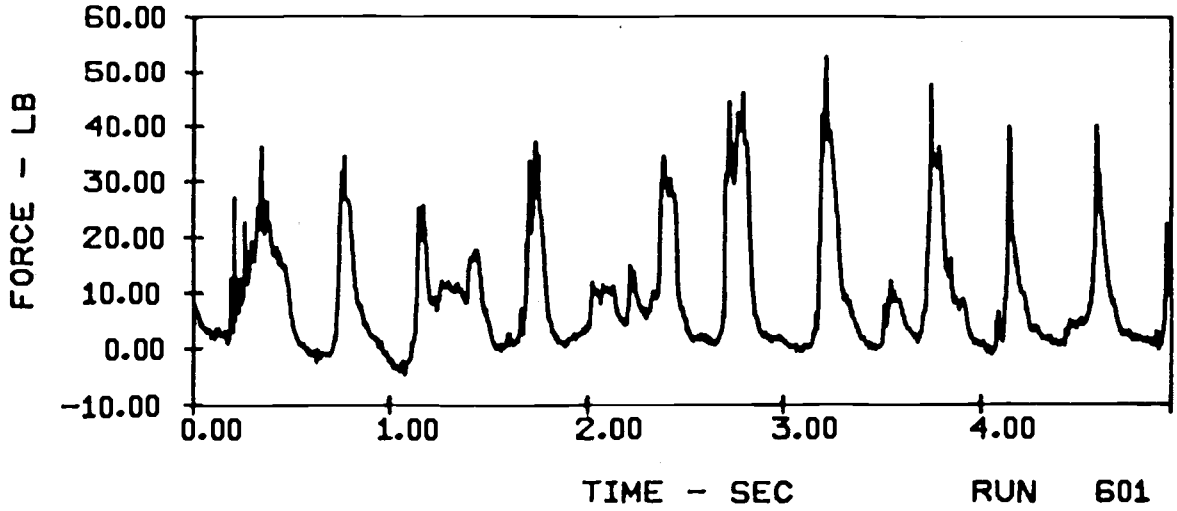


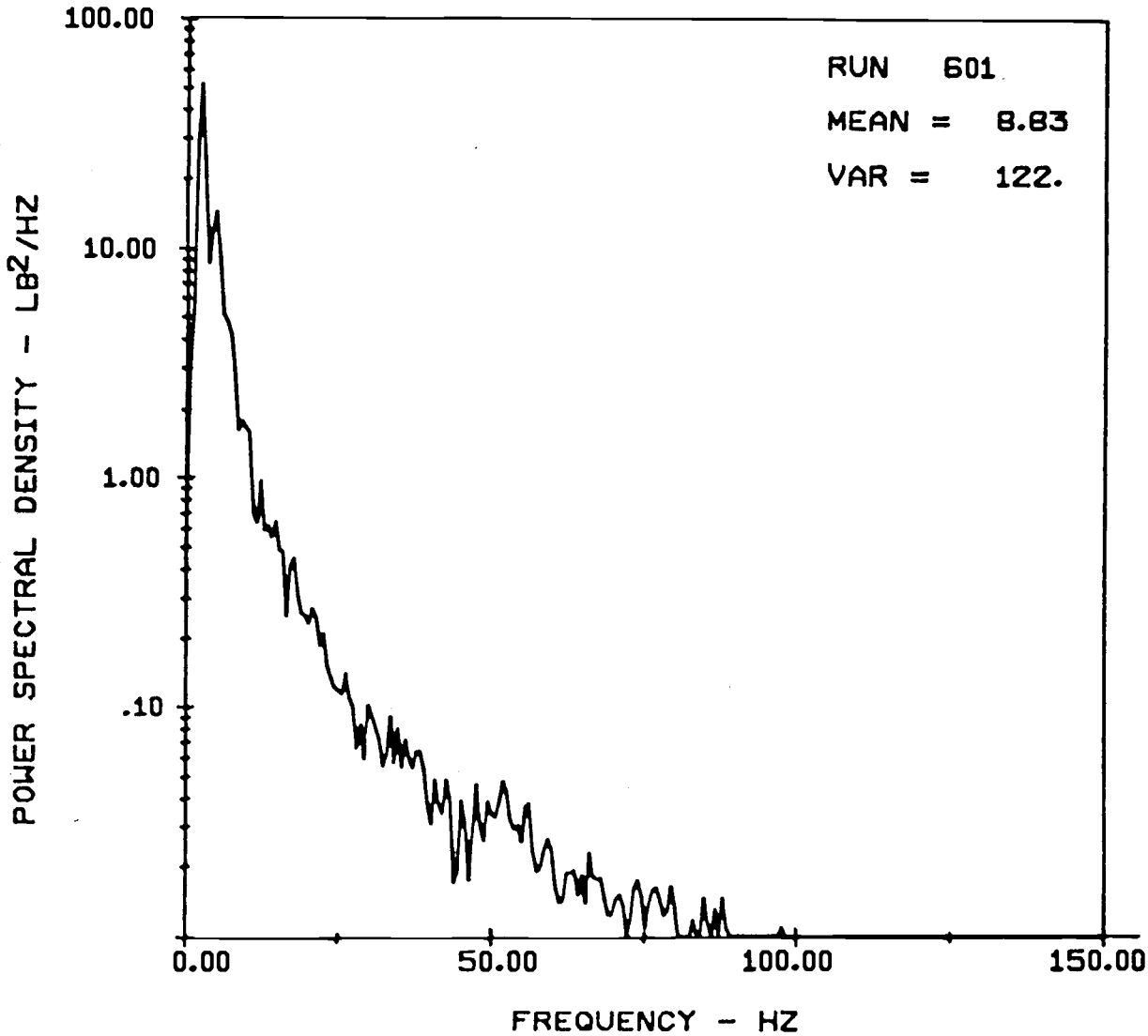


VERTICAL FORCES ON A SINGLE TUBE (V = 5 ft/sec)
IN EI16 SAND WITH 10" ARRAY HEIGHT AND 6" TUBE SPACING

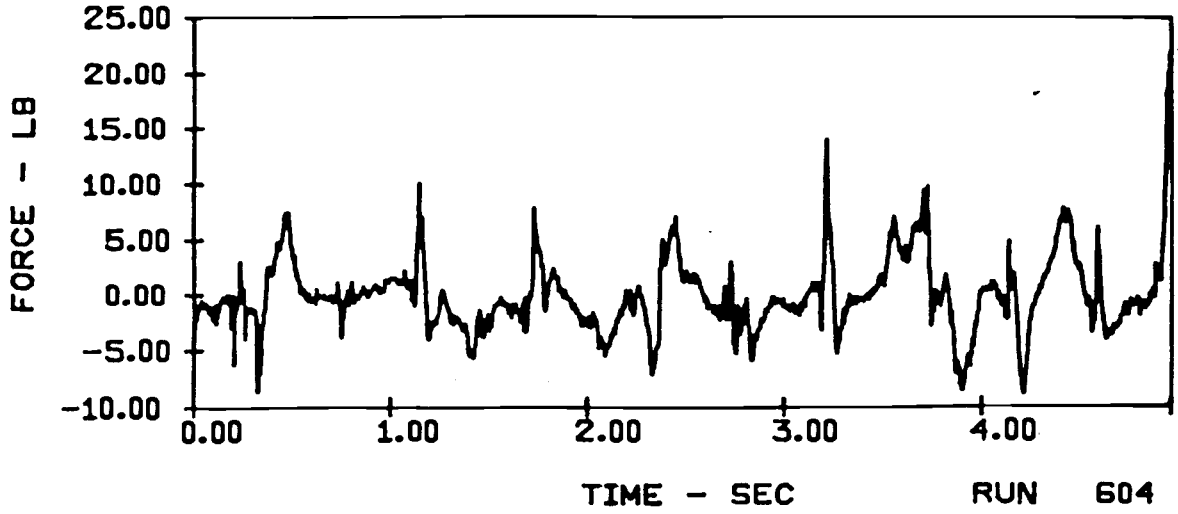


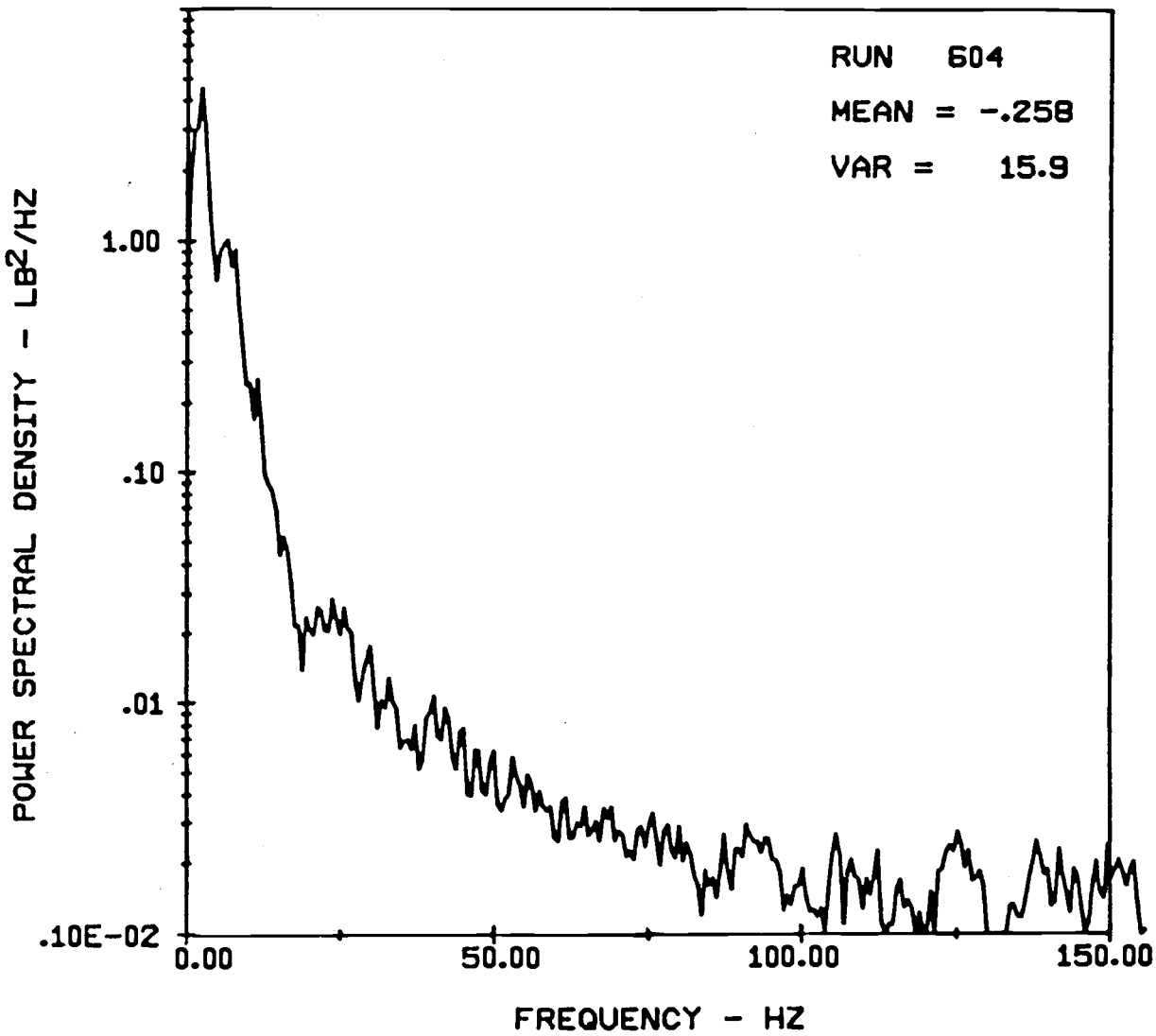


HORIZONTAL FORCES ON A SINGLE TUBE (V = 5 ft/sec)
IN EI16 SAND WITH 10" ARRAY HEIGHT AND 6" TUBE SPACING

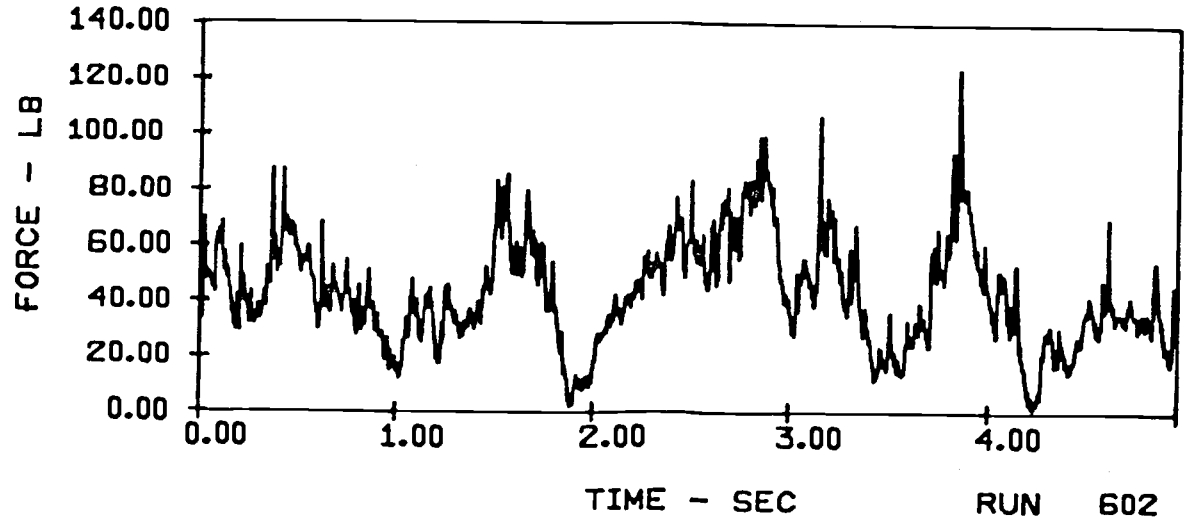


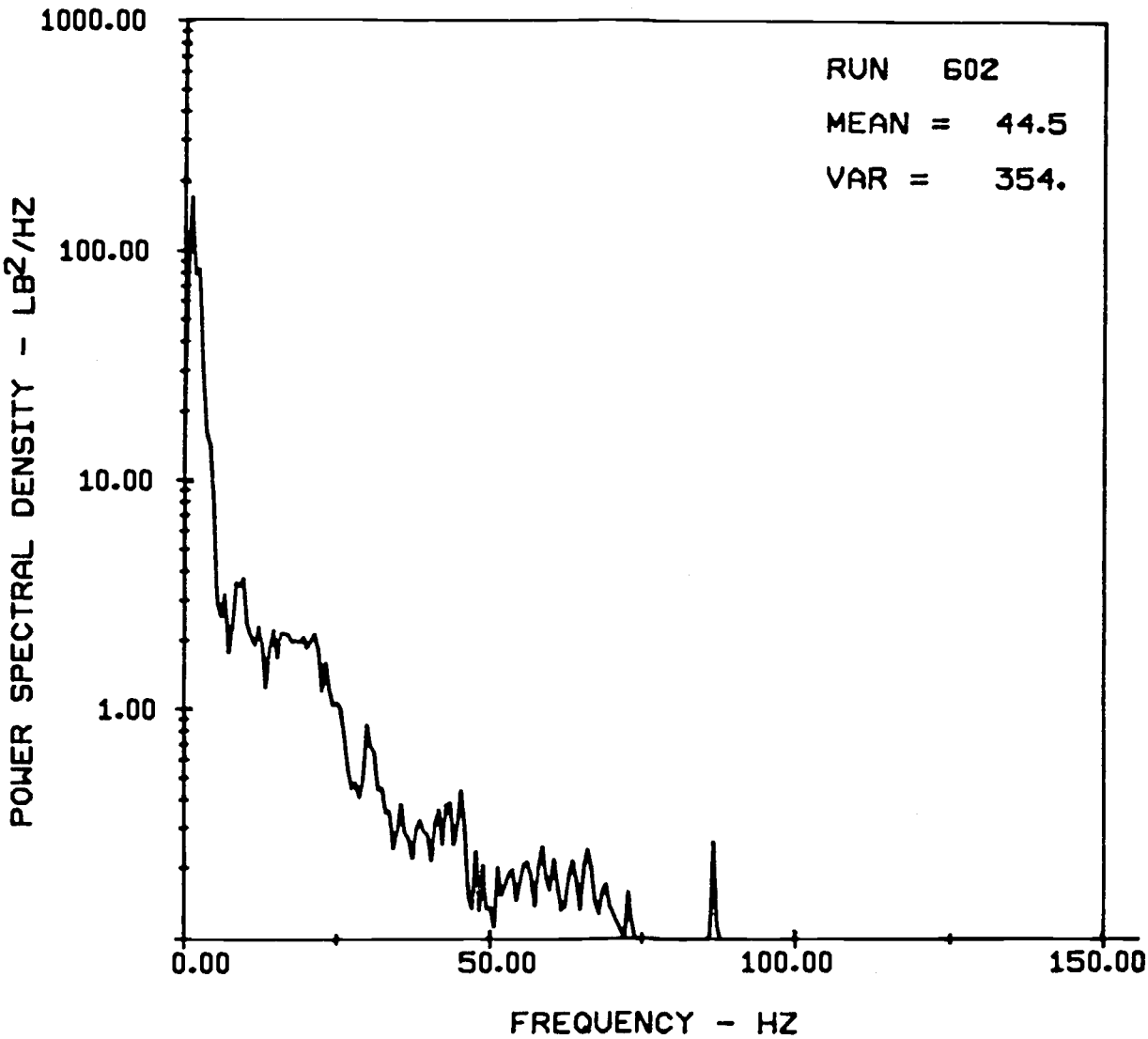


VERTICAL FORCES ON AN 8-TUBE ARRAY (V = 5 ft/sec)
IN EI16 SAND WITH 10" ARRAY HEIGHT AND 6" TUBE SPACING

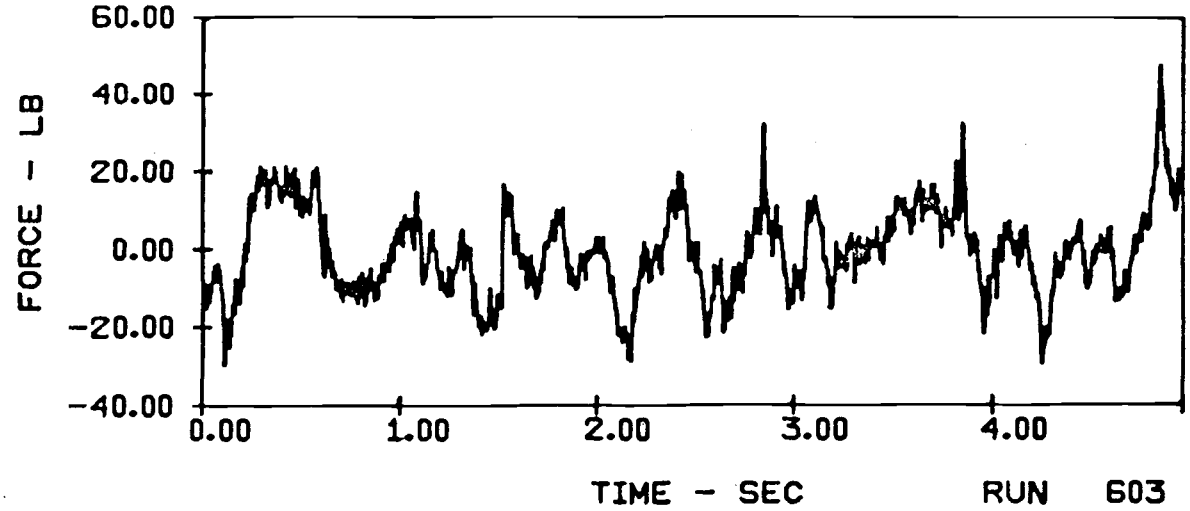


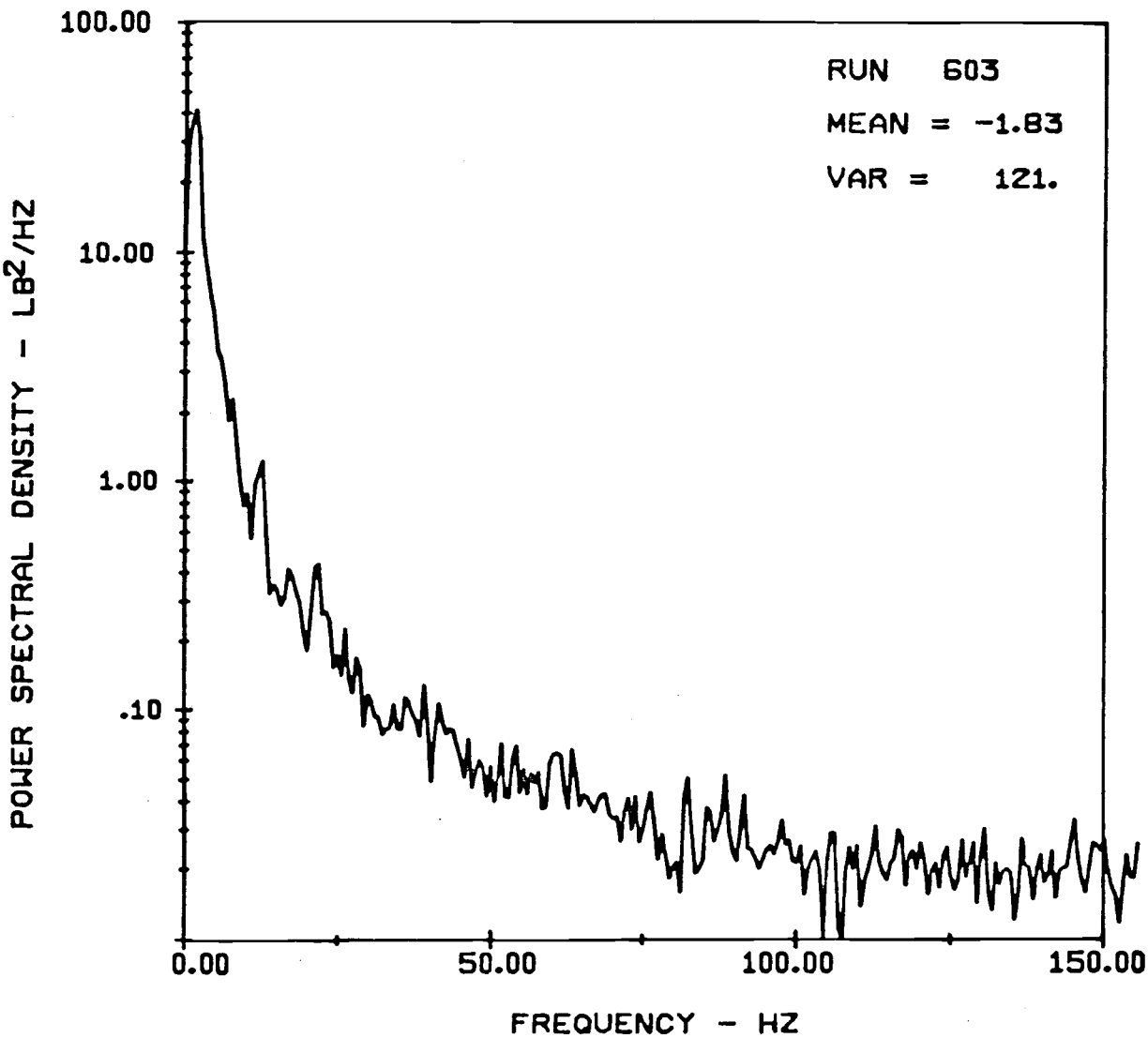


HORIZONTAL FORCES ON AN 8-TUBE ARRAY (V = 5 ft/sec)
IN EI16 SAND WITH 10 " ARRAY HEIGHT AND 6" TUBE SPACING

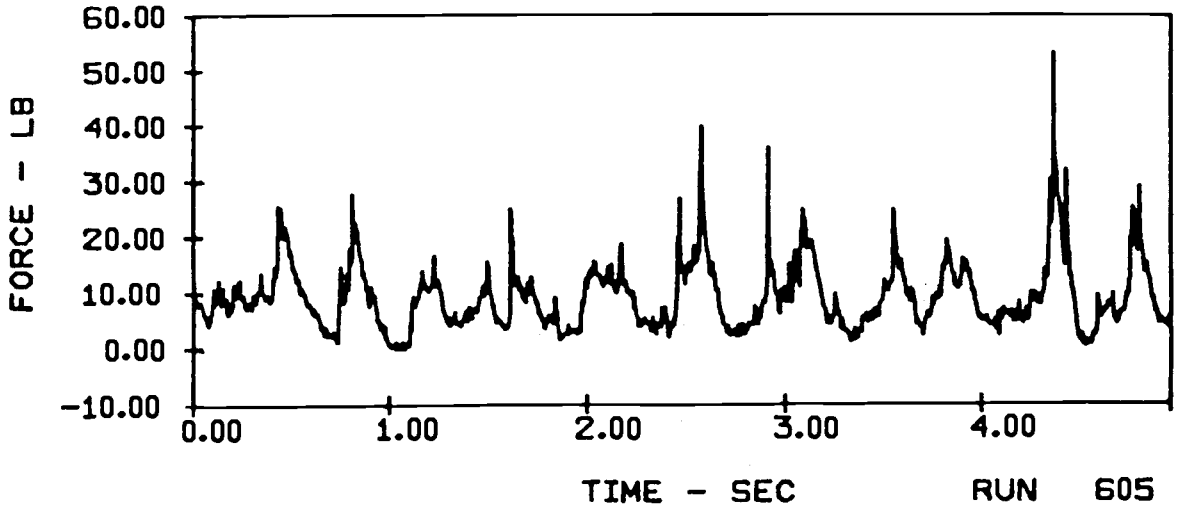


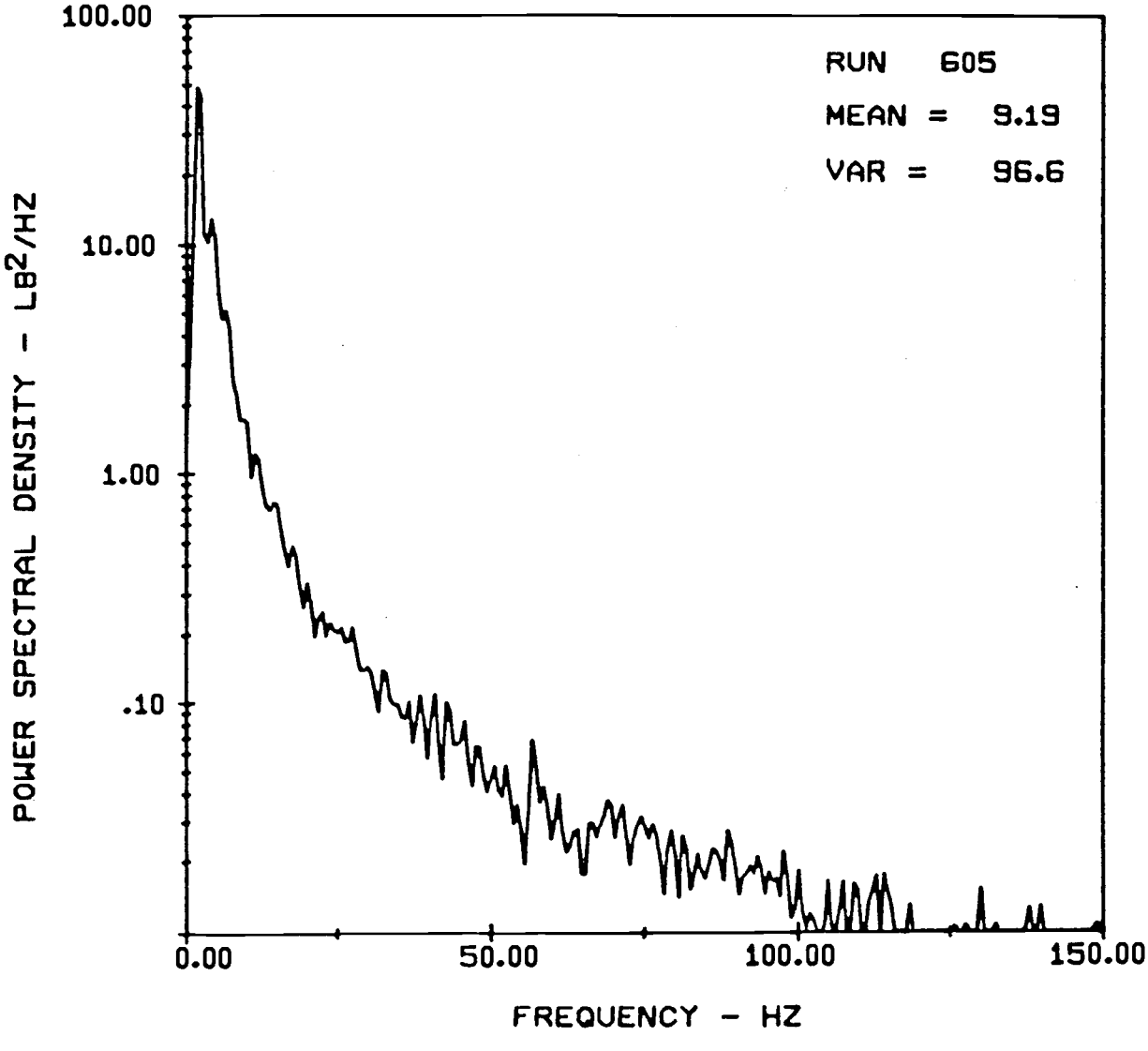


VERTICAL FORCES ON A SINGLE TUBE (V = 7 ft/sec)
IN EI16 SAND WITH 10" ARRAY HEIGHT AND 6" TUBE SPACING

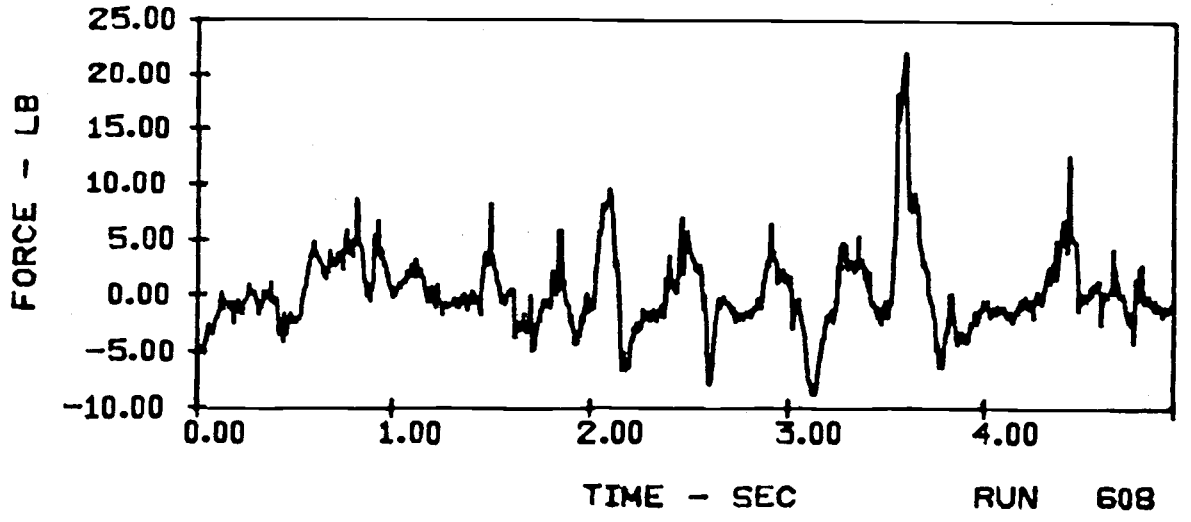


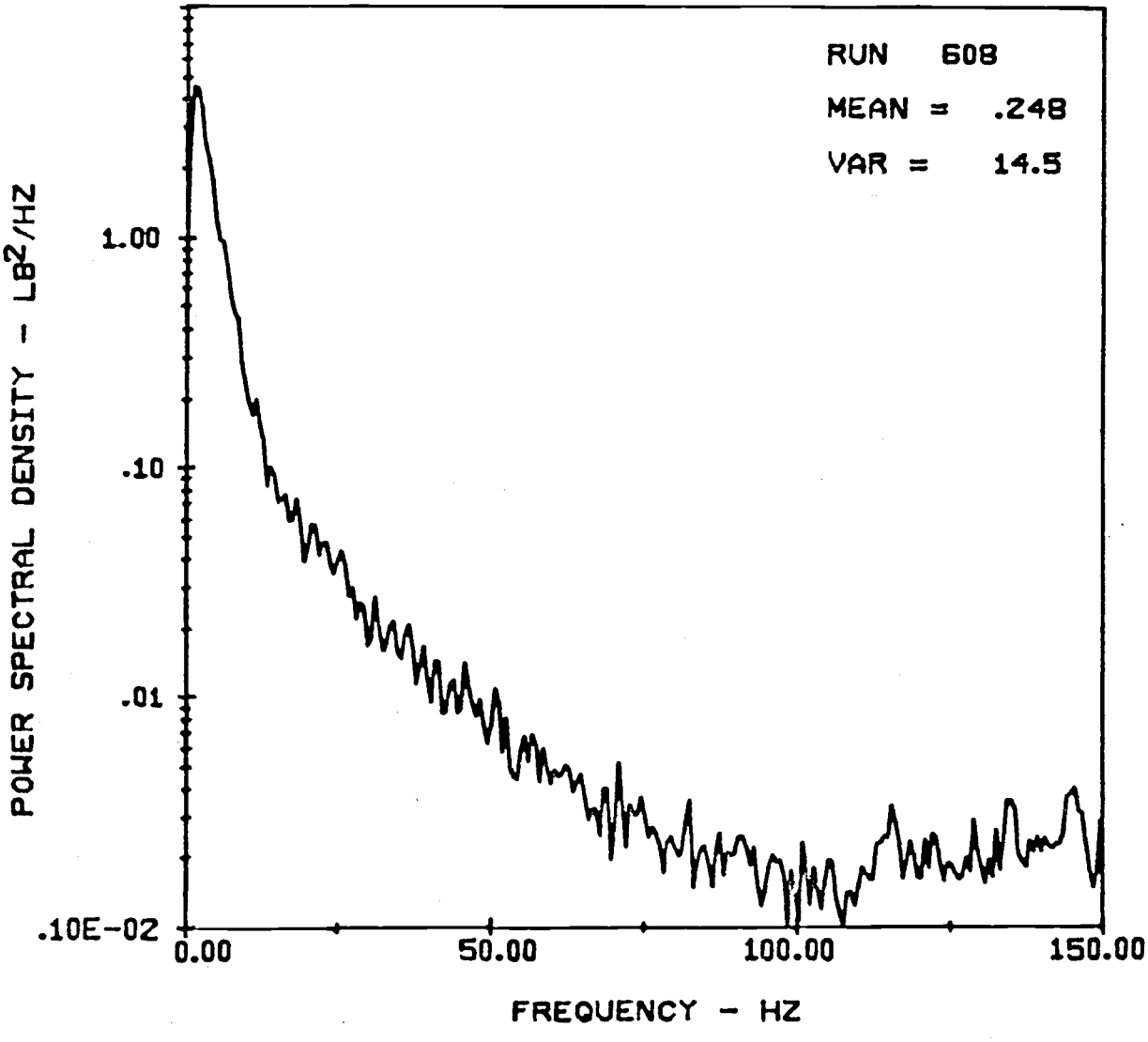


HORIZONTAL FORCES ON A SINGLE TUBE (V = 7 ft/sec)
IN EI16 SAND WITH 10" ARRAY HEIGHT AND 6" TUBE SPACING

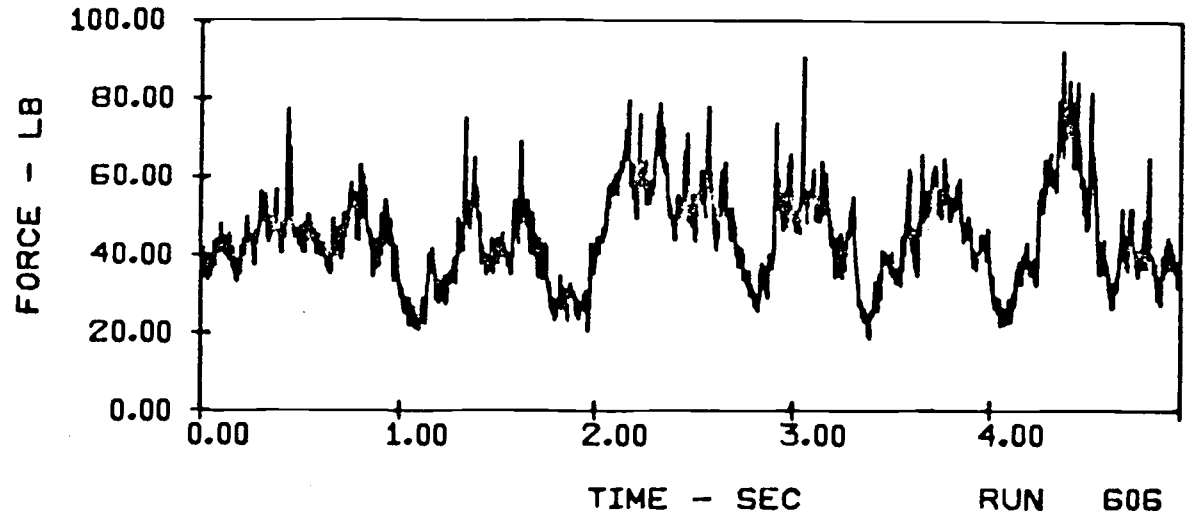


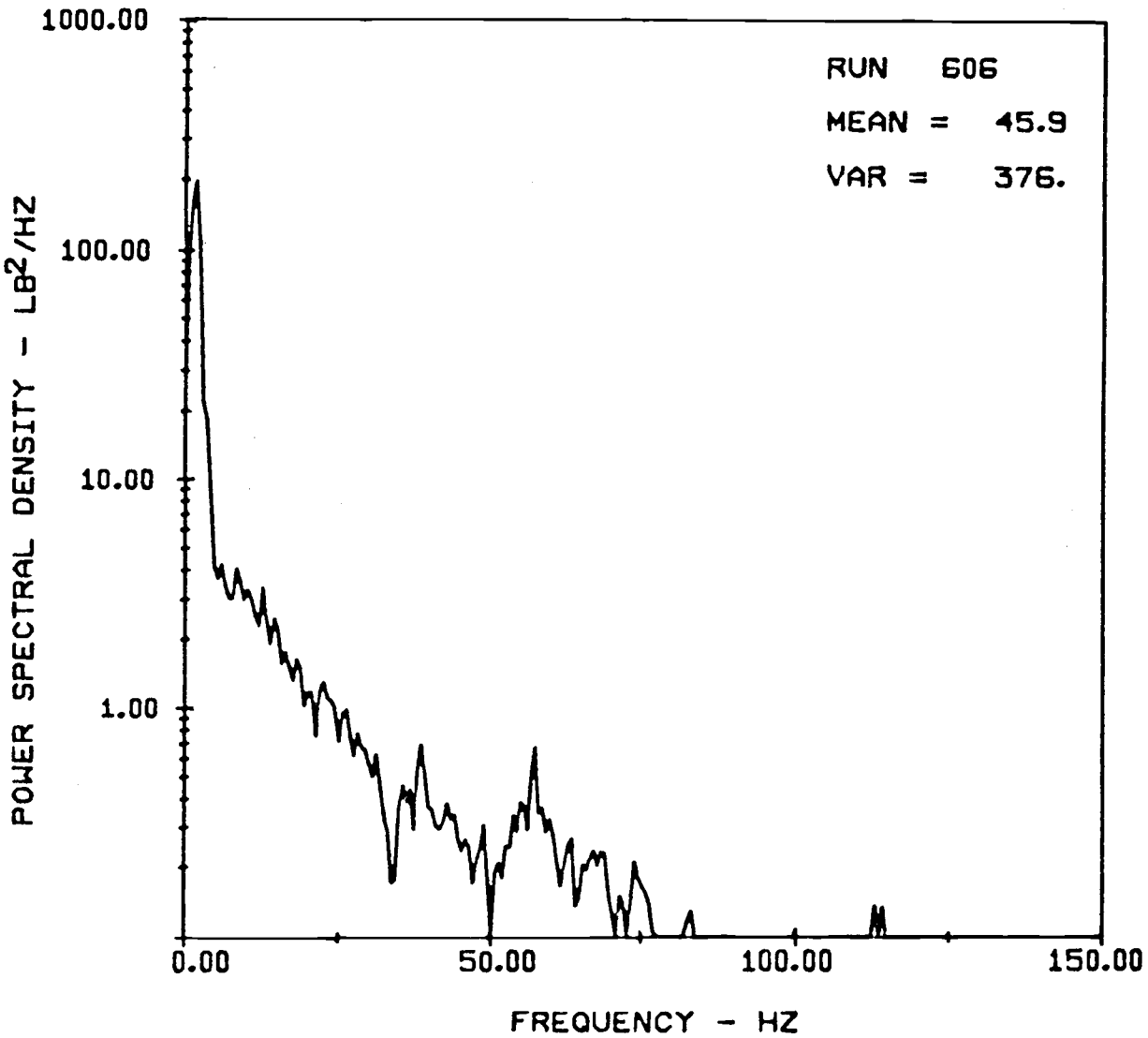


VERTICAL FORCES ON AN 8-TUBE ARRAY (V = 7 ft/sec)
IN EI16 SAND WITH 10" ARRAY HEIGHT AND 6" TUBE SPACING

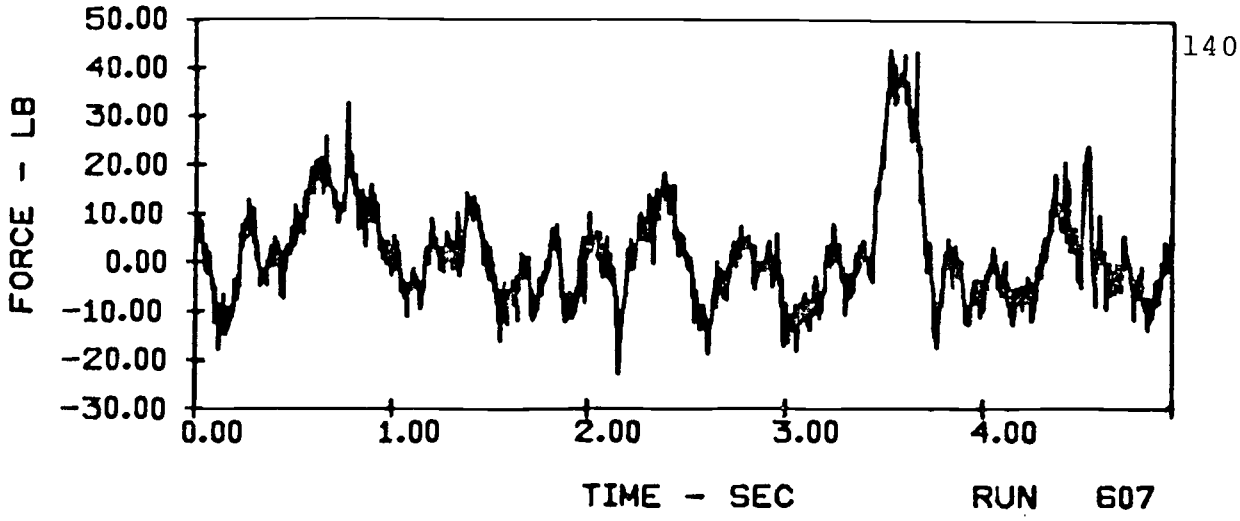


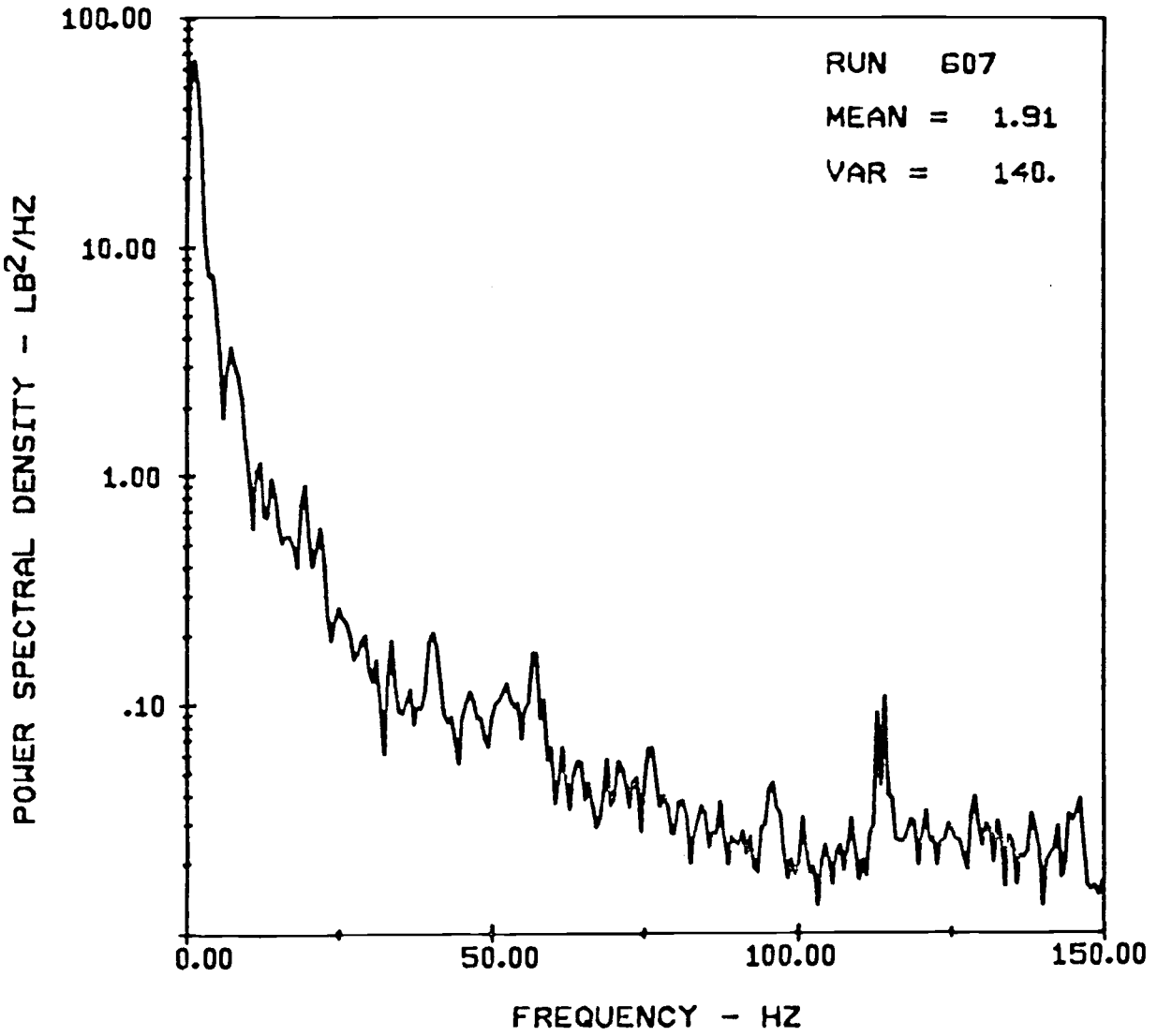


HORIZONTAL FORCES ON AN 8-TUBE ARRAY (V = 7 ft/sec)
IN EI16 SAND WITH 10 " ARRAY HEIGHT AND 6" TUBE SPACING

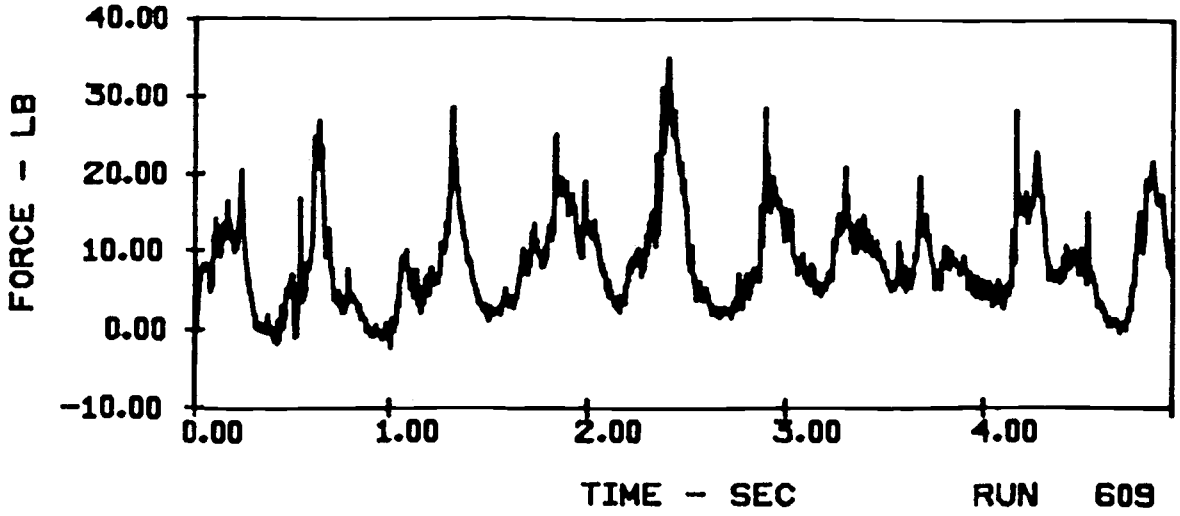


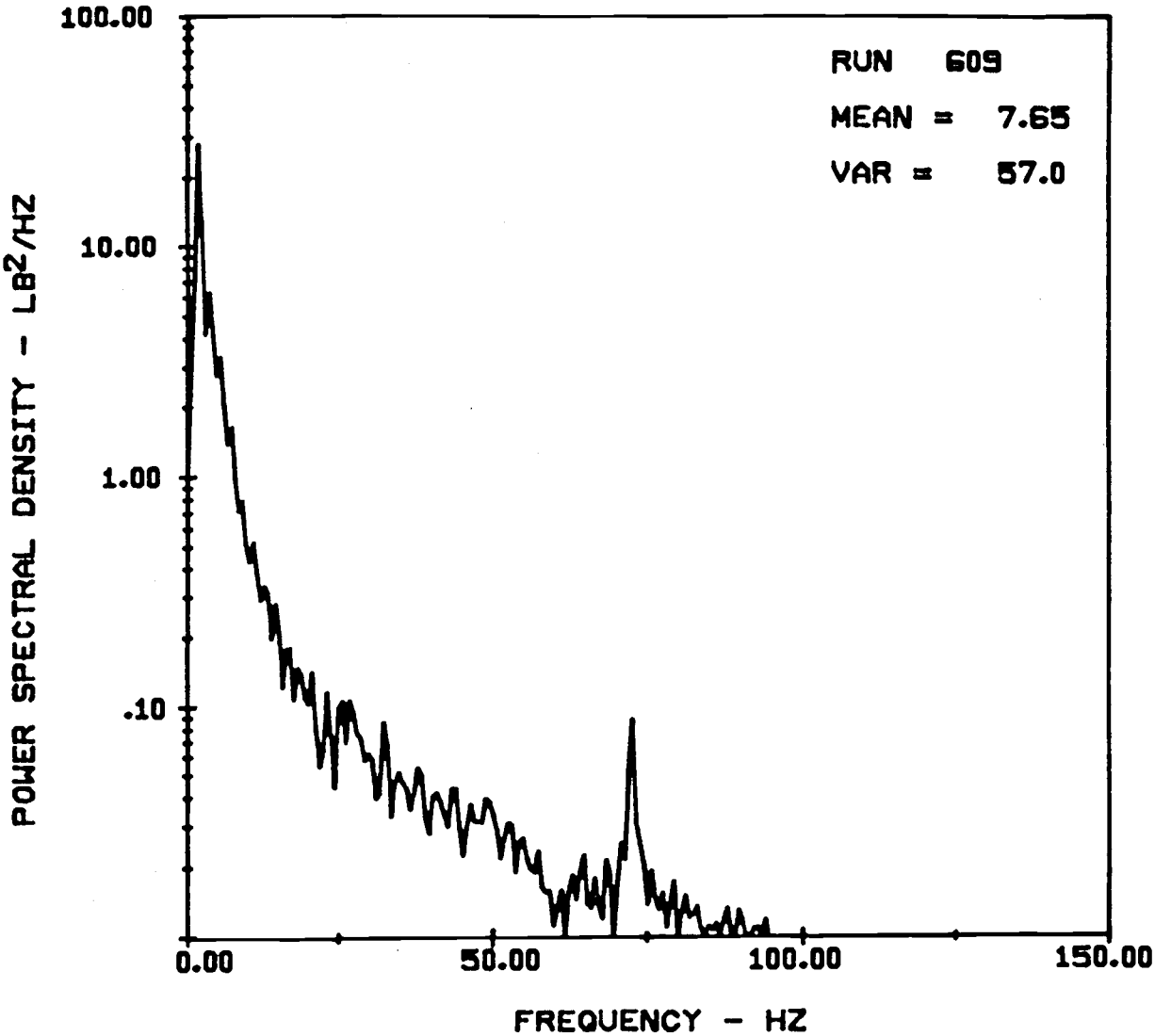


VERTICAL FORCES ON A SINGLE TUBE (V = 9 ft/sec)
IN EI16 SAND WITH 10" ARRAY HEIGHT AND 6" TUBE SPACING

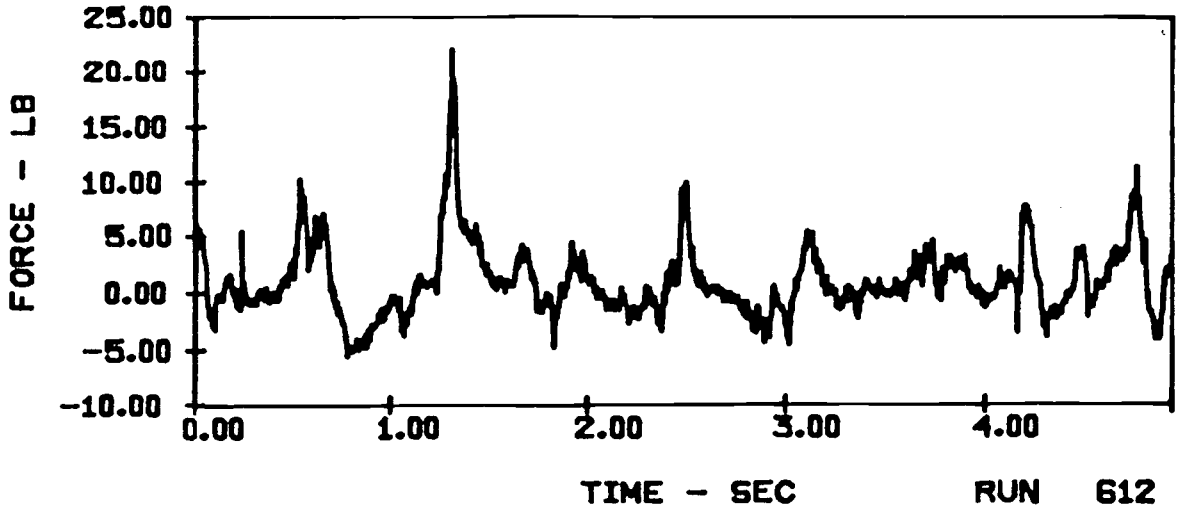


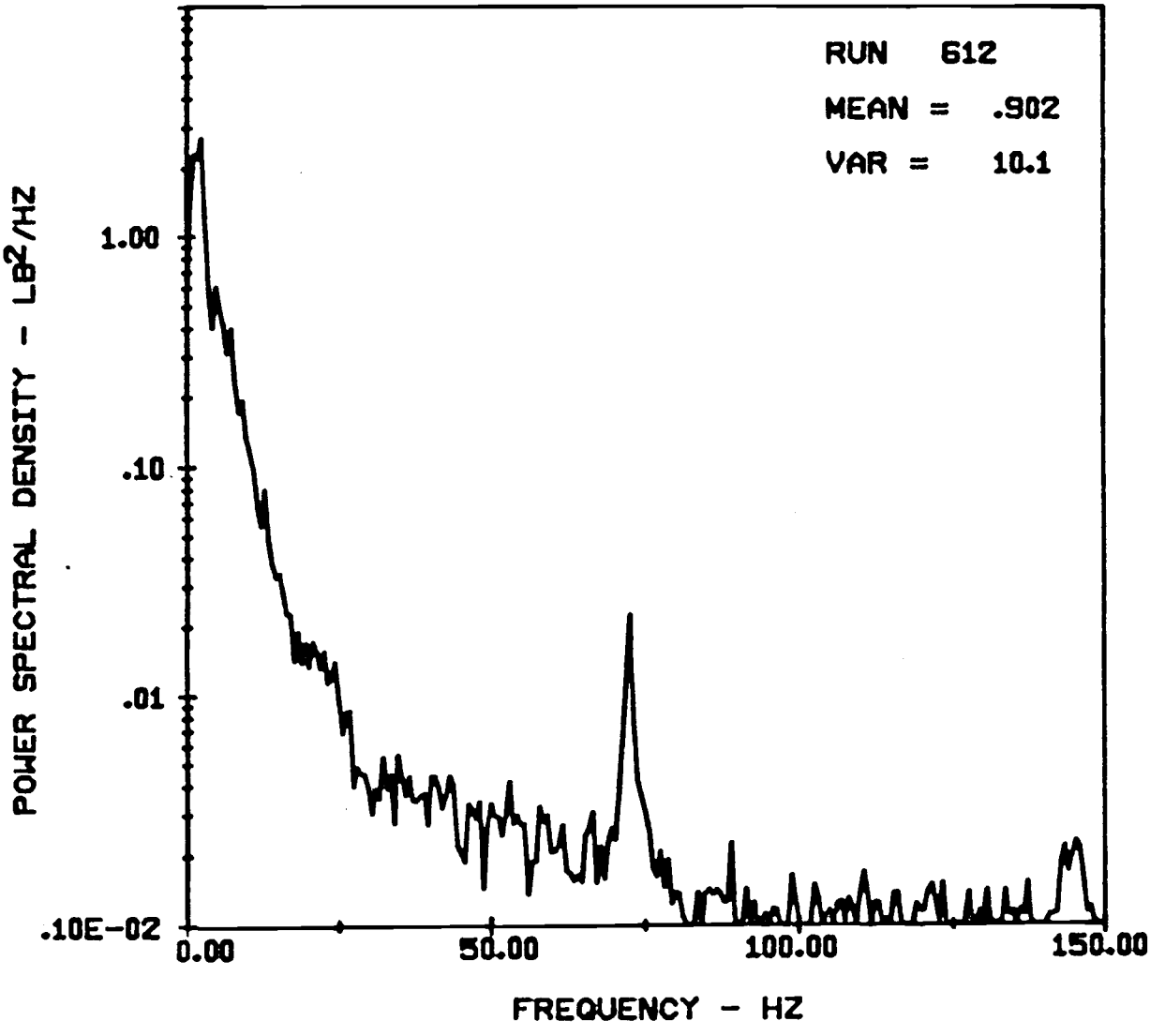


HORIZONTAL FORCES ON A SINGLE TUBE (V = 9 ft/sec)
IN EI16 SAND WITH 10" ARRAY HEIGHT AND 6" TUBE SPACING

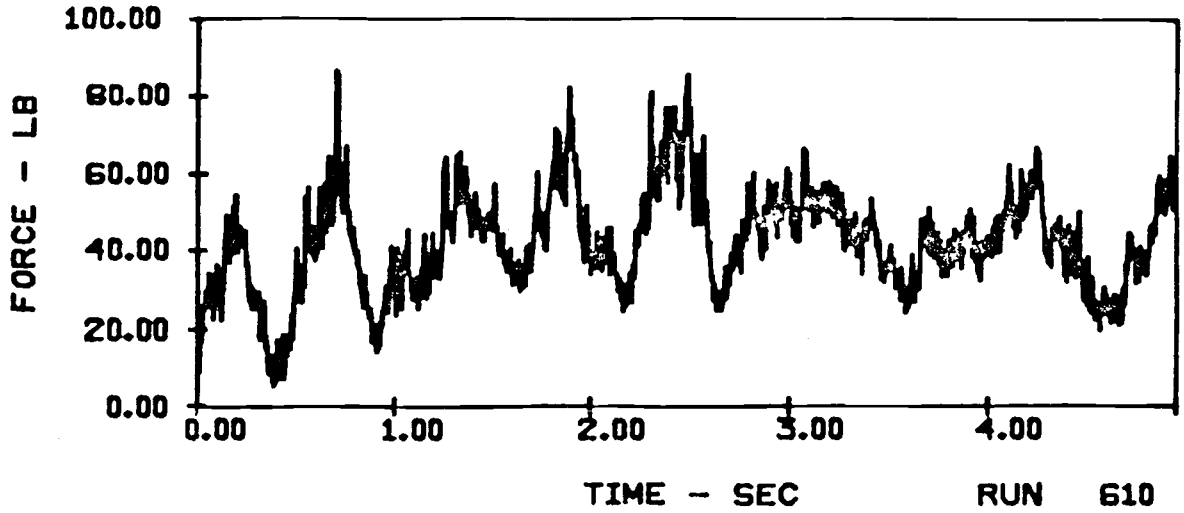


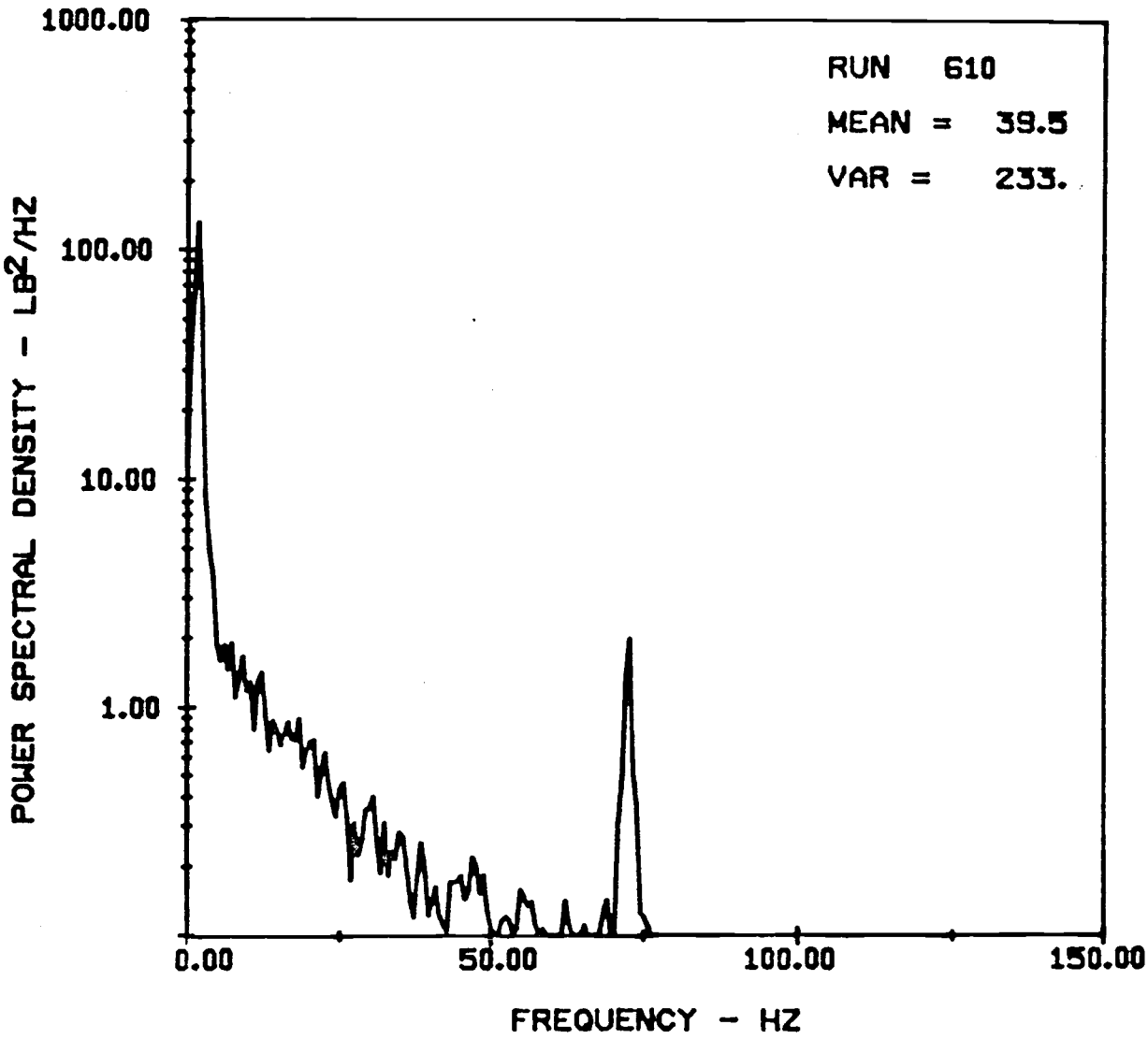


VERTICAL FORCES ON AN 8-TUBE ARRAY (V = 9 ft/sec)
IN EI16 SAND WITH 10" ARRAY HEIGHT AND 6" TUBE SPACING

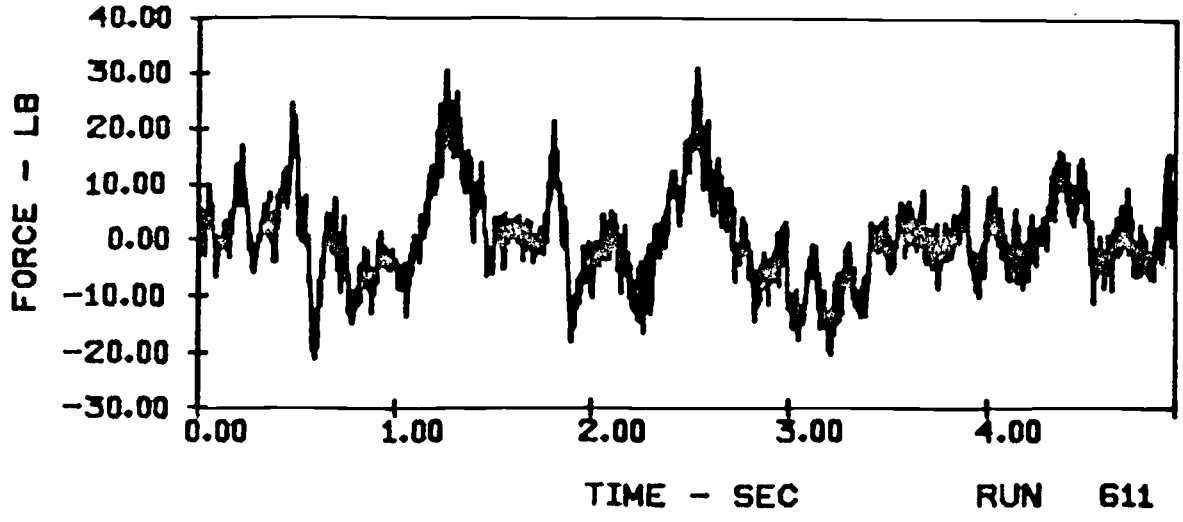


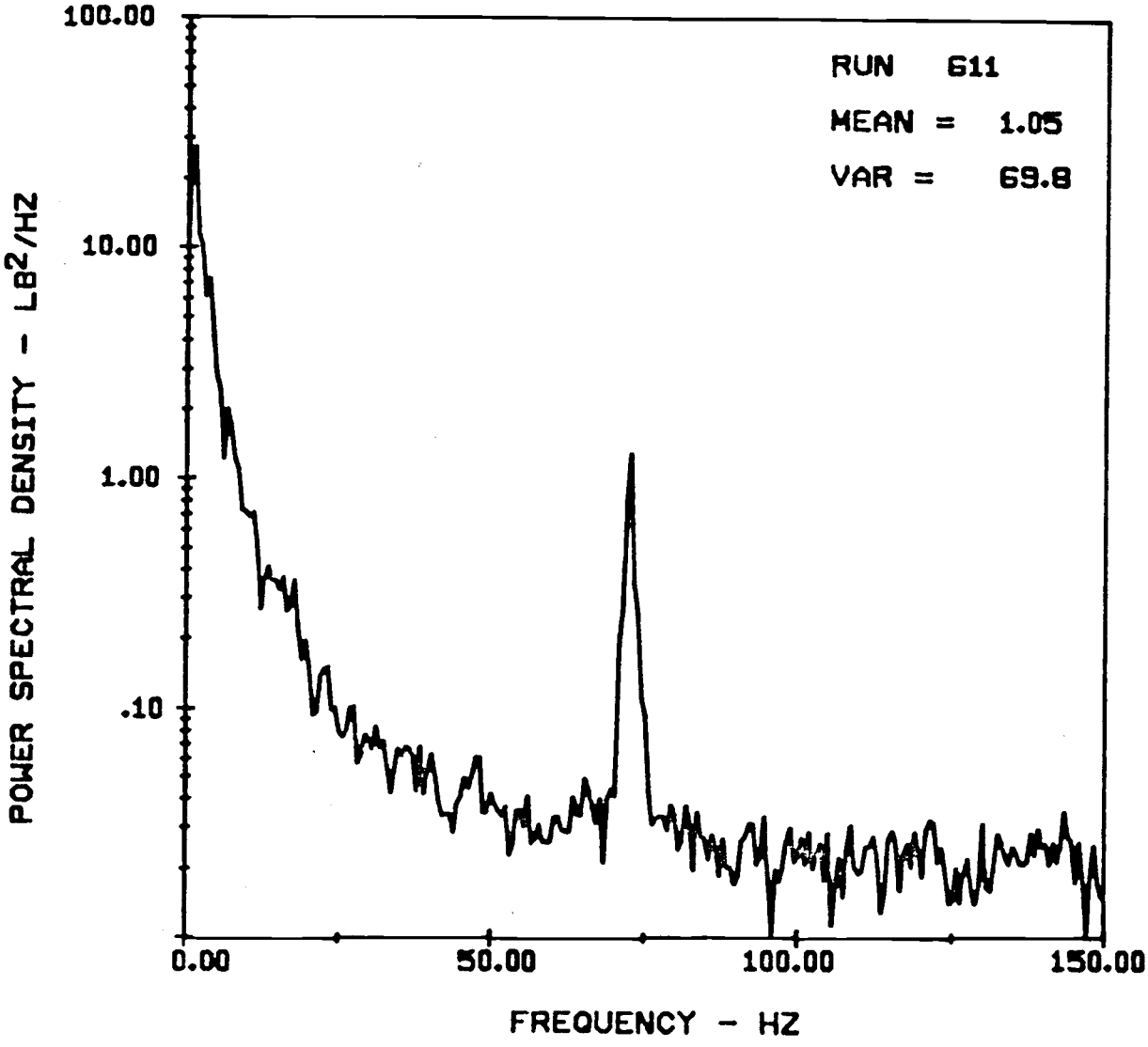


HORIZONTAL FORCES ON AN 8-TUBE ARRAY (V = 9 ft/sec)
IN EI16 SAND WITH 10 " ARRAY HEIGHT AND 6" TUBE SPACING

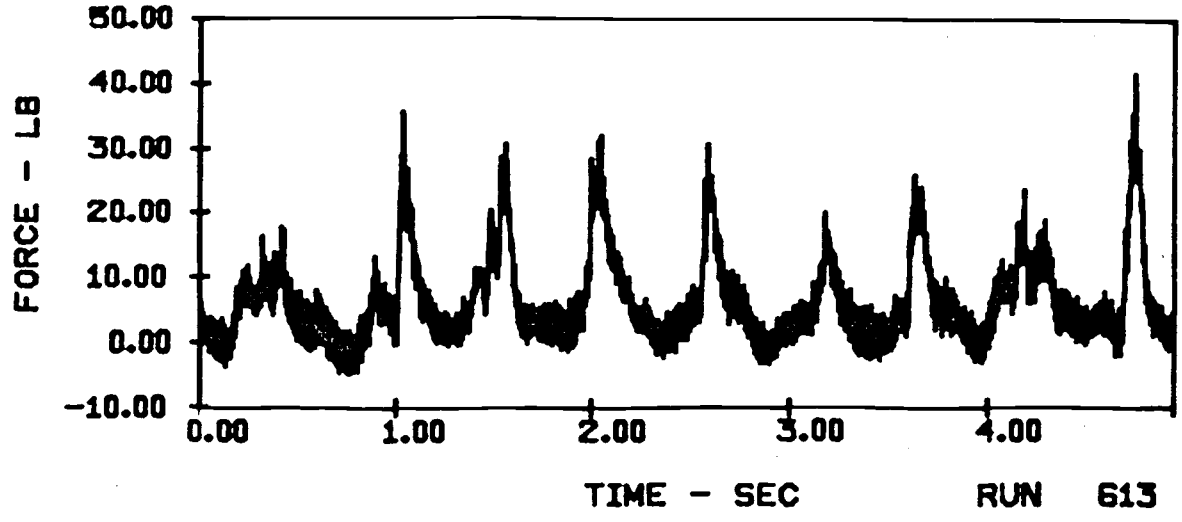


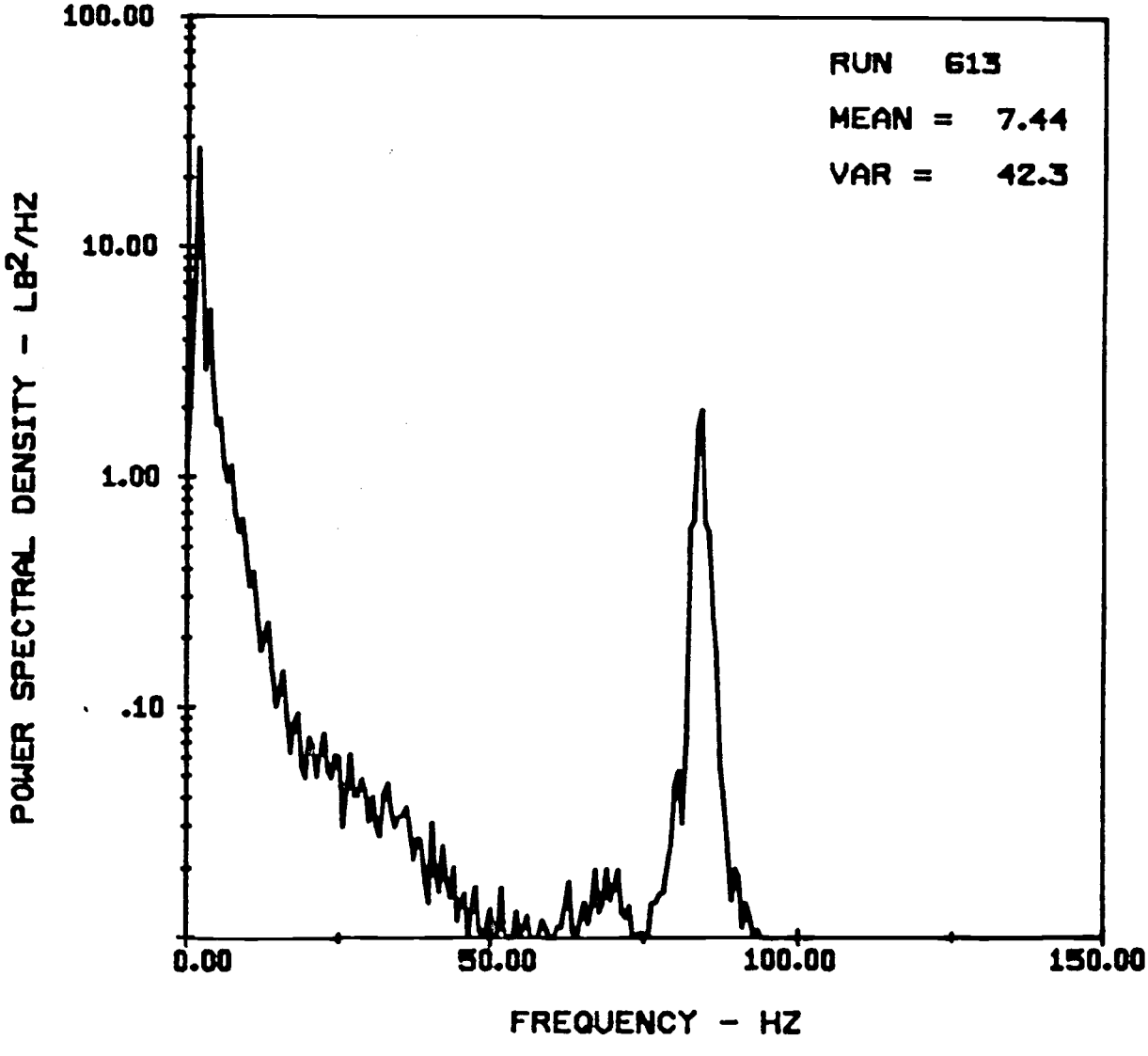


VERTICAL FORCES ON A SINGLE TUBE (V = 11 ft/sec)
IN EI16 SAND WITH 10" ARRAY HEIGHT AND 6" TUBE SPACING

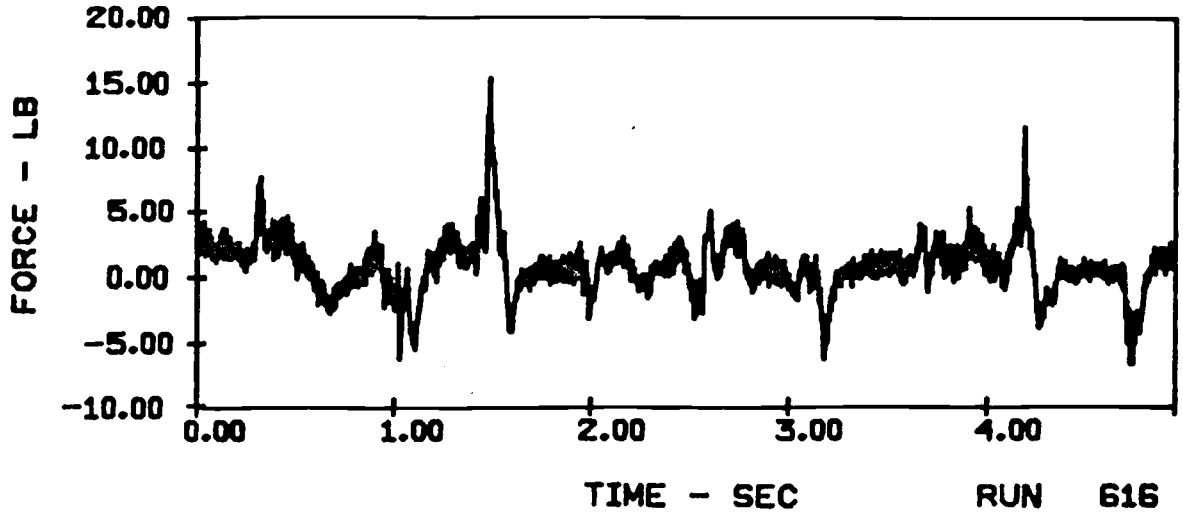


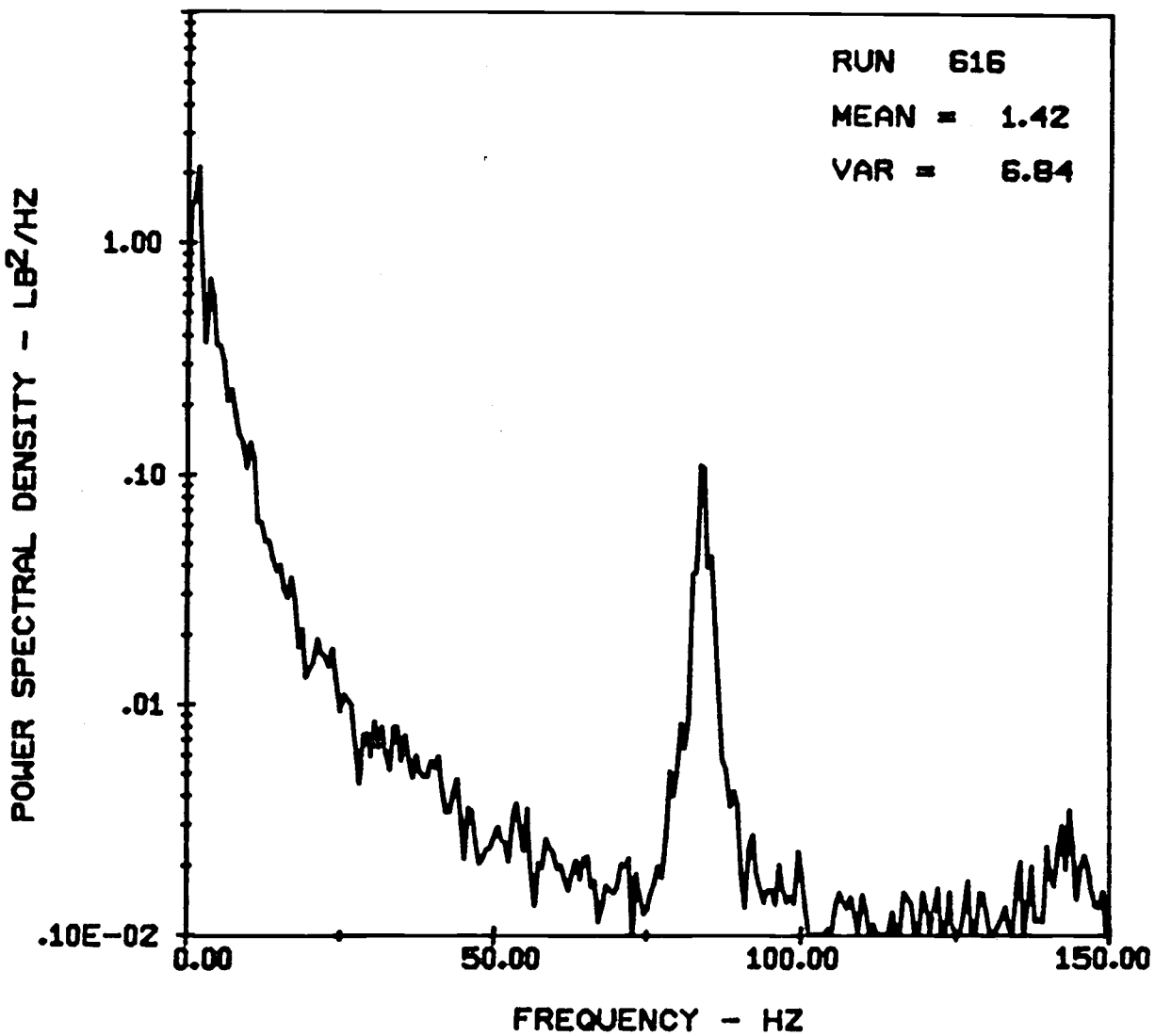


HORIZONTAL FORCES ON A SINGLE TUBE (V = 11 ft/sec)
IN EI16 SAND WITH 10" ARRAY HEIGHT AND 6" TUBE SPACING

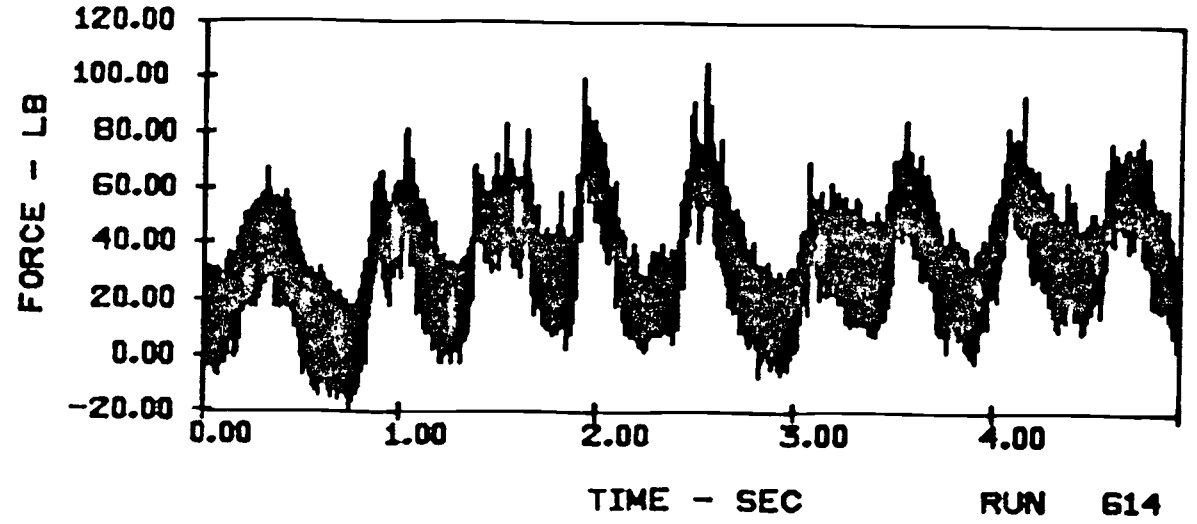


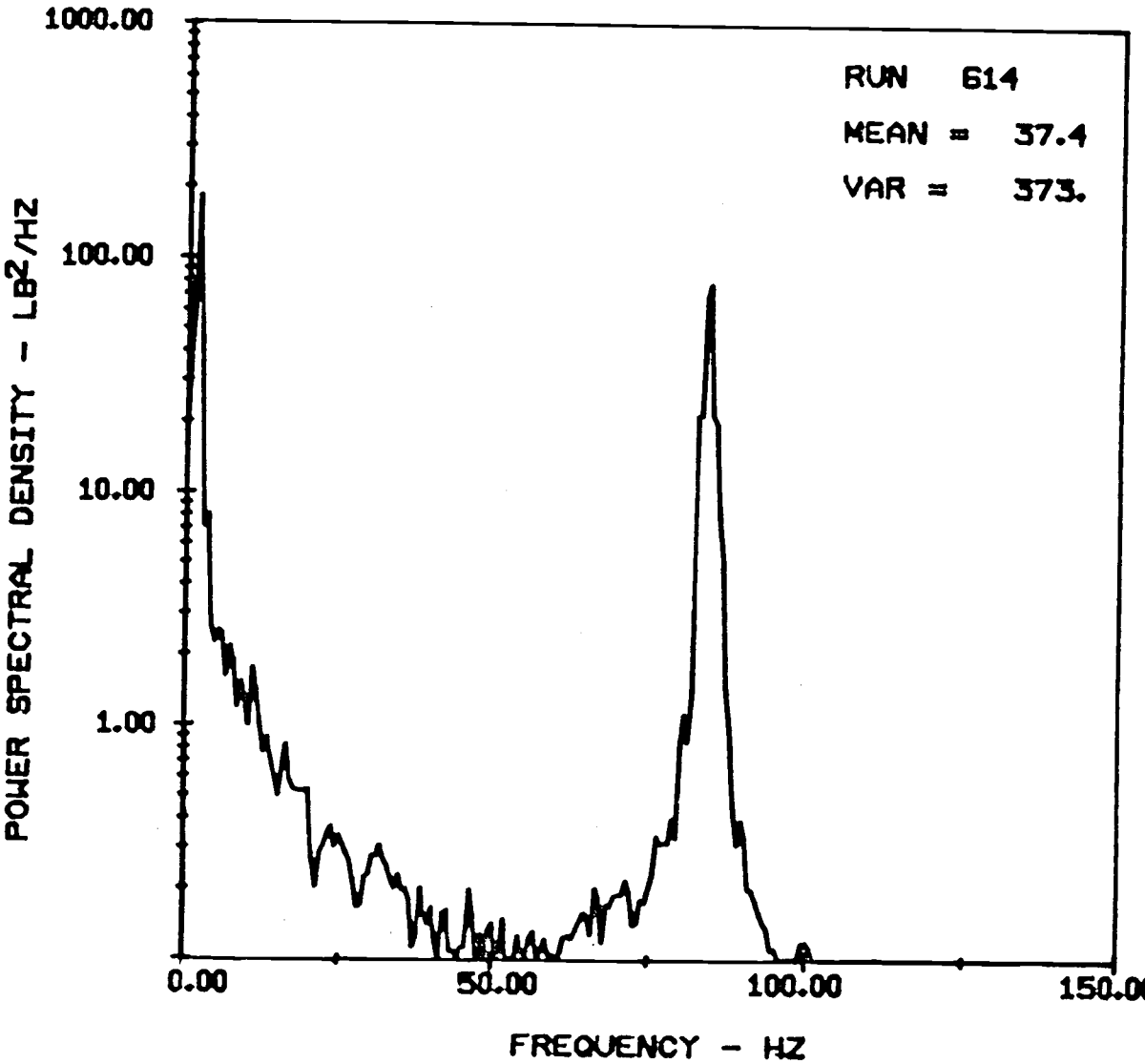


VERTICAL FORCES ON AN 8-TUBE ARRAY (V = 11 ft/sec)
IN E116 SAND WITH 10" ARRAY HEIGHT AND 6" TUBE SPACING

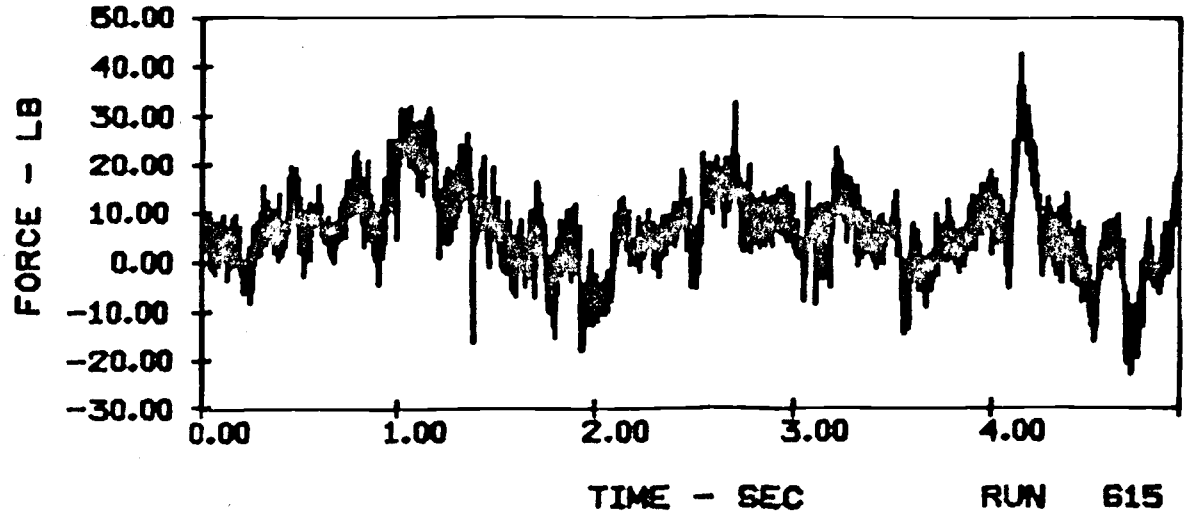


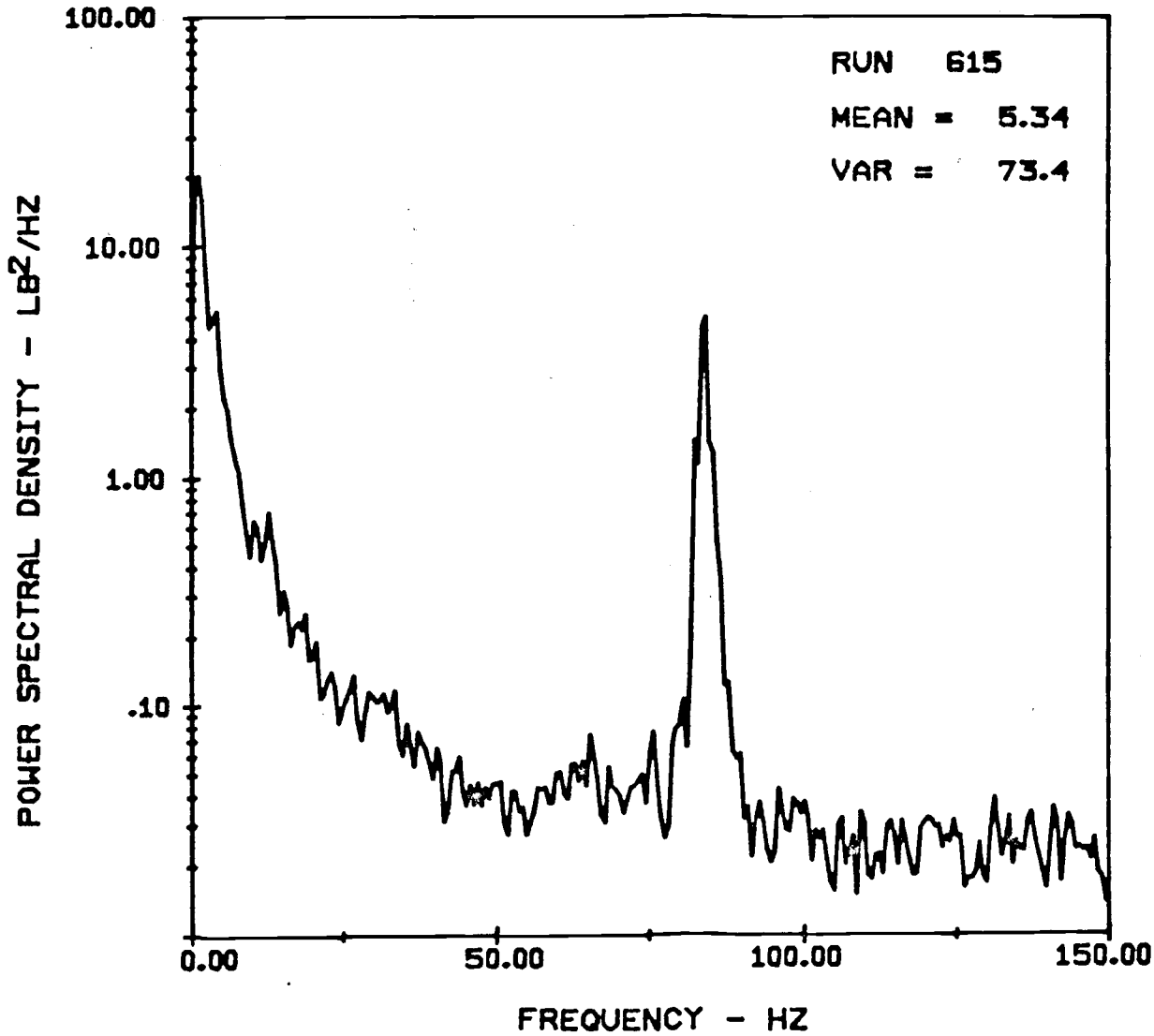


HORIZONTAL FORCES ON AN 8-TUBE ARRAY (V = 11 ft/sec)
IN EI16 SAND WITH 10 " ARRAY HEIGHT AND 6" TUBE SPACING

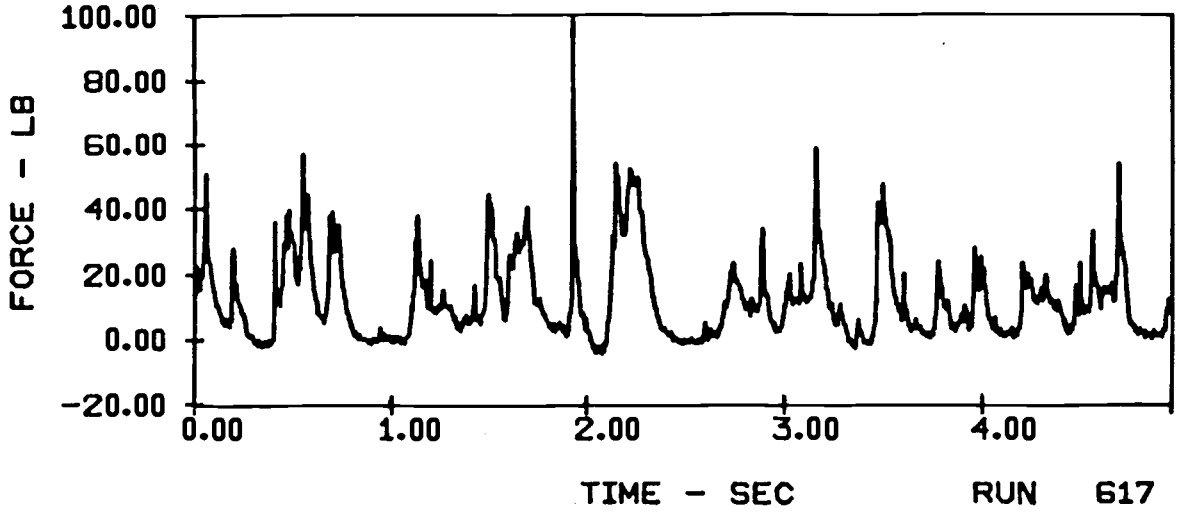


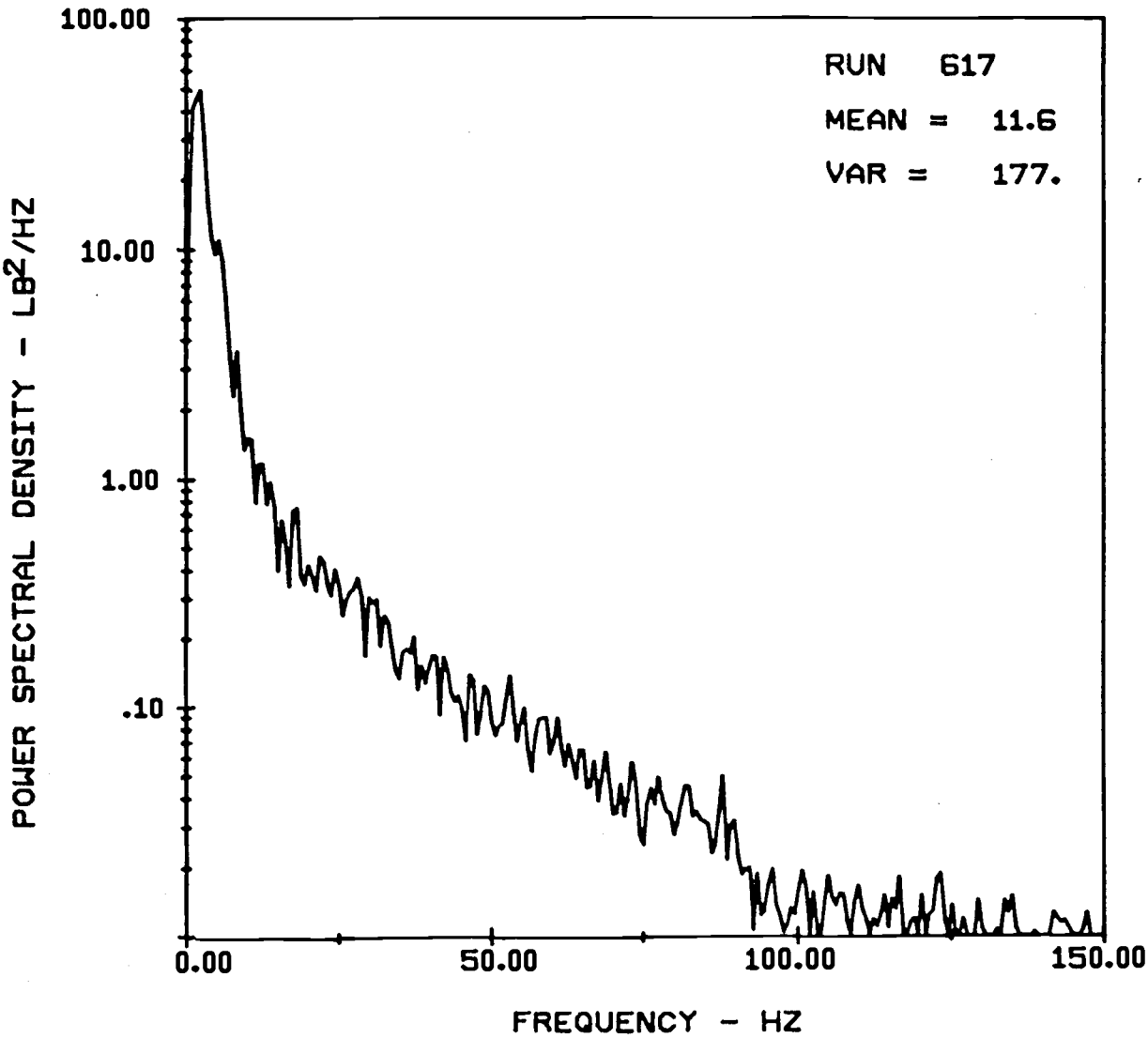


VERTICAL FORCES ON A SINGLE TUBE (V = 5 ft/sec)
IN EI16 SAND WITH 20" ARRAY HEIGHT AND 6" TUBE SPACING

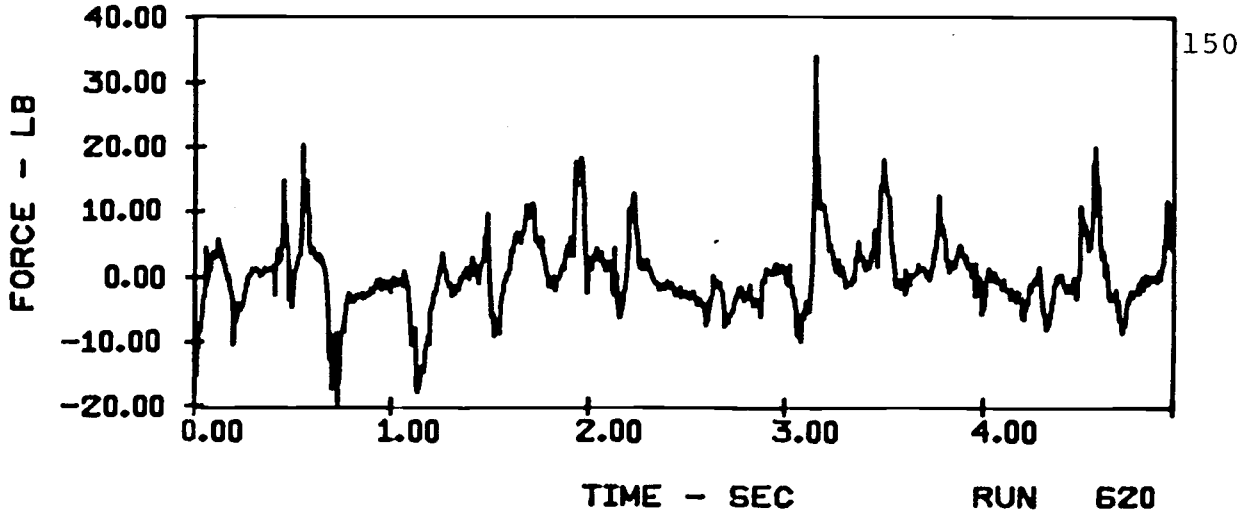


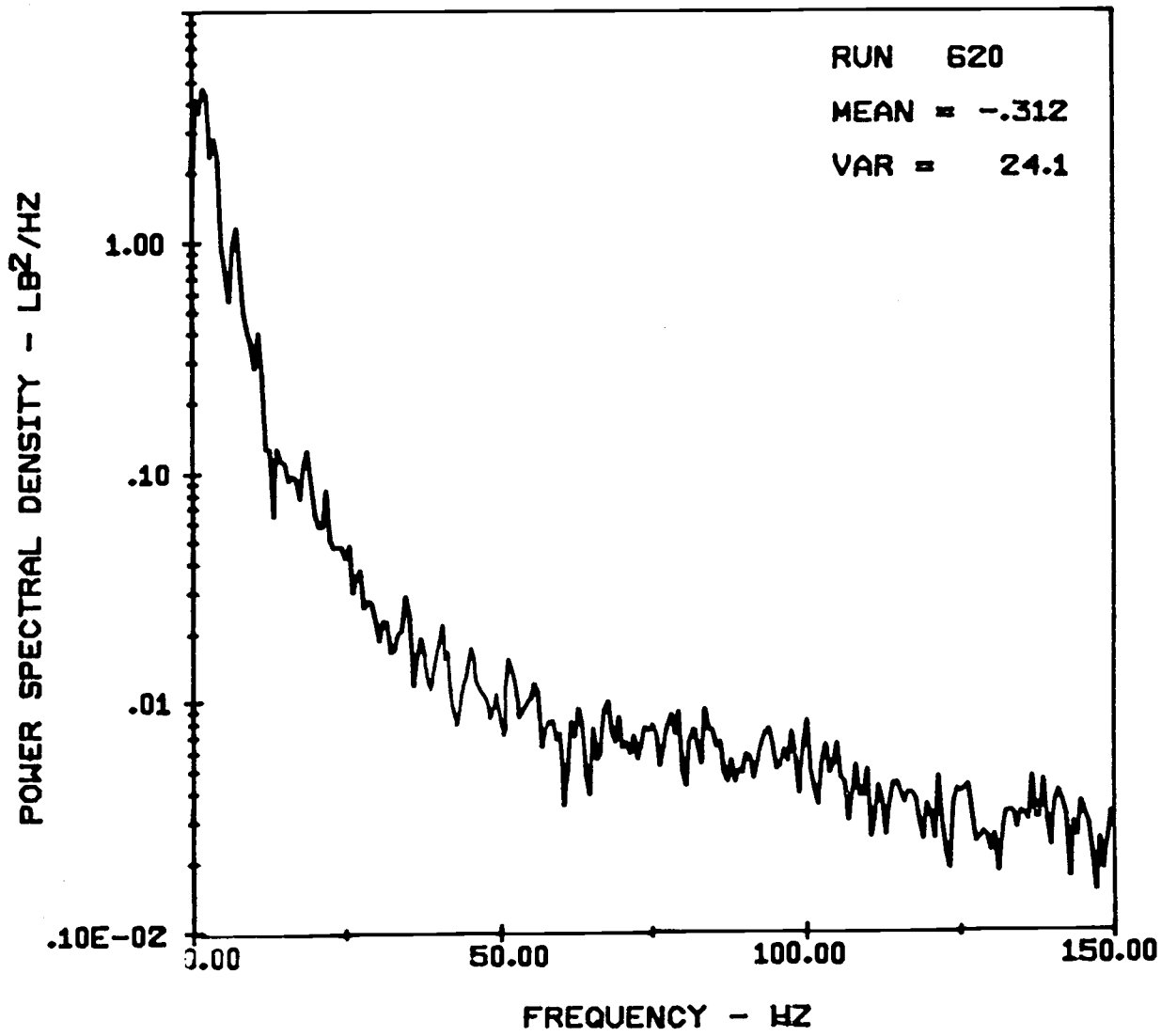


HORIZONTAL FORCES ON A SINGLE TUBE (V = 5 ft/sec)
IN EI16 SAND WITH 20" ARRAY HEIGHT AND 6" TUBE SPACING

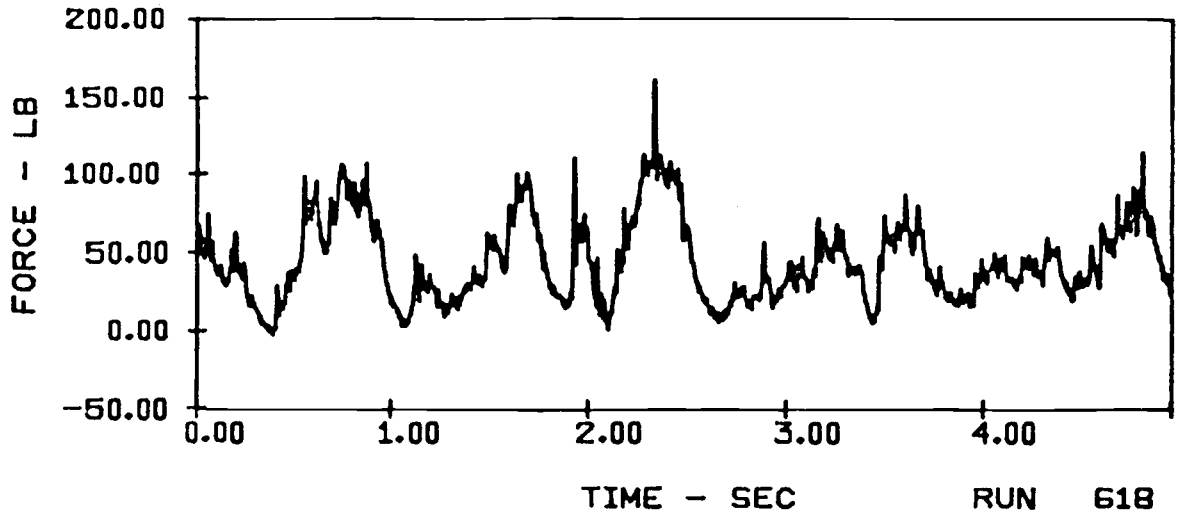


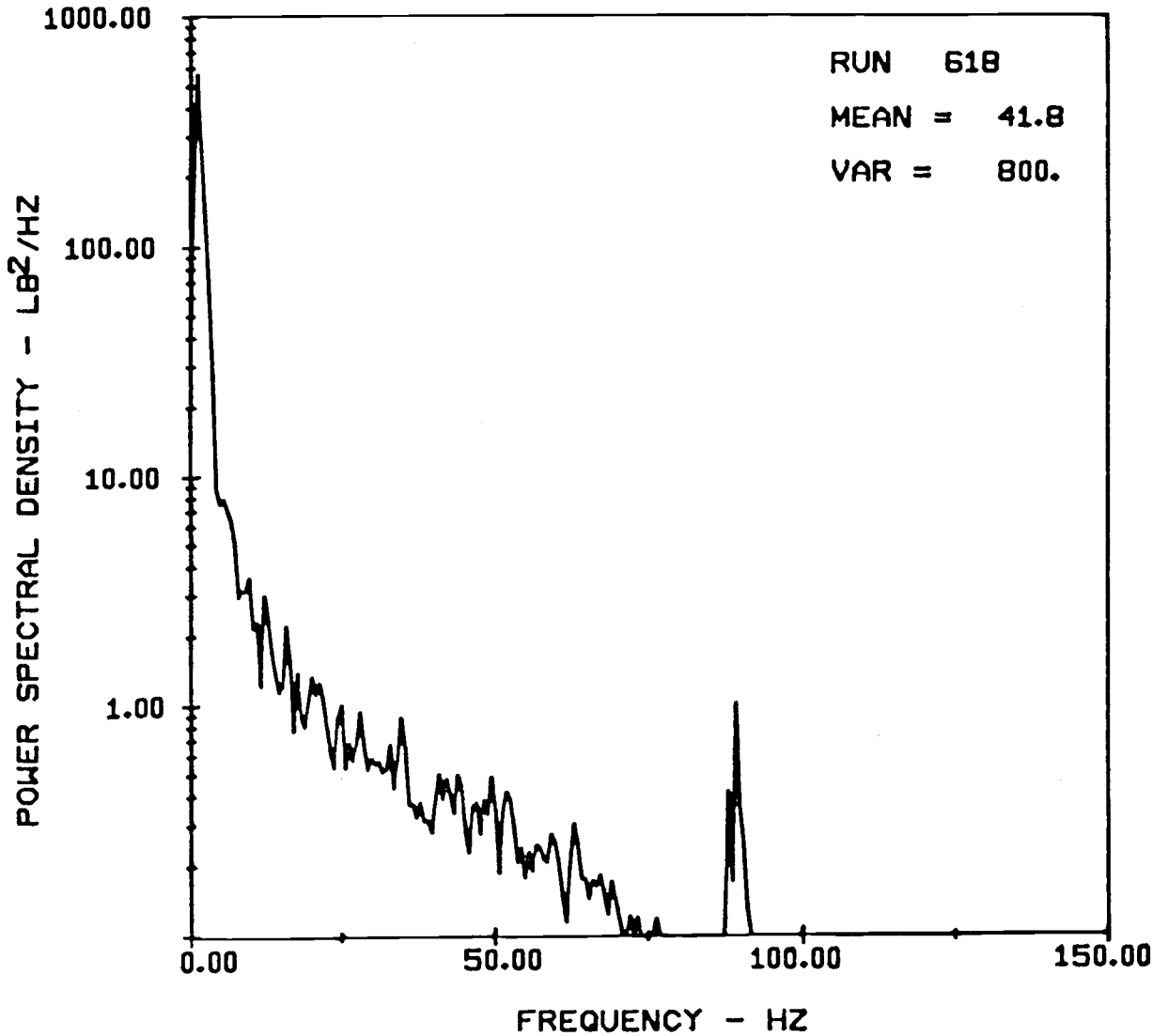


VERTICAL FORCES ON AN 8-TUBE ARRAY (V = 5 ft/sec)
IN EI16 SAND WITH 20" ARRAY HEIGHT AND 6" TUBE SPACING

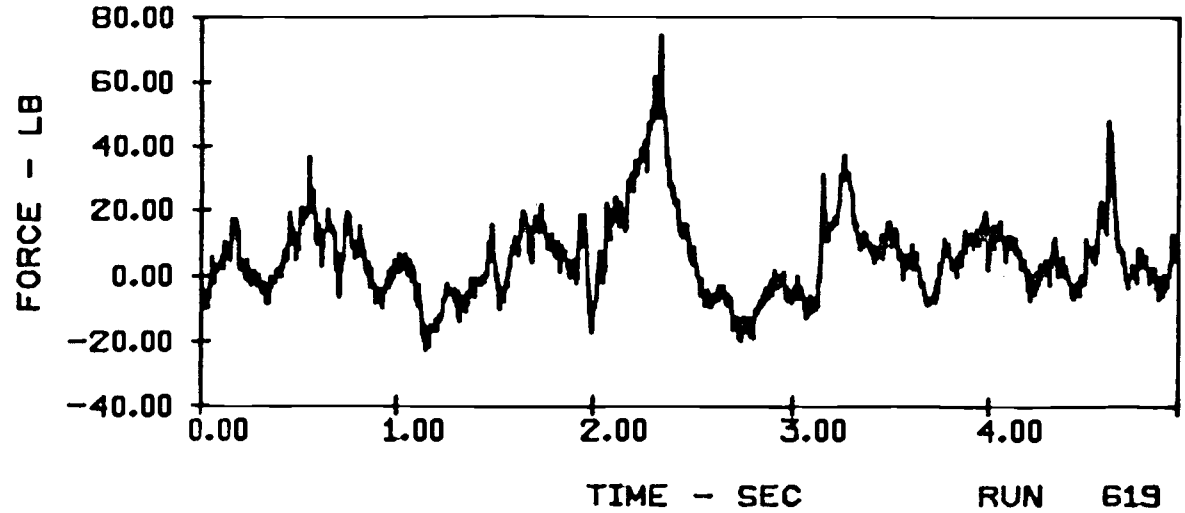


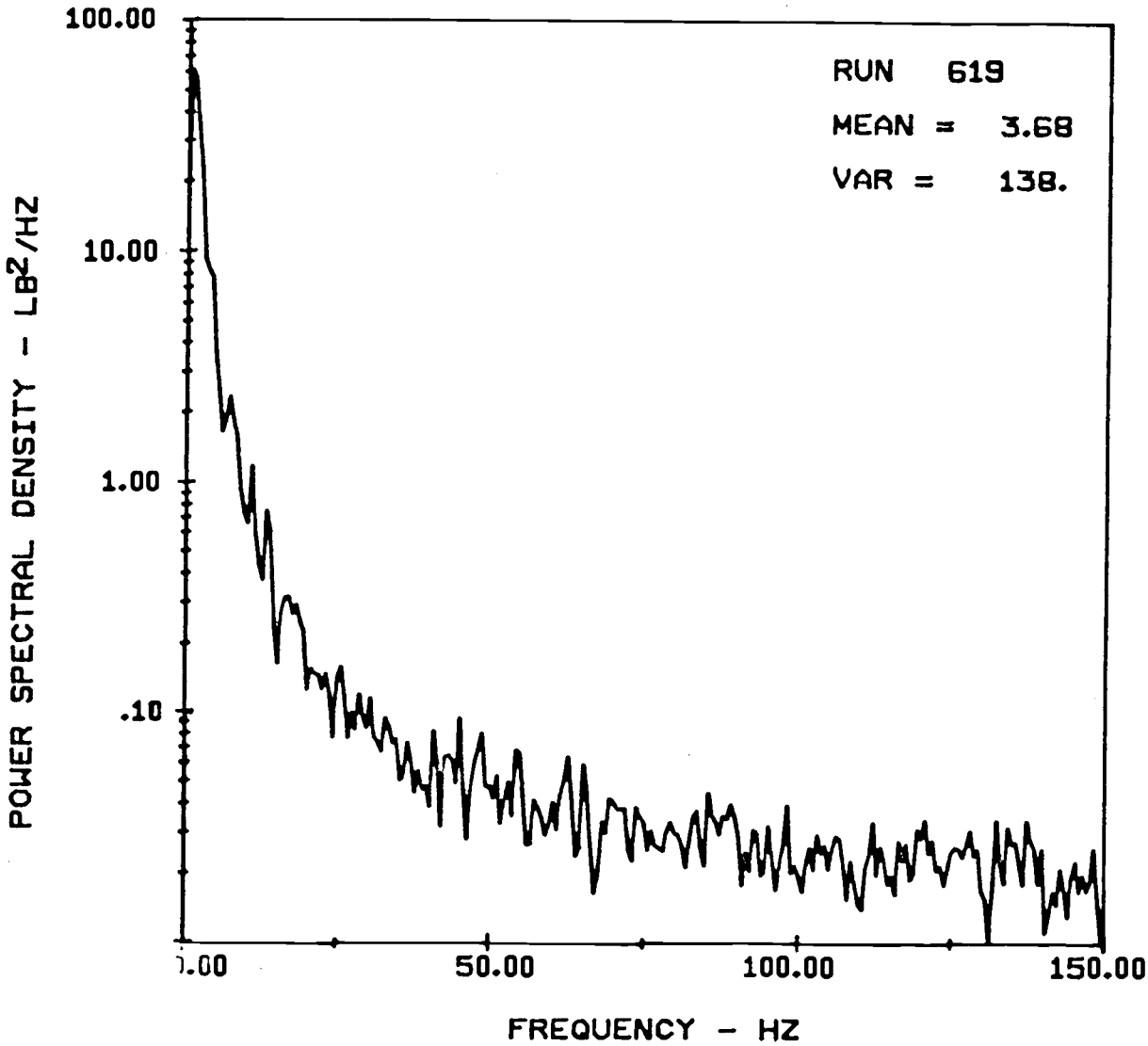


HORIZONTAL FORCES ON AN 8-TUBE ARRAY (V = 5 ft/sec)
IN EI16 SAND WITH 20 " ARRAY HEIGHT AND 6" TUBE SPACING

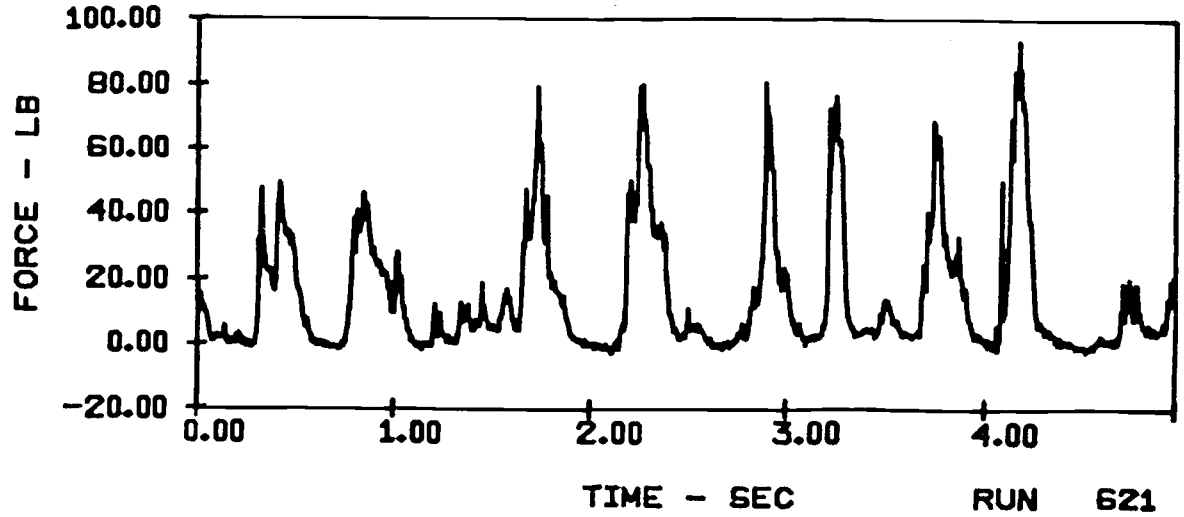


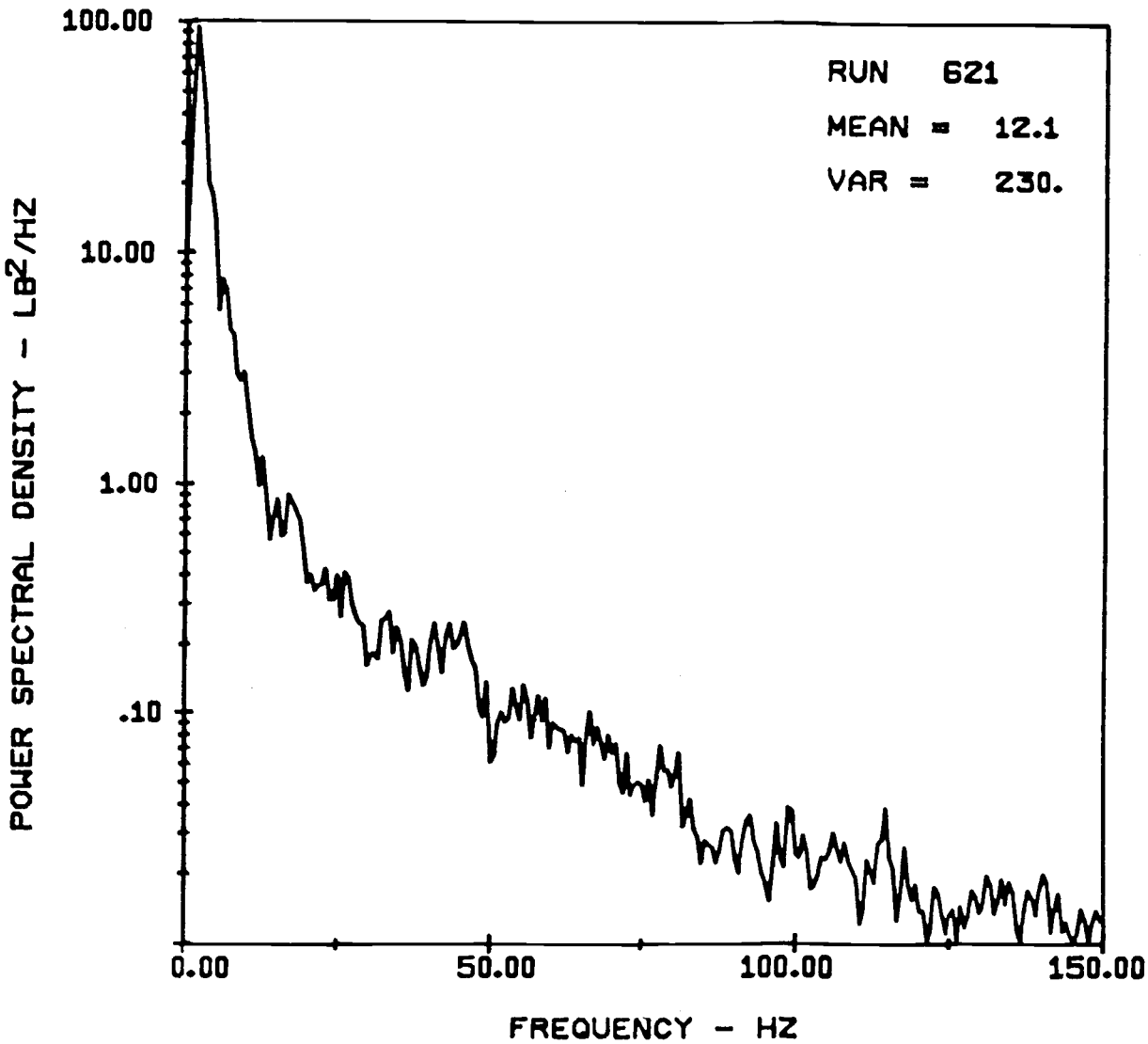


VERTICAL FORCES ON A SINGLE TUBE (V = 7 ft/sec)
IN EI16 SAND WITH 20" ARRAY HEIGHT AND 6" TUBE SPACING

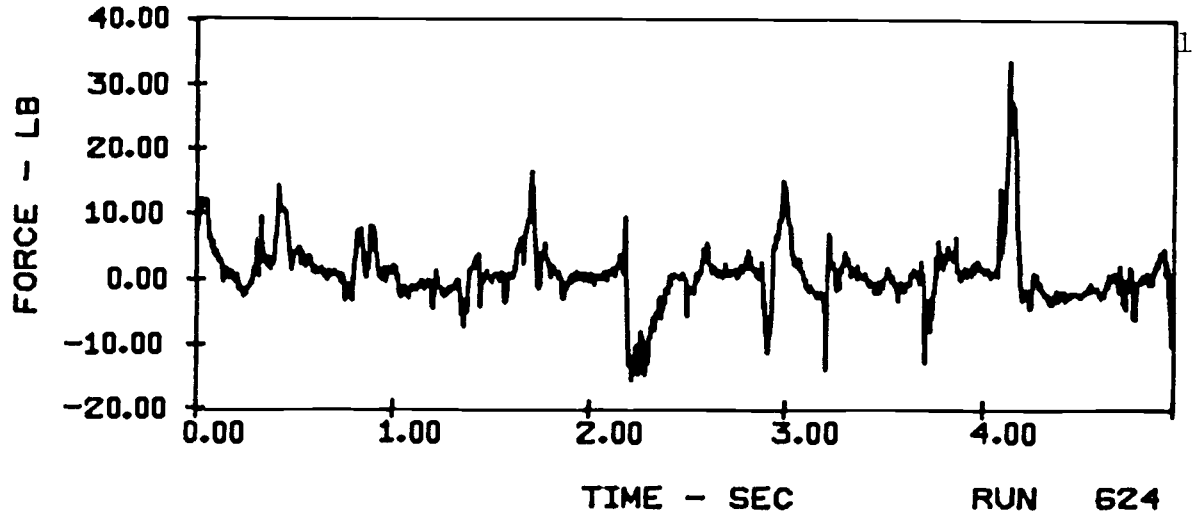


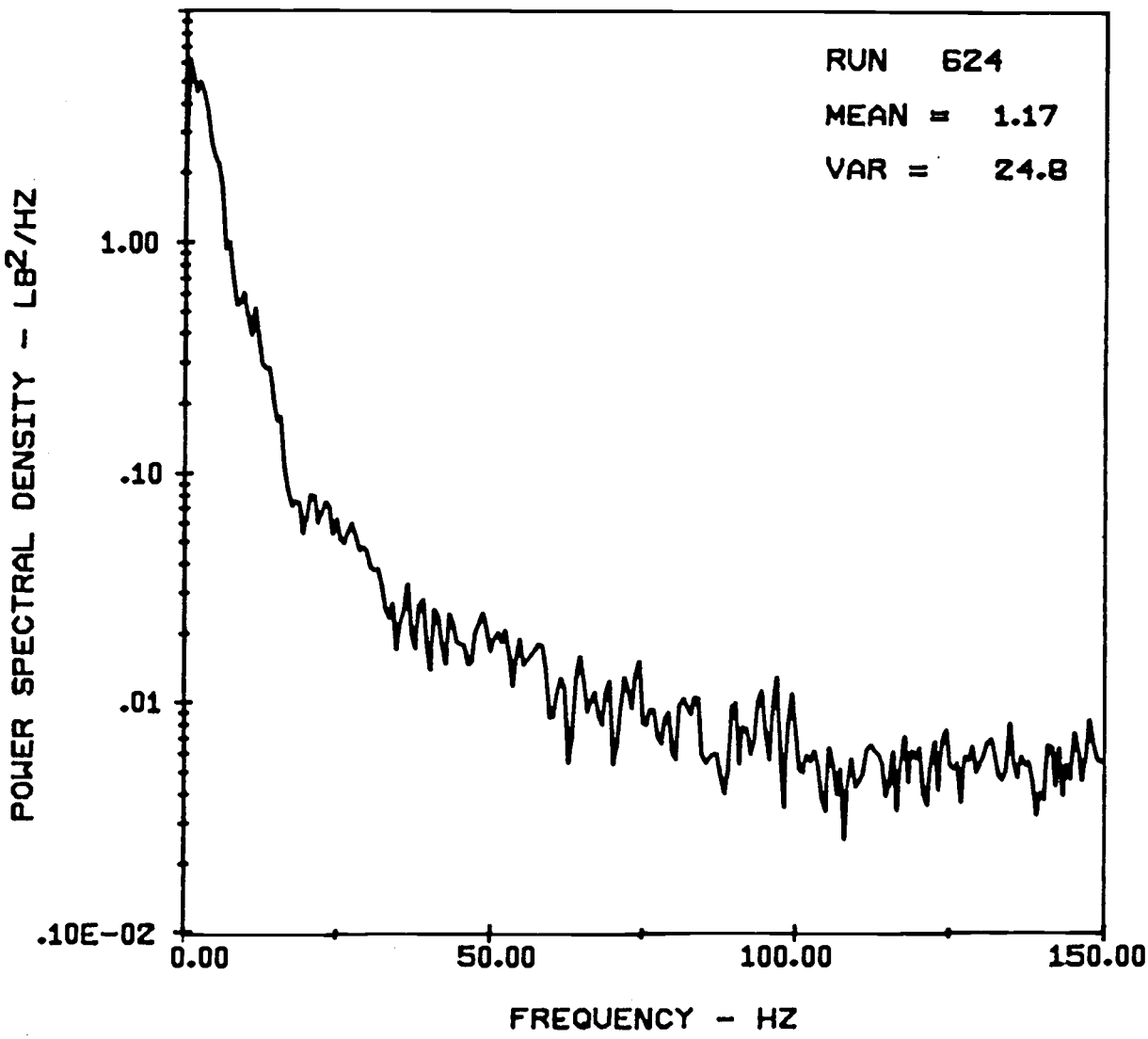


HORIZONTAL FORCES ON A SINGLE TUBE (V = 7 ft/sec)
IN EI16 SAND WITH 20" ARRAY HEIGHT AND 6" TUBE SPACING

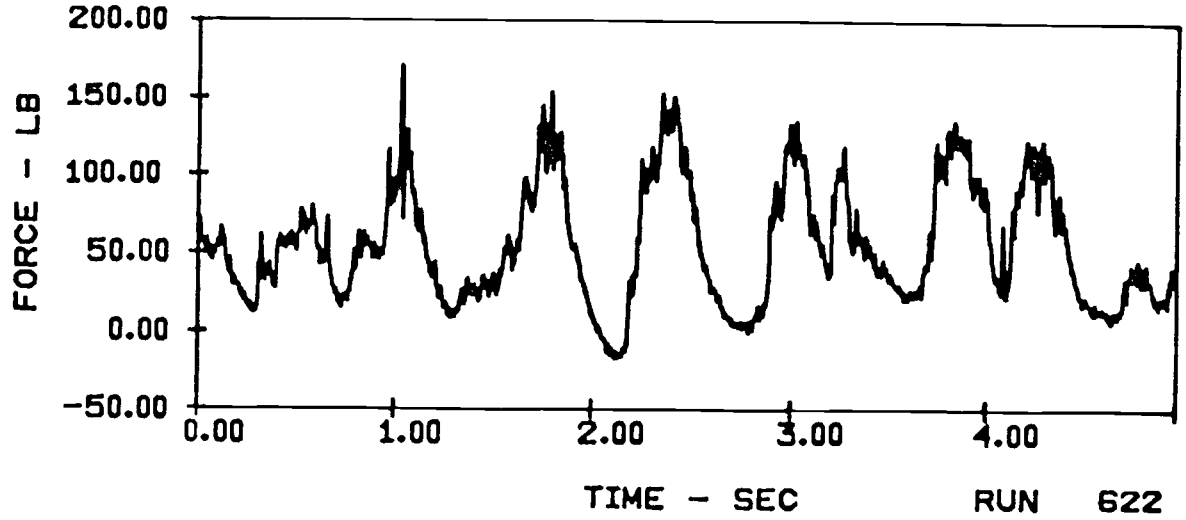


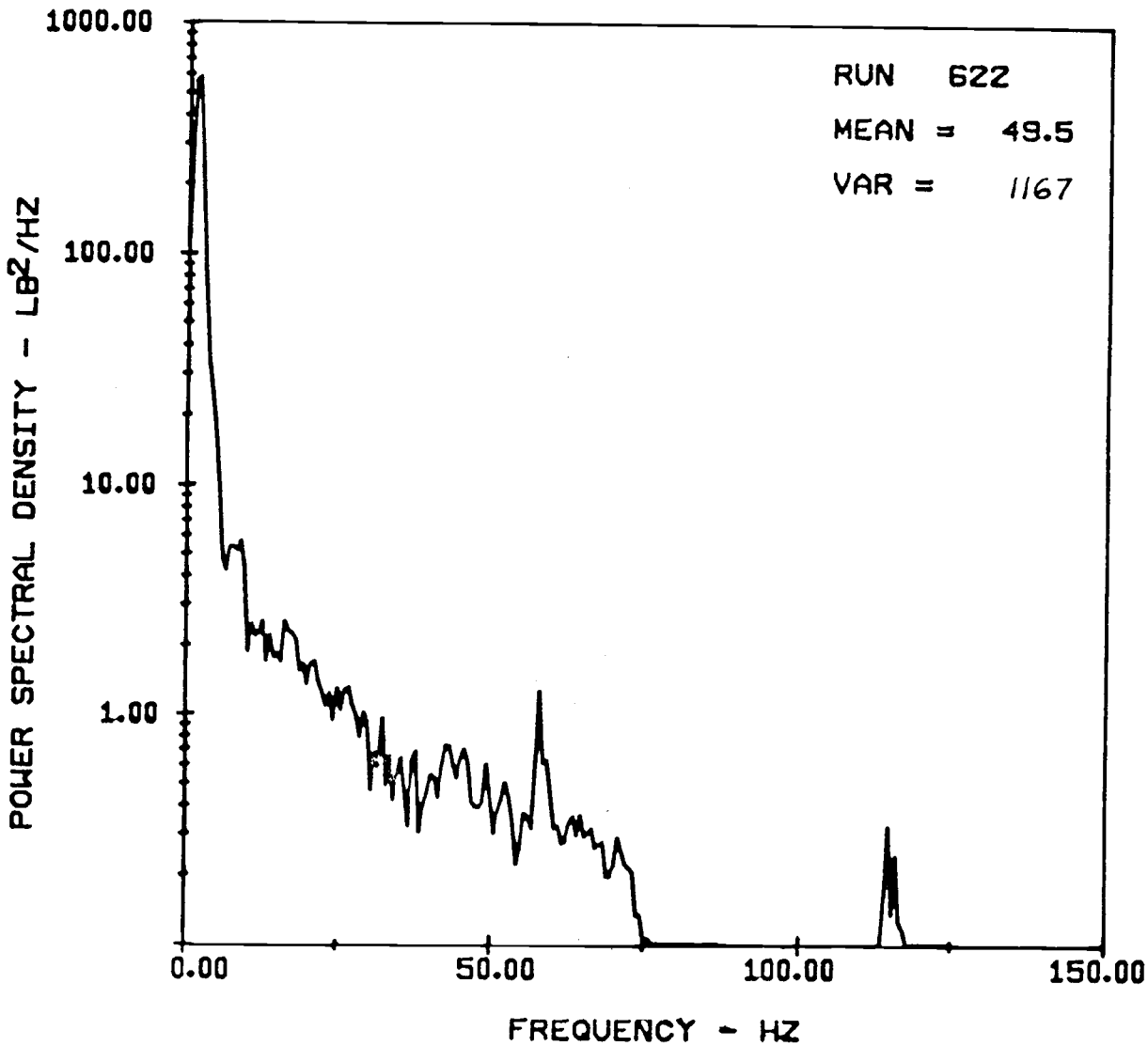


VERTICAL FORCES ON AN 8-TUBE ARRAY (V = 7 ft/sec)
IN E116 SAND WITH 20" ARRAY HEIGHT AND 6" TUBE SPACING

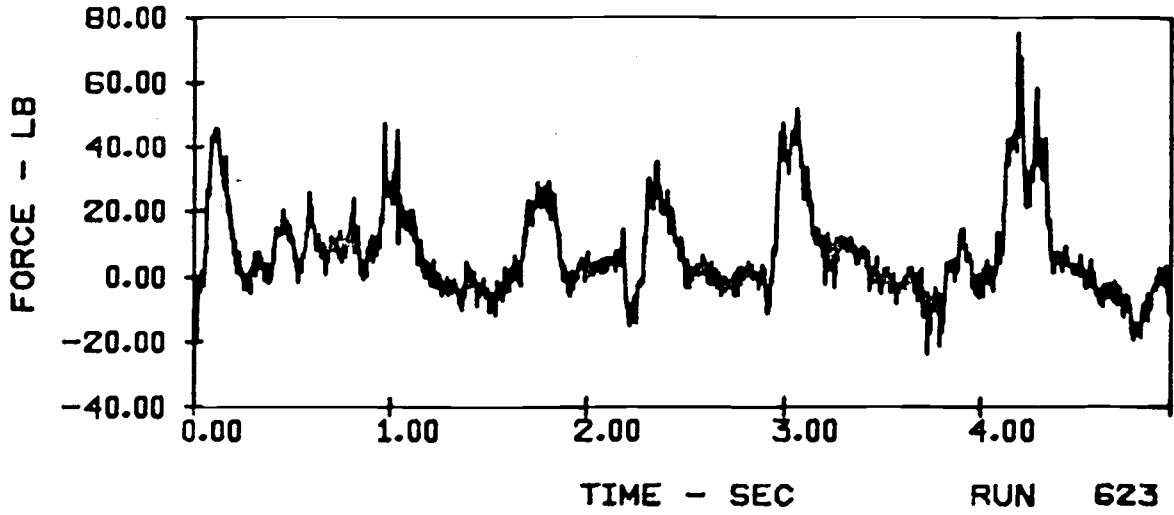


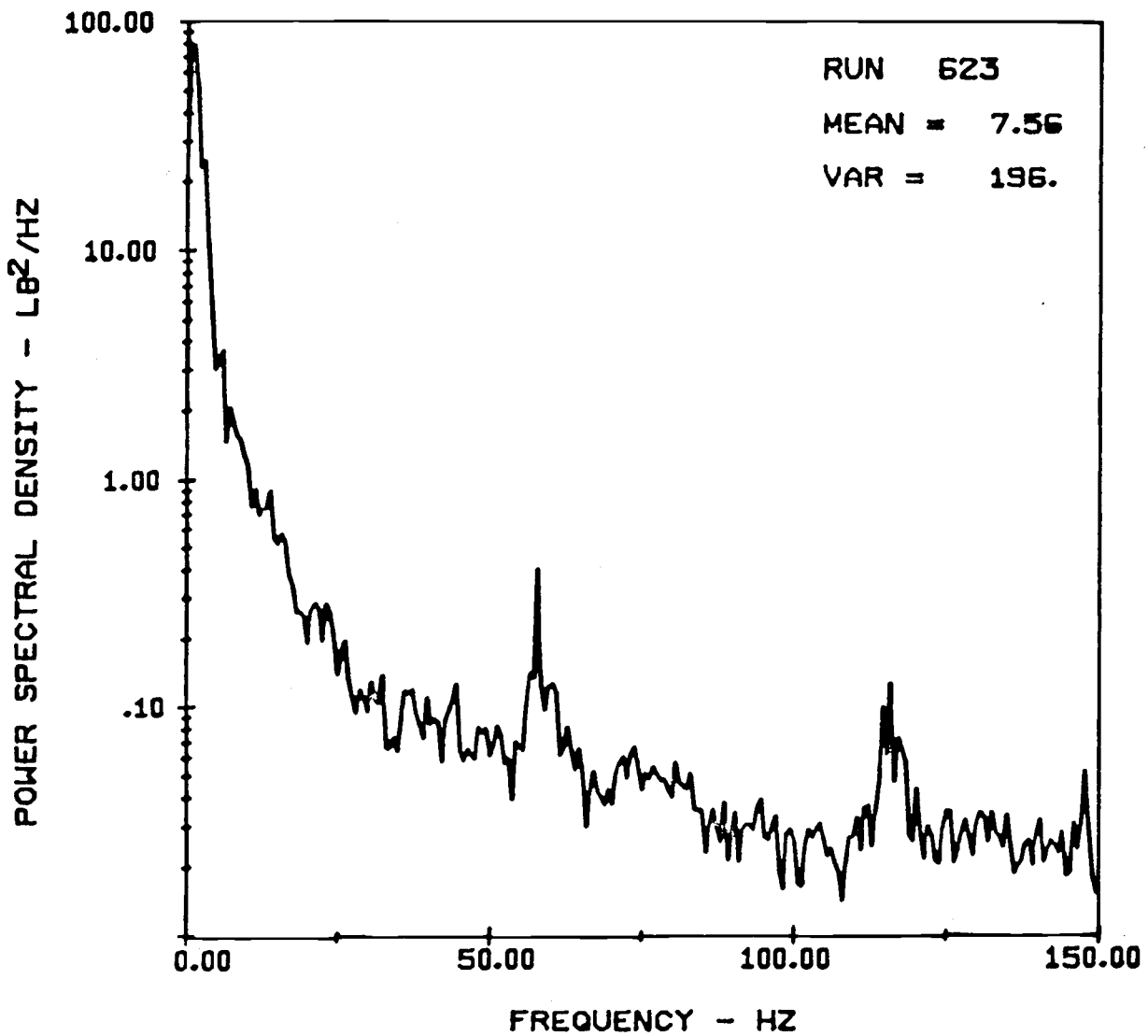


HORIZONTAL FORCES ON AN 8-TUBE ARRAY (V = 7 ft/sec)
IN EI16 SAND WITH 20 " ARRAY HEIGHT AND 6" TUBE SPACING

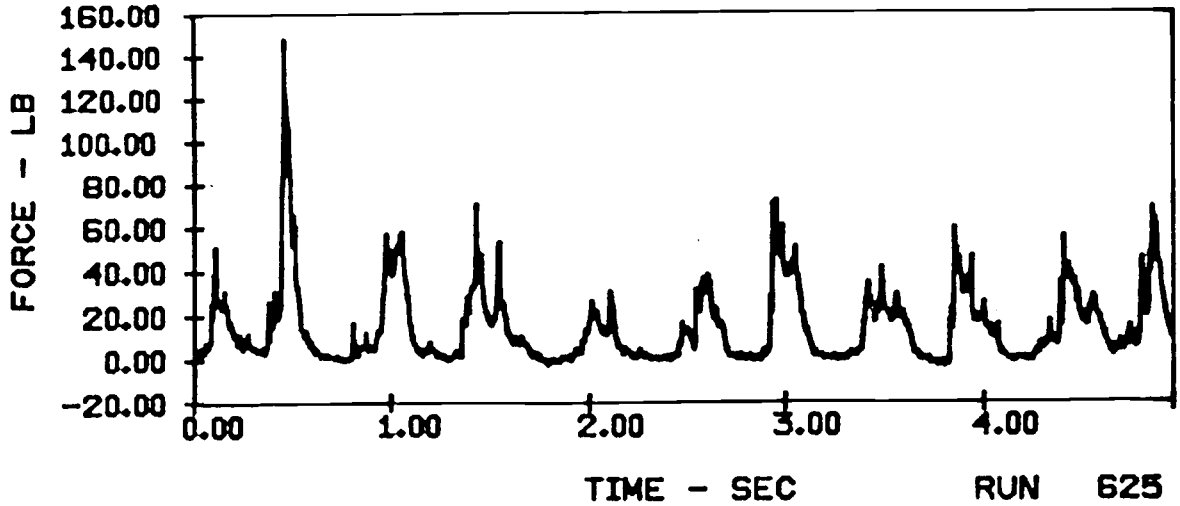


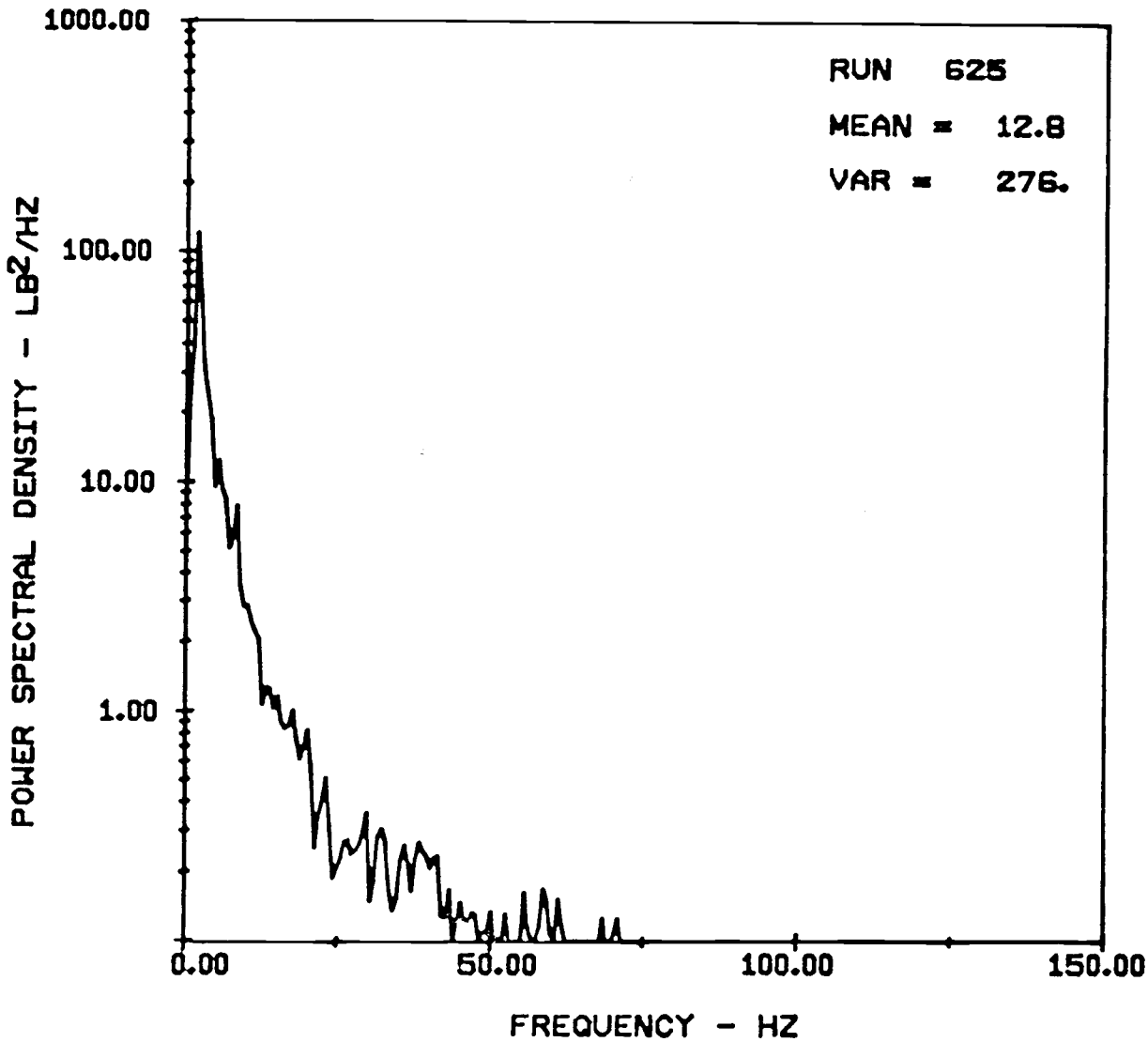


VERTICAL FORCES ON A SINGLE TUBE (V = 9 ft/sec)
IN EI16 SAND WITH 20" ARRAY HEIGHT AND 6" TUBE SPACING

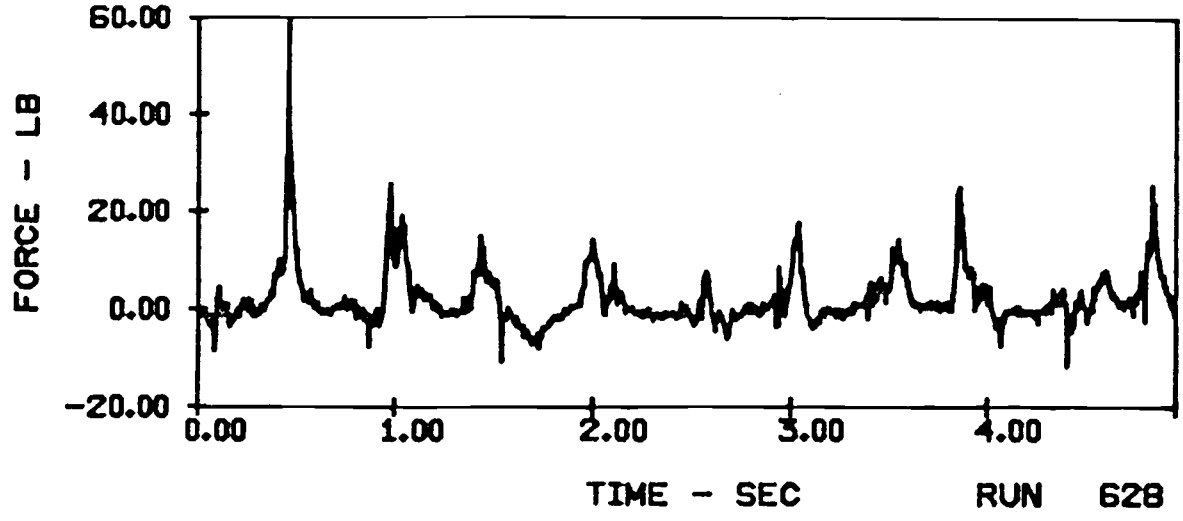


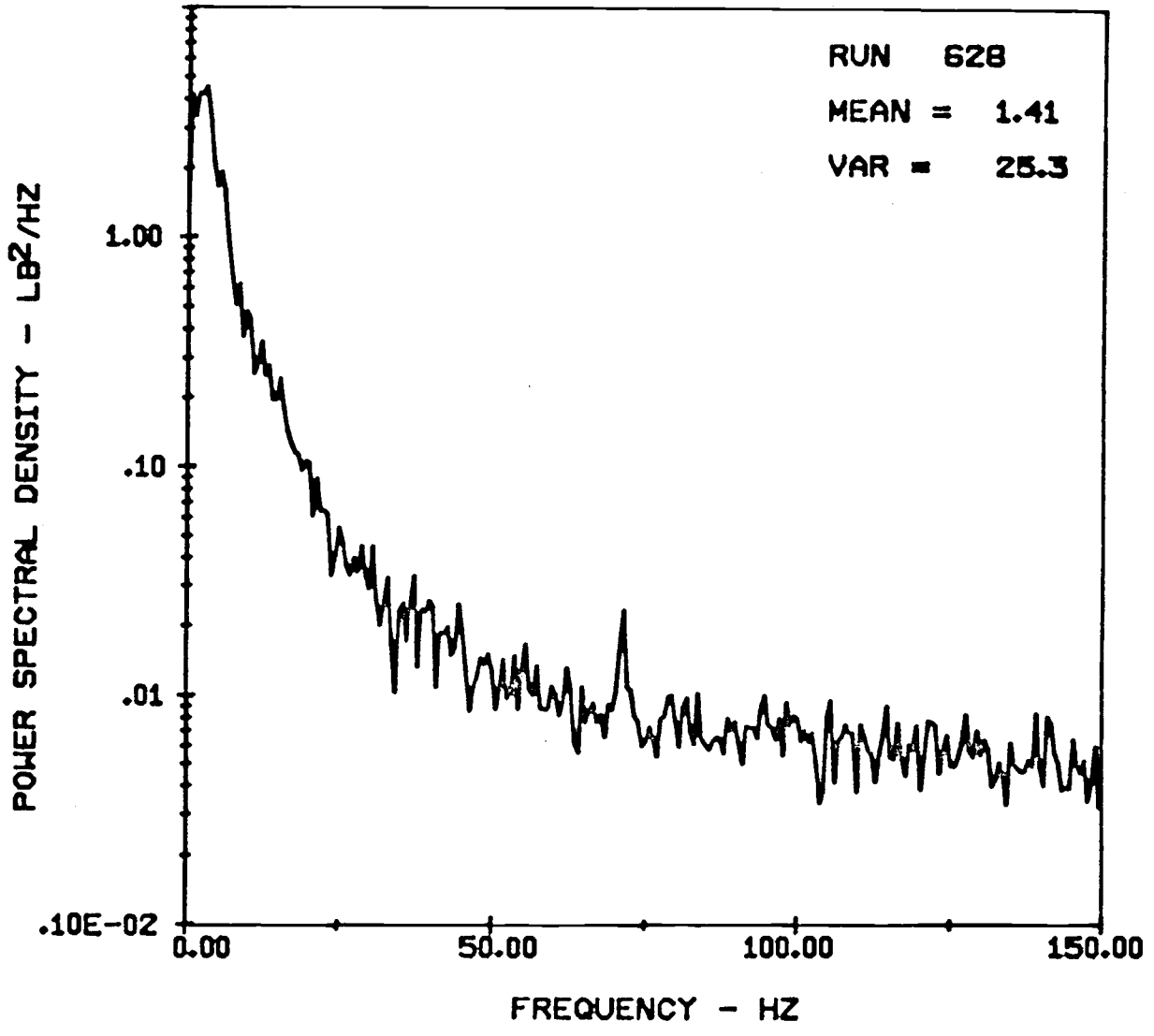


HORIZONTAL FORCES ON A SINGLE TUBE (V = 9 ft/sec)
IN EI16 SAND WITH 20" ARRAY HEIGHT AND 6" TUBE SPACING

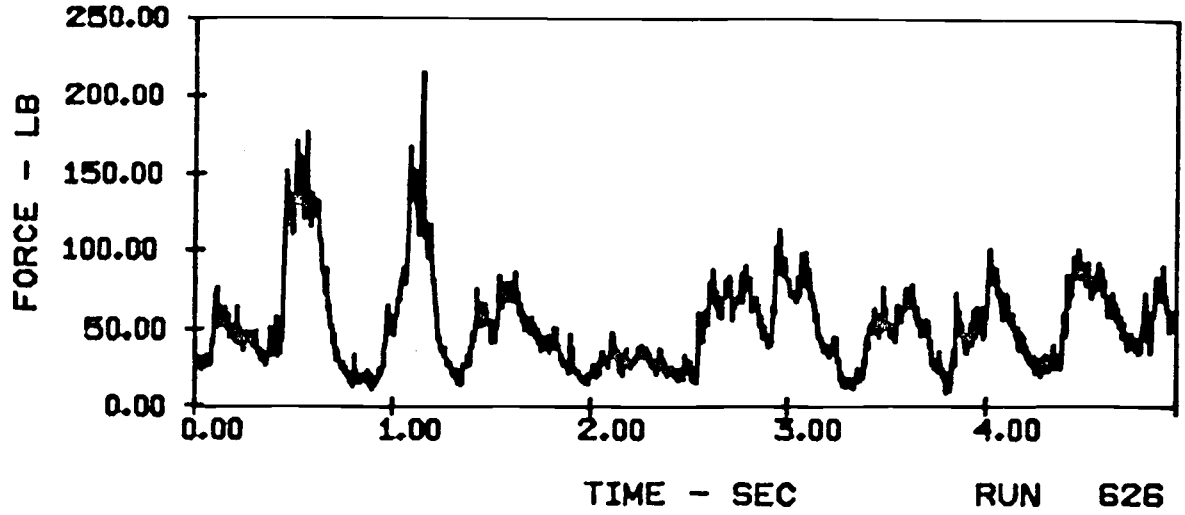


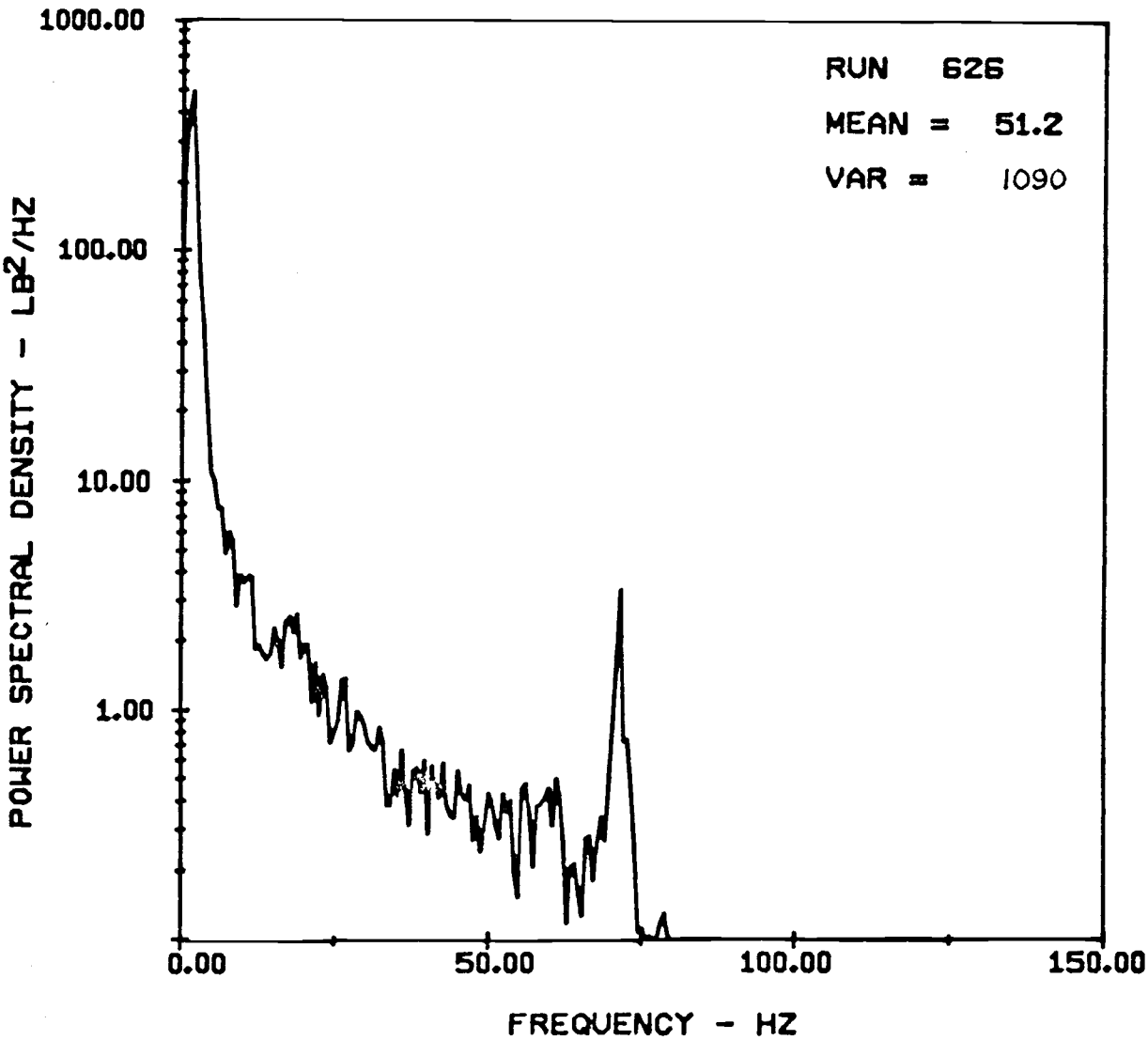


VERTICAL FORCES ON AN 8-TUBE ARRAY (V = 9 ft/sec)
IN E116 SAND WITH 20" ARRAY HEIGHT AND 6" TUBE SPACING

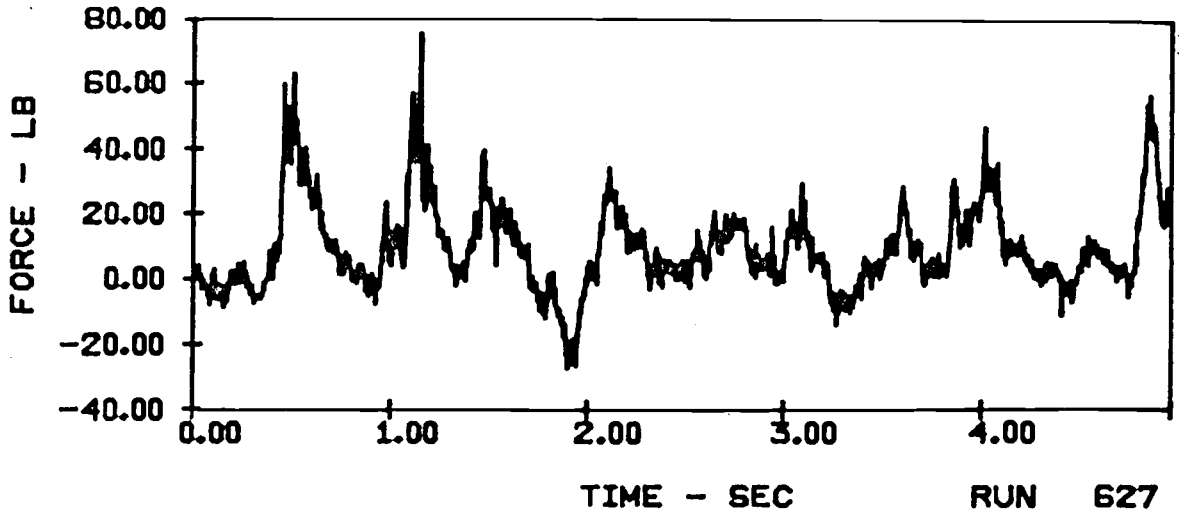


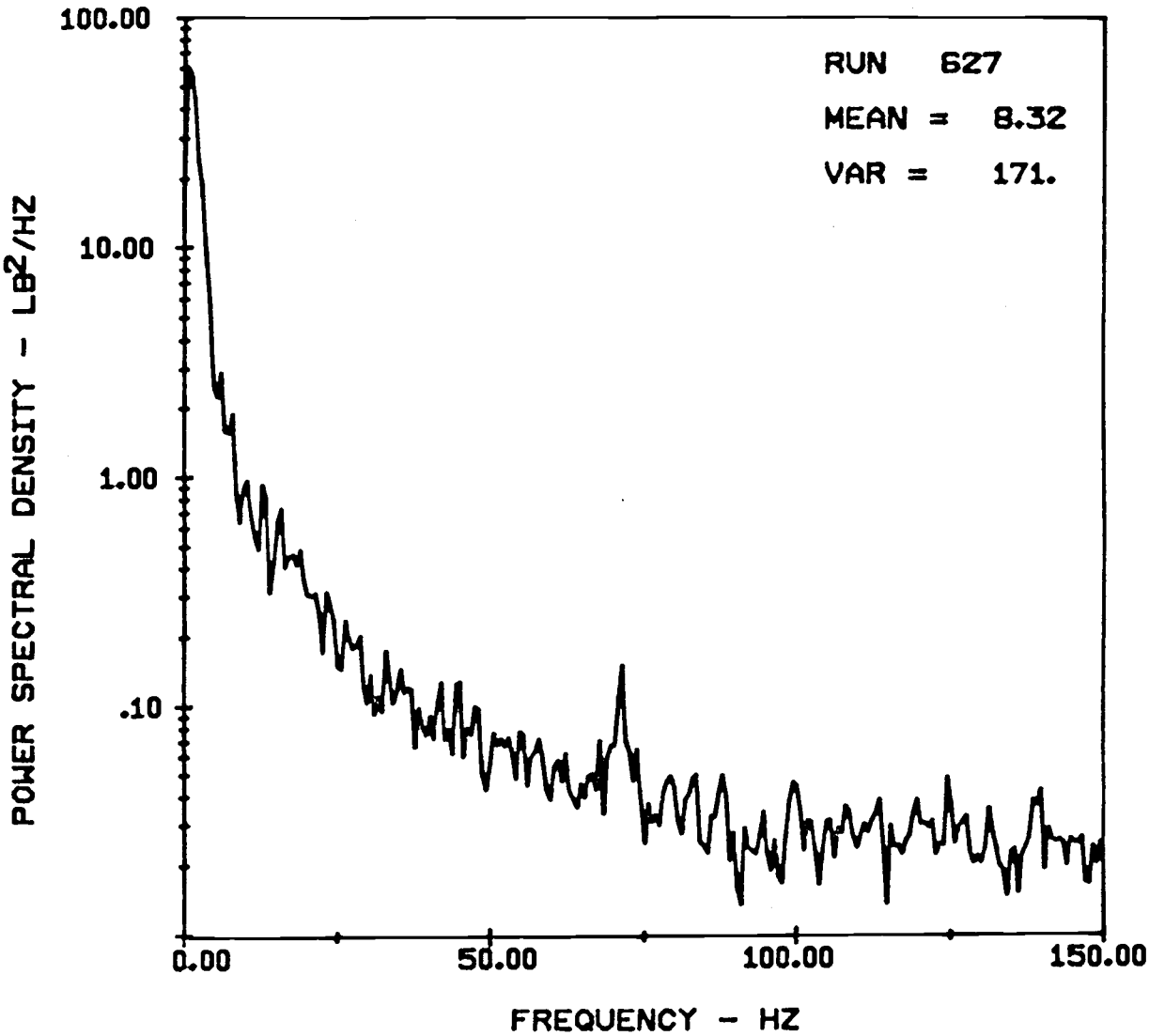


HORIZONTAL FORCES ON AN 8-TUBE ARRAY (V = 9 ft/sec)
IN E116 SAND WITH 20" ARRAY HEIGHT AND 6" TUBE SPACING

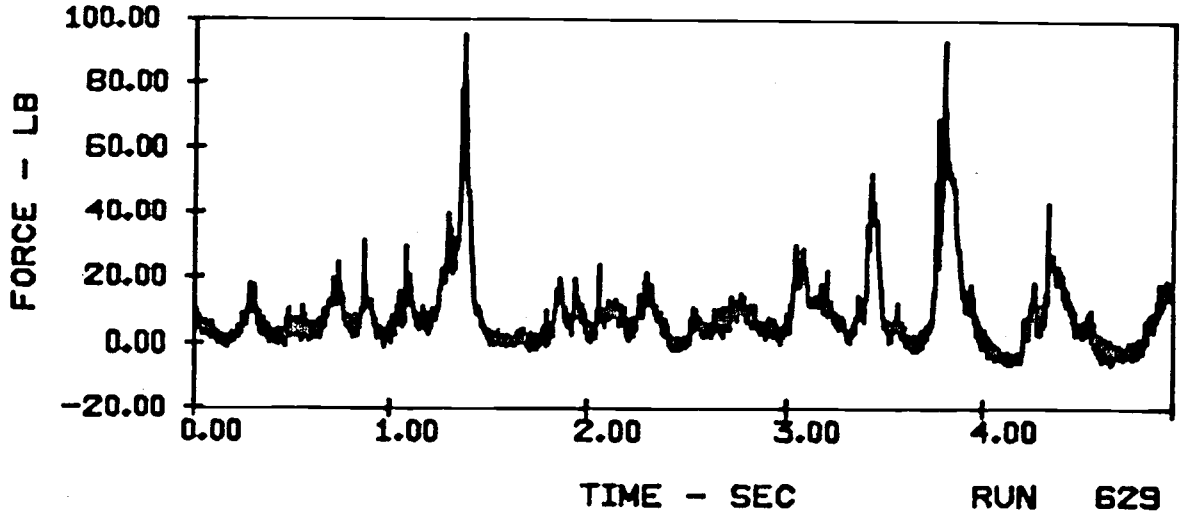


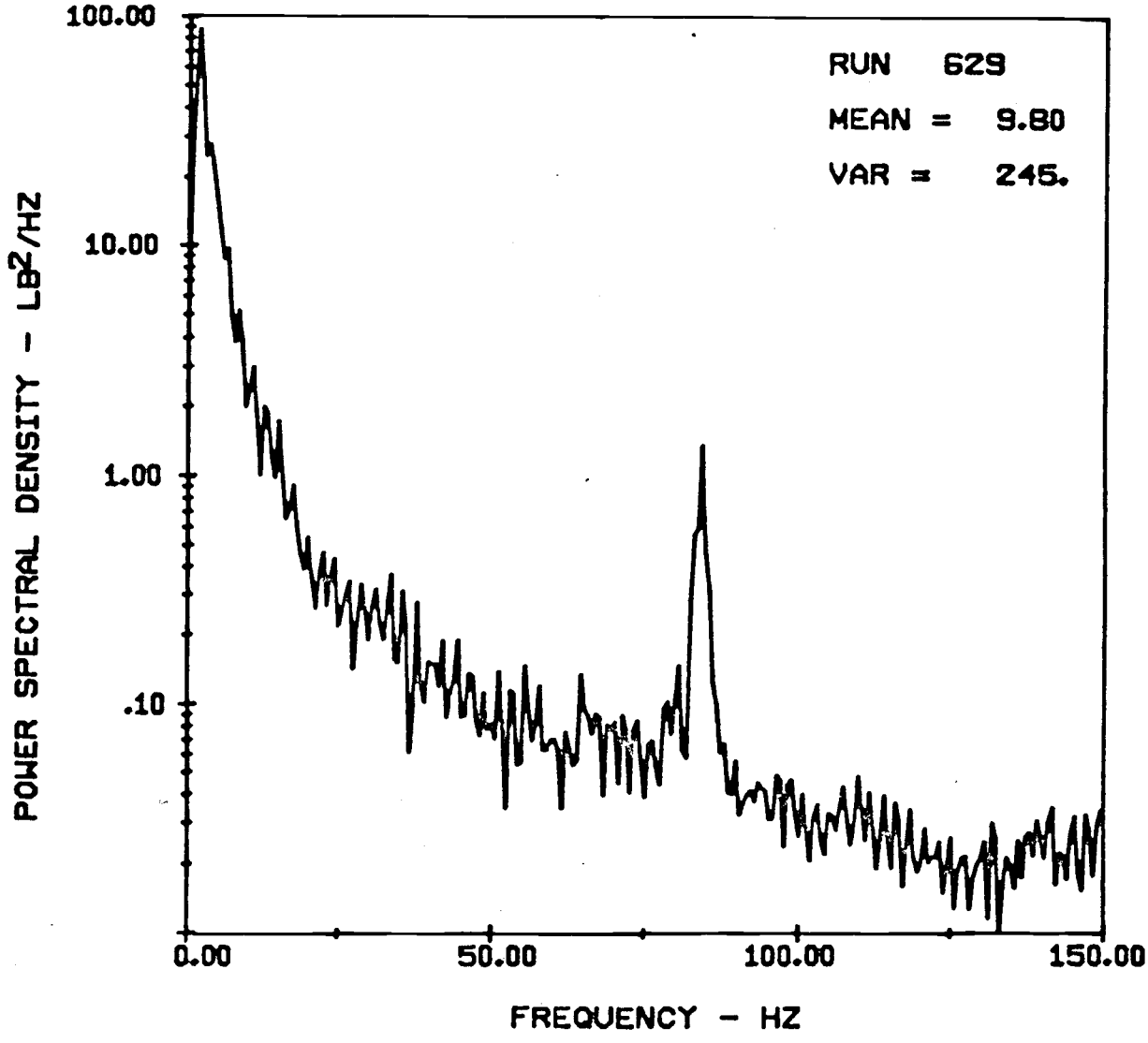


VERTICAL FORCES ON A SINGLE TUBE (V = 11 ft/sec)
IN EI16 SAND WITH 20" ARRAY HEIGHT AND 6" TUBE SPACING

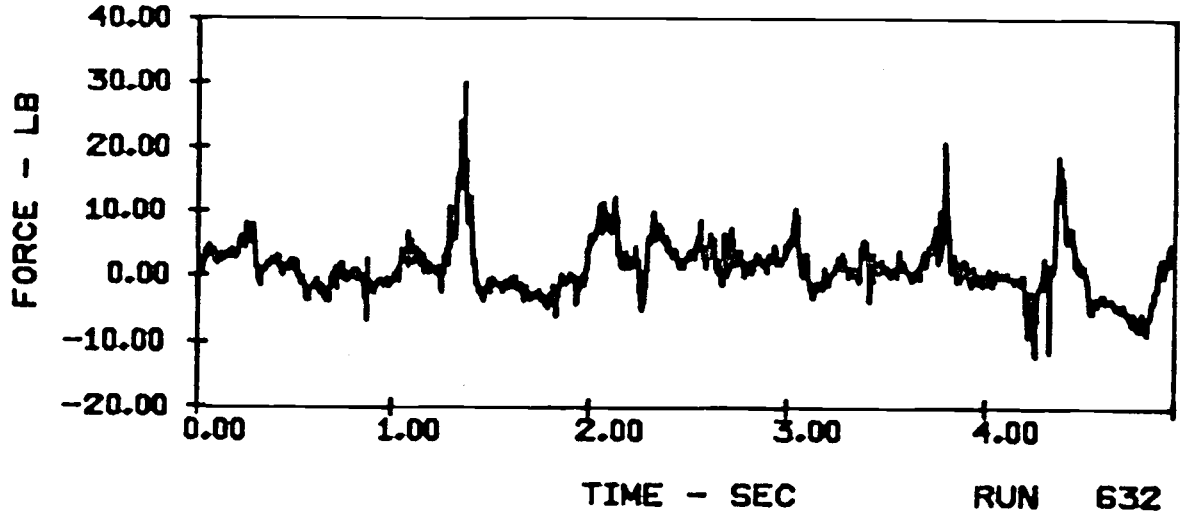


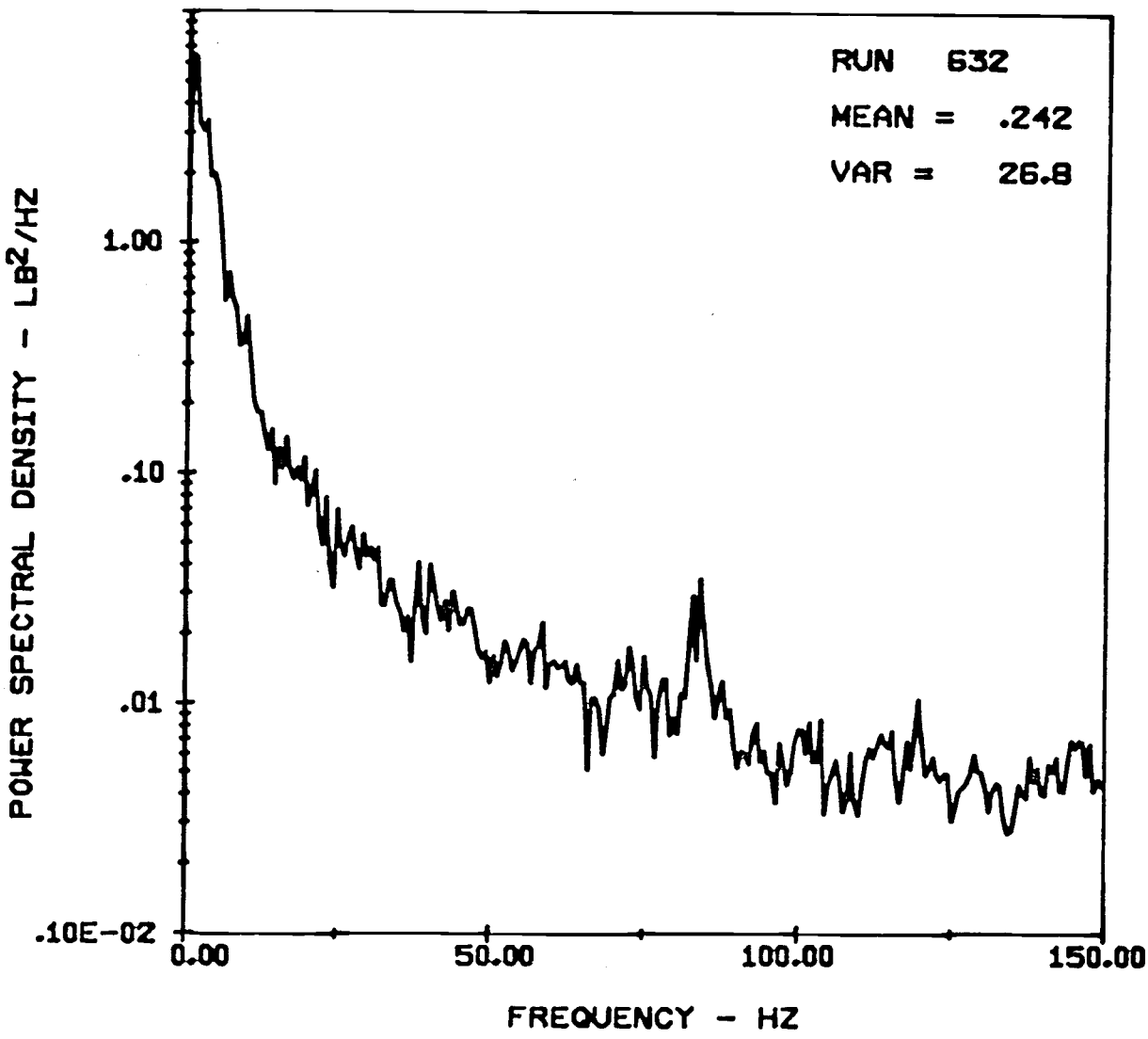


HORIZONTAL FORCES ON A SINGLE TUBE (V = 11 ft/sec)
IN EI16 SAND WITH 20" ARRAY HEIGHT AND 6" TUBE SPACI.G

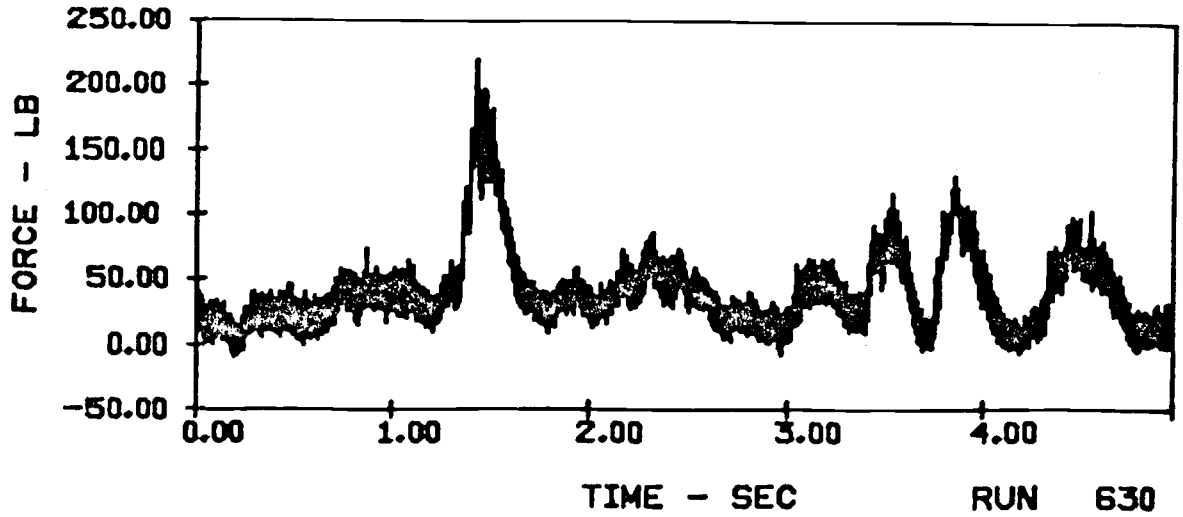


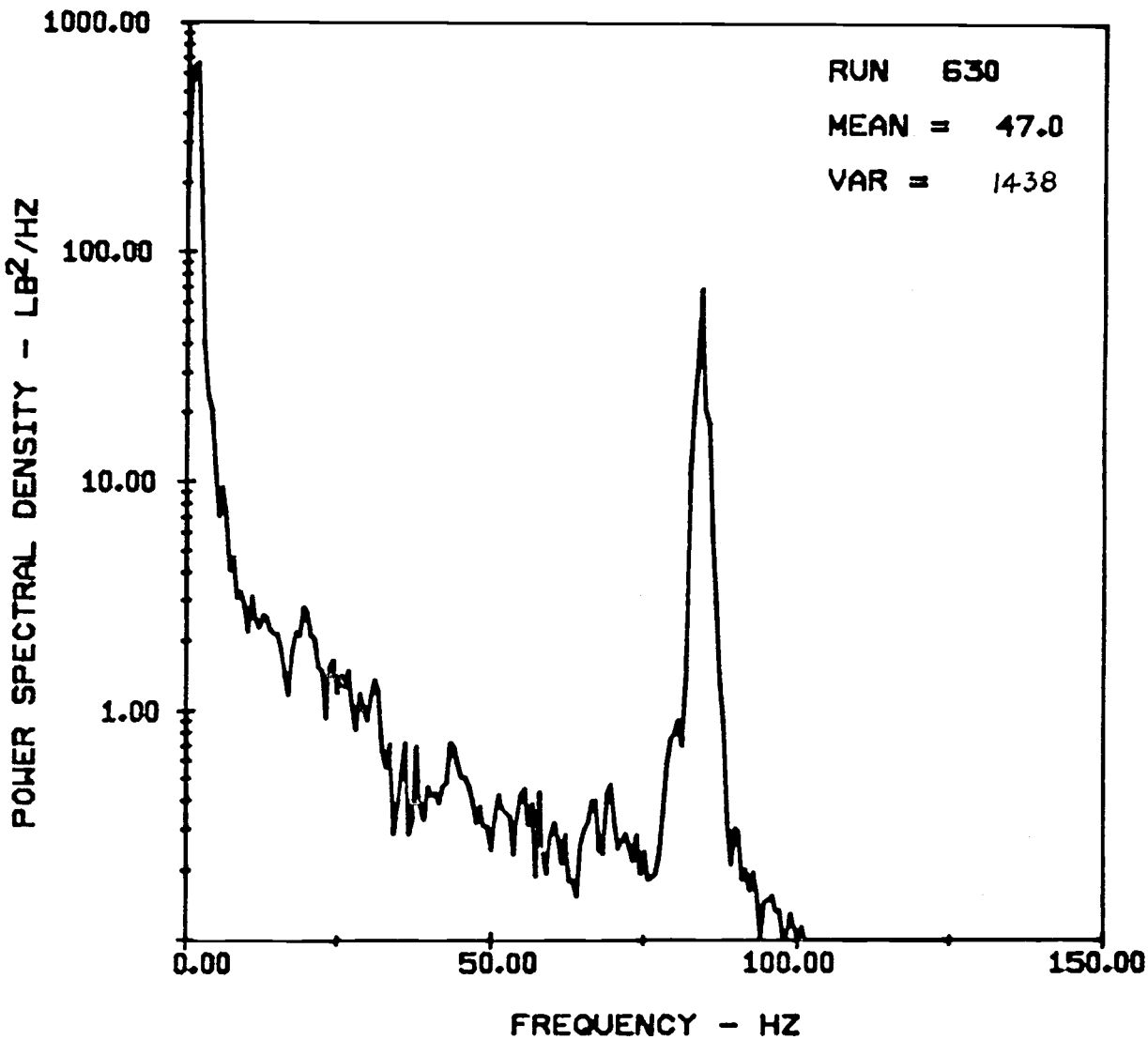


VERTICAL FORCES ON AN 8-TUBE ARRAY (V = 11 ft/sec)
IN E116 SAND WITH 20" ARRAY HEIGHT AND 6" TUBE SPACING

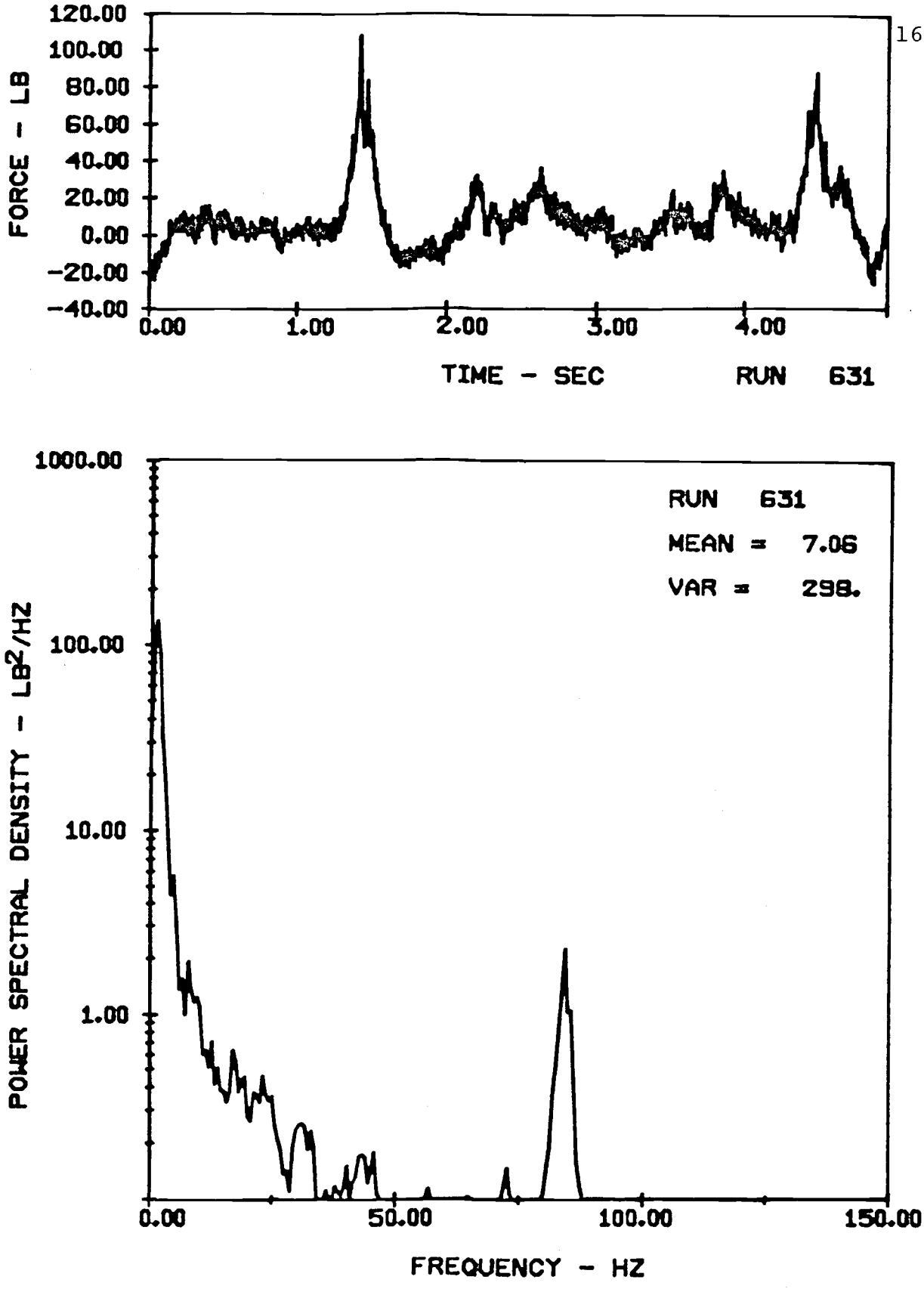


HORIZONTAL FORCES ON AN 8-TUBE ARRAY (V = 11 ft/sec)
IN EI16 SAND WITH 20 " ARRAY HEIGHT AND 6" TUBE SPACING